

CRANFIELD UNIVERSITY

S C LISLE-TAYLOR

CAVITATION PERFORMANCE OF PUMPED HYDROCARBONS

SCHOOL OF MECHANICAL ENGINEERING

PhD THESIS



## **IMAGING SERVICES NORTH**

Boston Spa, Wetherby

West Yorkshire, LS23 7BQ

[www.bl.uk](http://www.bl.uk)

**CONTAINS  
PULLOUTS**

## ACKNOWLEDGEMENTS

The work for this thesis was conducted under the supervision of Prof. R.L. Elder of Cranfield University, Mr I.N. Rhodes of BHR Group Limited and Mr A.G. Salisbury and Mr G. Webster of the project sponsors Hayward Tyler Fluid Dynamics in Luton. I express my thanks to all for their help, advice, encouragement and support throughout the duration of the project.

I would like to thank the staff of BHR Group Limited and Hayward Tyler Fluid Dynamics for all their help and advice. Especially Mr J. Harvey and Mr C. McDonnell at Hayward Tyler for their help during the design and fabrication of the test rig.

I would also like to express my gratitude to Hayward Tyler Fluid Dynamics for their sponsorship of this project without which it would not have happened.

Last but by no means least I would like to thank my wife Rebecca for her support, patience and understanding during some of the more stressful times of this work.

S C LISLE-TAYLOR.  
September 1997

## ABSTRACT

The phenomena of cavitation has been studied widely, as it can occur in all aspects of fluid flow. Although a very large body of research has been conducted over the years, some of the fundamental processes at work are not fully understood. This especially applies to the area of cavitation in fluids other than water, the bulk of research over the years having been conducted on water.

A study has investigated the various aspects of cavitation in hydrocarbon fluids, and how their cavitation performance compares to that of water. The study was conducted to aid the design and selection of centrifugal process pumps and to better the understanding of cavitation in hydrocarbon fluids from its inception to fully developed conditions.

Experimental data was gathered on water, kerosine and gas oil using a newly designed and constructed test rig. The effects of dissolved air and temperature were studied for each fluid, using a dual method multi fluid cavitation test rig. These two methods of cavitation induction were a centrifugal process pump and a two dimensional convergent-divergent nozzle test section. The test section was designed to model the flow passage of neighbouring blades on a centrifugal pump impeller which also incorporates inspection windows to observe the cavitating flows. The centrifugal pump was also used for driving flow through the nozzle.

The results and conclusions show the many differences of the cavitation process between water and hydrocarbons fuels and outline some of the fundamental aspects of the influential properties of the hydrocarbon fuels that affect cavitation. The principal conclusions are:-

1. The hydrocarbon liquids needed a greater  $NPSH_R$  than cold clean water at ambient temperatures, due to vaporous cavitation being enhanced by gaseous cavitation. (Shown for both test methods)
2. Incipient cavitation performance is proportional to the dissolved oxygen as a percentage of saturation value of the fluids tested (Nozzle tests). The performance increasing as the air content is lowered
3. The 3% nozzle efficiency drop of the fluids tested is dependent on the dissolved air as a percentage of the volume. The hydrocarbons showed a significant increase in cavitation performance with decreasing air content, water showed a negligible effect
4. One of the main factors affecting cavitation inception is the viscosity of the fluid. (Nozzle tests). The higher the viscosity the better the incipient cavitation performance.



## TABLE OF CONTENTS



ACKNOWLEDGEMENTS.	i
ABSTRACTS.	ii
TABLE OF CONTENTS.	iii
LIST OF FIGURES.	vii
LIST OF TABLES .	xiii
NOMENCLATURE .	xiv



<b><u>1. TOPIC OF INVESTIGATION</u></b>	<b><u>1</u></b>
<b>1.1 INTRODUCTION TO THE RESEARCH PROJECT.</b>	<b>1</b>
<b>1.2 THE CAVITATION PHENOMENON.</b>	<b>2</b>
1.2.1 HYDRODYNAMIC CAVITATION.	2
1.2.2 CAVITATION EROSION.	5
1.2.3 CAVITATION NOISE.	8
<b>1.3 CAVITATION IN HYDRAULIC MACHINES - CENTRIFUGAL PUMPS.</b>	<b>8</b>
1.3.1 DEFINITIONS OF CENTRIFUGAL PUMP TERMS.	8
1.3.1.1 NPSH, NPIH or NPSE.	8
1.3.1.2 SPECIFIC SPEED.	9
1.3.1.3 SUCTION TYPE NUMBER / SUCTION SPECIFIC SPEED.	10
1.3.1.4 THOMA CAVITATION COEFFICIENT.	10
1.3.2 THE EFFECT OF CAVITATION ON CENTRIFUGAL PUMPS.	10
1.3.3 PUMPING VARIOUS LIQUIDS.	12
<b>1.4 CONCLUSION.</b>	<b>13</b>
<b><u>2. LITERATURE REVIEW</u></b>	<b><u>14</u></b>
<b>2.1 INTRODUCTION.</b>	<b>14</b>
<b>2.2 THE THERMODYNAMIC EFFECT.</b>	<b>14</b>
2.2.1 CONCLUDING COMMENTS.	26
<b>2.3 GAS / AIR CONTENT EFFECTS.</b>	<b>26</b>
2.3.1 CONCLUDING COMMENTS	28
<b>2.4 HYDROCARBON PROPERTIES INFORMATION.</b>	<b>29</b>
<b>2.5 CONCLUSIONS OF LITERATURE REVIEW.</b>	<b>30</b>
<b><u>3. PUMP DESIGN</u></b>	<b><u>31</u></b>
<b>3.1 INTRODUCTION.</b>	<b>31</b>
<b>3.2 BASIC CENTRIFUGAL PUMP THEORY.</b>	<b>31</b>
<b>3.3 SELECTION OF PUMP DESIGN.</b>	<b>34</b>
3.3.1 PUMP SELECTION EXAMPLE - A SIMPLE CASE.	36
<b>3.4 BASIC PUMP DESIGN.</b>	<b>39</b>
3.4.1 SCALING.	40
3.4.2 TRADITIONAL HYDRAULIC DESIGN.	41
<b>3.5 CONCLUDING COMMENTS.</b>	<b>44</b>

<b>4. THE HYDROCARBON CAVITATION TEST RIG, (HCTR).</b>	<b>45</b>
<b>4.1 INTRODUCTION</b>	<b>45</b>
<b>4.2 THE TEST RIG DESIGN PROCESS.</b>	<b>45</b>
4.2.1 DESIGN 1	46
4.2.2 DESIGN 2	46
<b>4.3 THE FINAL TEST RIG DESIGN.</b>	<b>46</b>
4.3.1 CHOICE OF HYDROCARBON FLUIDS.	50
4.3.2 HYDRAULIC DETAILS	52
4.3.3 INSTRUMENTATION.	53
4.3.3.1 TEMPERATURE.	53
4.3.3.2 PRESSURE.	54
4.3.3.3 FLOW.	54
4.3.3.4 DISSOLVED AIR.	55
4.3.3.4 POWER METER.	55
4.3.3.4 TACHOMETER.	56
4.3.4 THE 2D VENTURI TEST SECTION.	56
<b>4.4 MATERIALS OF CONSTRUCTION AND MINOR DESIGN DETAILS.</b>	<b>58</b>
<b>4.5 SAFETY FEATURES OF THE DESIGN.</b>	<b>58</b>
<b>4.6 HYDRAULIC ANALYSIS OF THE TEST RIG DESIGN.</b>	<b>59</b>
4.6.1 CAVITATION CONDITIONS WITHIN TEST SECTION.	59
4.6.2 HYDRAULIC ANALYSIS OF THE TEST RIG.	60
<b>4.7 RETROSPECTIVE ANALYSIS OF THE TEST RIGS PERFORMANCE.</b>	<b>65</b>
4.7.1 HYDRAULIC DESIGN PERFORMANCE.	65
4.7.2 TEMPERATURE.	66
4.7.3 FLOW.	67
4.7.4 DISSOLVED OXYGEN / AIR CONTENT.	68
4.7.5 PRESSURE.	69
4.7.6 CONCLUSION.	70
<b>5. EXPERIMENTAL WORK.</b>	<b>71</b>
<b>5.1 INTRODUCTION.</b>	<b>71</b>
<b>5.2 WATER TESTS.</b>	<b>71</b>
5.2.1 WATER PUMP TESTS.	71
5.2.2 WATER NOZZLE TESTS.	72
<b>5.3 Kerosine TESTS.</b>	<b>73</b>
5.3.1 Kerosine PUMP TESTS.	74
5.3.2 Kerosine NOZZLE TESTS.	74
<b>5.4 GAS OIL TESTS.</b>	<b>75</b>
5.4.1 GAS OIL PUMP TESTS.	75
5.4.2 GAS OIL NOZZLE TESTS.	75



<b>REFERENCES.</b>	<b>144-151</b>
<b>APPENDIX A Test rig pump details.</b>	<b>153-158</b>
<b>APPENDIX B HCTR layout drawings.</b>	<b>159-161</b>
<b>APPENDIX C Hydraulic design information.</b>	<b>162-164</b>
<b>APPENDIX D Pump and nozzle curves for water.</b>	<b>165-183</b>
<b>APPENDIX E Pump and nozzle curves for kerosine.</b>	<b>184-192</b>
<b>APPENDIX F Pump and nozzle curves for gas oil.</b>	<b>193-201</b>
<b>APPENDIX G Photographs.</b>	<b>202-207</b>
<b>APPENDIX H Bubble dynamics.</b>	<b>208-222</b>

## LIST OF FIGURES

<b>FIGURE 1.2-1 CAVITATION IN A VENTURI</b>	<b>4</b>
FIGURE 1.2-2 TYPES OF HYDRODYNAMIC CAVITATION	5
FIGURE 1.2-3 CAVITATION EROSION	6
FIGURE 1.2-4 MODES OF BUBBLE COLLAPSE	6
FIGURE 1.2-5 EROSION LIFE CYCLE	7
FIGURE 1.2-6 RESISTANCE OF MATERIALS TO CAVITATION EROSION. (SOURCE: KNAPP ET AL, 1970)	7
FIGURE 1.3-1 NPSH AVAILABLE AND REQUIRED CURVES.	9
FIGURE 1.3-2 PUMP IMPELLER TYPES	9
FIGURE 1.3-3 CAVITATION CHARACTERISTIC OF A PUMP.	11
FIGURE 1.3-4 NPSH TEST ON TWO DIFFERENT LIQUIDS	12
<b>FIGURE 3.2-1 RADIAL CENTRIFUGAL PUMP - SINGLE STAGE SINGLE ENTRY.</b>	<b>31</b>
FIGURE 3.2-2 VELOCITY VECTORS FOR A CENTRIFUGAL PUMP IMPELLER.	33
FIGURE 3.2-3 LEAKAGE FLOW	33
FIGURE 3.3-1 A SIMPLE PUMP SELECTION CHART.	35
FIGURE 3.3-2 A PUMPING SYSTEM.	36
FIGURE 3.3-3 EFFICIENCY V SPECIFIC SPEED.	39
FIGURE 3.4-1 BLACK BOX APPROACH TO SCALING	40
FIGURE 3.4-2 HEAD COEFFICIENT VERSUS SPECIFIC SPEED	43
FIGURE 3.4-3 IMPELLER DIAMETER SHROUD DISTANCE RATIO GRAPH	43
<b>FIGURE 4.3-1 SCHEMATIC OF THE HYDROCARBON CAVITATION TEST RIG HCTR.</b>	<b>49</b>
FIGURE 4.3-2 CROSS SECTION OF 2D VENTURI TEST SECTION.	57
FIGURE 4.6-1 SCHEMATIC OF CONVERGENT DIVERGENT NOZZLE	60
FIGURE 4.6-2 SCHEMATIC OF TEST RIG.	61
FIGURE 4.6-3 PRESSURE AND FRICTION LOSSES DIAGRAM FOR TEST RIG.	62
<b>FIGURE 6.2-1 PUMP PERFORMANCE CURVES.</b>	<b>77</b>
FIGURE 6.3-1 EFFECT OF TEMPERATURE ON THE VACUUM PUMP NPSH TEST METHOD.	80
FIGURE 6.3-2 EFFECT OF TEMPERATURE ON THE SUCTION VALVE THROTTLING NPSH TEST METHOD ( 100% DISSOLVED OXYGEN OF THE SATURATION VALUE).	80

FIGURE 6.3-3 EFFECT OF TEMPERATURE ON THE SUCTION VALVE THROTTLING NPSH TEST METHOD ( <10% DISSOLVED OXYGEN OF THE SATURATION VALUE).	81
FIGURE 6.3-4 COMPARISON OF NPSH TEST METHODS : VACUUM PUMP AND SUCTION VALVE THROTTLING (TEMPERATURE 19°C).	81
FIGURE 6.3-5 COMPARISON OF NPSH TEST METHODS : VACUUM PUMP AND SUCTION VALVE THROTTLING (TEMPERATURE 30°C).	82
FIGURE 6.3-6 COMPARISON OF CRITICAL NPSH OF WATER, KEROSENE AND GAS OIL ( VACUUM PUMP METHOD AT 20°C )	82
FIGURE 6.3-7 COMPARISON OF CRITICAL NPSH OF WATER, KEROSENE AND GAS OIL ( VACUUM PUMP METHOD AT 30°C )	83
FIGURE 6.3-8 COMPARISON OF CRITICAL NPSH OF WATER, KEROSENE AND GAS OIL ( VACUUM PUMP METHOD 20°C AND 30°C )	83
FIGURE 6.4-1 EFFECT OF TEMPERATURE ON WATER CAVITATING IN THE NOZZLE (REF. PRESSURE 2.0 BAR)	85
FIGURE 6.4-2 EFFECT OF TEMPERATURE ON WATER CAVITATING IN THE NOZZLE. (REF. PRESSURE 1.5 BAR)	86
FIGURE 6.4-3 EFFECT OF TEMPERATURE ON WATER CAVITATING IN THE NOZZLE. (REF. PRESSURE 1.0 BAR)	87
FIGURE 6.4-4 EFFECT OF DISSOLVED OXYGEN ON WATER CAVITATING IN THE NOZZLE.	88
FIGURE 6.4-5 EFFECT OF FREE STREAM VELOCITY ON WATER CAVITATING IN THE NOZZLE.	89
FIGURE 6.4-6 EFFECT OF TEMPERATURE ON KEROSENE CAVITATING IN THE NOZZLE.	91
FIGURE 6.4-7 EFFECT OF TEMPERATURE ON KEROSENE CAVITATING IN THE NOZZLE.	92
FIGURE 6.4-8 EFFECT OF TEMPERATURE ON KEROSENE CAVITATING IN THE NOZZLE.	93
FIGURE 6.4-9 EFFECT OF DISSOLVED OXYGEN ON KEROSENE CAVITATING IN THE NOZZLE.	94
FIGURE 6.4-10 EFFECT OF FREE STREAM VELOCITY ON KEROSENE CAVITATING IN THE NOZZLE.	95
FIGURE 6.4-11 EFFECT OF TEMPERATURE ON GAS OIL CAVITATING IN THE NOZZLE.	97
FIGURE 6.4-12 EFFECT OF TEMPERATURE ON GAS OIL CAVITATING IN THE NOZZLE.	98
FIGURE 6.4-13 EFFECT OF TEMPERATURE ON GAS OIL CAVITATING IN THE NOZZLE.	99
FIGURE 6.4-14 EFFECT OF DISSOLVED OXYGEN ON GAS OIL CAVITATING IN THE NOZZLE	100
FIGURE 6.4-15 EFFECT OF FREE STREAM VELOCITY ON GAS OIL CAVITATING IN THE NOZZLE.	101
FIGURE 6.4-16 EFFECT OF DISSOLVED OXYGEN ON WATER, KEROSENE AND GAS OIL OR VARIOUS CAVITATION CONDITIONS.	102

FIGURE 6.4-17 EFFECT OF DISSOLVED AIR (% BY VOLUME DISSOLVED IN THE FLUID) ON WATER, KEROSENE AND GAS OIL FOR VARIOUS CAVITATION CONDITIONS.	105
FIGURE 6.5-1 COMPARISON OF NPSH TEST AND NOZZLE TEST DATA FOR WATER, KEROSENE AND GAS OIL.	106
<b><u>FIGURE 7.3-4 SCHEMATIC OF LEAKAGE OVER ONE BLADE OF AN UNSHROUDED IMPELLER.</u></b>	<b>113</b>
FIGURE 7.4-1 STILLS OF WATER CAVITATION IN THE NOZZLE ( $s=8.0$ : DISSOLVED AIR 100% OF SATURATION VALUE : REFERENCE PRESSURE 2.0 BAR)	122
FIGURE 7.4-2 KEROSENE CAVITATION JUST PRECEDING THE 3% EFFICIENCY DROP VALUE ( $s=10.5$ : DISSOLVED AIR 100% OF SATURATION VALUE : REFERENCE PRESSURE 2.0 BAR)	124
FIGURE 7.4-3 WATER CAVITATION JUST PRECEDING THE 3% EFFICIENCY DROP VALUE ( $s=9.5$ : DISSOLVED AIR 100% OF SATURATION VALUE : REFERENCE PRESSURE 2.0 BAR)	124
FIGURE 7.4-4 KEROSENE CAVITATION, COMPARABLE CONDITION TO THAT OF WATER IN FIGURE 7.4-1 ( $s=8.2$ : DISSOLVED AIR 100% OF SATURATION VALUE : REFERENCE PRESSURE 2.0 BAR)	125
FIGURE 7.5-1 AIR CONTENT EFFECT OF WATER ON CAVITATION IN A CENTRIFUGAL PUMP. (ORIGINAL SOURCE SCHOENEBERGER 1956 - NOT FOUND BY AUTHOR)	128
FIGURE 7.5-2 FORMATION IF AIR BUBBLES AROUND VAPOUR CAVITY.	130
FIGURE 7.5-3 ZONE OF GAS CONTENT EFFECT ON CAVITATION PERFORMANCE.	132
FIGURE 7.5-4 GASEOUS - VAPOROUS CAVITATION CHARACTERISTIC GRAPH FOR SEVERAL FLUIDS.	133
FIGURE 7.5-5 BOILING RANGE OF TYPICAL PETROLEUM FUELS.	136
<b><u>FIGURE A-1 MANUFACTURERS PUMP CURVES FOR THE MAIN CIRCULATING PUMP.</u></b>	<b>154</b>
FIGURE A-2 DIMENSIONS OF THE MAIN CIRCULATING PUMP	155
FIGURE A-3 PUMP SET DETAILS OF THE MAIN CIRCULATING PUMP.	156
FIGURE A-4 CROSS SECTION OF THE MAIN CIRCULATING PUMP.	157
FIGURE A-5 CROSS SECTION PARTS LIST.	158
<b><u>FIGURE B-1 MAIN LAYOUT ENGINEERING DRAWING OF THE HCTR.</u></b>	<b>160</b>
FIGURE B-2 MAIN FLOW LOOP ENGINEERING DRAWING.	161
<b><u>FIGURE C-1 MOODY FRICTION FACTOR CHART.</u></b>	<b>164</b>

**FIGURE D-1 NPSH CURVES FOR WATER - SUCTION VALVE**

**THROTTLING**

166

FIGURE D-2 NPSH CURVES FOR WATER - SUCTION VALVE THROTTLING	167
FIGURE D-3 NPSH CURVES FOR WATER - SUCTION VALVE THROTTLING	168
FIGURE D-4 NPSH CURVES FOR WATER - SUCTION VALVE THROTTLING	169
FIGURE D-5 NPSH CURVES FOR WATER - VACUUM PUMP METHOD	170
FIGURE D-6 NPSH CURVES FOR WATER - VACUUM PUMP METHOD	171
FIGURE D-7 NOZZLE EFFICIENCY TESTS FOR WATER : DISSOLVED OXYGEN » 100% OF SATURATION VALUE : FLUID TEMPERATURE 20°C	172
FIGURE D-8 NOZZLE EFFICIENCY TESTS FOR WATER: DISSOLVED OXYGEN » 100% OF SATURATION VALUE : FLUID TEMPERATURE 30°C	173
FIGURE D-9 NOZZLE EFFICIENCY TESTS FOR WATER : DISSOLVED OXYGEN » 100% OF SATURATION VALUE : FLUID TEMPERATURE 40°C	174
FIGURE D-10 NOZZLE EFFICIENCY TESTS FOR WATER : DISSOLVED OXYGEN » 100% OF SATURATION VALUE : FLUID TEMPERATURE 50°C	175
FIGURE D-11 NOZZLE EFFICIENCY TESTS FOR WATER : DISSOLVED OXYGEN » 50% OF SATURATION VALUE : FLUID TEMPERATURE 20°C	176
FIGURE D-12 NOZZLE EFFICIENCY TESTS FOR WATER : DISSOLVED OXYGEN » 50% OF SATURATION VALUE : FLUID TEMPERATURE 30°C	177
FIGURE D-13 NOZZLE EFFICIENCY TESTS FOR WATER : DISSOLVED OXYGEN » 50% OF SATURATION VALUE : FLUID TEMPERATURE 40°C	178
FIGURE D-14 NOZZLE EFFICIENCY TESTS FOR WATER : DISSOLVED OXYGEN » 50% OF SATURATION VALUE : FLUID TEMPERATURE 50°C	179
FIGURE D-15 NOZZLE EFFICIENCY TESTS FOR WATER : DISSOLVED OXYGEN <10% OF SATURATION VALUE : FLUID TEMPERATURE 50°C	180
FIGURE D-16 NOZZLE EFFICIENCY TESTS FOR WATER : DISSOLVED OXYGEN <10% OF SATURATION VALUE : FLUID TEMPERATURE 30°C	181
FIGURE D-17 NOZZLE EFFICIENCY TESTS FOR WATER : DISSOLVED OXYGEN <10% OF SATURATION VALUE : FLUID TEMPERATURE 20°C	182
FIGURE D-18 NOZZLE EFFICIENCY TESTS FOR WATER : DISSOLVED OXYGEN <10% OF SATURATION VALUE : FLUID TEMPERATURE 40°C	183



<b><u>FIGURE E-1 NPSH CURVES FOR Kerosine - Vacuum Pump Method</u></b>	<b>185</b>
FIGURE E-2 NPSH CURVES FOR Kerosine - Vacuum Pump Method	186
FIGURE E-3 NOZZLE EFFICIENCY TESTS FOR Kerosine : DISSOLVED OXYGEN » 50% OF SATURATION VALUE : FLUID TEMPERATURE 20°C	187
FIGURE E-4 NOZZLE EFFICIENCY TESTS FOR Kerosine: DISSOLVED OXYGEN » 50% OF SATURATION VALUE : FLUID TEMPERATURE 30°C	188
FIGURE E-5 NOZZLE EFFICIENCY TESTS FOR Kerosine : DISSOLVED OXYGEN » 100% OF SATURATION VALUE : FLUID TEMPERATURE 30°C	189
FIGURE E-6 NOZZLE EFFICIENCY TESTS FOR Kerosine: DISSOLVED OXYGEN » 100% OF SATURATION VALUE : FLUID TEMPERATURE 20°C	190
FIGURE E-7 NOZZLE EFFICIENCY TESTS FOR Kerosine : DISSOLVED OXYGEN » 20-25% OF SATURATION VALUE : FLUID TEMPERATURE 20°C	191
FIGURE E-8 NOZZLE EFFICIENCY TESTS FOR Kerosine : DISSOLVED OXYGEN » 20-25% OF SATURATION VALUE : FLUID TEMPERATURE 30°C	192
<b><u>FIGURE F-1 NPSH CURVES FOR GAS OIL - Vacuum Pump Method</u></b>	<b>194</b>
FIGURE F-2 NPSH CURVES FOR GAS OIL - Vacuum Pump Method	195
FIGURE F-3 NOZZLE EFFICIENCY TESTS FOR GAS OIL : DISSOLVED OXYGEN » 100% OF SATURATION VALUE : FLUID TEMPERATURE 20°C	196
FIGURE F-4 NOZZLE EFFICIENCY TESTS FOR GAS OIL: DISSOLVED OXYGEN » 100% OF SATURATION VALUE : FLUID TEMPERATURE 30°C	197
FIGURE F-5 NOZZLE EFFICIENCY TESTS FOR GAS OIL : DISSOLVED OXYGEN » 50% OF SATURATION VALUE : FLUID TEMPERATURE 30°C	198
FIGURE F-6 NOZZLE EFFICIENCY TESTS FOR GAS OIL: DISSOLVED OXYGEN » 50% OF SATURATION VALUE : FLUID TEMPERATURE 20°C	199
FIGURE F-7 NOZZLE EFFICIENCY TESTS FOR GAS OIL : DISSOLVED OXYGEN » 20-25% OF SATURATION VALUE : FLUID TEMPERATURE 20°C	200
FIGURE F-8 NOZZLE EFFICIENCY TESTS FOR GAS OIL : DISSOLVED OXYGEN » 20-25% OF SATURATION VALUE : FLUID TEMPERATURE 30°C	201

<b><u>FIGURE G-1 HYDROCARBON CAVITATION TEST RIG ; MAIN CIRCUIT</u></b>	<b>203</b>
FIGURE G-2 EARLY CAVITATION GROWTH IN GAS OIL	204
FIGURE G-2 APPROXIMATELY 3% EFFICIENCY DROP CAVITATION CONDITION IN GAS OIL	205
FIGURE G-2 FULLY DEVELOPED CAVITATION IN GAS OIL	206
FIGURE G-2 'SUPERCAVITATION' CONDITION IN GAS OIL	207
<b><u>FIGURE H-1 RAYLEIGH ENERGY ANALYSIS.</u></b>	<b>211</b>
FIGURE H-2 RAYLEIGH ANALYSIS: PRESSURE PROFILE NEAR A COLLAPSING BUBBLE.	215
FIGURE H-3 PORITSKI ANALYSIS	217

## LIST OF TABLES

<b><u>TABLE 4.3-1 COMPARISON OF PROPERTIES, KEROSENE AND GAS OIL</u></b>	<b><u>51</u></b>
TABLE 4.3-2 TEMPERATURE MEASURING POINTS	53
TABLE 4.3-3 PRESSURE MEASURING POINTS	54
TABLE 4.3-4 TURBINE FLOW METER DETAILS	54
TABLE 4.6-1 VALUES TO FIND FRICTION FACTOR F FROM THE MOODY CHART	62
TABLE 4.6-2 FRICTION HEAD LOSSES BETWEEN POINTS J AND C.	63
TABLE 4.6-3 FRICTION HEAD LOSSES BETWEEN POINTS D AND PUS.	63
TABLE 4.6-4 FRICTION HEAD LOSSES BETWEEN POINTS PDS AND J	63
TABLE 4.6-5 FRICTION HEAD LOSSES BETWEEN POINTS J AND B	64
TABLE 4.6-6 RESULTS FROM SPREADS SHEET FRICTION LOSS ANALYSIS.	64
<b><u>TABLE 7.2-1 SUMMARY OF TEST FLUID PROPERTIES.</u></b>	<b><u>108</u></b>
TABLE 7.3-1 NPSH ADJUSTMENT FOR WATER BETWEEN 19 AND 30°C.	111
TABLE 7.3-2 ASTM DISTILLATION FOR KEROSENE AND GAS OIL.	113
TABLE 7.3-3 NPSH ADJUSTMENT FOR KEROSENE AND GAS OIL BETWEEN 20 AND 30°C.	114
TABLE 7.5-1 SPRAKERS DATA FOR A TOP SUCTION PUMP ( 3550 RPM : 71M HEAD : 136 M3/HR )	131
TABLE 7.5-2 VISCOSITIES OF SOME CONSTITUENT FLUIDS OF KEROSENE AND GAS OIL.	136
<b><u>TABLE C-1 K FACTORS FOR TYPICAL FITTINGS.</u></b>	<b><u>163</u></b>

## NOMENCLATURE

<u>Symbol</u>	<u>Description</u>	<u>Units</u>
$a$	Acceleration.	$m/s^2$
$B$	Stepanoff's Thermal Cavitation Criterion.	-
$c$	Sonic velocity	$m/s$
$C_P$	Specific heat at constant pressure	$kJ/kgK$
$C_{pm}$	Minimum pressure coefficient (a function of attack angle)	-
$D, d$	Characteristic dimension, or cavity diameter	$m$
$E$	Unknown factor ( $0.3 > E > 1.0$ )	-
$f$	friction factor	-
$f$	A function of	-
$g$	Acceleration of gravity ( $9.81m/s^2$ )	$m/s^2$
$H$	Head of fluid	$m \text{ of fluid}$
$h, H$	Enthalpy	$kJ/kg$
$J'$	Mechanical Equivalent of Heat ( $\approx 102 \text{ kg m/kJ}$ or $\approx 778 \text{ ft lb/Btu}$ )	$kg \text{ m/kJ}$
$K$	loss coefficient for friction losses in a hydraulic fitting	-
$KE$	Kinetic energy	$J$
$K_i$	Incipient cavitation parameter - Experimentally determined	-
$K_s$	Specific Speed	-
$K_{SS}$	Suction type number or suction specific speed	-
$L$	Latent heat of vaporisation	$kJ/kg$
$L_c$	Length of cavity	$m$
$M$	Molecular weight	
$N$	Rotational speed	$rpm$
$NPIH$	Net Positive Inlet Head (The total inlet pressure head minus the vapour pressure in head)	$m \text{ of fluid}$
$NPSE$	Net Positive Suction Energy	$J/kg$
$NPSH_A$	Net Positive Suction Head Available	$m \text{ of fluid}$
$NPSH_{adj}$	Net Positive Suction Head Adjustment	$m \text{ of fluid}$
$NPSH_{crit}$	Net Positive Suction Head Critical (Usually at 3% head drop)	$m \text{ of fluid}$
$NPSH_R$	Net Positive Suction Head Required	$m \text{ of fluid}$
$NPSH$	Net Positive Suction Head	$m \text{ of fluid}$
$p, P$	Pressure	$Pa$
$P_s$	Equilibrium vapour pressure	$Pa$
$Q$	Volume Flow rate	$m^3/s$
$r, R$	Radius	$m$
$R$	Specific gas constant	$kJ/kmolK$
$\tilde{R}$	Universal Gas Constant ( $\approx 8.314$ )	$kJ/kmolK$
$\dot{R}$	Velocity	$m/s$

$\ddot{R}$	Acceleration	$m/s^2$
$r_v$	Vapour to liquid volume ratio	-
$r_f$	Reciprocal of liquid specific gravity	-
$t$	time	$s$
$T$	Temperature	$^{\circ}C, ^{\circ}K$
$U$	Velocity	$m/s$
$u$	Velocity parallel to the x axis	$m/s$
$V, \bar{V}$	Volume	$m^3$
$v$	Velocity parallel to the y axis	$m/s$
$v$	Specific Volume	$m^3/kg$
$V_R'$	Volume Ratio	-
$W$	Work done	$J$
$w$	Velocity parallel to the z axis	$m/s$
$X$	Length of cavitating region	$m$
$z$	Head of fluid	$m$

#### GREEK

$\gamma$	Surface tension	$N/m$
$\alpha$	Dissolved gas content	-
$\beta$	Henry's constant	-
$\phi$	Velocity potential	$m^2/s$
$\mu$	Viscosity	$kg/\mu s$
$\sigma$	Surface tension coefficient	-
$\tau$	Time for total collapse of a bubble	$s$
$\theta$	Angle	$^{\circ}$ or $rad$
$\pi$	Pi = 3.1416	$rads$
$\nu$	Kinematic viscosity	$m^3/kg$
$\eta$	Efficiency	-
$\beta$	Ratio of radius to initial radius ( $R/R_0$ )	-
$\rho$	Density	$kg/m^3$
$\sigma$	Cavitation coefficient	-
$\omega$	Angular velocity	$rad/s$
$\Delta$	A finite difference in a quantity	-
$\alpha$	Thermal diffusivity of the liquid	-
$\alpha^*$	Void fraction of gas phase	-
$\beta^*$	$\alpha/(1-\alpha)$	-
$\sigma^*$	Critical cavitation coefficient	-
$\sigma_{TH}$	Thoma Cavitation Criterion	-

## SUBSCRIPTS

<u>Symbol</u>	<u>Description</u>
$\infty$	Infinity
$\phi, \theta$	Spherical co-ordinates - Angle of rotation.
$0$	Initial condition
$1, 2, 3 \text{ etc.}$	Condition one, two, three, etc.
$a, atm.$	Atmospheric
$c$	Cavitating
$crit$	Pertaining to the critical value
$dyn$	Dynamic
$f$	Fluid
$fit$	Pertaining to a fitting
$fg$	Pertaining to the point of phase change between liquid and gas
$gauge$	Pertaining to a gauge reading
$g, gas$	Pertaining to gas
$in$	Inlet condition
$L, l, LIQ$	Pertaining to Liquid
$m$	Minimum non cavitating
$min$	Minimum value of
$max$	Maximum value of
$out$	Outlet conditions
$pipe$	Pertaining to a pipe
$PRED$	Predicted values
$r, R$	Radially or at the radius $r, R$
$REF$	Reference values
$s$	Static
$st$	Pertaining to surface tension
$t$	Condition at test section throat
$v$	Vapour
$vp$	Vapour pressure
$x, y, z$	in the direction of

## **1. Topic of investigation**

### **1.1 Introduction to the research project.**

When running a centrifugal pump on hydrocarbon fluids the Net Positive Suction Head; NPSH required for efficient running of the pump is different to that of the same pump running on cold clean water. However this difference in NPSH has never fully been quantified, although several correlations have been made based on fluid properties and thermodynamic effects, with varying degrees of accuracy. Most texts such as Stepanoff (1957 and 1965) and Anderson (1980) suggest that hydrocarbons give a better cavitation performance to that of water. After the analysis of all the available published data the author could find, it appears that this statement has very little experimental data supporting it, as compared to the well researched temperature effects of water, where the NPSH required decreases with increasing temperature.

The project sponsors, a pump company Hayward Tyler Fluid Dynamics of Luton, have a keen interest in the cavitation characteristics of hydrocarbons, especially with the emergence of sub-sea oil operations. The pumps used need to be more efficient and more reliable as their removal for repair and maintenance is costly. Although the main industry standard for hydrocarbon process pumps API 610 (1989), disallows any advantage from this different NPSH, this is probably because there is so little known about the effect. A much better knowledge of the effects of pumping hydrocarbons is therefore required before any advantage can be taken from this effect. Further research might also find possible operating conditions where the performance might be worse than that of cold water and create the need for a factor of safety to be applied. This research therefore set out to obtain a better understanding of pumped hydrocarbons, and the factors effecting all stages of hydrocarbon cavitation, from its onset to more fully developed stages where hydraulic performance is effected. The remainder of this chapter gives an introduction to the subject area of cavitation and introduces the terms used in its study.

## **1.2 The Cavitation phenomenon.**

The first observation of '*cavitation*' was made by Newton (1704), although he did not realise the effect was due to dissolved air in the water coming out of solution. The first scientist to demonstrate cavitation as a result of decreasing the liquid pressure below that of its vapour pressure was Reynolds (1873). However the first major investigations into cavitation started at the turn of the century by Barnaby and Thornycroft (1895). The investigations were undertaken because the destroyer HMS Daring and the first turbine powered ship the Turbinia did not meet their design speed performance. This problem was traced to poor propeller performance due to cavitation. This is the first occurrence in literature where the word '*Cavitation*' is used to describe the phenomenon.

Since the turn of the century cavitation has been widely studied. These studies can be separated into four main fields, depending on the way in which the cavitation is created.

1. Particle cavitation - this is caused by elementary particles such as protons rupturing a liquid, causing a bubble chamber to form.
2. Acoustic cavitation - this is caused by sound waves travelling within a liquid creating pressure variations.
3. Optical cavitation - this is created by photons of high energy light (laser) rupturing the liquid.
4. Hydrodynamic cavitation - this is caused by the variations in flow and pressure of a liquid created by the systems geometry.

This research project is only concerned with Hydrodynamic cavitation and the rest of this chapter therefore gives an introduction for the subject with particular reference to cavitation in centrifugal pumps. Two good texts for further general reading on cavitation are Young (1989) and Knapp, Daily and Hammitt (1970).

### **1.2.1 Hydrodynamic Cavitation.**

The process by which a bubble forms in a liquid and its subsequent activity i.e. growth or collapse within that liquid is known as *cavitation*. The bubble appears either by the



creation of a new cavity or by the expansion of a micro bubble nuclei which can be in suspension within the liquid, or attached to the liquids boundary surfaces or to particles within the bulk of the fluid. The growth of these bubbles or creation of new cavities is caused by the lowering of the local pressure either by static or dynamic processes. These bubbles may contain vapour, gas or both. Bubbles containing gas may grow by the diffusion of gas from the liquid into the cavity, or by a reduction in the local pressure, or by an increase in temperature. Cavities which contain vapour grow explosively with a reduction in local pressure. Vapour bubbles will also form and grow with an increase in temperature ,this effect is known as *boiling*.

The stage at which cavitation is just detectable is *incipient cavitation*. In theory it is the point when the local liquid pressure is just reduced below the liquids vapour pressure. However this is rarely the case in practice, as incipient cavitation starts well before the local pressure reaches the fluids vapour pressure. This early onset of incipient cavitation is mainly dependent on the liquid's state. If there is a high dissolved gas content in the liquid, a reduced pressure will cause the gas to come out of solution. Also small bubble nuclei, (even those not visible to the naked eye) and small solid particles in the fluid will act as nucleation sites for cavitation bubbles to form and grow at pressures above those of the vapour pressure. It is not fully understood how gas content, nuclei size and number density affect the pressures at which cavitation will start. *Desinent Cavitation* is the type and stage of cavitation just before cavitation disappears, due to increased pressure. At this point the cavities / bubbles collapse which can cause erosion and noise.

Hydrodynamic cavitation can occur within a fluid system, where there are the highest velocities. As any hydrodynamic system will obey Bernoulli's equation, these points of high velocity will have the lowest pressures.

$$\frac{p}{\rho} + \frac{u^2}{2} + gz = Const \quad \text{..Equ 1.2-1}$$

For example as a fluid passes through a venturi See Figure 1.2-1 the velocity will be at its maximum at the throat. Thus the fluid pressure at the throat will be lower than that further up or down stream.

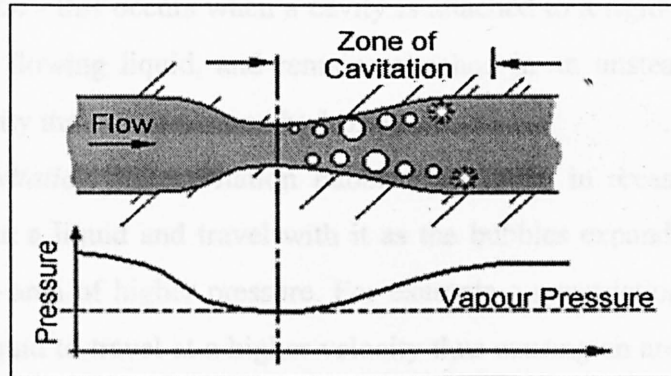


Figure 1.2-1 Cavitation in a Venturi

Theoretically, when this throat pressure is less than the vapour pressure of the fluid, cavitation bubbles will start to appear at the throat. These bubbles grow then shrink as they are swept down stream until they reach an area where the velocities are lower and thus the pressures are higher. The bubbles will then collapse with explosive forces, bubbles of pure vapour collapse more explosively as than bubbles with more gas / air content, this is because the vapour is more readily absorbed back into the fluid, and thus the bubbles collapse faster.

Bernoulli's equation can be rearranged to give a constant that is an indication of whether cavitation will occur within the system

$$\frac{P_1 - P_2}{\frac{1}{2} \rho u^2} = Const \quad \text{..Equ 1.2-2}$$

The constant is given the symbol  $\sigma$ , and  $p_2$  is usually taken as the vapour pressure of the fluid thus, a number known as the 'Sigma Cavitation Coefficient' is defined;

$$\sigma = \frac{P_1 - P_v}{\frac{1}{2} \rho u_1^2} \quad \text{..Equ 1.2-3}$$

In general there are three types of cavitation that occur in flowing liquids i.e. Hydrodynamic systems. See to Fig 1.2-2

- a) *Fixed cavitation* - this occurs when a cavity is attached to a rigid body immersed in the path of a flowing liquid, and remains attached in an unsteady condition. For example a cavity that forms over an hydrofoil.
- b) *Travelling cavitation* - is cavitation bubbles that form in areas of localised low pressure within a liquid and travel with it as the bubbles expand and subsequently collapse in an area of higher pressure. For example a constriction in the flow path causing the liquid to travel at a higher velocity thus causing an area of localised low pressure.
- c) *Vortex cavitation* - or 'tip' cavitation occurs in areas of high shear, such as the tips of ships propellers, and the cavities are formed in the low pressure areas in the centre of vortices.

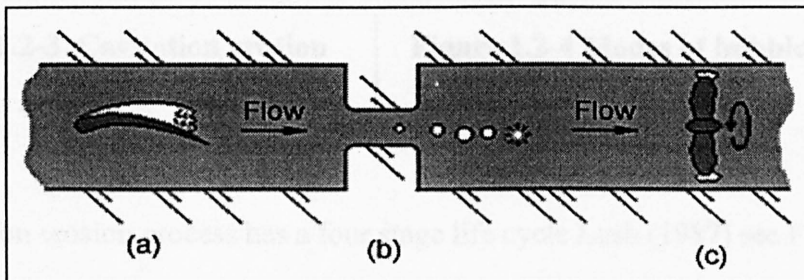
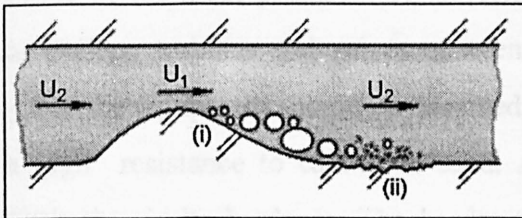


Figure 1.2-2 Types of Hydrodynamic cavitation

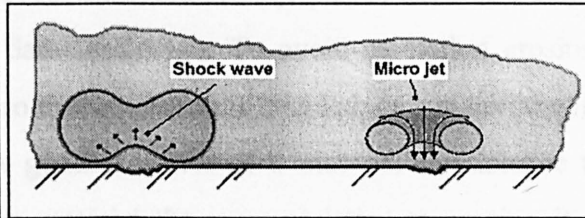
### 1.2.2 Cavitation Erosion.

Cavitation erosion is caused by the collapsing of the bubbles or cavities near the boundary surfaces of the liquid system (See Figure 1.2-3). The bubbles form at point (i) where the velocity is highest;  $u_1$ . They will subsequently collapse at around point (ii) where the velocity has slowed to  $u_2$ , causing the typical pitting of cavitation erosion. There are two schools of thought behind the process that causes the erosion (See Figure 1.2-4). The first is the thermal and pressure shocking of the material by the collapsing

bubble. The bubbles collapse in micro seconds sending out shock waves through the liquid with pressure differentials of up to 400 MPa Harrison (1952). The local fluid temperatures around the collapsing bubble have been calculated at 10,000 °K, Wheeler (1960), which can cause neighbouring materials to have temperature rises up to 1000°K. The second theory is that the bubbles collapse toroidally and produces a micro-jet of liquid through its centre which impinges on the materials surface with very high velocities 130-170m/s Plesset and Chapman (1971), and thus forces of very high magnitude are exerted on the materials surface. It is however probably caused by a mixture of both methods.



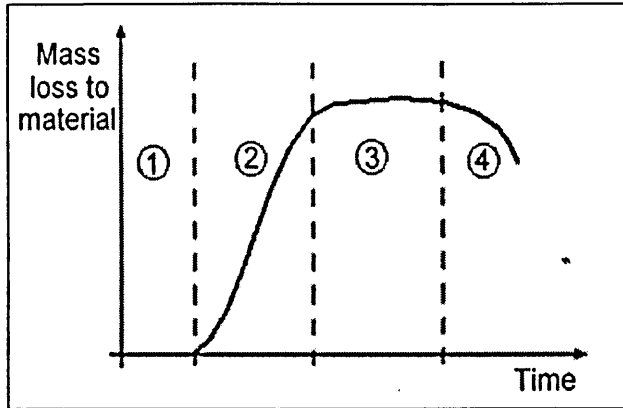
**Figure 1.2-3 Cavitation erosion**



**Figure 1.2-4 Modes of bubble collapse**

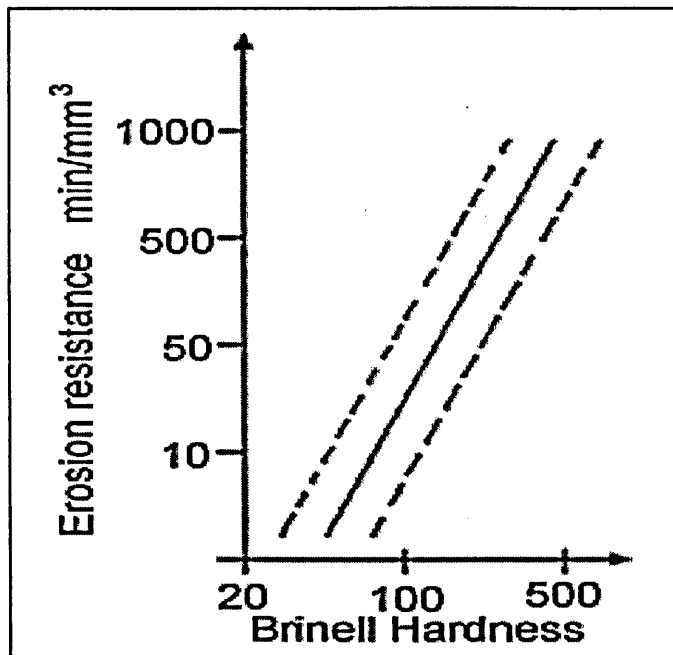
The cavitation erosion process has a four stage life cycle Lush (1987) see Figure 1.2-5.

1. *Incubation* - No material loss but damage is caused ,pitting in ductile area cracking in brittle areas, and the general fatiguing of the materials surface .
2. *Acceleration* - Material loss in small areas at first but will extend to the whole cavitation zone.
3. *Steady state* - Material is lost from the whole cavitation zone.
4. *Deceleration* - The rate of erosion declines as the loss of material changes the local flow conditions.



**Figure 1.2-5 Erosion life cycle**

The erosion of materials by cavitation can have damaging or even catastrophic effects. Some of the main problems of erosion occur in hydraulic equipment such as pumps, propellers, turbines and valves or even dam spillways. To avoid cavitation erosion, either the equipment should be designed so that cavitation is avoided, or a material with a high resistance to cavitation used. A good indicator of a material's resistance to cavitation is its hardness. The harder the material the more resistant to erosion it is likely to be, See Figure 1.2-6.



**Figure 1.2-6 Resistance of materials to cavitation erosion.**  
(Source: Knapp et al, 1970)

### 1.2.3 Cavitation Noise.

The most characteristic sign of cavitation is the noise it creates, which is caused by the collapsing bubbles. The noise covers a wide frequency band up to about 1MHz. The higher frequency noise is produced by small bubbles collapsing, low frequency noise, as well as vibration, is emitted by large bubbles collapsing. Noise has been used as a means of detecting and assessing cavitation inception and desinent and appears to be less subjective than visual quantification means.

## 1.3 Cavitation in Hydraulic Machines - Centrifugal Pumps.

### 1.3.1 Definitions of centrifugal pump terms.

Before looking into the effect of cavitation in centrifugal pumps, it is necessary to define some terms used when discussing cavitation in centrifugal pumps.

#### 1.3.1.1 *NPSH, NPIH or NPSE*

The terms refer to Net Positive Suction Head ( $m$ ), Net Positive Inlet Head ( $m$ ) or Net Positive Suction Energy ( $J/Kg$ ). For the purpose of this thesis NPSH will be used as it is the most widely use in the pumping industry. There are two forms of *NPSH* : there is net positive suction head available  $NPSH_A$ , this is the actual head available to accelerate the liquid into the inlet of the pump where;

$$NPSH_A = H_{atm} + H_{in} - H_v \quad \text{..Equ 1.3-1}$$

where  $H_{in}$  is the inlet total head

$$H_{in} = z_{in} + \frac{p_{in}}{\rho g} + \frac{U_{in}^2}{2g}$$

The dynamic term of the inlet total head is sometimes neglected as it can be of negligible magnitude. The net positive suction head required  $NPSH_R$ . Is the minimum *NPSH* to stop cavitation occurring, so as long as ;

$$NPSH_R < NPSH_A$$

cavitation is unlikely to occur See Figure 1.3-1

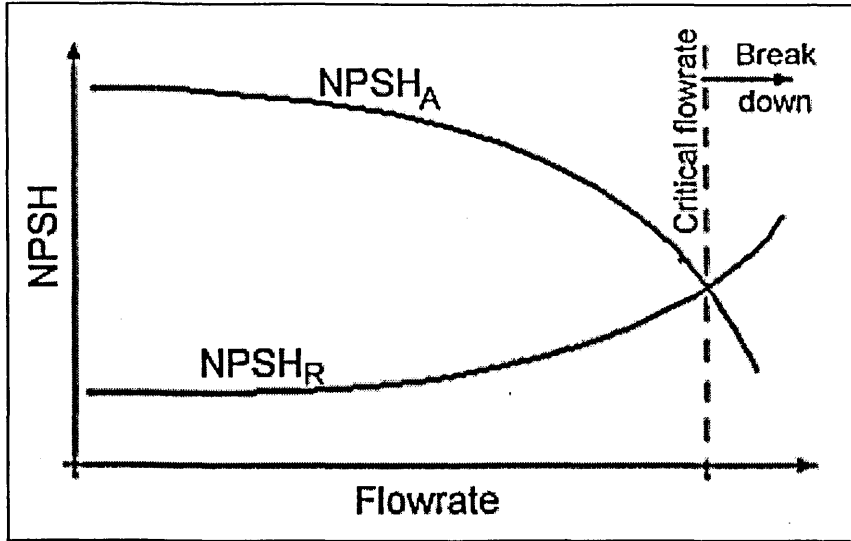


Figure 1.3-1 NPSH Available and Required Curves.

1.3.1.2 *Specific Speed.*

The specific speed of a pump ;  $K_S$  , is an indication of a centrifugal pumps design type. Low specific speeds (e.g.  $0 < K_S < 0.5$ ) indicate a radial type of pump. High specific speeds indicate an axial flow types (e.g.  $K_S > 4$ ) and in-between are the mixed flow types of pump, Refer to Fig 1.3-2. Specific speed is defined as;

$$K_S = \frac{\omega \sqrt{Q}}{(gH)^{3/4}} \quad \text{..Equ 1.3-2}$$

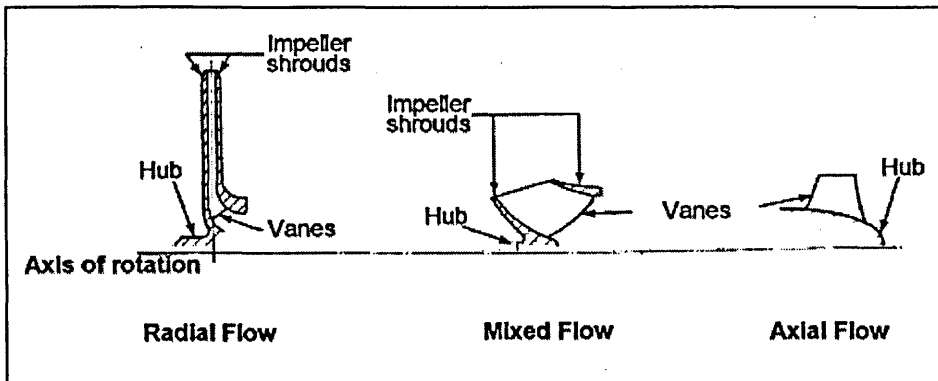


Figure 1.3-2 Pump impeller types

### 1.3.1.3 Suction Type Number / Suction Specific Speed

The suction type number of a pump  $K_{SS}$  gives an indication of the suction performance of the pump the higher the value the more likely it is to cavitate, and it is defined as;

$$K_{SS} = \frac{\omega \sqrt{Q}}{(g \text{ NPSH})^{3/4}} \quad \text{..Equ 1.3-3}$$

### 1.3.1.4 Thoma cavitation coefficient.

The Thoma cavitation coefficient which gives an indication of the likelihood of cavitation occurring. It is defined as;

$$\sigma_{TH} = \frac{NPSH_R}{(\text{Pump total head})} \quad \text{..Equ 1.3-4}$$

## 1.3.2 The effect of cavitation on centrifugal pumps.

There are several effects of cavitation on centrifugal pumps which are performance drop, erosion, noise, vibration and flow instabilities. Performance drop, is caused by cavities or bubbles blocking/choking up the impeller eye and vanes, thus restricting the flow through the pump. The loss in performance manifests itself in loss of head and reduction in flowrate. The method for determining the cavitation performance of a pump is a NPSH test. The pump is maintained at a constant flowrate and the inlet pressure is gradually reduced by means of a vacuum pump or throttling a valve on the suction line. Eventually the net head developed by the pump will start to drop, as the cavitation starts to block the impeller eye and vanes. This is usually performed at several flow rates including the Best Efficiency Point ; BEP. The *NPSH* at which the performance starts to be affected is known as the critical *NPSH* ( $NPSH_{CRT}$ ). The drop in performance is usually measured by a 3% fall from the non cavitating characteristic (See Figure 1.3-3). This does not signify incipient cavitation as it starts well before performance is affected. The rate at which performance is effected depends upon the pump type , higher specific speed pumps, e.g. axial flow, tend to have a more gradual fall in performance. This is because it is easier to block up the narrower blade passages in an impeller of a low



specific speed pump also the type of blade is more sensitive to attached bubbles thus causing earlier measurable effects.

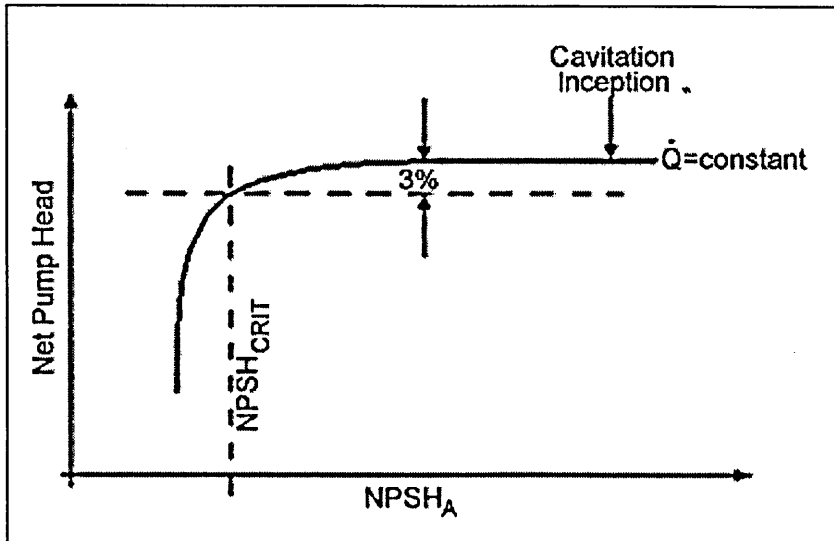


Figure 1.3-3 Cavitation characteristic of a pump.

Most pumps are designed to operate in the area just to the right of the point of 'performance breakdown' as to totally avoid the cavitation zone would mean the use of a much larger and therefore more expensive pump. For commercial reasons this is rarely done. Therefore most pumps can and do operate with some degree of cavitation, which creates the risk of erosion. Erosion encountered by centrifugal pumps and it can cause catastrophic failure, the modes of erosion have been covered earlier in this chapter. Noise and vibration is caused by the cavitation bubbles collapsing, the noise is more of a health and safety issue but the vibrations caused by the cavitation can cause mechanical damage to the pump.

These problems caused by cavitation are issues that the pump designer has to accommodate and in Chapter 3 the some pump design procedures show the effect of cavitation on the design and selection procedures of a centrifugal pump.

### 1.3.3 Pumping various liquids.

In general, the  $NPSH_R$  to pump cold water for a given application is known as there is a vast amount of test data available. Centrifugal pumps can subsequently be designed relatively accurately for a cold clean water application. Problems can arise when trying to pump other liquids, such as cryogenic liquids, petroleum products, even hot or de-aerated water. It has been known for a long time that the  $NPSH_R$  to pump liquids other than cold water is different from the  $NPSH_R$  for cold water, for the same application. Diagram Figure 1.3-4 is a schematic of an NPSH test, it shows for the same head drop, points A and B, water has a higher  $NPSH_R$  than the other liquid.

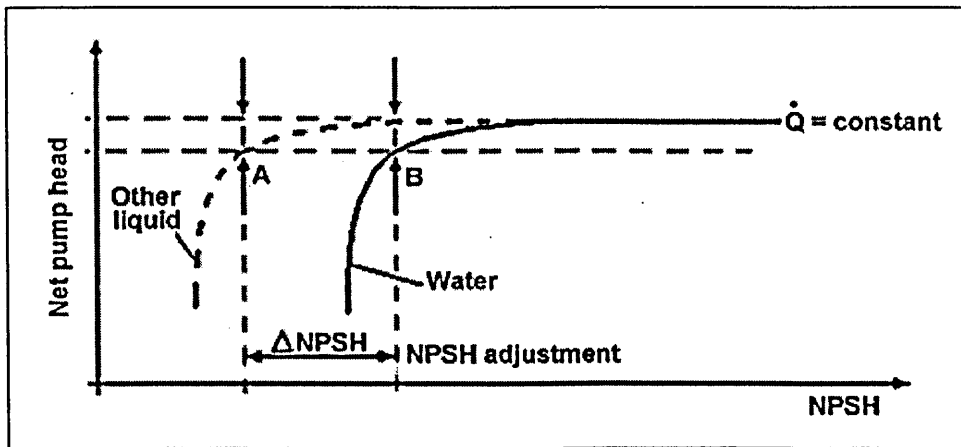


Figure 1.3-4 NPSH test on two different liquids

The difference between these  $NPSH_{crit}$  values is the net positive suction head adjustment  $\Delta NPSH$ . As most performance tests are carried out using cold water this adjustment factor must be taken into consideration, if another fluid is going to be used in the pump. The magnitude of  $\Delta NPSH$  and whether it is negative or positive is dependent on the fluid used. This 'thermodynamic effect' of the fluid can cause a pumps to be over or under designed, if an adjustment factor is not used or if the adjustment is not accurate enough. An over designed pump will perform its duty, but less effectively, it is also more expensive to build, and less competitive in the marketplace. An under designed pump will not meet the required duty. Information to

aid a pump designer in calculating the actual  $NPSH_R$  for any liquid is therefore extremely useful.

There have been many attempts to find a generic adjustment factor, both theoretically and experimentally. These factors and the knowledge to date about cavitation in liquids other than cold clean water will be discussed in greater detail in Chapter 2.

#### **1.4 Conclusion.**

Cavitation, at a first glance would seem to be a simple physical phenomenon. However as a subject it has been widely studied over the years and yet still there is disagreement regarding some of the fundamental mechanisms at work. A total solution to the thermodynamic effect of cavitation has eluded many researchers over the years, one solution working for some fluids but not for others. As a research project this work can at least hope to fill in part of the picture, in the area of cavitation in hydrocarbon fluids.

## **2. Literature review**

### **2.1 Introduction.**

Cavitation is an enormous field to encompass in one literature review therefore this review will focus on the main areas of interest to this research project. First experimental and theoretical works on *the thermodynamic effect* on cavitation will be examined. There has been a large volume of work conducted in this area, so an overview of the main works will be given.. The second area is the *gas/air content* effect on cavitation. It was thought to be important as hydrocarbons at STP contain large amounts of dissolved air in solution, as compared to water. As water has demonstrated gas / air content effects on cavitation, it was thought the much larger air content of the hydrocarbons will possibly produce a much larger effect. The final section of this review is not connected with cavitation as such, it is a review of the literature available on the properties of hydrocarbon fuels used in this research.

A subject area that was also examined, *cavitation bubble dynamics*, can be found in Appendix H. The subject was examined to provide some theoretical back up to the experimental work, but due to the large volume of experimental work that was undertaken this avenue was not pursued any further Appendix H attempts to give an introduction to this area, to give an appreciation of the factors effecting the development of cavitation bubbles

### **2.2 The Thermodynamic Effect.**

There have been many attempts to develop a generic theory for cavitation in various fluids and experimental studies performed on a wide variety of fluids at varying pressures and temperatures. This section gives a chronological account of the main theories and experimental studies.

The first works undertaken to try and ascertain the cavitation characteristics of various liquids were by Stahl and Stepanoff (1956) and Stepanoff (1957) who used an NPSH adjustment method. The method involves finding an adjustment factor for cavitation parameters such as  $\sigma$  or  $\sigma_{TH}$ , see Figure 1.3-4, so as to produce the same cavitation characteristics and the same effects for the same flow rate and pump speed. Stepanoff's adjustment method is known as the 'Thermal Cavitation Criterion' or 'B' factor, and is defined as Equation 2.2-1;

$$B = \frac{v_v \Delta h_f}{v_L L} = \frac{\bar{V}_v}{\bar{V}_L} \quad \text{..Equ 2.2-1}$$

Where  $B$  is the ratio of the vapour to liquid volume, not of the whole flow, as there is no equilibrium condition, it is merely an index of the fluids readiness to cavitate. Equations 2.2-3 can be arrived at by algebraic manipulation of Equ 2.2-1 and substituting the Clapeyron-Clausius Equation 2.2-2. Where  $\Delta h_f = \Delta T C_{p,L}$ ;  $\Delta T$  being the temperature increase corresponding to the enthalpy change;  $\Delta h_f$  between two points with pressure  $\Delta NPSH$  apart and  $\Delta P = \Delta NPSH / v_L$

$$J' \frac{h_{fg}}{v_v - v_L} = T \frac{\Delta P}{\Delta T} \quad \text{..Equ 2.2-2}$$

$$B = \Delta NPSH \frac{C_{p,L} T}{J'} \left( \frac{v_v}{v_L h_{fg}} \right)^2 \quad \text{..Equ 2.2-3}$$

The change  $\Delta NPSH$  is the difference in  $NPSH$  below that of the incipient cavitation point that causes a measurable cavitation effect i.e. a 3% head drop in performance.

Jacobs, et al (1959) and Jacobs (1961), attempt at an NPSH adjustment factor was more rigorous. It was a derivation of the thermodynamic properties and viscous friction effects, backed up with data on pumping liquefied gases. The theory consisted of, expressing the ratio of vapour to liquid-vapour volumes generated by a pressure drop as

a function of the fluid properties. Then assuming this volume ratio  $V_R'$  is constant for a pump, the ratio for different  $V_R'$  's for two different working fluids should be unity. As an outcome a 'Cavitation Tendency Quotient' was developed, which is expressed as;

$$\frac{T_A}{T_B} = \frac{(NPSH_m - NPSH_c)_A}{(NPSH_m - NPSH_c)_B} = \frac{f\left(\frac{v_g}{v_f}; h_{fg}; \frac{\partial h_f}{\partial p}\right)_A}{f\left(\frac{v_g}{v_f}; h_{fg}; \frac{\partial h_f}{\partial p}\right)_B} \quad \text{..Equ 2.2-4}$$

and  $V_R'$  can be expressed as

$$V_R' = \frac{\left(\frac{\Delta NPSH(\Delta h_f / \Delta p)}{h_{fg}}\right)^{v_g}}{v_f + \left(\frac{\Delta NPSH(\Delta h_f / \Delta p)}{h_{fg}}\right)^{v_g}} \quad \text{..Equ 2.2-5}$$

Salemman (1959) carried out an experimental investigation into the NPSH requirements of various liquids including Water, Butane, Benzene, Gasoline, Kerosine (degasified) and Freon-11. His results provided NPSH<sub>adj</sub> for these fluids at various temperatures although the Kerosine and Gasoline tests were only conducted at 21°C. He showed that the pumps performed with a reduced NPSH on other liquids compared to that on cold water, however he had difficulty proving either of the theories to any great extent. It is thought that this was due to experimental difficulties, such as trying to measure the vapour pressure accurately and some of the assumptions made in Stepanoffs; B theory and Jacobs  $V_R'$  theory. Surface tension effects are neglected, which can actually have a reducing effect on the vapour pressure at low temperatures. Also thermodynamic equilibrium was assumed for the  $V_R'$  theory i.e. all heat liberated by the pressure drop is converted into the latent heat of the vapour. This is not the case as some heat is converted into accelerating the fluid and super heated water may also exist for a short time. Also different modes of cavitation seemed to be apparent, dependent on temperature, pressure and fluid condition, i.e. gas/ air content.

Methods that try to correct the cavitation number such as the  $B$  thermal cavitation criterion can only represent an averaging of the cavitation conditions. Sarósy and Acosta (1961) showed that the same  $B$  value does not necessarily mean that the same cavitation conditions prevail. They experimented with water and freon-113 cavitating on a bluff body, and noted that the cavitation in the two liquids was distinctly different for the same  $B$  factor. The water cavities were clear and distinct, where as the freon-113 was an indistinct frothy cavity. This suggested that one of Stepanoff's basic assumptions was incorrect.

During the 1960's NASA conducted a vast amount of research on cavitation. Ruggeri and Gelder (1963) worked on cavitation in venturi flows with different purities of water, they showed that a comparison between de-mineralised, de-stilled and tap water indicated a negligible effect, at a given air content and over a temperature range of 19°C - 44°C. However air content did give a significant effect, the smaller the air content the better the cavitation performance of the venturi. Ruggeri and Gelder (1964) extended their work on cavitation in a venturi to include liquid nitrogen. In comparison with water it sustained nearly twice the effective tension of that of water ( $h_{\min} - h_v$ ), where.

$$h_{\min} - h_v = \frac{V_0^2}{2g} (K_i + C_{P,\min}) \quad \text{..Equ 2.2-6}$$

Ruggeri, Moore and Gelder (1965 March) then conducted tests with Ethylene Glycol in a venturi, they found that the incipient cavitation parameter was less than that of water but increased with temperature, where as water stayed constant until 27°C then decreased with increasing temperature. The next fluid to be examined in a cavitating venturi was Freon-114 as detailed in the three reports by Gelder , Moore and Ruggeri (1965), Gelder, Ruggeri and Moore (1966) and Moore and Ruggeri (1968). They found that for geometrically similar developed cavitation, a close to single cavitation parameter was obtained for freon-114, nitrogen and water, using the minimum cavity pressure as a reference. A method for estimating the minimum cavity pressure for developed cavitation in a venturi for a liquid is postulated, based on a known value for one test fluid. It was also found that the thermodynamic effect was proportional to the

wall pressure distribution, the greater the distribution the greater the effect. This would mean that as a pump speed or flow rate varies so would the pressure distribution between the blades and therefore the thermodynamic effect would alter. This would also indicate why the affinity law  $NPSH_R \propto N^2$  is not true. It was also found that Freon-114 indicated a decrease in the incipient cavitation parameter as temperature increased over a range of -18°C to 34°C, whereas there was no change for water over the range of 3°C to 50°C

This work at NASA conducted on Water, Freon-114, Liquid Nitrogen, and Ethylene Glycol culminated in two theories Moore and Ruggeri (1968) and Ruggeri and Moore (1969). The first a method for predicting a vapour to liquid-volume ratio, was arrived at by theoretical analysis coupled with experimental results.

$$\left(\frac{v_g}{v_f}\right)_{PRED} = \left(\frac{v_g}{v_f}\right)_{REF} \left(\frac{\alpha_{REF}}{\alpha}\right)^r \left(\frac{V_1}{V_{1,REF}}\right)^s \left(\frac{D}{D_{REF}}\right)^{1-s} \left[\frac{\left(\frac{\Delta X}{D}\right)}{\left(\frac{\Delta X}{D}\right)_{REF}}\right]^t \quad \text{..Equ 2.2-7}$$

The exponents  $r, s$  and  $t$  are determined experimentally as they depend on the heat transfer processes at work. The second was a method for predicting cavitation performance in pumps for various liquids, temperatures and rotative speeds. Equation 2.2-7 can be applied to a pump to give Equ 2.2-8 and therefore a corresponding  $\Delta H_v$  can be found from Equ 2.2-9.

$$\left(\frac{v_g}{v_f}\right)_{PRED} = \left(\frac{v_g}{v_f}\right)_{REF} \left(\frac{\alpha_{REF}}{\alpha}\right)^r \left(\frac{N}{N_{REF}}\right)^s \quad \text{..Equ 2.2-8}$$

$$\Delta H_v = J \left(\frac{\rho_g}{\rho_f}\right)^2 \left(\frac{L^2}{C_L T}\right) \left(\frac{v_g}{v_f}\right) \left(\frac{g_c}{g}\right) \quad \text{..Equ 2.2-9}$$

This can then be used to predict the change in NPSH from Equ 2.2-10

$$\frac{NPSH_{REF} + (\Delta H_v)_{REF}}{NPSH + (\Delta H_v)} = \left(\frac{N_{REF}}{N}\right)^2 \quad \text{..Equ 2.2-10}$$



The agreement between experimental and predicted values is very good, however the main draw back is that you need reference or empirical data for the theory to work.

Stepanoff (1964) in a supplement to his earlier work was able to reduce his equation 2.2-3 for  $B$  to the empirical relationship equation 2.2-11, by using experimental data on water, butane and freon-11

$$\Delta NPSH = \frac{64 \rho}{\rho_v (B')^2} \quad \text{..Equ 2.2-11}$$

Where

$$B' = \frac{B}{\Delta NPSH} = \frac{C_{P,L} T}{J'} \left( \frac{v_v}{v_L h_{fg}} \right)^2$$

he also stated some of the problems encountered in determining an accurate NPSH adjustment factor, these being:

1. The difficulty of measuring NPSH under high pressure.
2. No generally accepted or accurate means of detecting the measurable effect of cavitation.
3. The lack of good information on the thermal properties of many liquids.
4. Manufacturers usually only test pumps on cold clean water.

Spraker (1965) built on Jacobs theory by relating it to the thermal cavitation parameter  $B$  of two different fluids, denoted by subscripts 1 and 2, in equation 2.2-12.

$$\Delta NPSH = \frac{1}{\left( \frac{1}{R_2} - 1 \right)} \left( \frac{1}{B_2} - \frac{1}{B_1} \right) \quad \text{..Equ 2.2-12}$$

Where R is the volume percentage of fluid evaporated:  $R = \frac{V_v}{V_v + V_L}$

He compared this with experimental data on six pumps and fluids including water, butane, freon- 11, methyl alcohol, gasoline, fuel oil and crude oil. The data included Stepanoff's and Salemann's data as well as his own. With some basic assumptions he reduced equation 2.2-12 to equation 2.2-13, which appeared to fit the data with reasonable accuracy for the pure fluids. However with petroleum-based hydrocarbons there seemed to be an additional NPSH depression over that of the pure fluids having the same thermal cavitation parameter. The additional depression was temperature dependent, but it was not possible to find the physical property/ies responsible. He also concluded that the NPSH adjustment was only due to the fluid's properties and therefore was independent of the pump.

$$\Delta NPSH = f\left(\frac{1}{B}\right) \text{ ..Equ 2.2-13}$$

Barenboim (1966) used a technique where he related most of the common dimensionless terms that could possibly be related to the cavitation process. He then reduced this by removing the terms which have a small degree of influence. Then after experimental comparison with Salemann's data he concludes that:

$$Eu_u = f(Re_u, K)$$

$$Eu_u = \frac{gNPSH_{crit}}{u^2} \quad \text{and} \quad K = \frac{(L\rho_g)^2}{C_p T_g (\rho_l - \rho_g) p_v}$$

$$Eu_u = -1.928 \times 10^{-5} (K \cdot Re_u)^2 - 7.434 \times 10^{-10} (K \cdot Re_u) + 2.076 \times 10^{-2} \quad \text{..Equ 2.2-14}$$

Equation 2.2-14 was determined empirically and seemed to give a fairly satisfactory correlation to all of Salemann's data, the maximum deviation being 9%.

Ward and Sutton (1967) formulated a similar expression to Salemann's after correlating the available tests data at the time, they showed that equation 2.2-15 will give a good approximate value for  $\Delta NPSH$ .

$$\Delta NPSH = \frac{r_v}{B'} \quad \text{..Equ 2.2-15}$$

They also stated that the quantity of published data of pumps running on fluids other than water, was not good enough to make a reliable empirical correlation of cavitation performance. Even so, they found that using  $r_v \approx 0.8$  in equation 2.2-15 was as good as any other thermal cavitation criteria for most estimation purposes with a conventional pump.

Chivers (1970) postulated a theory based on Rayleigh's (1917) (see section 2.3 on bubble dynamics) bubble growth theories and pump characteristics. Chivers tried to predict the  $NPSH$  changes in water with temperature. This was excellent at predicting the point of performance breakdown, however correlation was not so good at inception, Equation 2.2-16. This was thought probably due to the lack of knowledge about bubble nucleation as the theory does not model this initial nucleation process very well. The bubble growth theory used is also most likely to occur at the BEP as other flow rates produce quasi-steady cavities which can alter the inlet conditions. The theory also relies on one test point being available. Chivers went on to try and predict the cavitation performance in other liquids using his theory. It showed agreement with his own and Salemann's experimental data, the degree of correlation increasing as the degree of cavitation increased. The theory however appeared to fail on Spraker's data until an empirical correction was made to the Reynolds number term. He also noted that Barenboim's theory, although giving a good correlation to Salemann's data, had to be empirically altered to match Spraker's data. It however only detracted slightly from the Salemann correlation. Chivers came to the conclusion that any theory trying to predict a small percentage head loss would have to be an extremely complex function, if it is to

be a comprehensive solution. A simpler solution however should be able to predict the more advanced stages of cavitation

$$NPIH = F \left\{ Kr \cdot (\text{Pr} \cdot \text{Re})^{1/2} r_f^{4/3} \frac{P_s}{P_{at}} \right\} \quad \text{..Equ 2.2-16}$$

where

$$Kr = \frac{Jh_{fg}^2 v_f}{v_g^2 C_p T P_s} \quad \text{..Equ 2.2-17}$$

Furness (1973) and (1974) performed various cavitation experiments with two-dimensional convergent-divergent nozzle, for water 41 to 110°C and Freon -15°C to 30°C. He found that the Stepanoff 'B' factor correlated well with the experimental data. The theory postulated by Chivers correlated more satisfactorily especially when a negative exponent of the Reynolds number; Re was used (i.e.  $\text{Re}^{-0.4}$ ). This is due to a nozzle operating inversely to a pump. In a nozzle, for a constant flow rate, a decrease in Re results in an increase in the pressure drop across it. The best results being achieved with the 3% head drop data.

Hutton and Furness (1974) using the data from the above experiments found that there was an apparent absence of any thermodynamic scale effect if the correct cavity vapour pressure (Measured value) is used in the calculation of  $\sigma_{TH}$  or  $NPSH$ . This has applications to passive flow devices such as nozzles and venturies but it might not be applicable to flows within hydraulic machinery e.g. pumps. Hutton and Furness concluded that more tests should be carried out to see if their findings would work for centrifugal pumps. If the findings were applicable to centrifugal pumps then a reliable method for accurately predicting the cavity vapour pressure needs to be found. The cavity vapour pressure which differs to the bulk fluid pressure, is thought to be due to local evaporative cooling of the liquid surrounding the cavity which provides the latent heat of vaporisation.

Holl, Billet and Weir (1975) worked on a different type of theory. It was still semi-empirical but it was based on dimensionless number groups, and experimental work on ogives. This '*entrainment theory*' expresses the temperature depression  $\Delta T$  between the bulk fluid temperature and the cavity temperature as a function of a set of dimensionless numbers. These numbers being Froude;  $Fr$ , Nusselt;  $Nu$ , Péclet;  $Pe$ , Reynolds;  $Re$ , Weber;  $We$  and Cavity length ( $Lc/D$ ). The cavity temperature depression  $\Delta T$  is used to give an indication of the stage of cavitation. The basic equations for this theory are;

$$\Delta T = \frac{C_Q}{C_A} \cdot \frac{Pe}{Nu} \cdot \frac{\rho_v}{\rho_L} \cdot \frac{\lambda}{C_P}$$

$$C_A = C_1 \{Lc/D\}^a$$

$$C_Q = C_2 Re^b Fr^c We^d \{Lc/D\}^e$$

$$Nu = C_3 Re^f Fr^g We^h Pr^i \{Lc/D\}^j$$

These four equations can be combined to create the general empirical formula Equ 2.2-18 the values of  $C_n$  and exponents  $a$  to  $p$  are experimentally determined;

$$\Delta T = C_4 \{Lc/D\}^k Re^l Fr^m We^n Pr^p Pe \frac{\rho_v}{\rho_L} \frac{\lambda}{C_P} \quad \text{..Equ 2.2-18}$$

Billet, Holl and Weir (1981) continued to check this '*entrainment theory*' on bluff bodies and venturis. It was found that there was a correlation between  $\Delta T$  and different degrees of cavitation on the bluff bodies and in the venturis. Their conclusion was that this theory was a reasonable alternative to the thermal /  $B$  factor type of theory. This theory however is still reliant on experimental data, as do most of the theories stated previously. These theories also tend to be only applicable to the fully developed stages of cavitation.

Kamiyama and Yamasaki (1981) investigated a theory based on an analogy of choked two-phase bubble flow. The fluid is considered to be a mixture of liquid vapour and

foreign gas, the bubbles all being of the same radius  $R$  and they showed that the sonic velocity in this mixture is;

$$C^2 = \left( \frac{d\rho_l}{dp_l} \right)^{-1} \cong \frac{g}{B(1-\alpha_v^*)^2} + \frac{(p_g + K)^2}{\rho K} \left( 1 - \frac{2\gamma}{3Rp_g} \right) \quad \text{..Equ 2.2-19}$$

$$= C_g^2 \left[ 1 + \frac{g(\beta^*)^2}{KBv_l} \left( 1 - \frac{2\gamma}{3Rp_g} \right)^{-1} \right]$$

Where:  $K = \beta^*_{ref} p_{g,ref}$  ..Equ 2.2-20

and:  $C_g^2 \cong \frac{(p_g + K)^2}{\rho_l K} \left( 1 - \frac{2\gamma}{3Rp_g} \right)$  ..Equ 2.2-21

If the point at which the throat velocity reaches the sonic velocity ( $u = C$ ) in Equ 1.2-3 is the point of cavitation inception, under a pressure  $p_l$  and void fraction  $\alpha_v^*$ , the cavitation number  $\sigma$  at critical conditions;  $\sigma^*$  using equation 2.2-19 becomes.

$$\sigma^* = 2\alpha_v^*(1-\alpha_v^*) \frac{1}{C^2} \left\{ \frac{2\alpha_v^*g}{B(1-\alpha_v^*)} + \frac{2(p_s - p_v) + (8\gamma/3R)}{\rho_l} \right\} \quad \text{..Equ 2.2-22}$$

This theory stood up reasonably well when compared to some experimental data on hot water and liquid hydrogen. The method is however restricted to cases where gas bubbles are entrained in the bulk fluid, and these nuclei play a large part in the gaseous cavitation. Its general use would also be difficult as parameters such as *mean void fractions* have to be measured, and the *nuclei distributions* known. It also does not include any effect of gas / air solubility, therefore it might not be useful for liquids such as hydrocarbons which have large air contents in solution

Thew and Hadji-Sheike (1979) and Chalaby and Thew (1982) and (1983) performed a large number of tests on water and ethylene glycol mixtures. This has particular relevance to the centrifugal pumps that act as car cooling pumps, which pump a mixture of water and anti-freeze. The following points were concluded from their investigations using venturis and small centrifugal pumps;

1. The cavitation number for ethylene glycol - water mixtures (45/55 EG/H<sub>2</sub>O) is considerably higher than that for water, at inception. It was also found that this difference decreases with pump speed, 36% at 3000 *rpm* and 18% at 4000 *rpm*. In both cases  $\sigma_i$  increases with rotational speed.
2. Increasing the concentrations of ethylene glycol reduces the thermodynamic effect until at 50% it is negligible,  $\sigma_{\text{CRIT}}$  was approximately the same for 95°C as it was for 25°C. Also pure ethylene glycol exhibits a reverse thermodynamic effect.
3. The air content had a significant effect at inception for all concentrations of water / ethylene glycol mixtures from 0-50%

This work was purely experimental and no theories were postulated to explain their conclusions, although several comments were made on existing theories, and why they were not applicable to binary mixtures.

Kamiyama and Yamasaki (1986) tested a theory based on their earlier work (1981), by using an orifice plate in a test rig and various organic fluids such as benzene, gasoline, kerosine and also Freon-12 which shows a large thermodynamic effect. The authors found good correlation for benzene and gasoline, but the experimental data for kerosene was slightly higher than the predicted values. The predicted values for Freon-12 showed a thermodynamic effect, but due to experimental problems the freon data was too unreliable to give a fully qualitative comparison. As this theory is based on flow through an orifice plate, its relevance to centrifugal pumps is limited, however it did achieved good correlation with experimental data.

### **2.2.1 Concluding comments.**

It can be seen from this review that there are large gaps in the research of the *thermodynamic* effects of different fluids on cavitation. Most of the research was carried out before the 1980's. It is not known whether later research has not been published due to industrial sensitivity or whether the amount of research being conducted has declined.

There is very little good data available on the thermodynamic effect in pumps. Most of it is old and difficult to obtain the raw data collected. Also the tests that have been performed, have been conducted on a relatively small number of fluid types. Some of the theories are too complex to easily apply to centrifugal pumps, or the fluid properties used are unavailable for certain fluids. In the main the B-factor theory by Stepanoff or its modifications still seem to be the most widely used for NPSH adjustments by pump designers , and is recommended by most pump design text books. However the limited number of fluid which have been tested for thermodynamic effects make it unwise to apply the theories to all fluids. The main standard for the petroleum industry API 610 (1989) now even disallows any advantage from the thermodynamic effect for petroleum pumps. Possibly due to this limited knowledge in the area, thus making NPSH adjustments potentially hazardous. So the only way in which this field will advance is by producing much more experimental data on the effect on a much larger number of fluids so adjustments become much more reliable

### **2.3 Gas / Air content effects.**

The gas or air content of fluids plays an important part in the process of cavitation, Although there is no clear understanding of the effect of gas content, this short review aims to present the basic relationships that have been found. As the study at hand is examining hydrocarbon cavitation, and the hydrocarbons being used contain 7 to 10 times more dissolved air by volume than water, a control on the air content and its effects on cavitation was thought to be as important as the thermodynamic effect.



The effect of dissolved air on cavitation has been studied by many researchers. Crump (1949) & (1951), Williams and McNulty (1956) and Ziegler (1955) were among the first. Their experiments were performed using venturians nozzles and water. Although they did not match quantitatively the general trend was the same. That was as the air content fell the fluid could sustain lower pressures before inception. Also using a venturi Hammitt et al (1967) found that  $\sigma_i$  varies linearly with gas content. This was backed up by Holl (1960) who conducted his work on hydrofoils. Holl also found  $\sigma_i$  varied inversely with the square of the velocity. Although gas content affects inception it has been found to have no effect on head / efficiency breakdown in hydraulic machines or venturi type nozzles, Pearsall (1972). Holl also stated that the total gas content of the fluid is made up of two parts: the dissolved gas content and the free gas content. The latter being small gas bubble nuclei (diameters of the range  $10^{-5}$  to  $10^{-3}$  cm, Hammitt (1972).) entrained within the bulk of the fluid. Gas nuclei are thought to be proportional to the dissolved oxygen content. It is very hard to obtain / measure number density values for these nuclei and very few researchers have collected data on them. This is an area where most researchers have little or no control and it probably accounts for the reason why quantitative measurements have failed to agree. A small number of experimenters have even failed to find the correlation between air content and inception such as Lehman (1964), although it is generally accepted that it is the case.

Recent works by Meyer, Billet and Holl (1989), Lui, Kuhn de Chizelle and Brennen (1993) and Brennen (1994) have conducted more work on the effect of free stream nuclei on cavitation. However no broad conclusions can be drawn in the relationship to cavitation, except that for water the nuclei, as the dissolved gas content, only affect inception and not head breakdown.

Although not directly related to this research it is worth mentioning that air content also has an effect on erosion rates. At high dissolved air contents (saturation and above) the large number of bubbles produced have a 'cushioning' effect reducing damage rates, Knapp et al (1970). However at very low air contents the reduction in the number of bubbles outweighs the increase in the explosive force of collapse, and erosion rates are

reduced, Iyengar and Richardson (1957). The maximum damage is therefore incurred somewhere between 0 and 100% of air saturation.

### **2.3.1 Concluding comments**

Gas / air content is an important factor when looking at cavitation inception, however it seems to be much less important at head breakdown. The role of free stream nuclei seem to play an important role, but it is a role which has not been fully quantified. No research could be found on gas content effects on liquids other than water. As some fluids retain large amounts of dissolved air as compared to water (for example Hydrocarbons) the air content effects could be even more important, possibly even affecting head break down. More detail can be found in the references cited but the broad conclusions are as above.

## **2.4 Hydrocarbon Properties Information.**

An extensive search was carried out for the properties of the hydrocarbon fluids to be used in the cavitation research. These being Kerosine and Gas Oil. Details on chemical composition and stoichiometric properties were easily found. However the properties such as Vapour pressure, Surface Tension coefficients, Dissolved \*air contents, Density, Viscosity and how they vary with temperature are a lot harder to source. This short review gives the best references found for hydrocarbon fuels data, to aide anyone conducting similar research.

Goodger (1982, 1993 & 1994) has produced a number of very useful guides to Fuel Technology which provides good general data for properties and are excellent guides for understanding the chemistry of hydrocarbon fuels. His 'Alternative Fuel Technology Series' V1 & V2, being particularly useful

A Rolls - Royce report (1981) has been an excellent source for more detailed information providing data on a wide range of properties of aviation fuels as they vary with temperature.

A book by Spiers (1955) also provides a very useful reference for fuels property data, although possibly a bit dated

Two reports on the dissolved air content of fuels have been found one by Ross (1970) from Shell Research Ltd and Cansdale (1978) from the R A E. They provide good data on the dissolved air quantities within various fuels and methods of dissolved air measurement.

An ESSO (1981) table produced in consultation with the American Petroleum Institute (API), the American Society for Testing and Materials (ASTM) and the Institute of Petroleum, was also helpful. It could correct hydrocarbon densities for a large range of temperatures.

## **2.5 Conclusions of Literature Review.**

This review has concerned itself with only a few aspects of cavitation, relative to the study at hand. There is an enormous amount of material published and a single literature review could not do justice to this volume of material. The review aimed to outline the main theories and findings in the field of interest to this project. For further reading several good reviews are available Young (1989) and Knapp et al (1970) who deal with the subject area in much greater detail, and are good sources for references. There are no major conclusions to be made from the review except that there needs to be a great deal more basic research on the effects of various fluids and gas content on cavitation, if a solution to the problem of cavitation prediction is to be found.

### **3. Pump Design**

#### **3.1 Introduction.**

There are a very wide variety of pump types, these however can be broken down into two main categories.

1. Positive displacement pumps - which include gear pumps, peristaltic pumps, lobe pumps, vane pumps, screw pumps, piston pumps and progressive cavity pumps. These all work on the general principle of physically displacing the fluid through the machine by various means, utilising either a reciprocating or rotary action.
2. Rotodynamic pumps - which includes all those types of pumps which utilise a bladed impeller and a volute or fluid collector. There are three general types radial, mixed and axial flow, and any number of design types, for example, single stage, multi-stage, end suction, top suction, vertical in line, double discharge, and any number of variations for fluid types.

This project is only concerned with the rotodynamic type of pump and particularly the radial flow centrifugal pump. Therefore this chapter aims to give an overview of centrifugal pump theory, selection and design. The fundamentals of pump theory, pump design and pump selection were studied to give a greater understanding of centrifugal pumps. Pump design is a large subject area with many different methods of design. It is not an exact science and a lot of design ability is gained from experience. This chapter gives an insight into the design theories and shows how cavitation can affect the design of a pump. Thus showing the importance of cavitation in its role with design. For more information refer to the literature cited.

#### **3.2 Basic centrifugal pump theory.**

A centrifugal pump is a machine for imparting energy to a liquid to result in a pressure increase and flow. It achieves this by means of a bladed impeller rotating within

stationary fluid collector, the impeller creates a forced vortex which discharges the liquid at a higher energy than the liquid entering it. This liquid is discharged into the volute of fluid collector with increased pressure and velocity. The casing then converts some of the velocity head into static head by channelling the liquid into the discharge area which is a diverging channel, see figure 3.2-1.

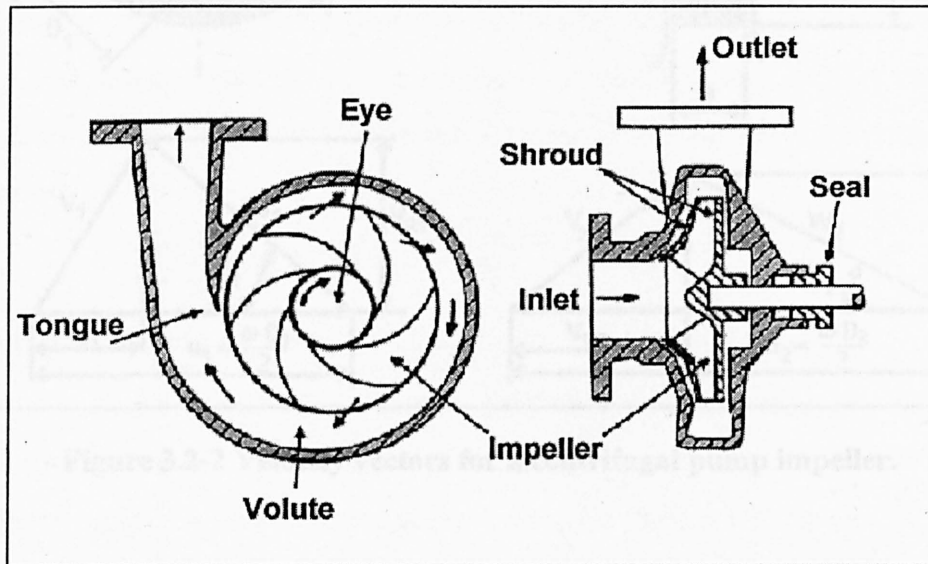


Figure 3.2-1 Radial centrifugal pump - Single stage single entry.

The work transferred to the fluid by the impeller can be estimated by the general equation to define the specific energy change and the component velocities within the pump, the Euler equation 3.2-1

$$gH_E = u_2 V_{u2} - u_1 V_{u1} \quad \text{..Equ 3.2-1}$$

Referring to velocity vector diagrams of the liquid, created by the impeller in figure 3.2-2, it can be said that;

$$gH_E = \frac{1}{2} \left[ (v_2^2 - v_1^2) + (u_2^2 - u_1^2) + (w_2^2 - w_1^2) \right]$$

The first term represents the total kinetic energy change and the last two terms represent the total static energy change.

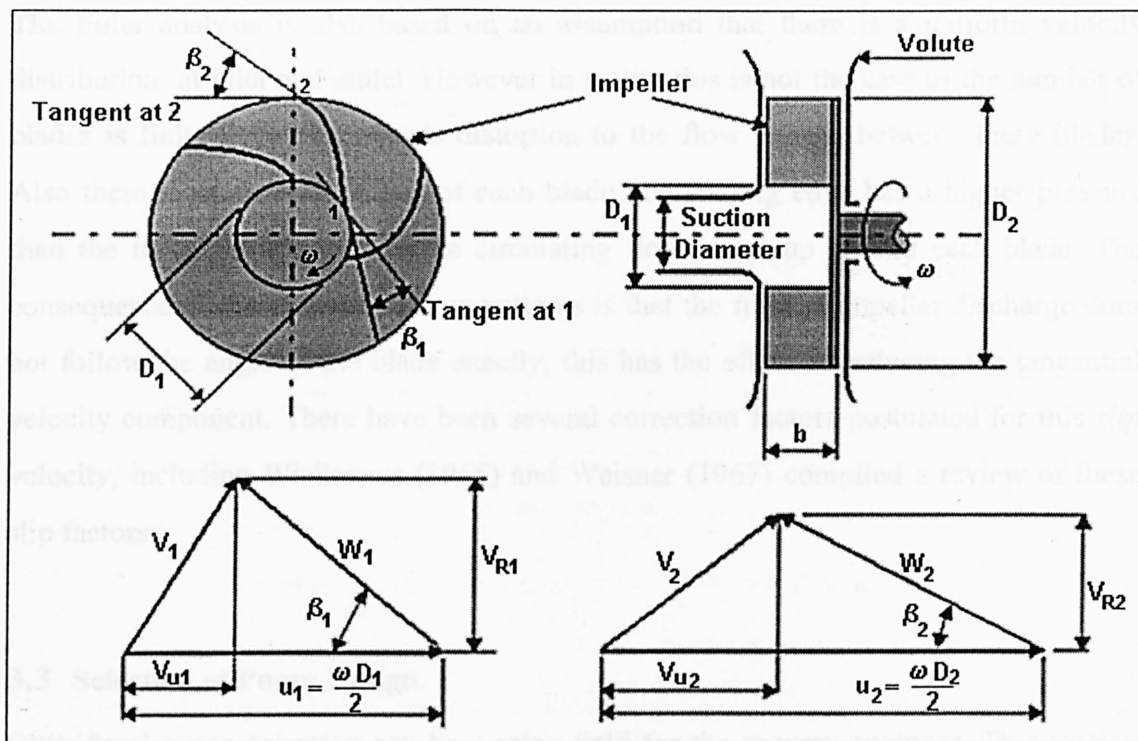


Figure 3.2-2 Velocity vectors for a centrifugal pump impeller.

for ideal behaviour of the pump, that is no inlet whirl into the impeller eye;  $V_{u2} = 0$  it can be shown that;

$$gH_E = u_2^2 - \frac{Q}{A_2} u_2 \cos(\beta_2)$$

This is obviously the ideal situation. In reality there are losses due to turbulence created as the fluid impinges on the blades, friction losses of the fluid on the pump casing, disk friction and leakage. Leakage flows are recirculation of fluid from a high pressure area to a low pressure area. For example for a shrouded impeller a proportion of the liquid flows around the top shroud through the wear ring and back to the impeller eye, see figure 3.2-3

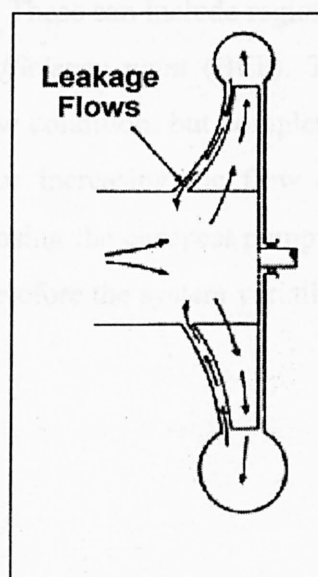


Figure 3.2-3 Leakage flow

The Euler analysis is also based on an assumption that there is a uniform velocity distribution at inlet and outlet. However in reality this is not the case as the number of blades is finite therefore there is distortion to the flow pattern between these blades. Also there is an aerofoil effect of each blade, the leading edge has a higher pressure than the trailing edge, therefore a circulating flow is set up around each blade. The consequence of these distorted flow patterns is that the fluid at impeller discharge does not follow the angle of the blade exactly, this has the effect of reducing the tangential velocity component. There have been several correction factors postulated for this *slip* velocity, including Wislicenus (1965) and Weisner (1967) compiled a review of these slip factors.

### 3.3 Selection of Pump Design.

Centrifugal pump selection can be a mine field for the unwary engineer. This section aims to give an introduction to some of the problems associated with selection, and gives an example of a simple selection procedure. For further information refer to four recent articles by Shields (1990 & 1995).

Most manufacturers of pumps provide the customer with charts to select a pump for given head and flowrate, Figure 3.3-1 shows a simple selection chart. However there can be problems if the pump is run at off design conditions. These can include region of instability on the head flow curve away from the *best efficiency point* (BEP). This means a pump may be suitable for a system under one flow condition, but completely unsuitable if the system resistance changes, decreasing or increasing the flow and putting the pump into an unstable operating region. So choosing the cheapest pump for one given head and flowrate may not be the best option. Therefore the system variations must be taken into account when making a decision.



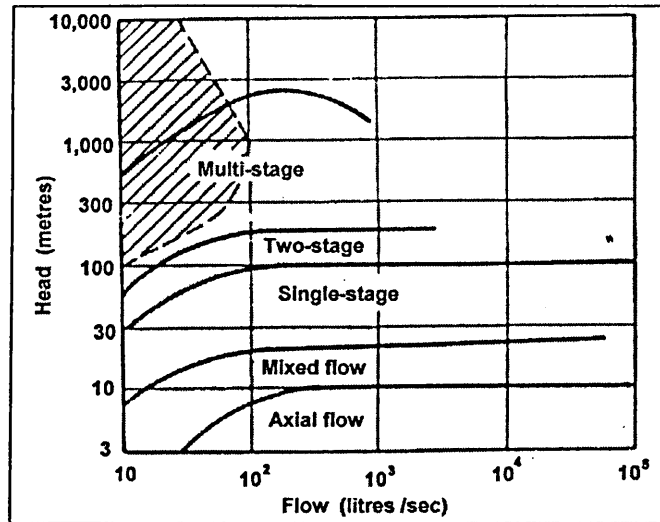


Figure 3.3-1 A simple pump selection chart.

The power characteristic of the pump driver can also have an effect on the pump selection. It can vary greatly from a rising power curve over the whole flow range, to a power curve that peaks at the BEP. The selection of the driver must be made in accordance with the highest power consumption. This can sometimes mean what you save on a cheaper pump you can lose on the need for a more expensive pump driver.

The pump data supplied by the manufacturer will almost certainly be based on tests on cold clean water. Changes in liquid density will mean a proportional change in pressure generated. For liquids less dense than water pump selection from manufacturers data is usually sufficient. For liquids more dense, pump casings, shafts, seals and bearings may not be adequate for the increase in pressure. Viscosity mainly effects the power and efficiency curves, increasing viscosity means more power consumption, resulting in lower efficiencies. There may also be a reduction in the head flow curve. Correction factors can be found in the Hydraulic Institute Standards (1983). Large viscosities will therefore result in the need for bigger drivers and the associated shafts and bearings etc. The viscous effect on the pumping system should also be examined carefully, as high losses can result in problems.

A wrongly selected pump can cause numerous problems including, noise and vibration when operating off of BEP, as well as imbalance in radial loading. The imbalance can affect performance as well as bearing, seal and shaft life. Cavitation can also arise at the higher flows as the  $NPSH_R$  increases and the  $NPSH_A$  decreases, not to mention the effects of fluid type.

### 3.3.1 Pump selection example - a simple case.

The following is a simple example to give an appreciation of the pump selection procedure. Usually the minimum data required to select a pump is, the duty flow rate ;  $\dot{Q}$  ( $m^3/s$ ), the duty head ;  $H$  ( $m$  of fluid), the fluid type and the net positive suction head available ;  $NPSH_A$  ( $m$  of fluid). It can be seen from equation 1.3-1 that the  $NPSH_A$  is a function of the pumping system and the fluid being pumped. The variables being,  $p_a$ , the pressure above the fluid being pumped,  $p_v$ , the vapour pressure of the fluid,  $h_{LOSSES}$ , are the friction losses in the pipes and fittings and  $p_s$ , is the static pressure lift, this can be positive or negative, see Figure 3.3-2.

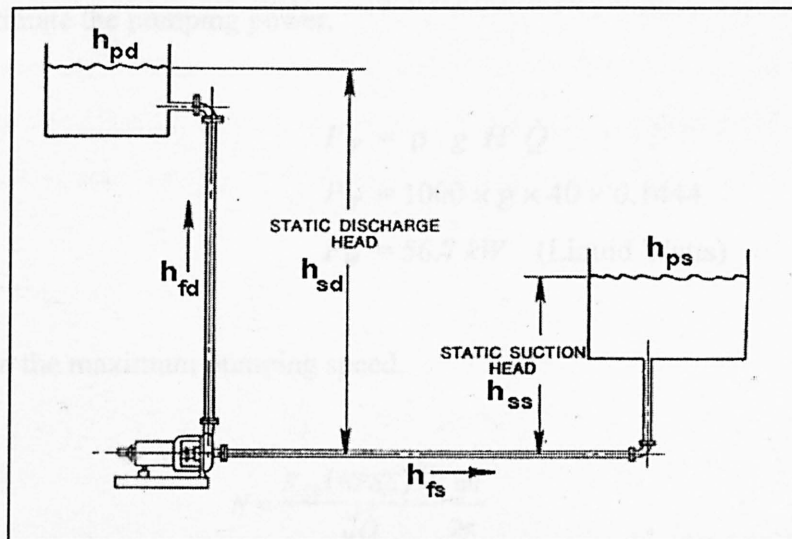


Figure 3.3-2 A pumping system.

So for this example if the following duty values are given

$$\dot{Q} = 520 \text{ m}^3/\text{hr} = 0.1444 \text{ m}^3/\text{s} \quad \text{Of cold clean water.}$$

$$H = 40\text{m}$$

$$NPSH_A = 5\text{m} \quad (NPSE_A = 49.05 \text{ J/kg})$$

1. First estimate a running speed. This should be based on the preferred driver.

- Electric motor A/C or D/C.
- Diesel engine. {As well as
- Petrol engine. {gear boxes
- Steam turbine. {as necessary
- Gas turbine.

For this example a 4-pole 50 Hz induction motor will be used as a starting point therefore

the synchronous speed  $N = 1450 \text{ rpm}$  this means the specific speed  $K_s$  is

$$K_s = \frac{2\pi N}{60} \frac{\sqrt{\dot{Q}}}{(gH)^{3/4}} = \frac{2\pi \cdot 1450}{60} \frac{\sqrt{0.1444}}{(g \times 40)^{3/4}}$$

$$K_s = 0.6545$$

2. Next estimate the pumping power.

$$P_w = \rho g H \dot{Q}$$

$$P_w = 1000 \times g \times 40 \times 0.1444$$

$$P_w = 56.7 \text{ kW} \quad (\text{Liquid Watts})$$

3. Calculate the maximum pumping speed.

$$N = \frac{K_{SS} (NPSE)^{3/4}}{\sqrt{\dot{Q}}} \frac{60}{2\pi}$$

Therefore  $K_{SS}$  needs to be found;

$$K_{SS} = \frac{2\pi N \sqrt{\dot{Q}}}{60(NPSE_A)^{3/4}}$$

$$K_{SS} = 3.113$$

For a single stage single entry centrifugal pump  $K_{SS} = 3.25$  is the optimum value Salisbury (1982). Therefore the maximum speed can be found by setting  $K_{SS}$  to this value, which will allow us to see if the correct pump speed and motor has been found.

$$N = \frac{3.25(9.81 \times 5)^{3/4}}{\sqrt{0.1444}} \frac{60}{2\pi} = 1514 \text{ rpm}$$

Therefore the synchronous speed of 1450 rpm as chosen was the closest out of all the synchronous speeds for a 50Hz induction motor to this maximum. The initial estimated value of  $N$  was the best for the type of drive chosen. Otherwise it should be calculated with a new estimate of the speed i.e. back to step 1.

4. Now using a graph such as Figure 3.3-3 based on a Worthington Pump and Machinery Company plot which can be found in most pumping text books. The data is based purely on empirical data. With the values of  $\dot{Q} = 144.4 \text{ l.s}^{-1}$  and  $K_s = 0.6545$ , an efficiency for the pump can be found. In this case from the graph it can be seen that a conservative reading of the overall pump efficiency is  $\eta_p \approx 0.85$

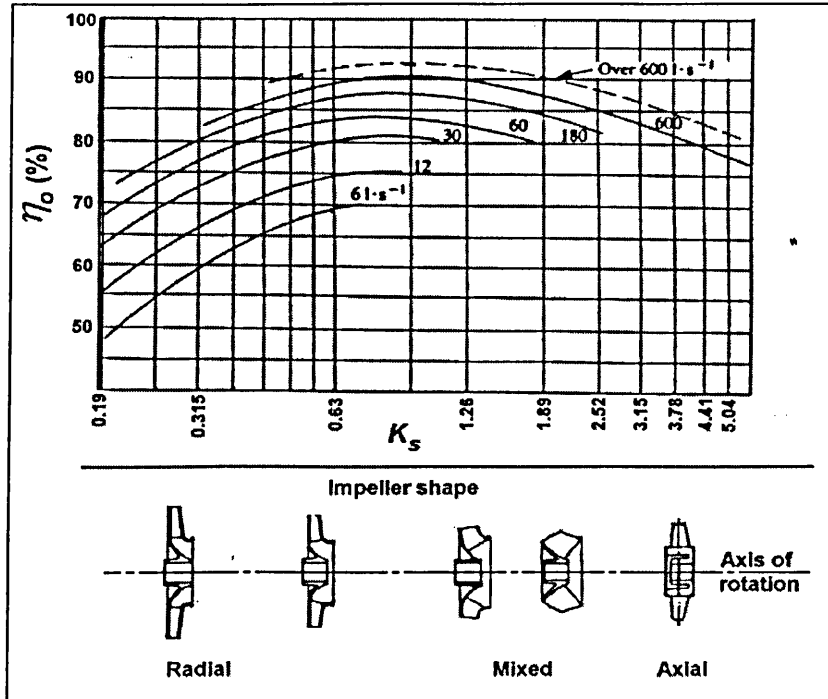


Figure 3.4-1 Efficiency v Specific speed.

5. Find the pump input power.

$$P_{IN} = \frac{\rho g H \dot{Q}}{\eta_P}$$

$$\approx 67 \text{ kW}$$

From these steps the basic specification of the pump has been determined. That is a radial single stage, single suction pump of specific speed  $K_S = 0.6545$ , synchronous motor speed  $1450 \text{ rpm}$  and shaft power  $67 \text{ kW}$  with an hydraulic or pump efficiency  $\approx 85\%$ .

### 3.4 Basic Pump Design.

There are two generally accepted methods of designing a rotodynamic pump, scaling and designing for the duty point. Scaling utilises an existing design to obtain the new design, based on various scaling laws. Designing from the duty point information, basically means designing the pump from scratch, utilising various laws and design

criteria. This section will only deal with the hydraulic aspects of pump design. Pump casings, seals, shafts and bearings will not be covered.

### 3.4.1 Scaling.

One of the easiest ways used to design a centrifugal pump is to use an existing design and scale it. Any given family of centrifugal pumps, that is pumps of similar specific speed should follow the scaling laws equation 3.4-1. These are arrived at from a black box approach to a pump, see Figure 3.4-1, where the various inputs and outputs of the pump are examined.

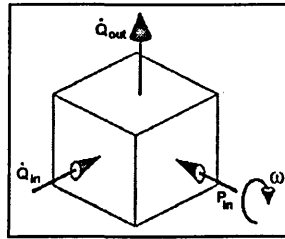


Figure 3.4-1 Black box approach to scaling

$$\frac{P}{\rho \omega^3 D^5} = f \left\{ \frac{\dot{Q}}{\omega D^3}; \frac{gH}{\omega^2 D^2}; \frac{\rho \omega D^2}{\mu} \right\} \quad \text{..Equ 3.4-1}$$

(1)                      (2)    (3)    (4)

- (1) Power Coefficient.                      }
- (2) Flow Coefficient.                      All these terms are deemed to be
- (3) Head Coefficient.                      constant.
- (4) Reynolds Number; Re.

From dimensional analysis of equation 3.4-1 the following approximate scaling laws can be arrived at, where the subscripts 1 and 2 indicate the existing pump and the pump to be scaled respectively.

$$\frac{\dot{Q}_1}{\dot{Q}_2} = \frac{N_1 D_1}{N_2 D_2} \quad ; \quad \frac{H_1}{H_2} = \frac{N_1^2 D_1^2}{N_2^2 D_2^2} \quad ; \quad \frac{P_1}{P_2} = \frac{N_1^3 D_1^3}{N_2^3 D_2^3}$$

The impeller diameter  $D$  is used as the characteristic dimension for the pump and all other dimensions are scaled on the same ratio. Scaling provides a quick method of producing a pump design, and is used widely in industry where time is an important factor. It does not however necessarily mean that it will be the best design for the duty, even if the pump it was scaled from was.

### 3.4.2 Traditional Hydraulic Design.

There are many different methods of designing a pump from scratch. The method chosen is usually made on the preference of the particular hydraulic designer. The following design method is one method of designing a basic impeller for a centrifugal pump. It can be seen from the following design steps, just to find the inlet and outlet diameters and the distance between the shrouds, pump design is a lengthy process. It also evolves a certain amount of empirical data, and experience in choosing the right method and data. This section will not investigate pump design in any great depth, for further information consult Stepanoff (1957 & 1965), Lobanoff (1985), Gongwer (1941), Anderson (1980) and Neumann (1991).

1. The impeller inlet eye diameter can be calculated from ;  $D_e = k(\dot{Q}/N)^{1/3}$  (m) where  $k \approx 4.66$ . Using the pump selection example from section 3.31

$$D_e = 4.66 \left( \frac{\dot{Q}}{N} \right)^{1/3} = 4.66 \left( \frac{0.1444}{1450} \right)^{1/3} = 0.216m$$

2. The shaft diameter can be estimated for two different shaft types;

$$\text{Overhung} \quad D_s = 118(kW/N)^{1/3} \quad (mm)$$

$$\text{Through} \quad D_s = 127(kW/N)^{1/3} \quad (mm)$$

For an overhung shaft. 
$$D_s = 118 \left( \frac{kW}{N} \right)^{1/3} = 118 \left( \frac{66.7}{1450} \right)^{1/3} = 42.3mm$$

Therefore a hub diameter of approximately 50mm, will create a blockage in the impeller eye, this needs to be taken into account.

Therefore

$$D_e = \sqrt{\left(\frac{\pi D_e^2}{4} + \frac{\pi D_s^2}{4}\right) \frac{4}{\pi}} = \sqrt{\left(\frac{\pi 0.216^2}{4} + \frac{\pi 0.05^2}{4}\right) \frac{4}{\pi}} = 0.2217m$$

3. Check this value with the Optimised Eye Theory which states in the following equation for a well designed pump  $K_1 = 1.8$  and  $K_2 = 0.23$ .

$$NPSH_R = \frac{K_1 V_{m1}^2 + K_2 U_{1E}^2}{2g}$$

$$NPSH_R = \frac{1.8 \left(\frac{\dot{Q}4}{\pi D_e^2}\right)^2 + 0.23 \left(\frac{\pi N D_e}{60}\right)^2}{2g} = \frac{1.8(43.74)^2 + 0.23(16.83)^2}{2g} = 4.6m$$

therefore as the  $NPSH_A (= 5m)$  is greater than the  $NPSH_R$  cavitation should be avoided.

4. To find the outlet diameter  $D_2$  refer to Figure 3.4-2.

with a  $K_S = 0.655$   $HC = 0.57$ , where  $HC = 2gH/(U_2^2)$

$$U_2^2 = 2g40 / 0.57 = 1376.8$$

$$U_2 = 37.1 \text{ m/s}$$

For a given speed  $N$  it can be said that  $D_2 = (60U_2)/(N\pi) = 0.489 \text{ m}$ .



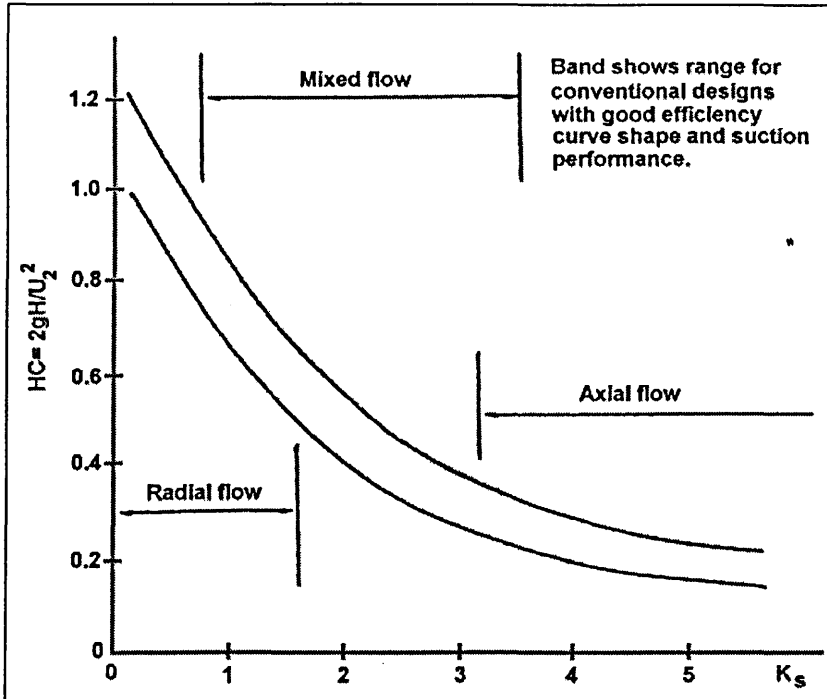


Figure 3.4-2 Head coefficient versus specific speed

5. To find the distance between the shrouds use the middle line on Figure 3.4-3 it can be seen that the ratio of  $D_2 / b_2 = 12$   
 therefore  $b_2 = 0.041\text{m}$ .

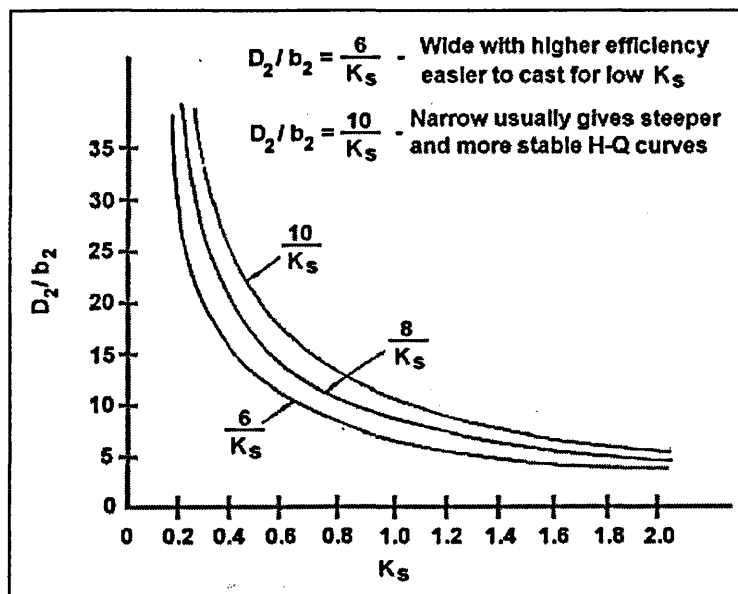


Figure 3.4-3 Impeller diameter shroud distance ratio graph

### **3.5 Concluding comments.**

It can be seen from these simplified design and selection methods that the NPSH plays a fundamental part in the overall sizing of a pump. Therefore accurate calculation of NPSH *required* and *available* is necessary, otherwise the pump selected or designed will not perform to the duty required, or will be bigger than actually needed, i.e. more expensive.

## **4. The Hydrocarbon Cavitation Test Rig, (HCTR).**

### **4.1 Introduction**

To carry out the experimental investigation of the *thermodynamic* effect of hydrocarbon cavitation for this research project, a test rig was required. The test rig was to combine a two dimensional venturi test section and a centrifugal test pump. The two dimensional venturi test section was to be used to perform a detailed analysis of the thermodynamic effect. It is used as a simple model of one blade passage of a radial pump impeller. Tests were also to be performed on the centrifugal pump to obtain data for NPSH tests on hydrocarbons. The test rig will also allow comparisons between the two methods. This chapter details tests rigs design process, and a detailed description of the final design. A critical appraisal of the test rigs performance during the research is also given.

### **4.2 The test rig design process.**

The basic design of the test rig was to consists of a main test loop with two receivers, a bypass loop with a heat exchanger, a centrifugal pump and a two dimensional venturi test section in the main loop. The test section to be used is the two dimensional convergent divergent nozzle as used by Furness (1973) and Chivers (1967) in their PhD theses. The rest of their original test rig had been dismantled and scrapped. Most of the pipe work and tanks for the new test rig were already in existence as parts of two old test rigs, that the author was given access to. However several modifications were to be made to these existing parts and several new parts fabricated. The general layout of the rig stayed the same throughout the design process. The main design alterations were due to changes in the test fluids to be used, and cost implications. The remainder of this section will give a summary of the designs considered and the reasons why various design features were discarded. A full description of the final test rig design will be given in section 4.3.

### **4.2.1 Design 1**

The first cavitation test rig design consisted of the main flow loop, two reservoir tanks with a process pump, pumping fluid from one to the other and a return line between the tanks containing the test section. It also included a bypass loop through a heat exchanger. Stainless steel wetted parts and appropriate seals were to be used as the projects sponsors initial choice of test fluids to be used were water, propane and kerosine. The other design features were a vacuum pump to be used for degassing and NPSH tests, a fluid actuator for re-pressurisation and a propane recovery system. All instrumentation, the process pump, vacuum pump and all other electric appliances were to be of intrinsically safe construction. The cost of this rig, designed to accommodate the fluids stated above, was prohibitive, therefore it was rejected by the sponsors.

### **4.2.2 Design 2**

One of the main cost areas of the first design was the intrinsically safe equipment, that was needed because propane was being used as one of the test fluids. After an extensive search for an alternative fluid was completed Gas Oil was chosen in replacement (For more details see Section 4.3.1). The need for intrinsically safe equipment could therefore be eliminated. The second test rig design was very similar to the first, the main change being the alteration from intrinsically safe electrical equipment to standard electrical equipment. Also a system for retrieving the propane from the test rig was no longer needed. This test rig was also deemed to be too expensive.

## **4.3 The final test rig design.**

The final design was to exclude the fluid actuator which was also a major cost, the implications of this is discussed later on in this chapter.




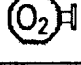
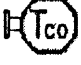

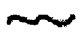
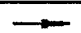

The initial design process involved drawing to scale on a CAD layout drawing all the existing component parts e.g. the two vessels, the pipework heat exchangers and valves. They were then arranged like a jigsaw puzzle into a test rig design. This design criteria

was a compromise between keeping the costs down on one hand and having a working test rig on the other. Costs were to be kept low by trying to utilise the existing parts with as few modifications as possible, and minimising the number of new parts needed for the test loop. The design for the test rig could not be finalised until the main circulating pump had been specified, and the pump could not be specified without a hydraulic analysis of the final test loop design. This 'Catch 22' situation was resolved by estimating the size of pump needed and designing connecting pipes to suit. Then an analysis of flow loop was carried out to size the pump more accurately. (This analysis was an iterative process and was carried out on a spread sheet package, details can be found in section 4.6.)

Having specified the pump type no suitable pump for the test rig was available from the project sponsors within the time limits of the research project. Enquiries were made to one of sponsors' sister companies Sterling SPP Ltd, who were able to provide a suitable, process pump within the time limits. The pump provided was a research and development model of a new line of Sterling LaBour process pumps, specific speed  $K_s = 0.455$  a copy of the performance curves and pump dimensions can be found in Appendix A.

The pump specification and therefore pump design type having now been finalised the test rig design could be completed. There were some last minute changes to the final detailed design, as a problem arose the day before the detail drawings of the new and modify parts of the test rig were due to be given to the manufacturing contractors. The area in the laboratory in which the test rig was due to be installed was changed by the laboratory manager. This meant that several alterations to the test rig design had to be made so it would fit within the new area of the laboratory, and new support structures had to be designed. The modifications to the design were not thought to alter the friction head losses within the test rig to any great extent. Also as the pump was specified to be slightly oversized for the calculated duty, to cope with any margins of error. Therefore alterations were thought to be negligible on the effect of the test rigs hydraulic operation. As time was short, the modifications were made to the drawings which were sent off to be fabricated. A subsequent analysis of the final design showed that the alterations made a negligible change to the calculated hydraulic performance of the rig.

The final detailed design drawings of the test rig can be found in Appendix B, and a photograph in Appendix G however it is easier to describe how the test rig operates and the theory behind some of the design features by looking at the test rig schematic Figure 4.3-1 the key for which can be found below.

Key for figure 4.3-1			
	Pressure gauge.	①	Main Circulating pump as described previously.
	Temperature sensor.	②	Main fluid holding tank.
	Turbine flow meter.	③	Intermediate settling tank .
	Dissolved oxygen probe, with a retractable housing.	④	Convergent divergent nozzle test section.
	Temperature cut out for the main pump.	⑤	Cooling water pump - Grundfos CR16-30/2 vertical multi-stage inline pump.
	Valve - each valve is numbered on the schematic.	⑥	8,000 gallon cold water sump, used a source for cooling water.
	Free surface of Liquid.	⑦	Serpentine heat exchangers, two identical h/x's connected in parallel.
	Air or vapour flow direction.	⑧	Liquid interceptor - to protect the vacuum pump.
	Liquid flow direction.	⑨	Vacuum pump - Sunvic.

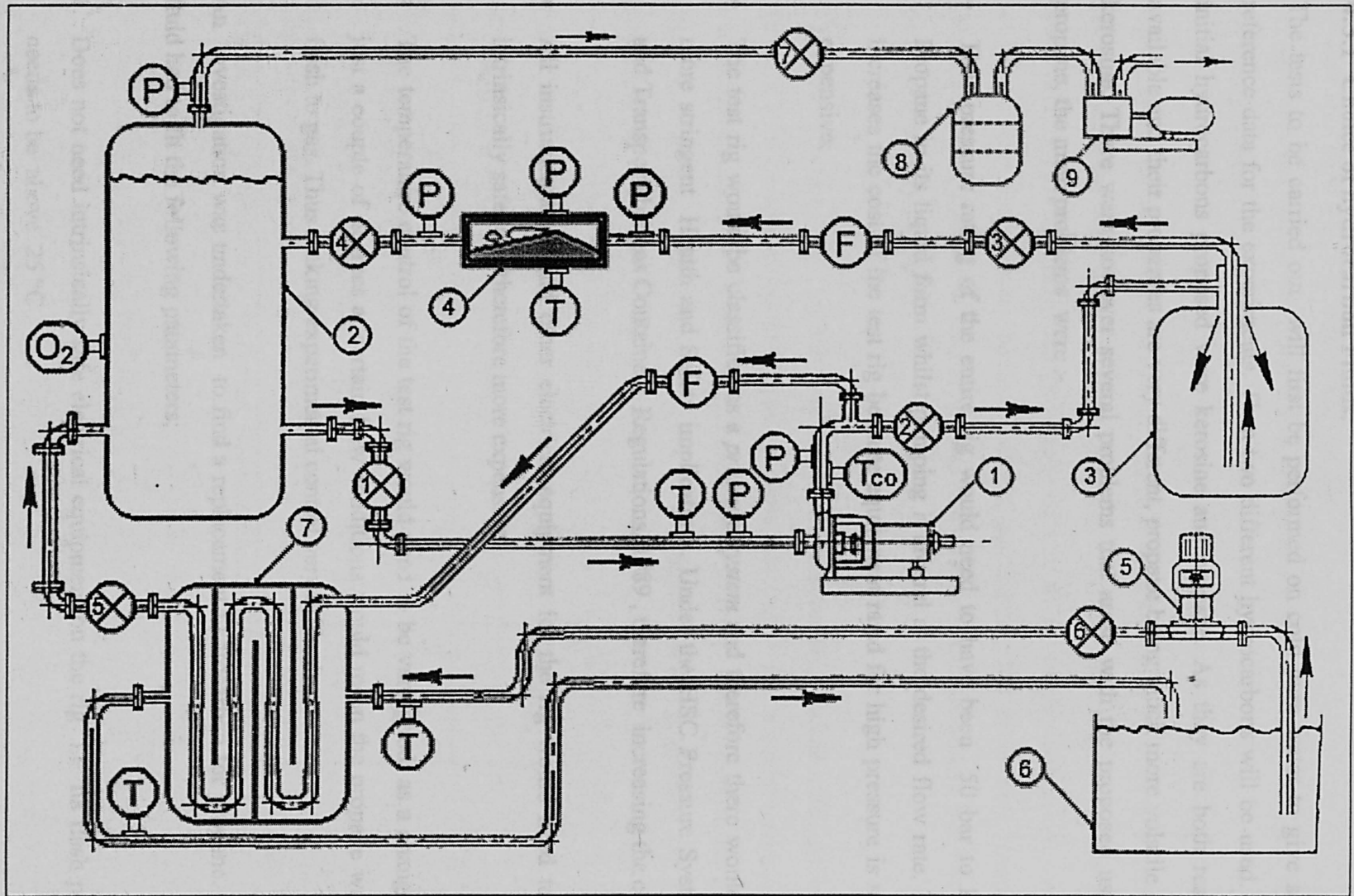


Figure 4.6-1 Schematic of the Hydrocarbon Cavitation Test Rig, HCTR.

#### 4.3.1 Choice of hydrocarbon Fluids.

The tests to be carried out will first be performed on cold pure water to give some reference data for the experiments. Then two different hydrocarbons will be used. The initial hydrocarbons proposed were kerosine and propane. As they are both readily available and their properties are very different, propane being much more volatile than kerosine. There were however several problems that arose with the proposed use of propane, the main problems were :-

- The pressure rating of the entire rig would need to have been 50 bar to keep Propane in its liquid form whilst pumping it around at the desired flow rate. This increases the cost of the test rig because equipment rated for high pressure is more expensive.
- The test rig would be classified as a *pressure system* and therefore there would be more stringent Health and Safety implications. Under the HSC Pressure Systems and Transportable gas Containers Regulations, 1989 , therefore increasing the cost.
- All instrumentation and other electrical equipment for the rig would need to be intrinsically safe, and therefore more expensive.
- The temperature control of the test rig would need to be very good, as a change of just a couple of degrees at certain flow conditions would mean the propane would flash to gas. Thus making experimental control very difficult.

An investigation was undertaken to find a replacement hydrocarbon for propane. The fluid had to fit the following parameters;

1. Does not need intrinsically safe electrical equipment on the rig i.e. its flash point needs to be above 25 °C .
2. Readily available and low cost.



3. Relatively different thermodynamic properties from kerosene.
4. Does not need a high pressure rated test rig.
5. Minimise the number of Health & Safety regulations that need to be complied with
6. Easily controlled experimentally.

A lengthy search was conducted to find a suitable hydrocarbon that could be found that satisfied all these conditions, and that was more volatile than kerosene. Among the more volatile pure hydrocarbons potentially of use, as far as physical properties are concerned were cyclohexane, hexane, toluene, and heptane but these were nonviable because of cost ( £100's per Litre). Nonane was a less volatile alternative but was also made nonviable by its cost.

A hydrocarbon that is less volatile than kerosene was eventually chosen, this fluid being gas oil, a choice endorsed by the project sponsors. Although it is not a pure hydrocarbon it is easily handled, the properties are measurably different from kerosene, and it is cheap and readily available. Table 4.1 lists some fluid properties for these hydrocarbons.

<i>Property</i>	<i>Kerosine</i>	<i>Gas Oil</i>
Density at 1 atm and 20°C (g/cm <sup>3</sup> )	0.775	0.849
Flash Point (°C)	40	70
Dynamic viscosity (cP) @ 20°C	1.3	5.4
Vapour Pressure @ 20°C (m)	0.138	31x10 <sup>-6</sup>
Specific Heat Capacity KJ/K kg @ 20°C	2.09	2.05

**Table 4.3-1 Comparison of Properties, Kerosine and Gas Oil**

### 4.3.2 Hydraulic details

The Fluid under test is pumped from the main fluid holding tank by the main circulating pump, into the intermediate settling tank. The fluid then returns to the main fluid holding tank via the test section. There is also a bypass loop that returns a proportion of the fluid to the main holding tank, from the discharge side of the main circulating pump. The bypass includes two serpentine heat exchangers connected in parallel. Valves 2 and 5 are used for adjusting the proportion of flow between the main flow loop and the bypass loop. Valve 4 is used for adjusting the back pressure in the test section, which will vary the cavitation conditions within the test section. Valve 1 can be used for varying the suction pressure to the pump for NPSH tests. NPSH tests can also be performed by the use of the vacuum pump connected to the top of main holding tank. The other use for the vacuum pump is to de-gas the test fluid. The vacuum pump is protected by a liquid interceptor to stop any liquid reaching it. The return line to the main holding tank delivers the fluid into the top of the tank so any gas or vapour bubbles arriving at the top of the tank will reabsorb and settle back into the fluid, before passing into the main pumps inlet line, taken from near the bottom of the tank. The intermediate tank between the main pump and the test section has an inlet at the top and the outlet at the bottom. This is so any gas or vapour pulled out of solution by cavitation in the pump or caused by valve 2 will be reabsorbed at the top of this higher pressure tank before entering the test section line.

The test line is long and straight so that the flow has a fully developed flow profile when it reaches the test section. The cruciforms located in the inlet and outlet of the turbine meter were thought to be enough flow straightening to eliminate any whirl effects before the test section. The test section is positioned just up stream of the inlet back to Tank 1. This is to aide in the de-gassing of the test fluids. Under cavitating conditions the venturi will cause the air to come out of solution and remain in bubble form as it enters the top of the main tank, thus making it easier to remove with the vacuum pump.

The cooling water for the serpentine heat exchangers is provided from an 8000 gallon cold water sump. It is pumped through the heat exchangers using a multistage vertical in-line

pump connected via reinforced PVC hose, then returned to the sump. The sump was calculated to be a big enough heat sink to provide the cooling needs of the test rig.

### 4.3.3 Instrumentation.

The instrumentation permanently attached to the test rig consists of temperature sensors, pressure gauges, a dissolved oxygen probe and a electrical power meter. Other instruments such as tachometers for pump speed, and DVM's were used when necessary.

#### 4.3.3.1 Temperature.

Temperature is measured at five points around the test rig, see table 4.3-2.

No.	Measuring point	Accuracy
1.	Inlet to the main circulating pump.	$\pm 0.5^{\circ}\text{C}$
2.	Inlet to the Test Section.	$\pm 0.5^{\circ}\text{C}$
3.	Throat of the Test Section	$\pm 0.1^{\circ}\text{C}$
4.	The cooling water inlet to the heat exchangers	$\pm 1^{\circ}\text{C}$
5.	The cooling water outlet from the heat exchangers	$\pm 1^{\circ}\text{C}$

**Table 4.3-2 Temperature measuring points**

The RTD temperature sensors 1-3 enable the fluid temperature in the test rig to be monitored accurately and also so the test fluids physical properties can be found accurately on property v temperature graphs. The sensors were surrounded in stainless steel sheaths, numbers 1 and 2 were 3mm in diameter and number 3 was 2mm in diameter to try and reduce any interference to the flow field in the venturi throat. Sensor 3 was positioned approximately 15mm downstream of the actual throat so it would not interfere with cavitation inception. The sensors number 4 and 5 are to give an indication that the heat exchanger is working.

#### 4.3.3.2 Pressure.

Pressure is measured at five points around the test rig by Budenburg standard test gauges, see table 4.3-3 The pressure sensors at points 1 and 2 are used for performance tests on the pump and are positioned in accordance with the pump test standard BS 5316:Part 2:1977. Gauges 3 4 and 5 are used to measure the throat efficiency of the test section. Gauge 6 on top of Tank 1, is used to measure the vacuum or pressure above the free surface of the fluid in the main holding tank.

No.	Measuring point	FSD	Accuracy
1.	Inlet to the main circulating pump.	-1 to 1.5 bar	-ve scale $\pm 0.017$ bar +ve scale $\pm 0.015$ bar
2.	Outlet from the main circulating pump.	0 to 10 bar	$\pm 0.02$ bar
3.	Inlet to the Test Section.	0 to 10 bar	$\pm 0.02$ bar
4.	Throat of the Test Section.	-1 to 1.5 bar	-ve scale $\pm 0.017$ bar +ve scale $\pm 0.015$ bar
5.	Outlet from the Test Section.	-1 to 10 bar	$\pm 0.02$ bar
6.	Above the fluids free surface in the main holding tank.	-1 bar to 1 bar	-ve scale $\pm 0.034$ bar +ve scale $\pm 0.07$

**Table 4.3-3 Pressure measuring points**

#### 4.3.3.3 Flow.

Two turbine flowmeters were used one of nominal diameter 3" in the main test line and the other of nominal diameter 1.5" in the heat exchanger bypass line. The output frequency is converted to a voltage, 0-5 volts being equal to 0  $\Rightarrow$  FSD. The voltage outputs from the flow meters was read on a two channel digital volt meter.

Nominal size	Operating Range m <sup>3</sup> /hr	Error %	Repeatability %	Effect of a Viscosity change 1 ctS $\Rightarrow$ 10 ctS at percentages of flow range		
				10%	50%	100%
3"	16 -180	0.5	0.05	-1%	-0.5%	-0.5%
1.5"	3.5 - 45	0.5	0.05	-1.5%	+0.25%	+0.5%

Q-Flo Turbine Flow meters Manufactured by Quadrina Ltd, Letchworth

**Table 4.3-4 Turbine flow meter details**

The maximum viscosity encountered with the test fluids was gas oil at 20°C which is approximately 6 cSt (Table 4.3-4) The viscosity effect on the turbine meter was therefore ignored as the added errors were low.

#### **4.3.3.4 Dissolved air.**

A dissolved oxygen content meter was used, to infer a dissolved air content of the test fluids. The oxygen sensing probe is installed in the main holding tank, and a retractable housing is used so the probe can be isolated without affecting the test fluid. The measurement system consists of a polarographic O<sub>2</sub> sensor (Clark type) and a Dissolved oxygen transmitter / microprocessor analyser. The theory behind the measurement system is complex. It consists of a sensor with a working electrode (Cathode), a counter electrode, and a reference electrode (Anode), with an oxygen permeable Teflon<sup>®</sup> coated membrane which separates the electrodes from the fluid being measured. The transmitter provides a polarising voltage to the cathode (-550 to -750 mV). The oxygen molecules migrate through the membrane and are reduced at the cathode, whilst oxidation occurs at the anode. The oxidising anode metal being transferred to the electrolyte. This electrolyte completes the ion conduction circuit between anode and cathode. This current measured by the transmitter is proportional to the partial pressure of the oxygen in the medium. A similar sensor has been used by Cansdale (1978) on aviation fuels, and compared well with gas liquid chromatography results. The inference of dissolved air by measurement of dissolved oxygen was aided by a report by Ross (1970) which gives detailed results on the quantities of dissolved oxygen and nitrogen within fuels.

( 12.5mm T type sensor with microprocessor analyser; Manufactured by Mettler Toledo)

#### **4.3.3.5 Power meter.**

This was a three phase electricity meter, a solid state microelectronic kilowatt hour meter, with maximum error of  $\pm 1\%$  of full scale.

(Responder 3 - Manufactured by response company Ltd, Winchester )

#### 4.3.3.6 Tachometer.

The tachometer was microprocessor controlled meter with an optical sensor. The FSD 3 - 99,999 rpm, accuracy of  $\pm 1$  digit and a resolution of 0.001.

#### 4.3.4 The 2D venturi test section.

The 2D venturi test section as stated before was used by Furness and Chivers, (full details of the design and design criteria of the test section can be found in Chivers (1967)). The venturi has proved to be an excellent tool in the study of cavitation over the years, some of the many studies are cited in the literature review. The cavitation conditions within the venturi are claimed to be like those found in a centrifugal pump. A cross sectional diagram can be seen in figure 4.3-2. The main body of the test section is machined out of a single piece of stainless steel, with a 54mm by 54mm square bore through the centre. A wedge insert in the bottom of the test section creates the convergent and divergent channel with a throat area of 21mm by 54mm. The venturi has two cast perspex viewing windows one located on the side and the other located on top. The windows are used for visual inspection of the cavitation within the test section. Cavitation inception can be seen and measurements of cavity length made from the side window: The top window was be used for lighting up the test section and for the use of a strobe light. It was also possible to take photographic and video footage of the cavitation through the side window.

Key for Figure 4.3-2	
No.	Description
①	Side window.
②	Top window.
③	Downstream pressure tapping.
④	Upstream reference pressure tapping.
⑤	Throat pressure tapping.
⑥	Reference temperature sensor tapping.
⑦	Throat temperature tapping.
⑧	O-ring end seals.

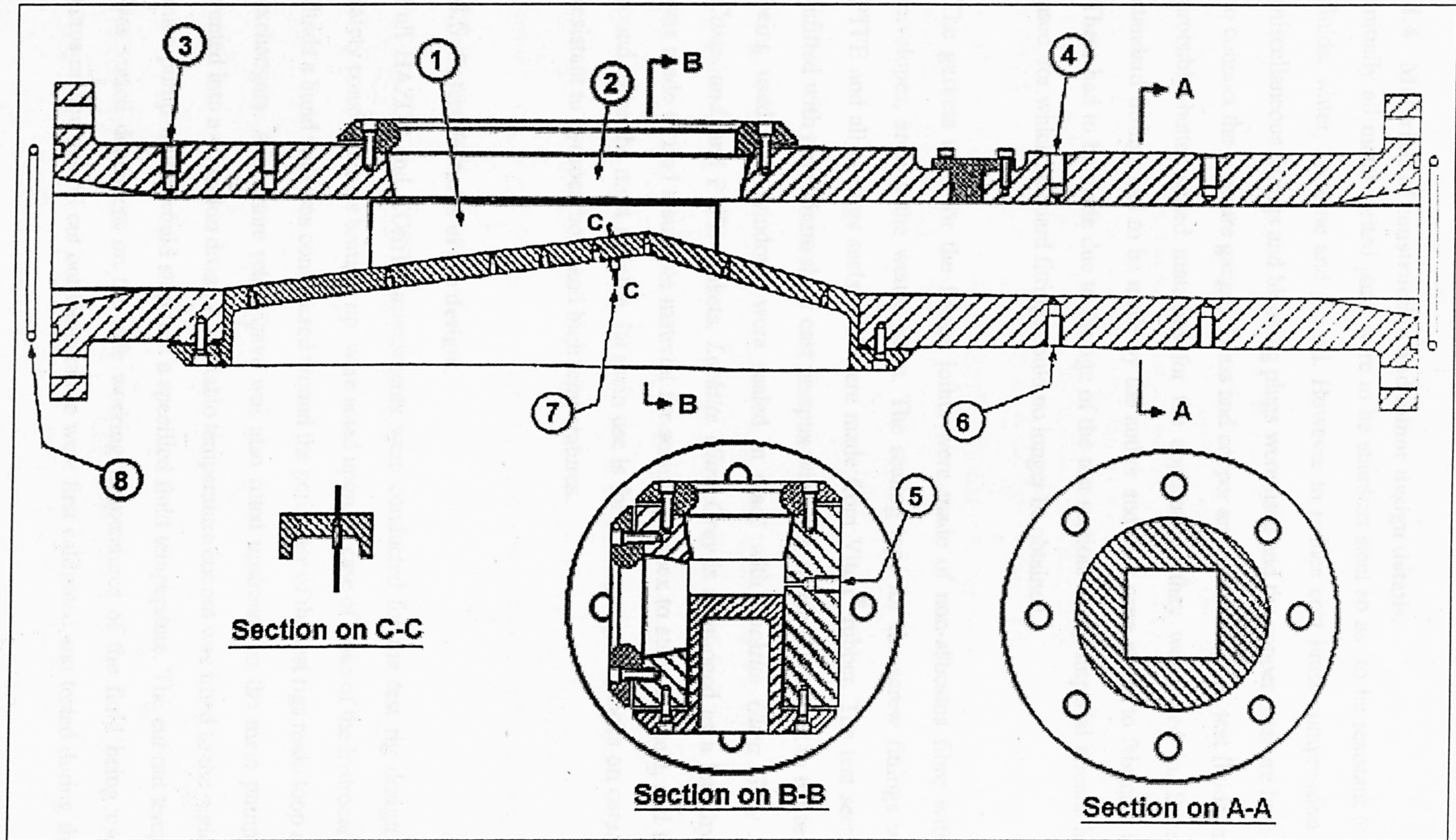


Figure 4.3-2 Cross section of the 2D venturi test section.

#### **4.4 Materials of construction and minor design details.**

Initially all metal wetted parts were to be stainless steel so as to be resistant to the test fluids, water, kerosine and gas oil. However to reduce cost brass compression fittings, miscellaneous fittings and blanking plugs were used and the copper pressure lines utilised to connect the pressure gauges. Brass and copper are resistant to the test fluids, and were probably better suited materials for the applications they were used in. Several non standard fittings had to be made by the author and they were easier to fabricate in brass. These had to be made due to the age of the test section. Many imperial threads had been used, for which standard fittings could no longer be obtained.

The gaskets used for the flange joints were made of non-asbestos fibre with PTFE envelopes, around the wetted parts. The sealing tape for the screw fittings was also PTFE and all O-rings seals used were made from Viton<sup>®</sup> rubber. The test section was refitted with new 25mm thick cast perspex windows, which is resistant to the test fluids being used. The windows were sealed in place with *Loctite Ultra Grey Silicone Compound*, and PTFE gaskets. *Loctite Ultra Grey* is mentioned as a lengthy search was made to find a suitable material for sealing perspex to stainless steel, and this was found to be the most suitable. Its main use is for sealing engine blocks on cars, so it is resistant to hydrocarbons and high temperatures.

#### **4.5 Safety features of the design.**

Full HAZOP and COSHH assessments were conducted for the test rig design and all safety considerations brought up were acted upon. In case of leaks of the hydrocarbon test fluids a bund wall was constructed around the perimeter of the test rigs main loop and heat exchangers. A pressure relief valve was also fitted upstream on the main pump, which vented into a 45 gallon drum. A variable temperature cut out was fitted to the outlet of the main pump which would stop it at a specified fluid temperature. The cut out temperature was varied dependent on the safe working temperatures of the fluid being used. The kerosine and gas oil cut out temperature were first calibrated and tested during the water



test phase. Two manually operated emergency stops were also located at strategic points which would stop the main pump.

#### 4.6 Hydraulic analysis of the test rig design.

This section details the hydraulic analysis of the test rig to enable the correct specification of the main circulation pump. As the analysis of the friction losses involves iterative calculations it was carried out on three spread sheets, one each for water, kerosine and gas. To show the assumptions and formulas behind the spread sheet analysis the following calculations show the first iteration for water. Friction factors for pipes were taken from a Moody chart and Friction factors for fittings were taken from a standard table (see Appendix C).

##### 4.6.1 Cavitation Conditions Within Test section.

To size the pump it was necessary to know the conditions that need to be achieved within the test section. Data in the Furness (1973) thesis was utilised and it was found that the conditions in the test section that would give a cavitation number;  $\sigma_o = 5$  in water at 20°C would mean the venturi would be cavitating with a very low throat efficiency. In other words complete cavitation breakdown would be achieved in the venturi, ( $\sigma_{3\%} = 6.75$ ). The pump was therefore sized so as to achieve this cavitation condition in the venturi. Therefore from the equation  $\sigma_o = \frac{P_o - P_v}{\frac{1}{2} \rho V_o^2}$  the maximum flow rate needed in the test section can be found.

Properties of water	$P_v = 2340 \text{ Pa}$	@ 20°C
	$\rho = 987 \text{ Kg/m}^3$	@ 20°C
	$v = 9.01 \times 10^{-7}$	@ 20°C

Assuming an gauge pressure of 1 bar at the reference point; o ,see figure 4.6-1 ,

Therefore; 
$$P_o = P_{o, gauge} + P_{atm} = 2.0132 \times 10^5 \text{ Pa}$$

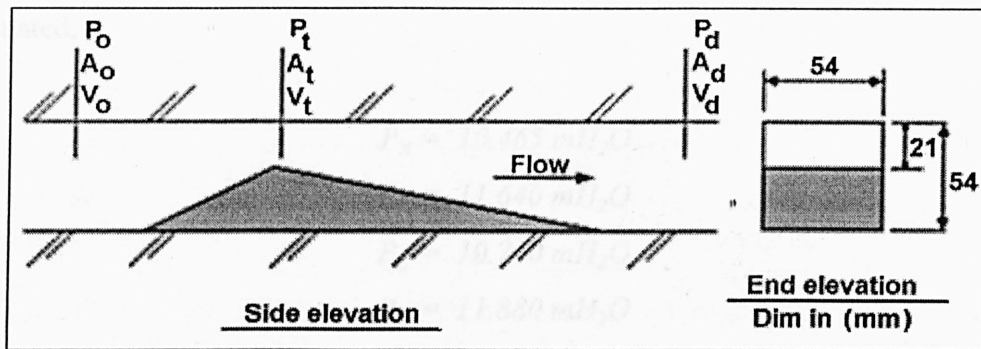


Figure 4.6-1 Schematic of Convergent Divergent Nozzle

The velocity at the reference point is therefore

$$V_o^2 = \frac{P_o - P_v}{\frac{1}{2} \rho \sigma} = \frac{2 \cdot 0132 \times 10^5 - 2340}{0.5 \times 987 \times 5} = 80.64$$

$$V_o = 8.98 \text{ m/s}$$

The maximum flowrate needed in the test section is

$$Q_o = V_o \times A_o = 8.98 \times (0.054 \times 0.054) = 0.0262 \text{ m}^3/\text{s}$$

$$= 94.32 \text{ m}^3/\text{hr}$$

#### 4.6.2 Hydraulic analysis of the test rig.

With reference to the following two diagrams Fig 4.6-2 and Fig 4.6-3 the following parameters are known. Assuming  $P_1 = P_{\text{atm}} = 1.0132 \times 10^5 \text{ Pa}$ , and that the free surface of fluid in tank 1 is at a point A above the datum. The heights of points B, C and D

above the datum are also known, the absolute pressures at these points can be calculated.

$$P_A = 10.465 \text{ mH}_2\text{O}$$

$$P_B = 11.640 \text{ mH}_2\text{O}$$

$$P_C = 10.740 \text{ mH}_2\text{O}$$

$$P_D = 11.880 \text{ mH}_2\text{O}$$

The flow rate  $Q_2 = Q_0 = 26.2 \text{ l/s}$

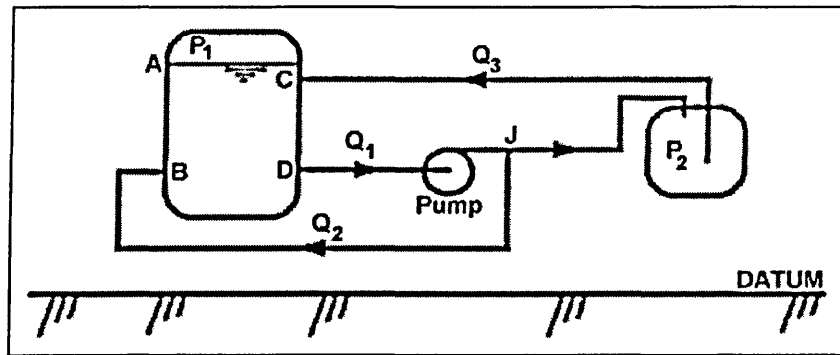


Figure 4.6-2 Schematic of Test Rig.

The pressures at  $P_j$ ,  $P_{ds}$  and  $P_{us}$  can be written in equation form as.

$$P_j = P_c + hf(J-C) = P_b + hf(J-B) \quad \text{..Equ 4.6-1}$$

$$P_{ds} = P_j + hf(P_{ds}-J) \quad \text{..Equ 4.6-2}$$

$$P_{us} = P_d - hf(D-P_{us}) \quad \text{..Equ 4.6-3}$$

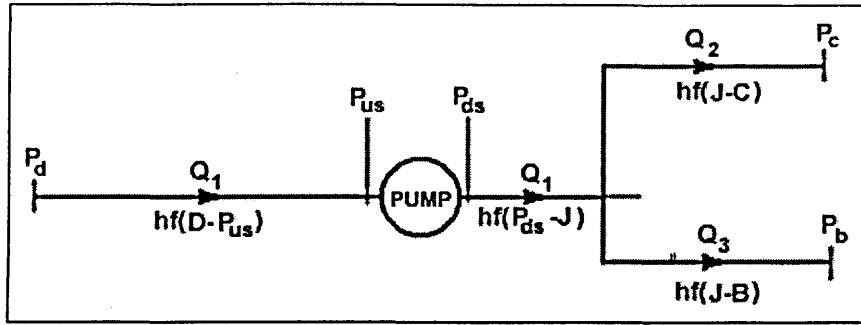


Figure 4.6-3 Pressure and Friction losses diagram for Test Rig.

The  $hf$  value is the friction head loss between the points in brackets. These losses are made up by a combination of the losses in the pipes;  $h_{pipe}$  and the losses in the fittings;  $h_{fit}$  where.

$$h_{pipe} = \frac{4fu^2l}{2gd} \quad \text{..Equ 4.6-4}$$

$$h_{fit} = \frac{Ku^2}{2g} \quad \text{..Equ 4.6-5}$$

Where the constants  $f$  and  $K$  are taken from a Moody chart and a K factor table respectively (See Appendix C). To continue with the calculations we need values for  $Q_1$  and  $Q_3$  these are therefore estimated.

$$\begin{aligned} \text{Assume } Q_3 = 3 \text{ l/s} \quad \Rightarrow \quad Q_1 &= Q_3 + Q_2 = 3 + 26.2 \\ Q_1 &= 29.2 \text{ l/s} \end{aligned}$$

To find the friction factor  $f$  from the Moody chart the Relative Roughness  $k/d$  and the Reynolds Number  $Re$  need to be found, these are easy to calculate from the given information and therefore are just tabulated in Table 4.6-1 below.

Nom Diameter	1.5"	3"	3"	4"	4"	2"
Flow	$Q_3$	$Q_1$	$Q_2$	$Q_1$	$Q_2$	$Q_1$
Internal diameter; d (mm)	25mm	77.9mm	77.9mm	103mm	103mm	30mm
Velocity (m/s)	6.11	5.49	6.12	3.53	3.17	41.29
Relative Roughness $k/d$ ( $k = 0.002$ for Stainless steel Pipe)	$8 \times 10^{-5}$	$2.57 \times 10^{-5}$	$2.57 \times 10^{-5}$	$1.95 \times 10^{-5}$	$1.95 \times 10^{-5}$	$6.67 \times 10^{-5}$
Reynolds No.	$1.7 \times 10^5$	$4.7 \times 10^5$	$5.3 \times 10^5$	$4.02 \times 10^5$	$3.6 \times 10^5$	$1.4 \times 10^6$

Table 4.6-1 Values to find Friction factor  $F$  from the Moody Chart

From Equations 4.6-4 and 4.6-5 and the values in Table 4.6-1 the friction losses in various sections of the test rig can be found, the results are tabulated in tables 4.6-2 to 4.6-5.

<i>Friction loss caused by, (at flow rate <math>Q_2</math>)</i>	<i>No. Off / length (m)</i>	<i>K or f</i>	<i><math>h_{pipe}</math> or <math>h_{fit}</math> (<math>mH_2O</math>)</i>
3" StSt pipe	12.42 m	0.0035	3.434
4" StSt pipe	1 m	0.0036	0.284
3" Elbows	3	0.9	4.154
Full bore valve	3	0.2	0.923
Expansion 2" to 3"	1	0.35	0.538
Expansion 3" to 4"	1	0.2	0.308
Divergent part of Nozzle	1	0.55	0.840
Convergent part of Nozzle	1	0.4	0.615
Tee Junction (Through side)	1	1.8	2.769
3" Pipe to Tank	1	1.0	1.538
4" Pipe to Tank	1	1.0	0.511
Tank to 3" Pipe	1	0.5	0.769
Turbine Flow Meter	1	0.6	0.923
<b>Total Losses hf(J-C)</b>	-	-	17.607

**Table 4.6-2 Friction head losses between points J and C.**

<i>Friction loss caused by, (at flow rate <math>Q_1</math>)</i>	<i>No. Off / length (m)</i>	<i>K or f</i>	<i><math>h_{pipe}</math> or <math>h_{fit}</math> (<math>mH_2O</math>)</i>
4" StSt pipe	4.32 m	0.0035	0.374
3" StSt pipe	1 m	0.0034	0.084
Reducer 4" to 3"	1	0.4	0.254
Tank to 4" Pipe	1	0.5	0.318
4" Elbows	2	0.9	1.143
<b>Total Losses hf(D-<math>P_{us}</math>)</b>	-	-	2.173

**Table 4.6-3 Friction head losses between points D and  $P_{us}$ .**

<i>Friction loss caused by, (at flow rate <math>Q_1</math>)</i>	<i>No. Off / length (m)</i>	<i>K or f</i>	<i><math>h_{pipe}</math> or <math>h_{fit}</math> (<math>mH_2O</math>)</i>
2" StSt pipe	0.60 m	0.0031	0.183
2" Elbow	1	0.9	1.720
<b>Total Losses hf(<math>P_{ds}</math>- J)</b>	-	-	1.903

**Table 4.6-4 Friction head losses between points  $P_{ds}$  and J**

<i>Friction loss caused by, (at flow rate <math>Q_3</math>)</i>	<i>No. Off / length (m)</i>	<i>K or f</i>	<i><math>h_{pipe}</math> or <math>h_{fit}</math> (<math>mH_2O</math>)</i>
1.5" StSt pipe	9.97 m	0.0042	12.753
1.5" Pipe to tank	1	1	1.904
Elbows 1.5"	9	0.9	15.420
Tee Junction (Through Side)	1	1.8	3.427
Two Heat exchangers in parallel <sup>Pb</sup>	0.5	45.0	42.834
<b>Total Losses hf(J-B)</b>	-	-	76.338

**Table 4.6-5 Friction head losses between points J and B**

It can be seen from equation 4.6-1 that

$$P_j = P_c + hf(J-C) = P_b + hf(J-B)$$

$$\therefore P_j = P_c + hf(J-C) = 10.740 + 17.607 = 28.347 \text{ m } H_2O$$

$$\therefore hf(J-B) = P_j - P_b = 28.347 - 11.640 = 16.707 \text{ m } H_2O$$

This does not match the value of  $hf(J-B)$  obtained in Table 4.6-5 therefore the assumed value for  $Q_3$  was wrong. Therefore another guess should be made, and the calculations repeated until a values of  $hf(J-B)$  match. The following information was produced from the spread sheet hydraulic analysis, to aide in specifying a pump.

<i>Fluid (Density at 20 °C)</i>	<i>Pump Head</i>	<i>Pump Head (m <math>H_2O</math>)</i>	<i>Max. Flow Rate Needed (<math>m^3/hr</math>)</i>
<b>Water</b> ( $\rho=987\text{kg/m}^3$ )	20.497 m $H_2O$	20.497	99.31
<b>Kerosine</b> ( $\rho=800\text{kg/m}^3$ )	25.394 m Kerosine	20.583	110.47
<b>Gas Oil</b> ( $\rho=860\text{kg/m}^3$ )	24.699 m Gas oil	21.521	106.86

**Table 4.6-6 Results from spreads sheet friction loss analysis.**

<sup>Pb</sup> The K factor for these two identical serpentine heat exchangers was found experimentally, by measuring the pressure drop across them at various flow rates. The No off = 0.5 because they are set up in parallel and would therefore half the frictional resistance across them.

The pump was sized to give a slightly higher delivery of pressure and flow to account for any errors occurring in the analysis as a result of the assumptions made. The main sources of error being a mixture of the following two areas:-

1. The same sigma value for breakdown cavitation condition in water ( $\sigma = 5$ ) was also used for the kerosine and gas oil analysis. No data was available on these fluids in a cavitating venturi to make any adjustment for thermal effects.
2. Discrepancies in the friction loss coefficients between theory and the real case.

The oversizing of the pump should compensate for these errors. The maximum delivery of the pump being  $132 \text{ m}^3/\text{hr}$  at  $37 \text{ mH}_2\text{O}$  and a closed valve head of  $62.5 \text{ mH}_2\text{O}$ .

#### **4.7 Retrospective analysis of the test rigs performance.**

This section will give an overview of how the test rig performed during the experimental phase. It will point out the areas for possible future improvements in the design and instrumentation used. This test rig review is split into various sections dealing with the hydraulic design and the various measurement areas.

##### **4.7.1 Hydraulic design performance.**

The design of the intermediate tank to reabsorb gas and vapour bubbles into the liquid, its inlet at the top and outlet downward facing at the bottom of the tank worked well. All bubbles were reabsorbed before entering the test line, even when there was extensive cavitation caused by the valve just up stream of the tank. No visible bubbles could be seen entering the test section with any of the test fluids used, even with the use of a strobe light.

The drowned suction of the test pump made it difficult to perform low flow NPSH tests on the hydrocarbons. Although tests of below 40% of BEP flowrate were not performed as it would have been impossible to conduct them. The 3% drop on the 40% of BEP

flowrate could only just be achieved with the hydrocarbon fluids. Thus at lower flowrates a 3% drop would not have been achieved.

The suction valve throttling tests proved to be impossible to perform with the hydrocarbons. The readings were too unstable, perhaps due to the cavitation bubbles caused by the throttling valve entering the pump. Hydrocarbons have approximately seven times more air in solution than water, so the cavitating throttling valve would have presented a near two phase mixture to the pump inlet. A settling tank in-between the throttling valve and the pump would have possibly cured the instabilities, but the cost of another tank and the time to modify the rig were prohibitive.

All the cavitation conditions needed in the test section for the test matrix were achievable. The tests section could easily be controlled from cavitation inception to complete efficiency breakdown, with the range of constant reference pressures 1, 1.5 and 2 bar.

#### **4.7.2 Temperature.**

The temperature stability of the test rig was excellent. On the constant flow NPSH tests the average maximum temperature variation was 0.5°C. The nozzle tests where the flow was varied had average maximum temperature variation of 1°C. The higher temperature tests had less variation than the ambient tests, as the higher temperature differential between the test flow and the coolant flow meant the system was more controllable.

The test fluid was heated purely by circulating the fluid with the main pump, without the cooling circuit on. The main drawback with this being the length of time to attain higher test temperatures. An immersion heater could have speeded this operation up, but with the use of hydrocarbons it was thought safer to just use the pump. The highest temperature attained by this method of heating was 56°C, as the test rig attained a thermal equilibrium with the ambient air in the laboratory. That is the convection and



radiation of heat from the test rig was equal to the heat input by the pumps work on the fluid. Lagging the pipes and tanks would have meant higher temperatures could have been achieved, but larger heat exchangers would be needed for the lower temperature tests. As heat losses from the test rig through convective and radiation effects would be negligible. The lagging for a test rig of this size was also expensive and was ruled out on cost grounds, as well as the fact that no other heat exchangers were available.

Only one problem was encountered with the temperature sensors although it happened several times. The sensor in the venturi throat would start leaking when under pressure or letting in air under vacuum. This was due to a minute crack appearing on the sensors tip. It was thought at first due to the sensor being located in the cavitation zone, and its surface was eroding due to the cavitation. However on the third occasion this happened the new sensor had not been subjected to any cavitation, and a vacuum test was conducted. The sensor leaked air from the tip, therefore it was deduced that it was a manufacturing fault. A replacement sensor was inspected with a microscope for cracks, and the problem did not occur again.

The accuracy of the thermocouples could have also have been improved. However this would have been more expensive and as the test temperatures were low the a variation in temperature of a degree does not significantly change the vapour pressure of the fluids used. The thermocouples accuracy of  $0.1^{\circ}\text{C}$  was therefore thought to be more than adequate, however if higher temperature tests are to be conducted, temperatures would need to be monitored much more accurately.

#### **4.7.3 Flow**

The turbine flow meters were very reliable and of high accuracy thus flow measurement errors were very low. Only one problem occurred during testing. If the pump was turned off with a high flowrate in the test line the test section venturi would create a water hammer effect. This happened a couple of times during initial test rig trials, and eventually resulted in the collapse of the 3" turbine meters journal bearings. The test

rigs procedures were subsequently changed, to only allow low flow shutdowns. The only other area which could be improved was the read out which was in volts, it would have been easier if these were displayed in actual flow rates.

#### **4.7.4 Dissolved Oxygen / Air content**

For the most part the polarographic oxygen sensor used was reliable and compared well with theoretical values of dissolved oxygen levels for water kerosine and gas oil. However two problems were encountered, the first occurring after a months testing. The sensor began to drift, this was traced to a small crack in the glass surrounding the cathode. After the sensor was repaired its reaction time was much faster, thus casting doubt over the results of the whole of the first months testing, not just from the point when the sensor began to drift. The tests were subsequently all repeated, which proved the sensor had not been working properly since it was installed. The second problem encountered with the sensor happened during the last week of testing with water. The sensor started to drift erratically, on water with a dissolved oxygen content known to be approximately 100% of the saturation value. The sensor would read the correct value for a couple of hours then rapidly vary from between approximately 130% to 55%. No problem with the sensor could be found and it worked perfectly for the rest of the tests. But for two and a half weeks these variations happened randomly throughout the day and night, and no source of external interference could be found. The drift eventually disappeared and is still something of an enigma. This polarographic type of oxygen sensor is a big improvement on previously used methods in cavitation research. The Van Slyke apparatus being the main instrument used by the likes of Furness and Pearsall. This could only measure samples, usually taken at the beginning and the end of each test run. The polarographic oxygen sensor used by the author gave continuous readings of the oxygen content of the fluid under test.

The control of the dissolved oxygen / air content was better than expected. It was thought that without the fluid actuator it might be impossible to conduct the tests at low oxygen levels. After a vacuum is used to de-aerate the test fluid the actuator would then

have be used to re-pressurise the test rig with de-aerated fluid. The main pump's performance would not be affected as it would not be operating under reduced NPSH. The venturi tests were initially to be performed at 100 % , 50% and approximately 0% of the air saturation value of the fluids. The 100% saturation value was obviously easy to maintain, with the free surface in the main holding tank being left open to atmosphere. The 50% value could also be maintained fairly easily by slowly degassing with the vacuum pump to 50% and maintaining the vacuum approximately 0.5 ⇒ 0.6 bar absolute above the free surface. This did not affect the main pump's performance to any great extent and all test conditions in the venturi could be achieved. The problem came when trying to achieve approximately 0% saturation and run the tests. It was possible to degas water, kerosine and gas oil to near 0% with a near total vacuum above the free surface, however the test conditions could not be achieved. The vacuum caused adverse suction conditions which effected the performance of the main pump, i.e. causing cavitation breakdown. However it was possible to reduce this vacuum slightly and to run the test at a slightly higher oxygen level. It was possible to keep water below 10% of the saturation value and perform all the tests needed. Kerosine and gas oil proved to be more difficult. The best that could be achieved was to maintain the level at around 25% of the saturation value. It also took a fair amount of preparation for each low oxygen test run and adjustments during the runs, especially for the hydrocarbons which reabsorbed air more readily than water. The tests would have been easier to perform, less time consuming and the zero oxygen content values could have been achieved if a fluid actuator had been used. Although good results have been achieved without one this is obviously an area where the test rig could be improved in the future.

#### **4.7.5 Pressure.**

The pressure gauges worked well with no problems and the large analogue dials were good for visualising any instabilities in the pressure readings and the acuracy was high so the errors in the head and nozzle efficiency were low. In the main pressure reading were fairly stable this meant that any reading errors were low. An improvement could be made in the accuracy of the sensors but this would have meant a greater cost.

#### **4.7.6 Conclusion.**

The test rig proved to be a good tool for this cavitation research project, it gave stable conditions and very repeatable results. The main drawback in the instrumentation was that it had to be manually logged then manually entered onto a computer to analyse. A full data acquisition system would be an vast improvement on the present system. However the money and the time to set one up was not available for this project, but such a system would be advisable for any future investigation. Although standard instruments were used they were capable of a high degree accuracy therefore the magnitude of the errors was low. The use of a fluid actuator would also be advisable for any further air content work. In the main part the areas in which improvements could be made are really a question of finance. If future cavitation research is conducted on the HCTR facility, the points mentioned in this section should be addressed.

## **5. Experimental Work.**

### **5.1 Introduction.**

This chapter describes the experimental work undertaken, in chronological order. The experiments covered work on water, kerosine and gas oil. The tests used a centrifugal pump and two dimensional venturi for easier visualisation of the cavitation. A comparison study on NPSH tests methods was also undertaken, suction valve throttling and vacuum pump methods. The temperature range studied was 20 to 50°C for water and 20 to 30°C for the hydrocarbons. The effect of the dissolved oxygen content was also studied (hence inferring the dissolved air content). Experimental procedures were set-up during the testing process rather than before, as the limitations of the rig and the fluid conditions that could be achieved were not known. The pump and nozzle tests performed on the various fluids were similar. The water tests will therefore be explained in detail, but to stop any repetition only the details relevant to the other fluids will be discussed in the relevant sections. This chapter only describes the experimental work that was carried out, all results and discussion are contained within the chapters 6 and 7.

### **5.2 Water tests.**

As Ruggeri and Gelder (1963) found that the effect of the water quality, i.e. tap, demineralised and de-stilled water had a negligible effect, so filtered tap water was used for the tests. The tests performed are broken into two clear section, first the pump tests and secondly the nozzle tests, which will now be discussed separately.

#### **5.2.1 Water Pump Tests.**

The first test to be performed on the pump was to characterise its head-flow curve and efficiency. These were compared with the manufacturers data, after being corrected for speed (Test 2950 rpm, Manufacturers 2900) using the affinity laws, and the curves matched up well. This was done in order to check on the pump and to find the

maximum flow and BEP (Best Efficiency Point), which were  $112\text{m}^3/\text{hr}$  at  $53\text{m}$  of fluid and  $100\text{m}^3/\text{hr}$  at  $57.5\text{m}$  fluid respectively. The next tests to be performed on the pump were NPSH tests, as laid out by the Hydraulic Institute Standards (1983). Both the vacuum pump and suction valve throttling tests were conducted. Tests were performed at  $20^\circ\text{C}$  and  $30^\circ\text{C}$ , with a maximum variation of  $0.5^\circ\text{C}$  per test run and flow rates of 40, 60, 80 and  $100\text{m}^3/\text{hr}$ . The suction valve throttling tests were also conducted at dissolved oxygen contents of 100% and  $<10\%$  of saturation, and for each test condition a repeat test was made. The low oxygen content suction valve throttling tests were achieved by first circulating the water under a hard vacuum. The nozzle would act as a sort of separator, introducing a two phase flow into the top of the main tank, making the removal of the air easier. After the desired air content had been reached, the fluid level in the main tank was gradually raised, so there was only a small area of fluid free surface (possible by the main tank having a domed top), the vacuum would then be released before a test run. As there was only a small free surface area of water in contact with the air, re-absorption was very slow, and a test run could be completed with very little change in the level of dissolved oxygen. The process was repeated before each test run. The fluid temperatures were attained by running the test rig, with no cooling water until the desired temperature was reached. The cooling water was then turned on and adjusted until the temperature remained steady.

As dissolved air was removed from the water during the vacuum pump NPSH tests, it was necessary to re-saturate the water with air at the end of each test run. This was so there was a consistent oxygen level at the start of each test run. The water was re-saturated by circulating the water and bubbling air up through the main tank, until the 100% saturation was achieved. The NPSH curve for the above tests can be found in Appendix D from which the 3% head drop data could be read for each test condition.

### **5.2.2 Water Nozzle tests.**

The tests conducted on the nozzle are similar to tests conducted by previous researchers, Furness (1973), Pearsall and McNulty (1955) and Hammitt et al (1967). They were

conducted for reference data, to compare the hydrocarbon data to. Pearsall and McNulty's (1955) throat efficiency parameter ( $\eta_t = [P_d - P_t] / [P_o - P_t]$ ) was used as a measure of cavitation, and when plotted against the free stream velocity it gives a similar characteristic curve to that of a pump NPSH test. A characteristic curve along which cavitation inception, 3% efficiency drop, and fully developed cavitation ( taken arbitrarily at a nozzle efficiency of 40% ) could be found, Inception being visually noted, the other points being calculated from the results plots. A note of average cavity length was also taken visually using a stroboscope.

To obtain this characteristic curve the upstream reference pressure  $P_o$  was held constant, whilst the free stream velocity was gradually increased until cavitation breakdown conditions were achieved in the nozzle. Up stream pressures of 1, 1.5 and 2 bar were chosen, after several initial test runs, to be the best for the operational envelope of the test rig. Test runs were then completed for temperatures at approximately 20, 30 40 and 50°C (Variation of 0.2 to 0.3°C) with water at dissolved oxygen concentrations of 100%, 50% and <10% of saturation, for each test run a repeat test was made. Dissolved Oxygen levels within the water were adjusted by similar means to the pump tests, however a partial vacuum could be maintained, thus prolonging the length of time the oxygen content could be kept at the lower levels.

The resulting Efficiency - Free stream velocity curves are in Appendix D, the resulting analysis and the effect of the various test conditions on  $\sigma_i$   $\sigma_{3\%}$  and  $\sigma_{fd}$  are discussed in later chapters.

### **5.3 Kerosine Tests.**

After the water tests were completed the test rig had to be drained, cleaned and dried. This was so there was no cross contamination of fluids. The water was first drained from the test rig, at all the low points. Areas where water could be trapped e.g. valves, instrumentation pressure tubes, pressure gauges etc. were removed, dried and replaced. A hot air blower was used to circulate hot air through the rig, the laboratory heaters

were turned up and the rig was left for several days to dry. As a final precaution the rig was re-sealed and a hard vacuum was pulled for several days, to remove any remaining moisture. The kerosine was then pumped into the test rig via a fuel filter using a small internal gear pump.

### **5.3.1 Kerosine Pump Tests.**

First the head-flow and efficiency tests were performed on the pump, maximum flow and the BEP were similar to those of water. It was then the intention to repeat the same NPSH tests on kerosine as on water. However although no problems were encountered with the vacuum pump method of test at 20°C or 30°C. Attempts to conduct NPSH tests using the suction valve throttling method were impossible. The readings were too unstable and it became impossible to record any data, the reasons behind this will be discussed in a later chapter. The NPSH curve for the above tests can be found in Appendix E from which the 3% head drop data was found for each test conditions.

### **5.3.2 Kerosine Nozzle Tests.**

The kerosine nozzle tests were conducted much the same as the water tests, however due to safety reasons they were only conducted at 20°C and 30°C. The dissolved oxygen levels in kerosine proved to be more difficult to maintain than with water. There were no problems at 100% and 50% of saturation but to maintain a saturation level of <10% during a test run was impossible, as the kerosine re-absorbed air at a much faster rate. After several trials it was found that a saturation level of between 20-25 % was possible to maintain relatively easily. The resulting Efficiency - Free stream velocity curves are in Appendix E, the subsequent analysis and the effect of the various test conditions on  $\sigma_i$ ,  $\sigma_{3\%}$  and  $\sigma_{fd}$  will be discussed in later chapters. The cavity length data was harder to obtain, because of the nature of the cavitation although inception was an easily defined point



## **5.4 Gas Oil Tests.**

The kerosine was drained from the test rig, and it was cleaned and dried as before. The gas oil was then pumped into the rig via a fuel filter.

### **5.4.1 Gas Oil Pump Tests.**

The tests performed were the same as those for kerosine. Similar problems were encountered with the suction valve throttling method of NPSH test and therefore they were not performed. The NPSH curves for the tests using the vacuum pump method can be found in Appendix F

### **5.4.2 Gas Oil Nozzle Tests.**

The nozzle tests conducted were also similar to the kerosine nozzle tests. Including the same problem with the low oxygen content levels. The lowest achievable oxygen content that was maintainable for the duration of a test was 20-25% of saturation. The point of incipient cavitation was easily noted, but as with kerosine subsequent cavity lengths were hard to define, see results and discussion. The efficiency - free stream velocity plots can be found in Appendix F.

## 6. Results of experimental work.

### 6.1 Introduction.

This chapter describes the results of the experimental work undertaken and is broken up into four main areas. First section looks at the comparison of the standard pump curves for the three fluids. The Second section examines the NPSH tests undertaken, looking at the differences between the NPSH test methods, and the differences between the fluids. The nozzle results are tackled in the third section examining the effects of dissolved oxygen, temperature, and fluid type. The final section looks at comparisons between the nozzle results and the pump NPSH tests. Discussion and comments on the results are left until the next chapter.

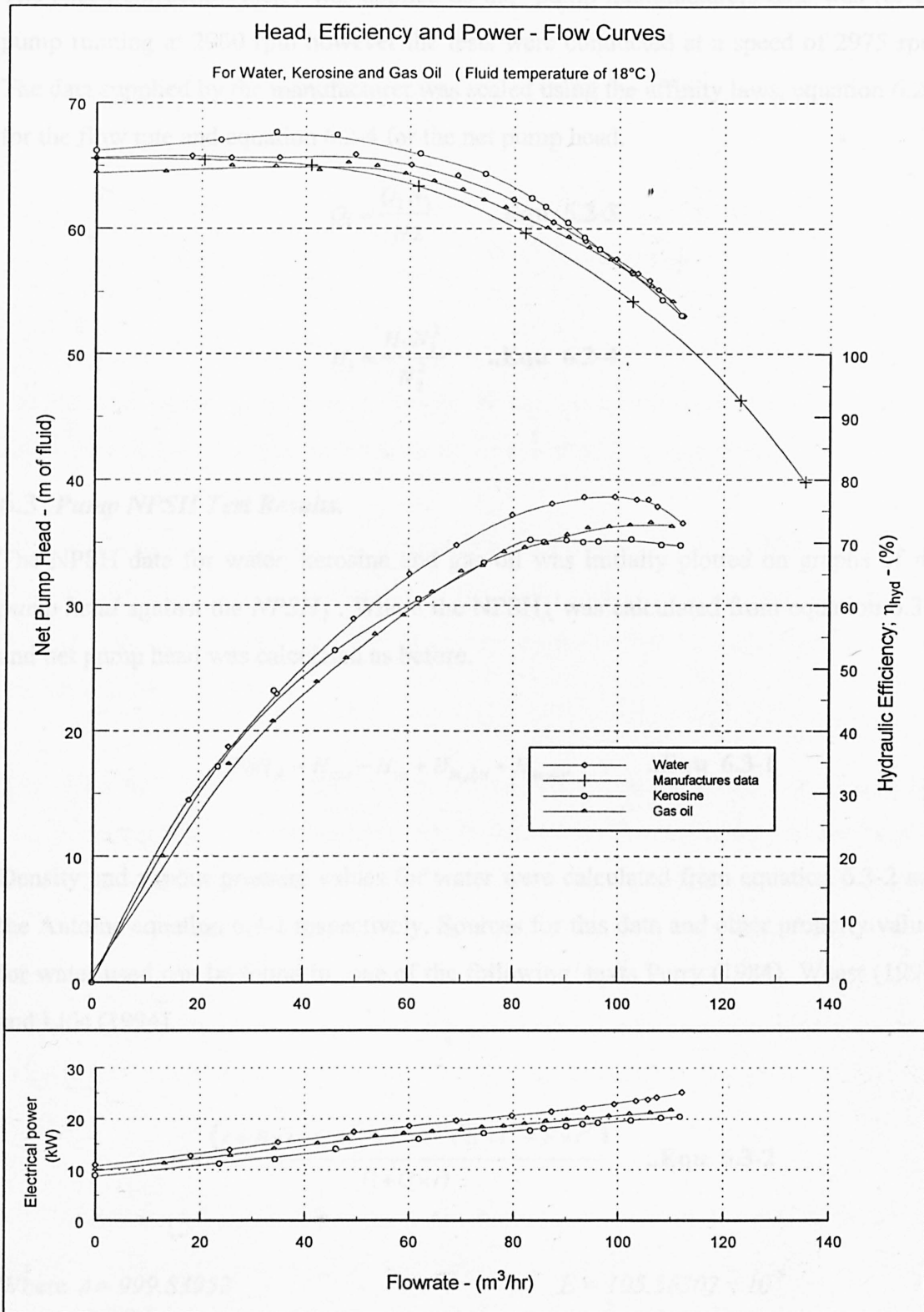
### 6.2 Pump Performance Curve Tests Results.

The pump performance curves (See figure 6.2-1) plots *head-flow*, *efficiency-flow* and *power-flow* characteristics, for water, kerosine, gas oil. The manufacturers *head-flow* data has also been included, after it was corrected for speed. The net pump head is found from equation 6.2-1.

$$\text{Net pump head; } H_{net} = \frac{(P_{out} - P_{in})}{\rho g} + \frac{(V_{out}^2 - V_{in}^2)}{2g} + (z_{out} - z_{in}) \quad \text{..Equ 6.2-1}$$

and the pumps hydraulic efficiency is found from equation 6.2-2

$$\text{Hydraulic efficiency; } \eta_{hyd} = \frac{(\text{Hydraulic power})}{(\text{Shaft power})} = \frac{(Qg\rho H_{net})}{(\text{Electrical power input} \times \eta_{motor})} \quad \text{..Equ 6.2-2}$$



**Figure 6.2-1 Pump Performance Curves.**

The speed correction factor was applied as the pump manufacturers data was for the pump running at 2900 rpm however the tests were conducted at a speed of 2975 rpm. The data supplied by the manufacturer was scaled using the affinity laws, equation 6.2-3 for the flow rate and equation 6.2-4 for the net pump head.

$$Q_1 = \frac{Q_2 N_1}{N_2} \quad \text{..Equ 6.2-3}$$

$$H_1 = \frac{H_2 N_1^2}{N_2^2} \quad \text{..Equ 6.2-4}$$

### 6.3 Pump NPSH Test Results.

The NPSH data for water, kerosine and gas oil was initially plotted on graphs of *net pump head* against the  $NPSH_A$ . Where the  $NPSH_A$  was calculated from equation 6.3-1 and net pump head was calculated as before.

$$NPSH_A = H_{atm} - H_{vp} + H_{in,dyn} + H_{in,stat} \quad \text{..Equ 6.3-1}$$

Density and vapour pressure values for water were calculated from equation 6.3-2 and the Antoine equation 6.3-1 respectively. Sources for this data and other property values for water used can be found in one of the following texts Perry (1984), Weast (1990) and Lide (1994).

$$\rho = \frac{(A + B \times t - C \times t^2 - D \times t^3 + E \times t^4 - F \times t^5)}{(1 + G \times t)} \quad \text{..Equ 6.3-2}$$

Where  $A = 999.83952$

$$B = 16.954176$$

$$C = 7.9870401 \times 10^{-3}$$

$$D = 46.170461 \times 10^{-6}$$

$$E = 105.56302 \times 10^{-9}$$

$$F = 280.54253 \times 10^{-12}$$

$$G = 16.87985 \times 10^{-3}$$

$t = \text{Fluid temperature in } ^\circ\text{C}$

$$P_{vp} = \exp \left\{ A_1 - \frac{A_2}{A_3 + T} \right\} \text{ ..Equ 6.3-3}$$

Where  $A_1 = 23.195$

$A_3 = -0.4629 \times 10^2$

$A_2 = 0.314 \times 10^4$

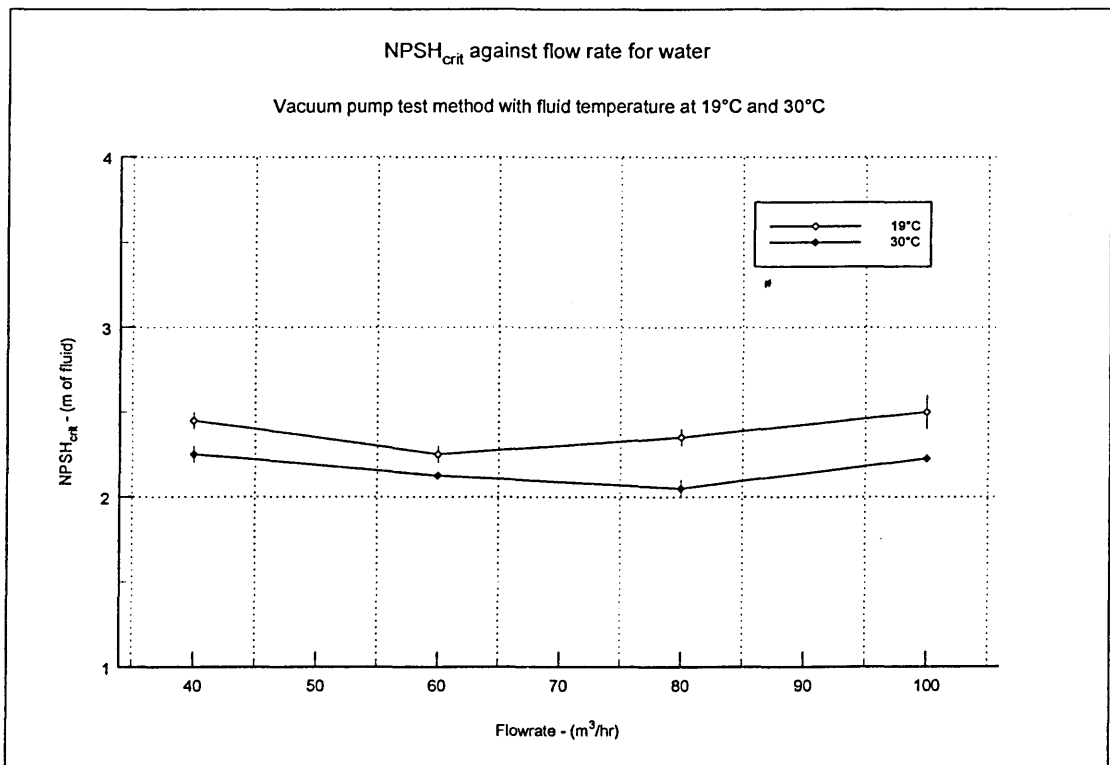
$T = \text{Fluid temperature in } ^\circ\text{C}$

Density and vapour pressure data for gas oil was taken from Birkett (1995). Kerosine density and vapour pressure data was taken from Rolls-Royce Ltd (1981).

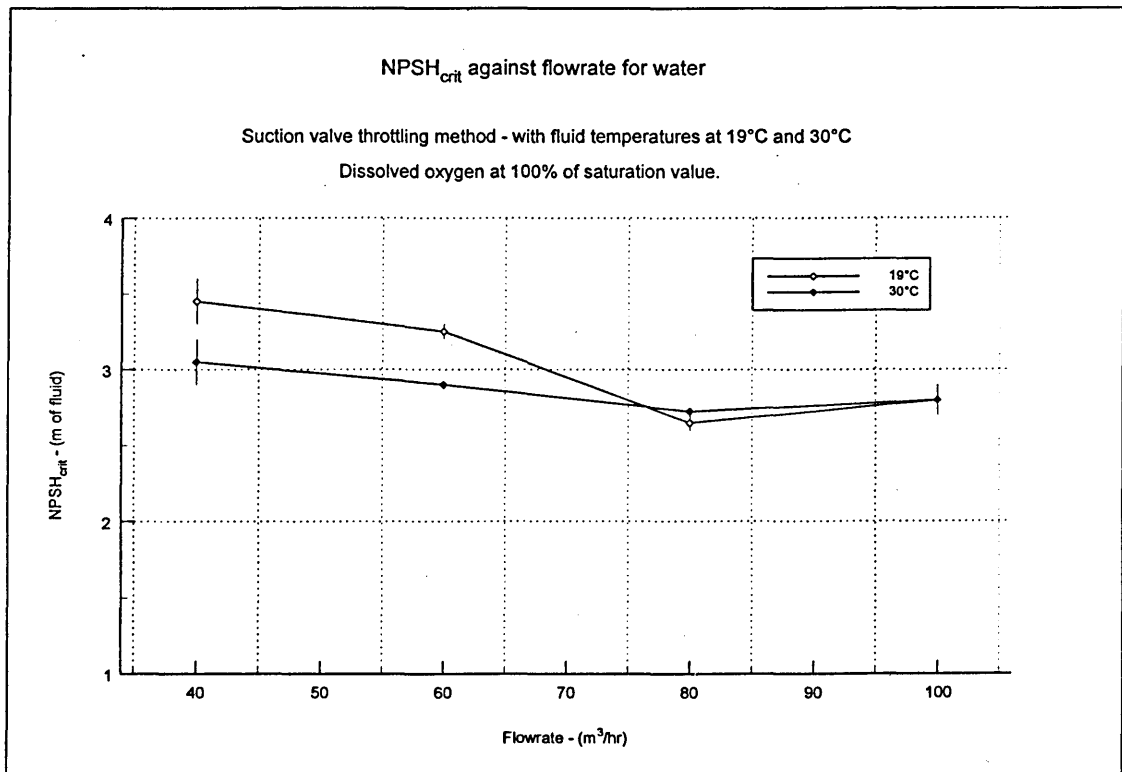
From the resultant NPSH curves (found in appendices D, E and F),  $\text{NPSH}_{\text{crit}}$  at a 3% drop in head from flat line head could be found, for each of the four flow rates the tests were conducted at. These were then plotted on graphs of  $\text{NPSH}_{\text{crit}}$  against flow rate for the various conditions.

The effect of NPSH test method on the critical NPSH was examined first of all (Note this comparison can only be made for water as suction valve throttling was not possible for the hydrocarbons.) Figures 6.3-1, 6.3-2 and 6.3-3 show the effect of temperature on the two methods, the vacuum pump method and suction valve throttling with water at 100% and <10% dissolved oxygen saturation. Figures 6.3-4 and 6.3-5 compare the different NPSH test methods at constant temperatures of 20°C and 30°C. Note that there were two test points taken for each flow rate at each condition the value shown is the average.

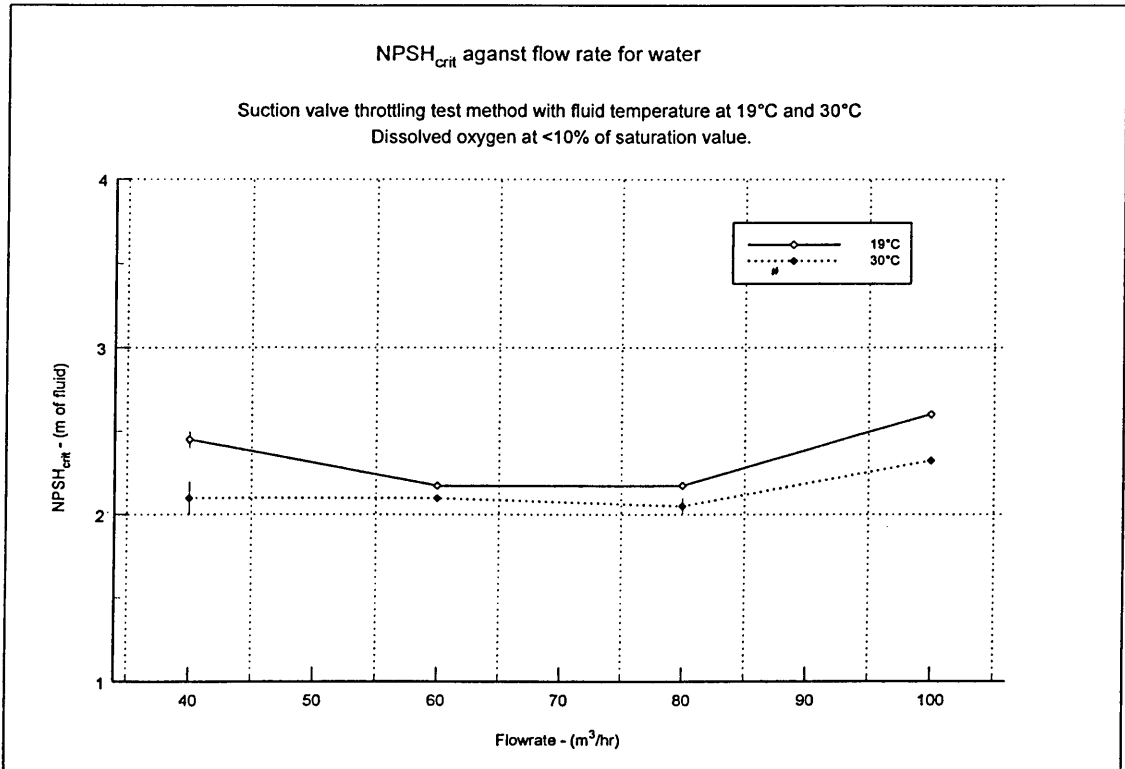
Figures 6.3-6, 6.3-7 and 6.3-8 show the comparisons between the critical NPSH for kerosine, water and gas oil. The comparisons are made for the same test method at temperatures of 20°C and 30°C.



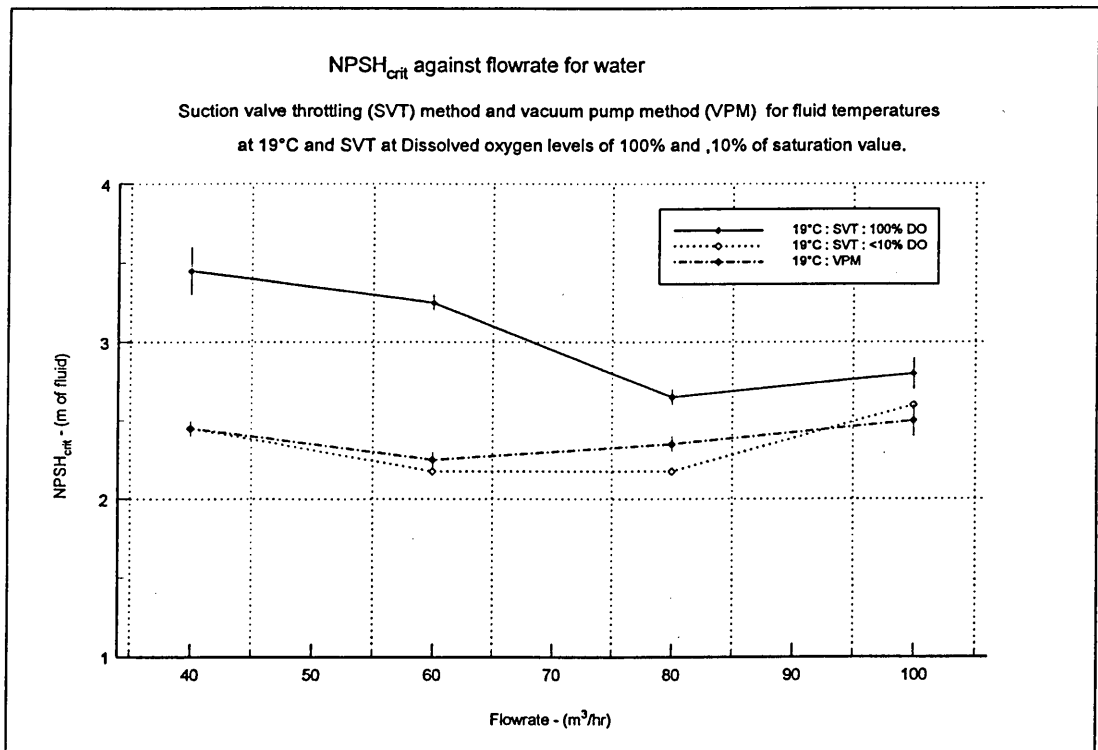
**Figure 6.3-1 Effect of temperature on the vacuum pump NPSH test method.**



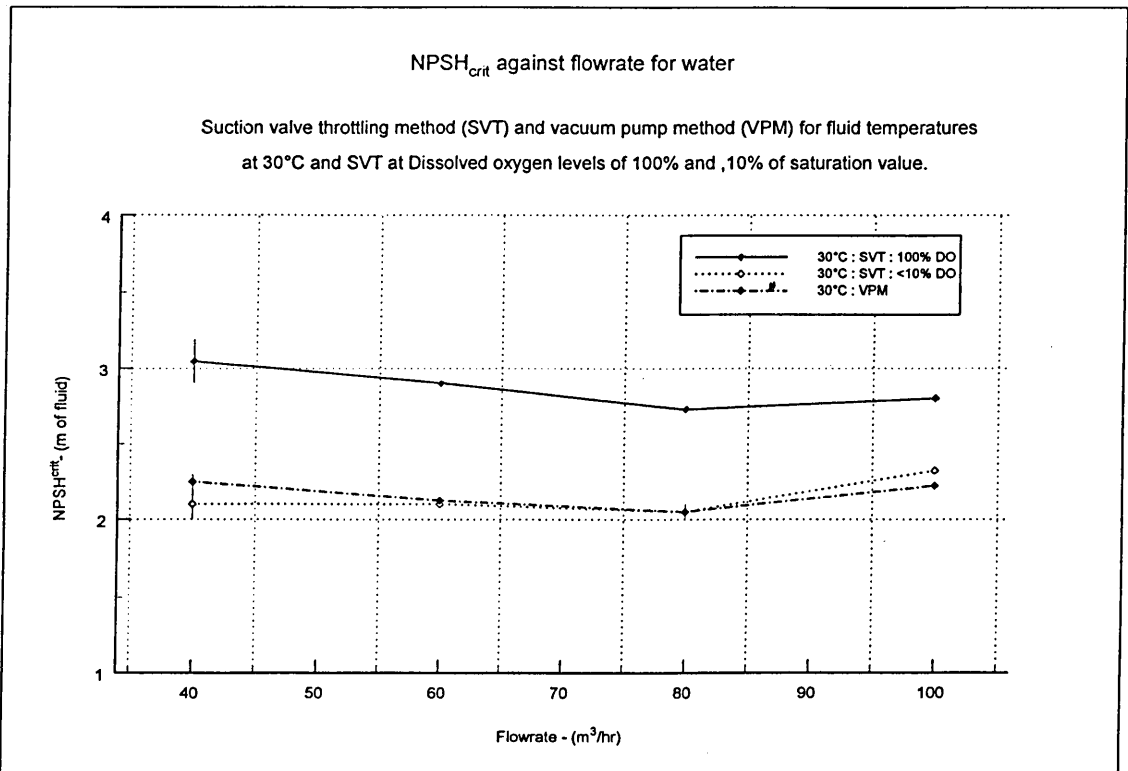
**Figure 6.3-2 Effect of temperature on the suction valve throttling NPSH test method ( 100% dissolved oxygen of the saturation value).**



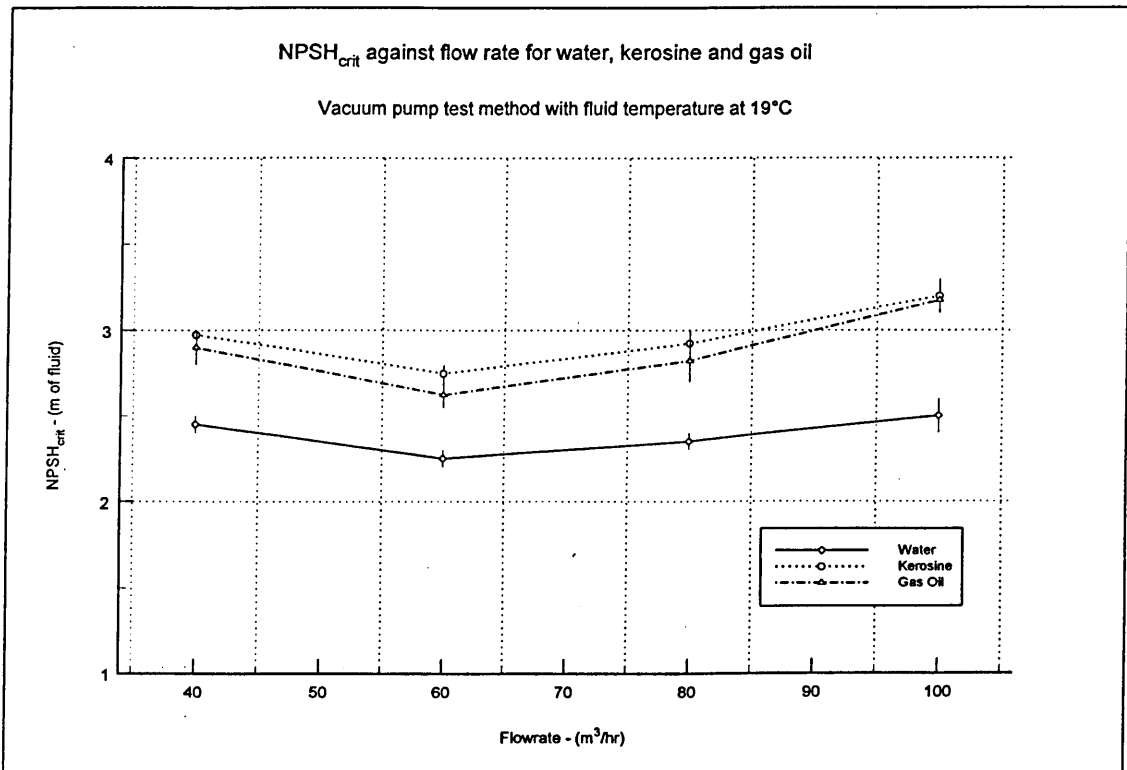
**Figure 6.3-3 Effect of temperature on the suction valve throttling NPSH test method (<10% dissolved oxygen of the saturation value).**



**Figure 6.3-4 Comparison of NPSH test methods : Vacuum pump and suction valve throttling (Temperature 19°C).**

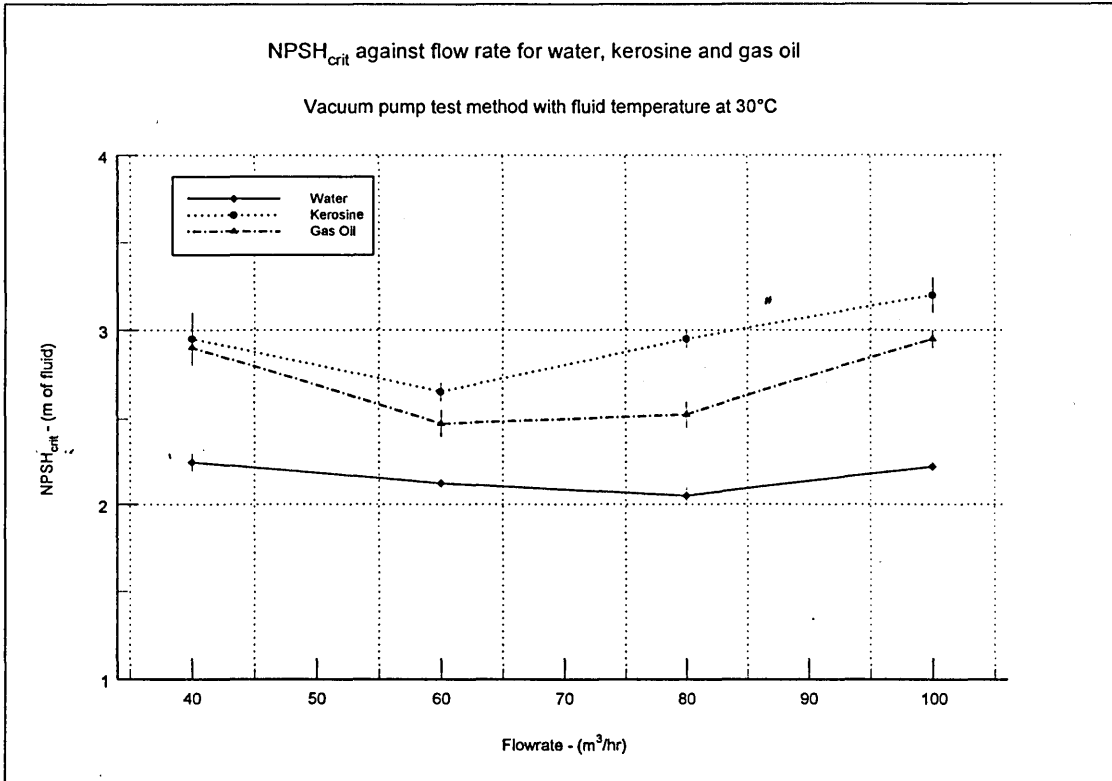


**Figure 6.3-5 Comparison of NPSH test methods : Vacuum pump and suction valve throttling (Temperature 30°C).**

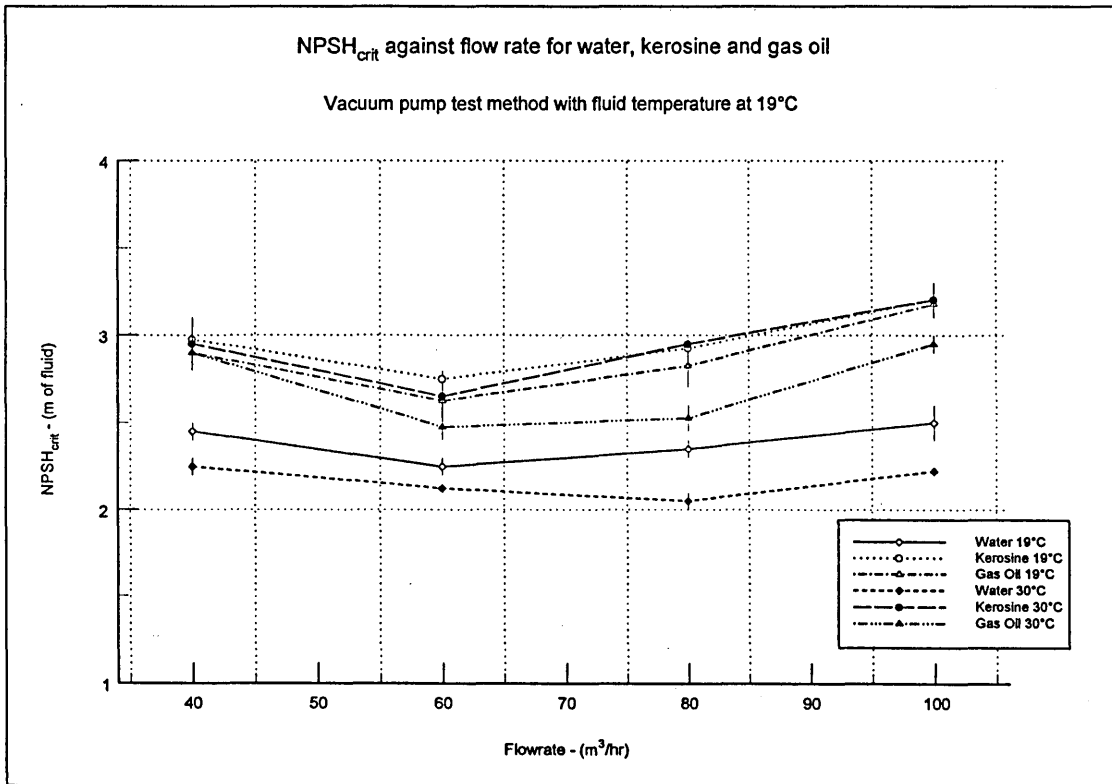


**Figure 6.3-6 Comparison of critical NPSH of water, kerosine and gas oil ( Vacuum pump method at 19°C )**





**Figure 6.3-7 Comparison of critical NPSH of water, kerosine and gas oil ( Vacuum pump method at 30°C )**



**Figure 6.3-8 Comparison of critical NPSH of water, kerosine and gas oil ( Vacuum pump method 19°C and 30°C )**

## 6.4 Nozzle Test Results.

The nozzle tests results are broken down into four sections water, kerosine, gas oil and the comparison of the three fluids. The effect of fluid temperature, free stream velocity and dissolved oxygen are shown on incipient cavitation;  $\sigma_i$ , the 3% drop in efficiency;  $\sigma_{3\%}$  and fully developed cavitation  $\sigma_{fd}$ . The data for the fluids was initially plotted on *Nozzle efficiency* (Equation 6.4-1) against *free stream velocity (F.S.V.)* graphs for ease of display and analysis. If the F.S.V was converted to sigma (Equation 6.4-2) the drop off points on the curves would overlap making it

$$\eta_N = \frac{(P_d - P_t)}{(P_o - P_t)} \quad \text{..Equ 6.4-1}$$

$$\sigma = \frac{(P_o - P_v)}{\frac{1}{2} \rho V_o^2} \quad \text{..Equ 6.4-2}$$

harder to obtain  $\sigma_{3\%}$  and  $\sigma_{fd}$ . The free stream velocity was therefore read from the graphs for the condition required and converted by equation 6.4-2. As the free stream velocity at visually noted incipient cavitation was recorded this could be directly converted into  $\sigma_i$ . (The nozzle efficiency plots for water, kerosine and gas oil can be found in appendices D, E and F respectively)

### 6.4.1 Water nozzle results.

From the tests the effect of dissolved oxygen, temperature and free stream velocity could be shown on cavitation at  $\sigma_i$ ,  $\sigma_{3\%}$  and  $\sigma_{fd}$ . First the effect of temperature over the range of 20°C to 50°C can be shown on the following three graphs ( Figures 6.4-1 to 6.4-3 ). They show data for the reference pressures 2.0, 1.5 and 1.0 bar respectively for the three cavitation conditions at three different dissolved oxygen concentrations, each condition is represented by two test points. As the temperature over this range showed no significant effect, as expected ( Furness (1973) and Chivers (1967) ), all the results were then plotted to see the effect of dissolved oxygen on the cavitation conditions  $\sigma_i$ ,  $\sigma_{3\%}$  and  $\sigma_{fd}$ , Figure 6.4-4 and the effect of free stream velocity can be seen in Figure 6.4-5. These last two plots displayed the averaged values with a band showing the maximum and minimum values.

Temperature effect on the cavitation coefficient  $\sigma$  for the nozzle (Water).

For inception, 3% efficiency drop and fully developed cavitation at various dissolved oxygen content levels and reference pressure 1.5bar

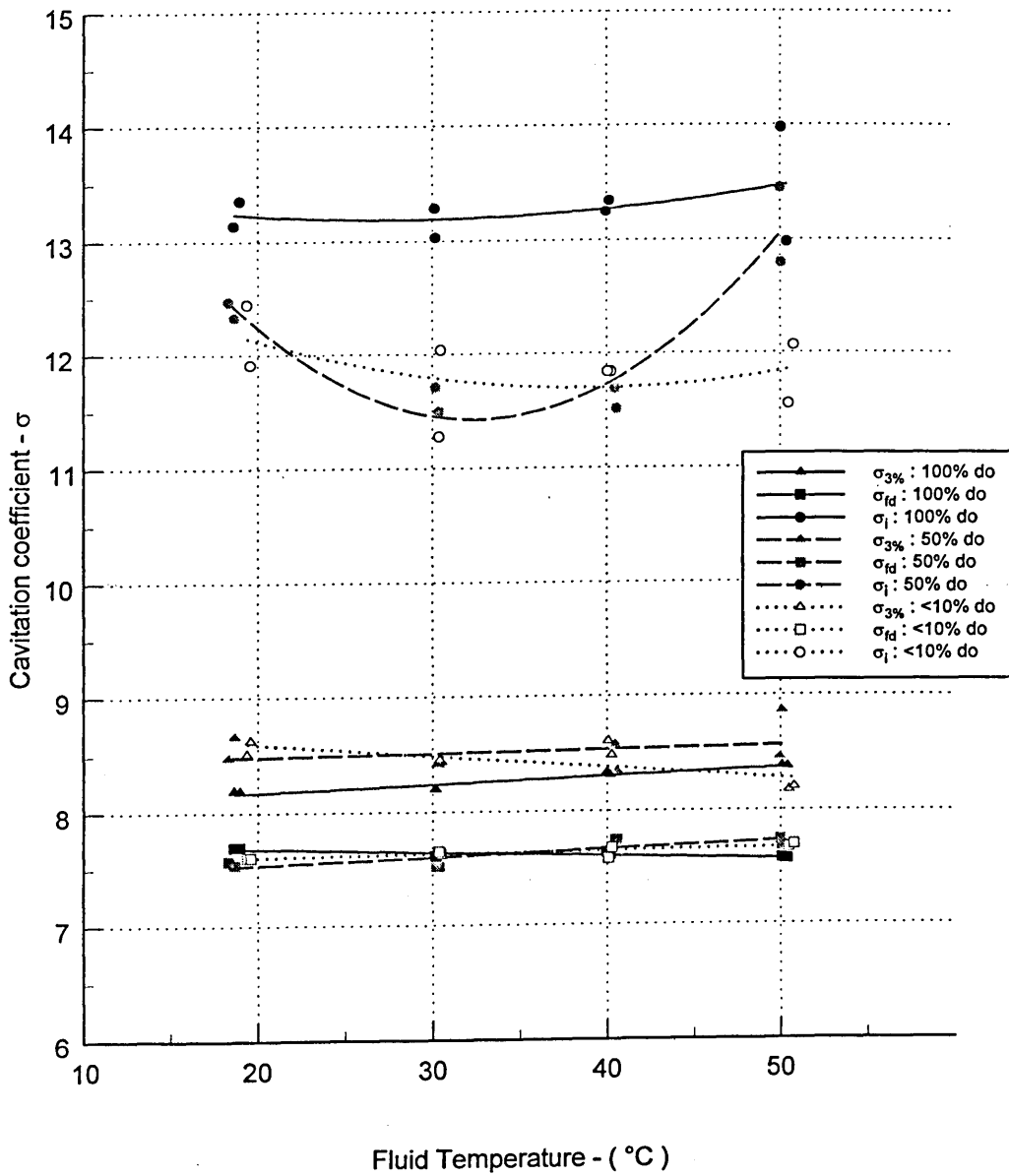


Figure 6.4-1 Effect of temperature on water cavitating in the nozzle. (Ref. pressure 2.0 bar)

Temperature effect on the cavitation coefficient  $\sigma$  for the nozzle (Water).

For inception, 3% efficiency drop and fully developed cavitation at various dissolved oxygen content levels and reference pressure 2.0 bar

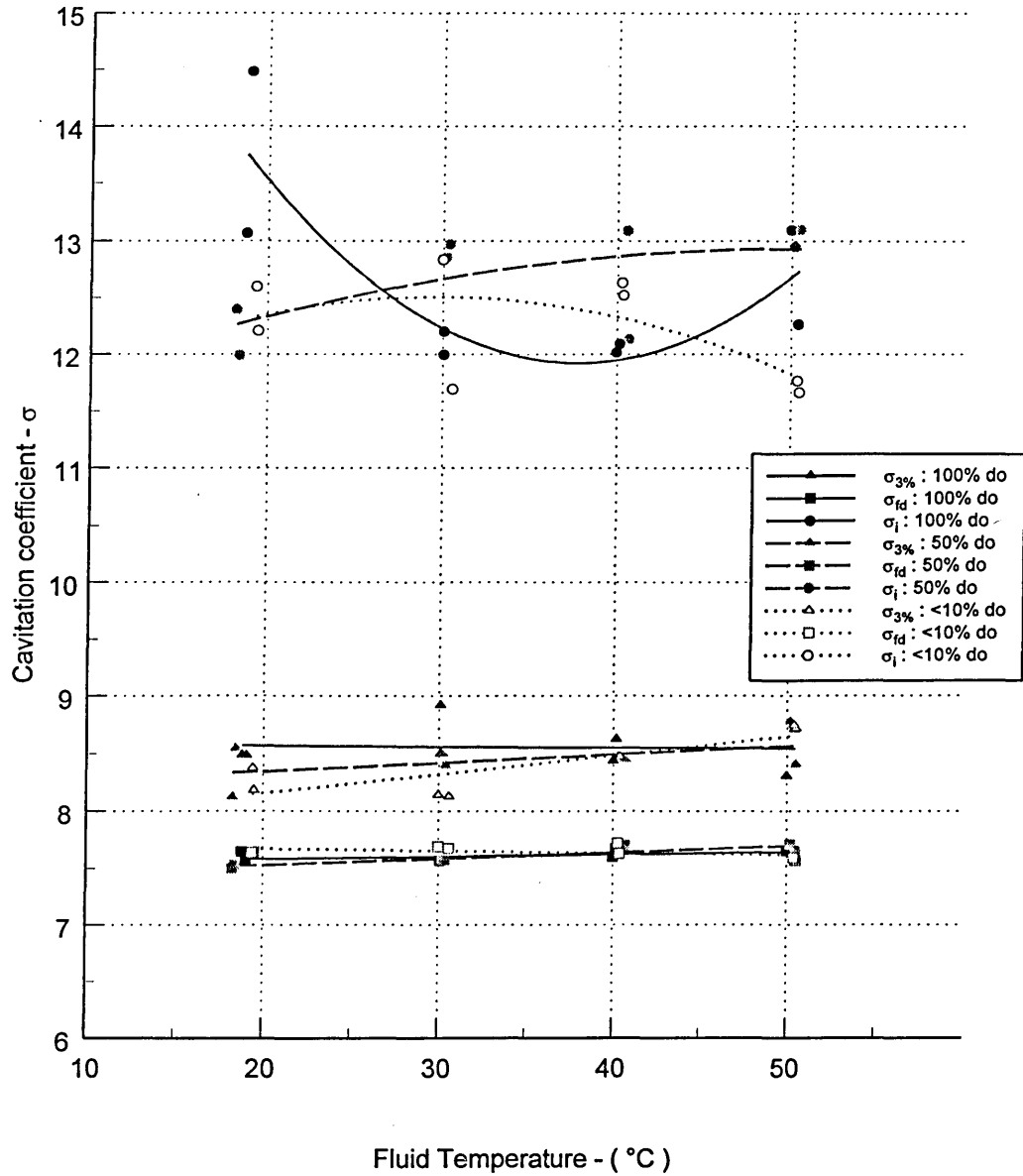


Figure 6.4-2 Effect of temperature on water cavitating in the nozzle. (Ref. pressure 1.5 bar)

Temperature effect on the cavitation coefficient  $\sigma$  for the nozzle (Water).

For inception, 3% efficiency drop and fully developed cavitation at various dissolved oxygen content levels and reference pressure 1.0 bar

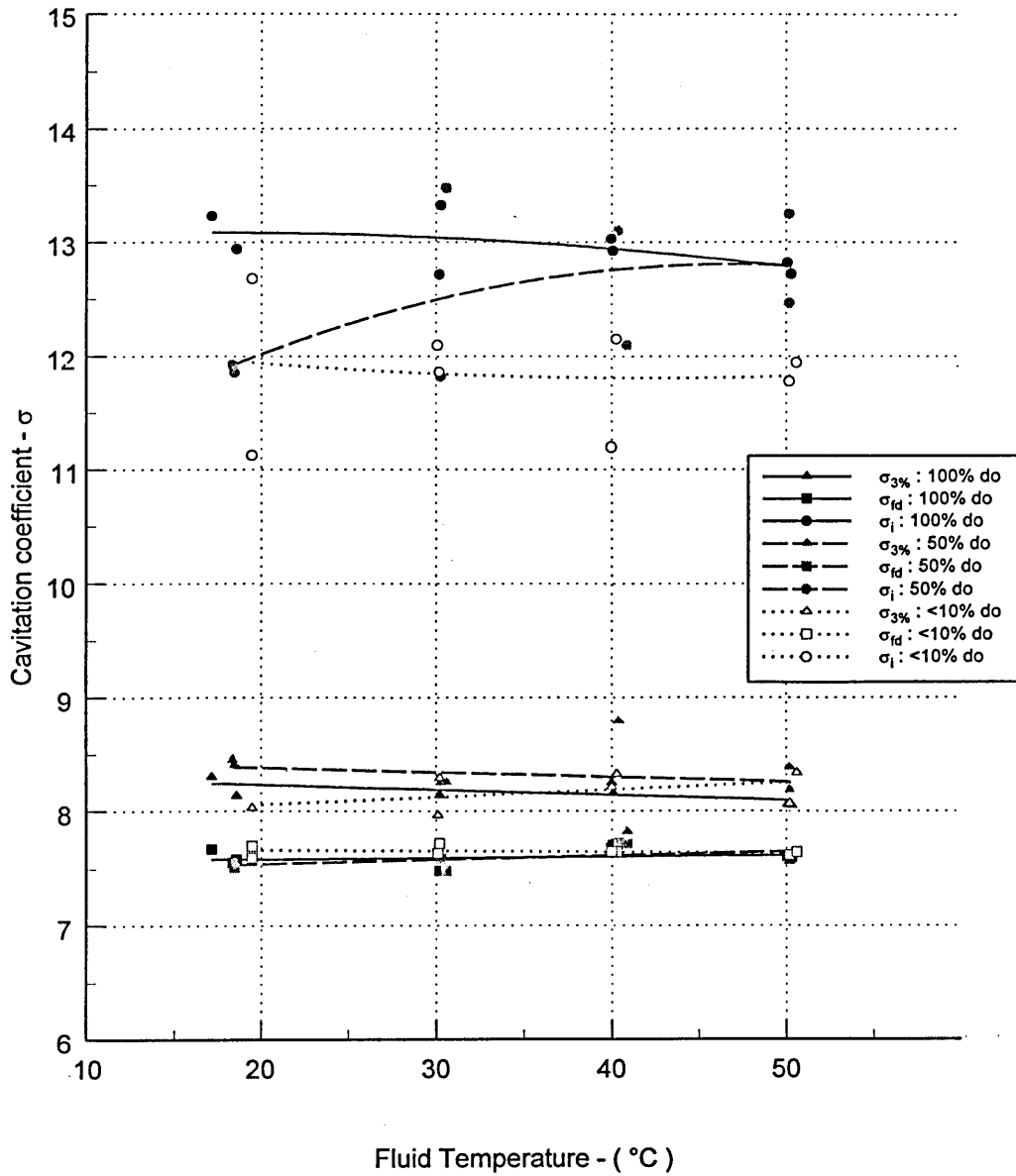


Figure 6.4-3 Effect of temperature on water cavitating in the nozzle. (Ref. pressure 1.0 bar)

Effect of dissolved oxygen on the cavitation coefficient  $\sigma$   
for the nozzle (Water)

For inception  $\sigma_i$ , 3% efficiency drop  $\sigma_{3\%}$  and fully developed  $\sigma_{fd}$  cavitation  
at reference pressures 2.0, 1.5 and 1.0 bar

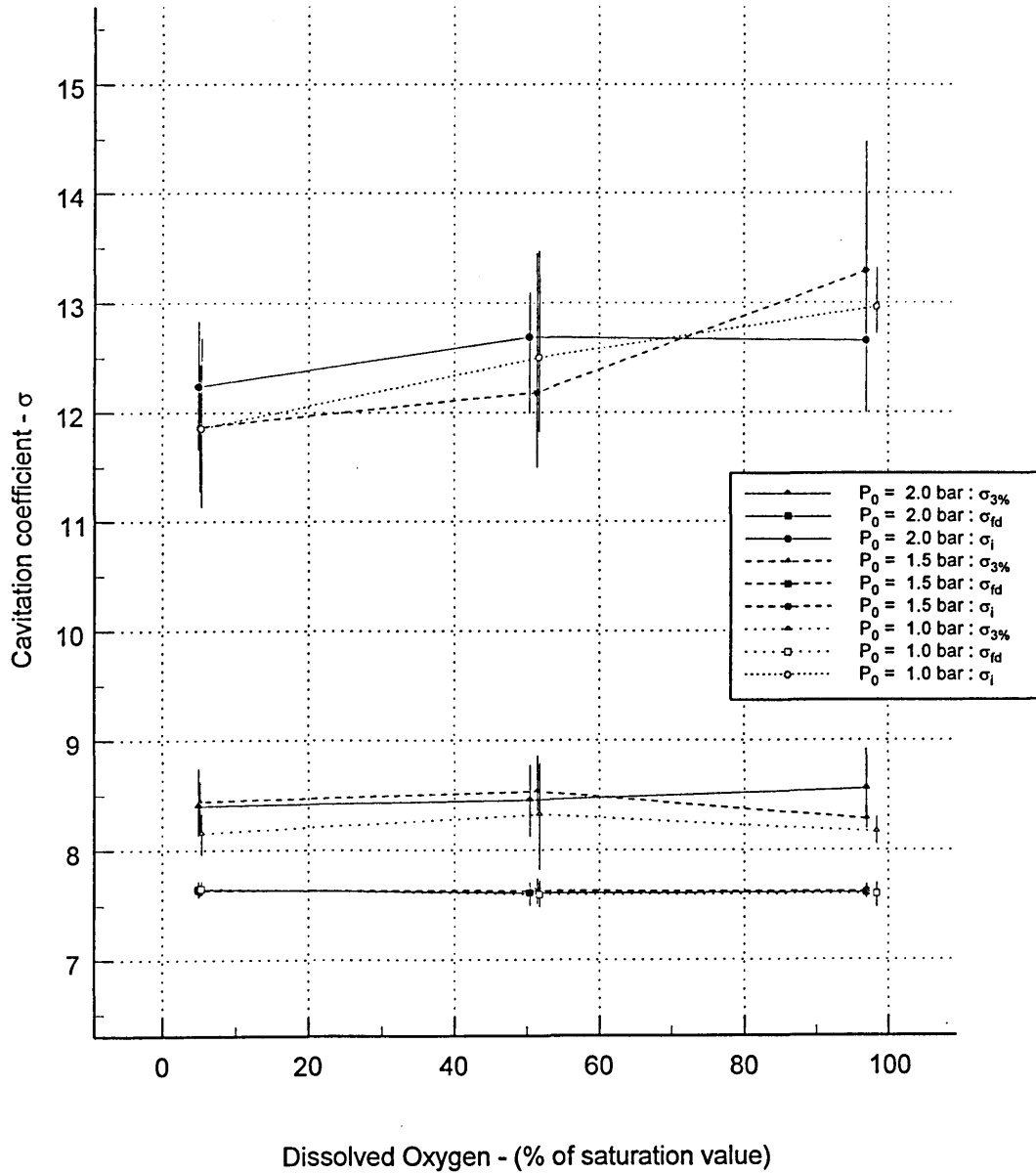
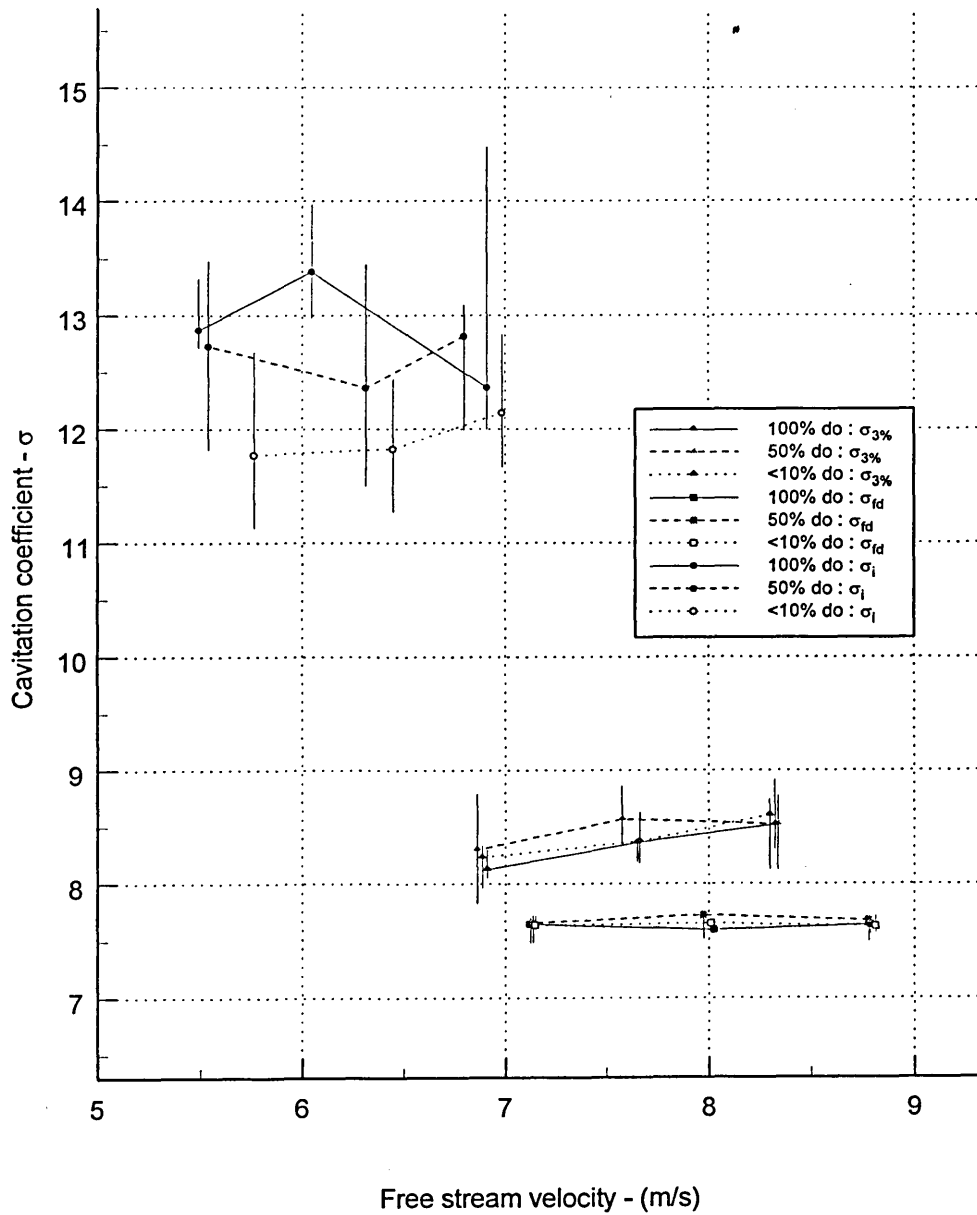


Figure 6.4-4 Effect of dissolved oxygen on water cavitating in the nozzle.

### Effect of free stream velocity on the cavitation coefficient $\sigma$ for the nozzle (Water)

For inception  $\sigma_i$ , 3% efficiency drop  $\sigma_{3\%}$  and fully developed  $\sigma_{fd}$  cavitation.



**Figure 6.4-5 Effect of free stream velocity on water cavitating in the nozzle.**

### 6.4.2 Kerosine Nozzle Results.

As with water the effect of dissolved oxygen, temperature and free stream velocity could be shown on cavitation at  $\sigma_i$ ,  $\sigma_{3\%}$  and  $\sigma_{fd}$ . Figures 6.4-6 to 6.4-8, show the effect of temperature between 20°C and 30°C on the reference pressures 2.0, 1.5 and 1.0 bar respectively for the three cavitation conditions at three different dissolved oxygen concentrations. The temperature over this range showed no significant effect so all the results were plotted to see the effect of dissolved oxygen on the cavitation conditions  $\sigma_i$ ,  $\sigma_{3\%}$  and  $\sigma_{fd}$ , Figure 6.4-9 and the effect of free stream velocity, Figure 6.4-10.



Temperature effect on the cavitation coefficient  $\sigma$  for the nozzle (Kerosine).

For inception, 3% efficiency drop and fully developed cavitation  
at various dissolved oxygen content levels and reference pressure 2.0 bar

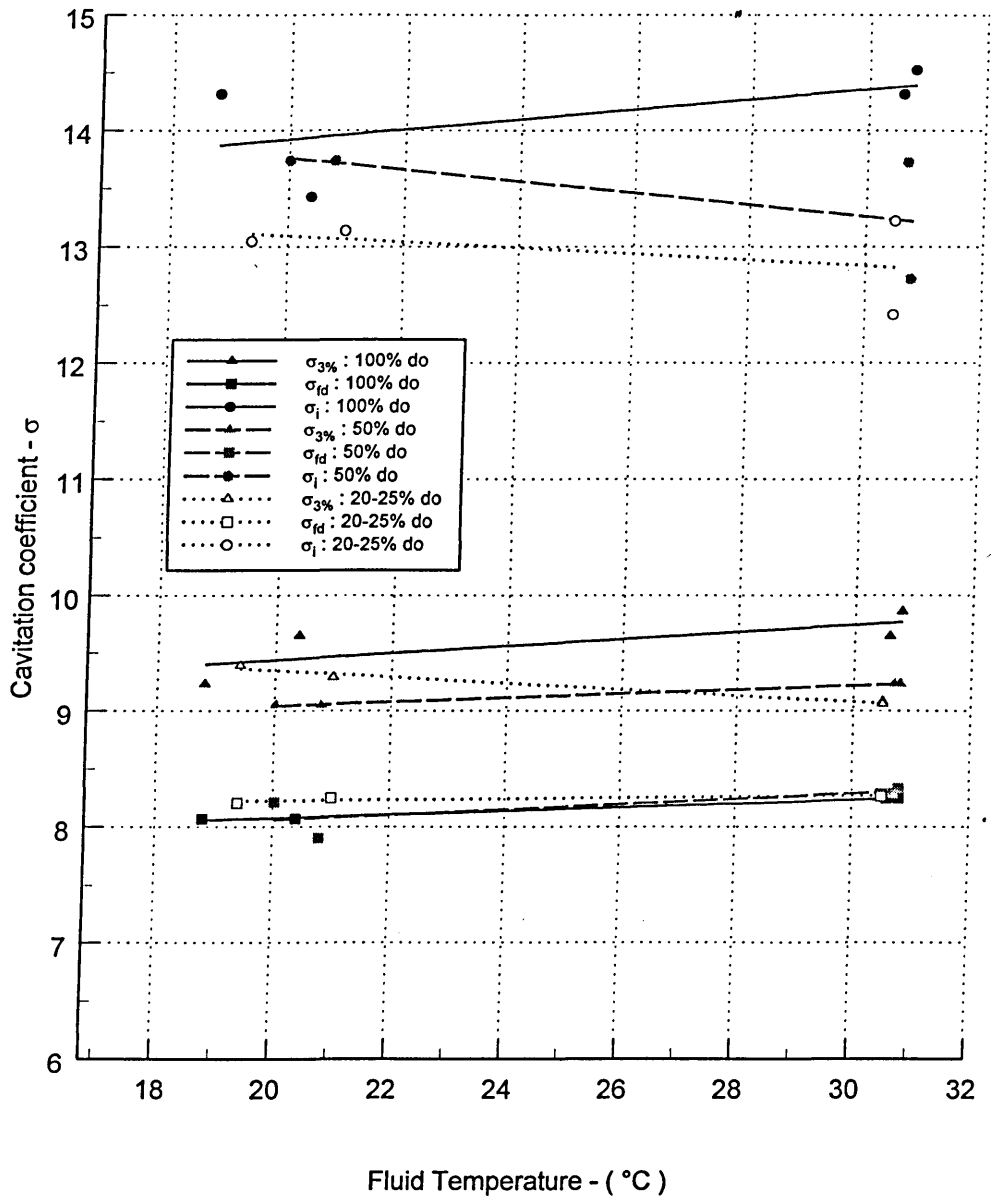


Figure 6.4-6 Effect of temperature on kerosine cavitating in the nozzle.  
(Ref. pressure 2.0 bar)

Temperature effect on the cavitation coefficient  $\sigma$  for the nozzle (Kerosine).

For inception, 3% efficiency drop and fully developed cavitation at various dissolved oxygen content levels and reference pressure 1.5 bar

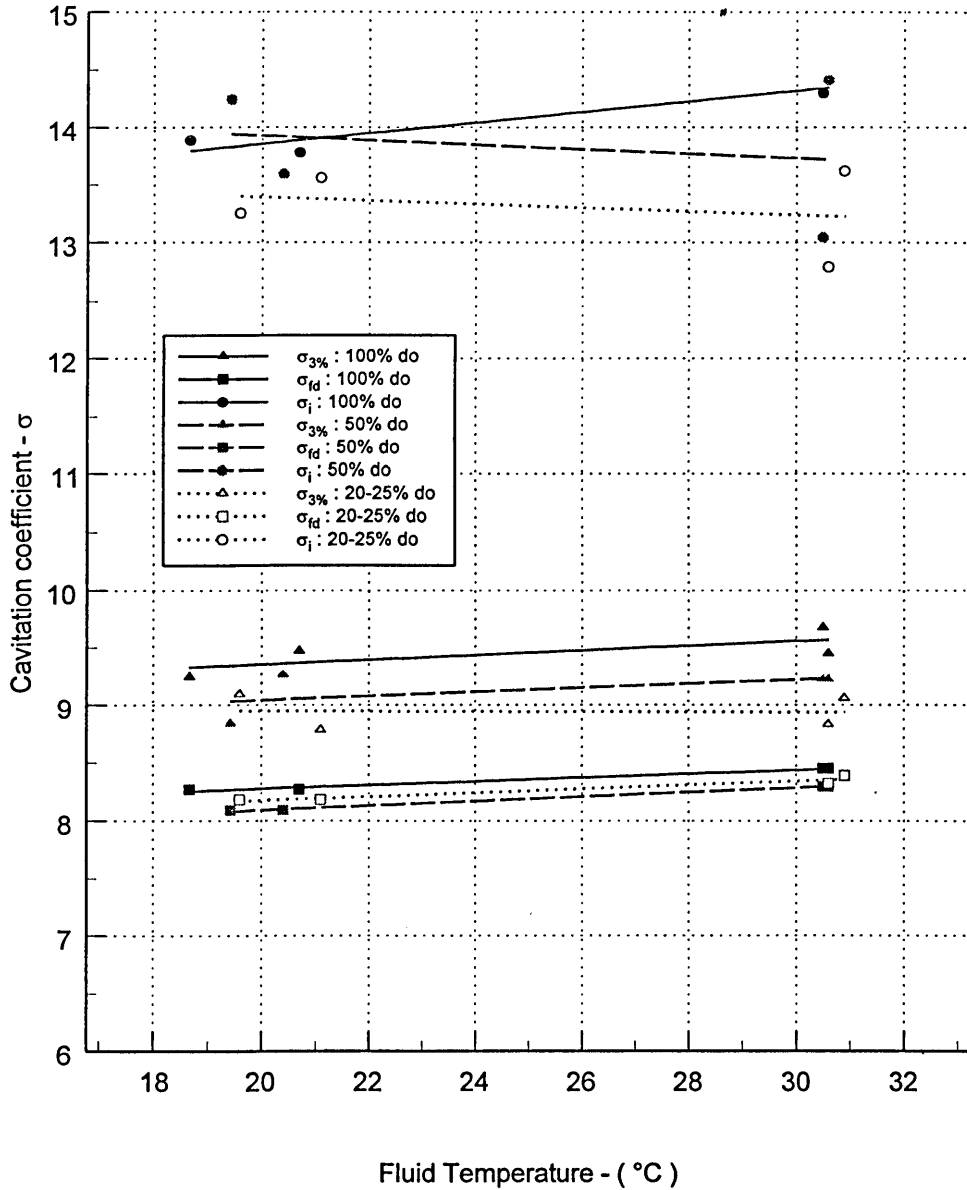


Figure 6.4-7 Effect of temperature on kerosine cavitating in the nozzle. (Ref. pressure 1.5 bar)

Temperature effect on the cavitation coefficient  $\sigma$  for the nozzle (Kerosine).

For inception, 3% efficiency drop and fully developed cavitation at various dissolved oxygen content levels and reference pressure 1.0 bar

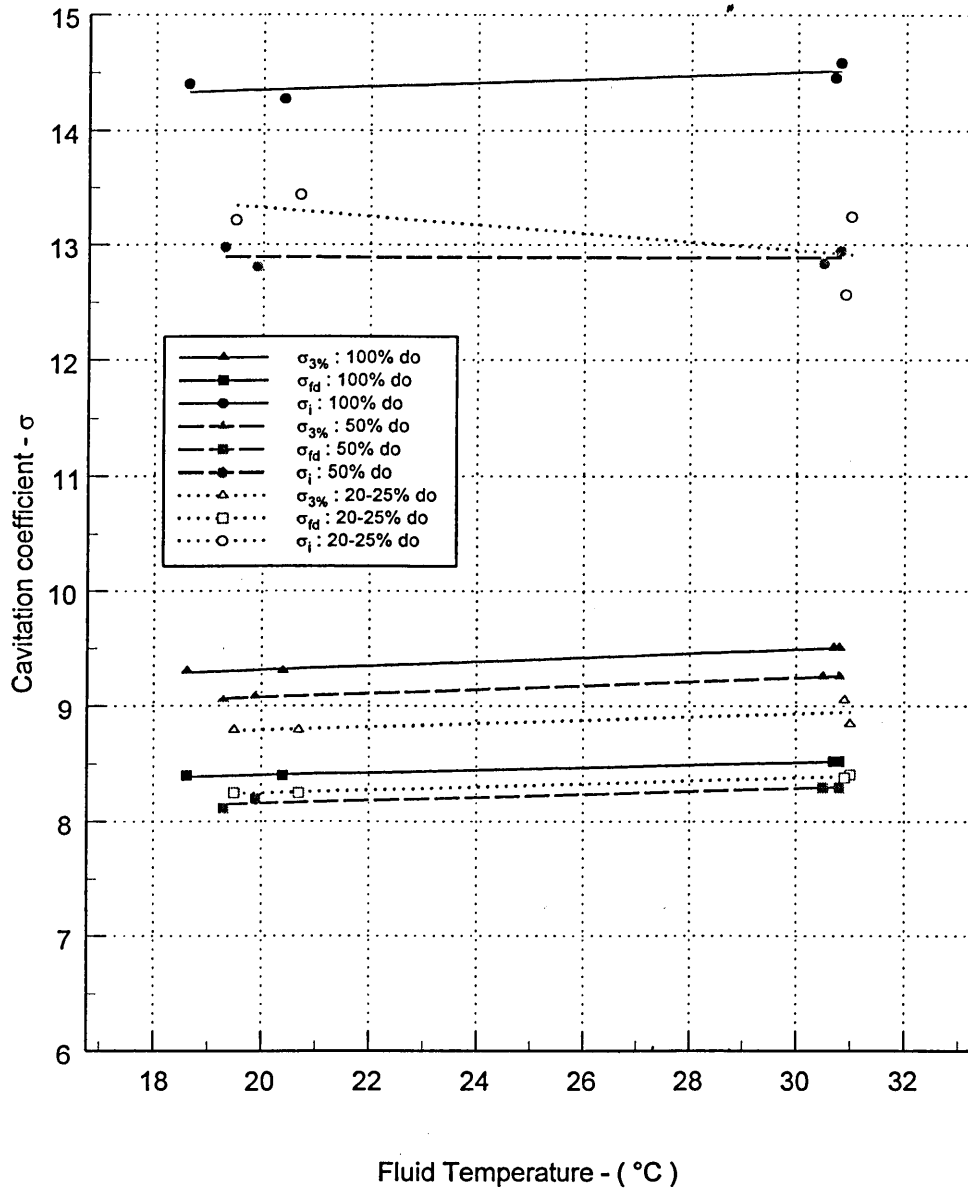


Figure 6.4-8 Effect of temperature on kerosine cavitating in the nozzle. (Ref. pressure 1.0 bar)

Effect of dissolved oxygen on the cavitation coefficient  $\sigma$   
for the nozzle (Kerosine)

For inception  $\sigma_i$ , 3% efficiency drop  $\sigma_{3\%}$  and fully developed  $\sigma_{fd}$  cavitation  
at reference pressures 2.0, 1.5 and 1.0 bar

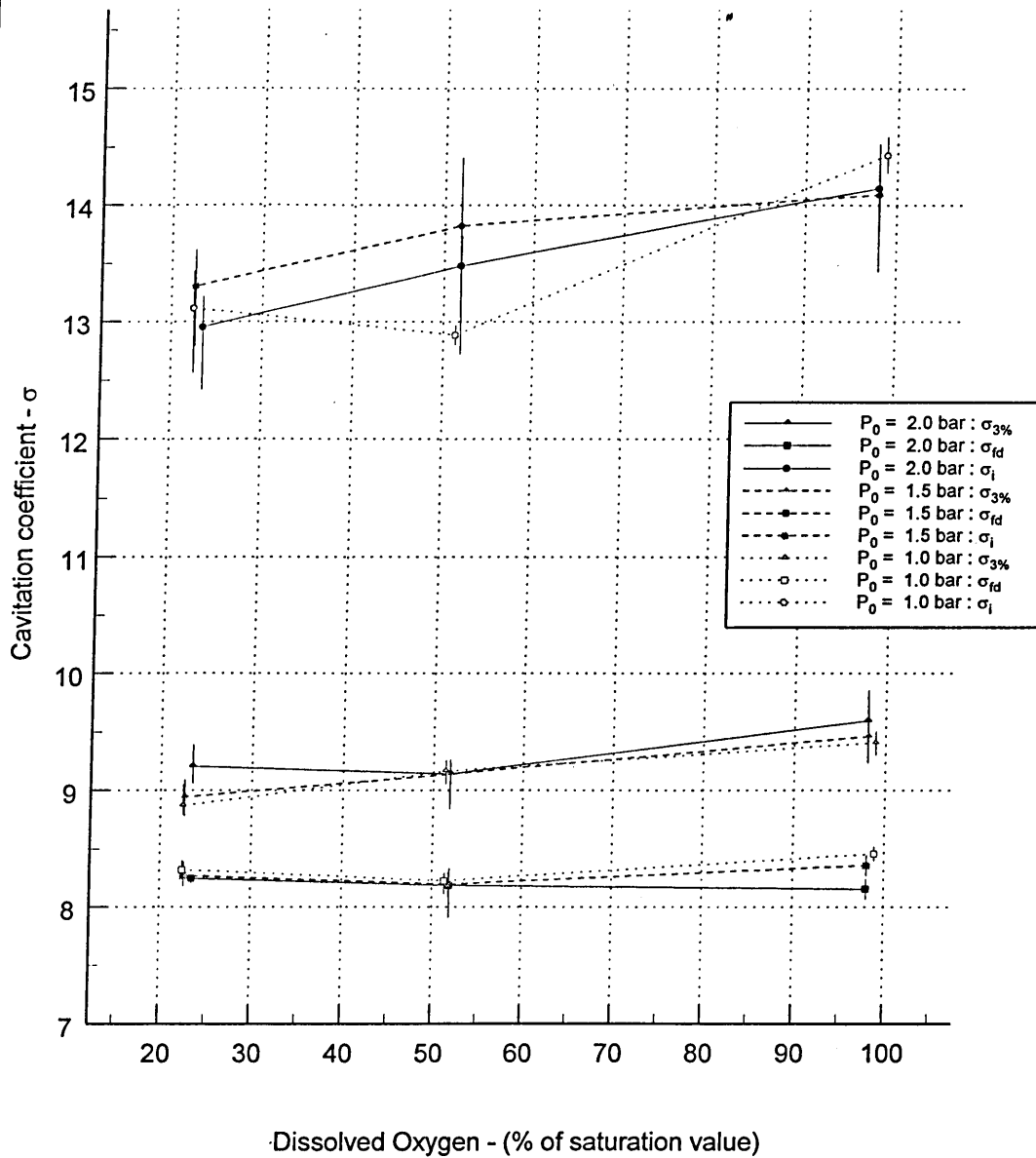


Figure 6.4-9 Effect of dissolved oxygen on kerosine cavitating in the nozzle.

Effect of free stream velocity on the cavitation coefficient  $\sigma$   
for the nozzle (Kerosine)

For inception  $\sigma_i$ , 3% efficiency drop  $\sigma_{3\%}$  and fully developed  $\sigma_{fd}$  cavitation.

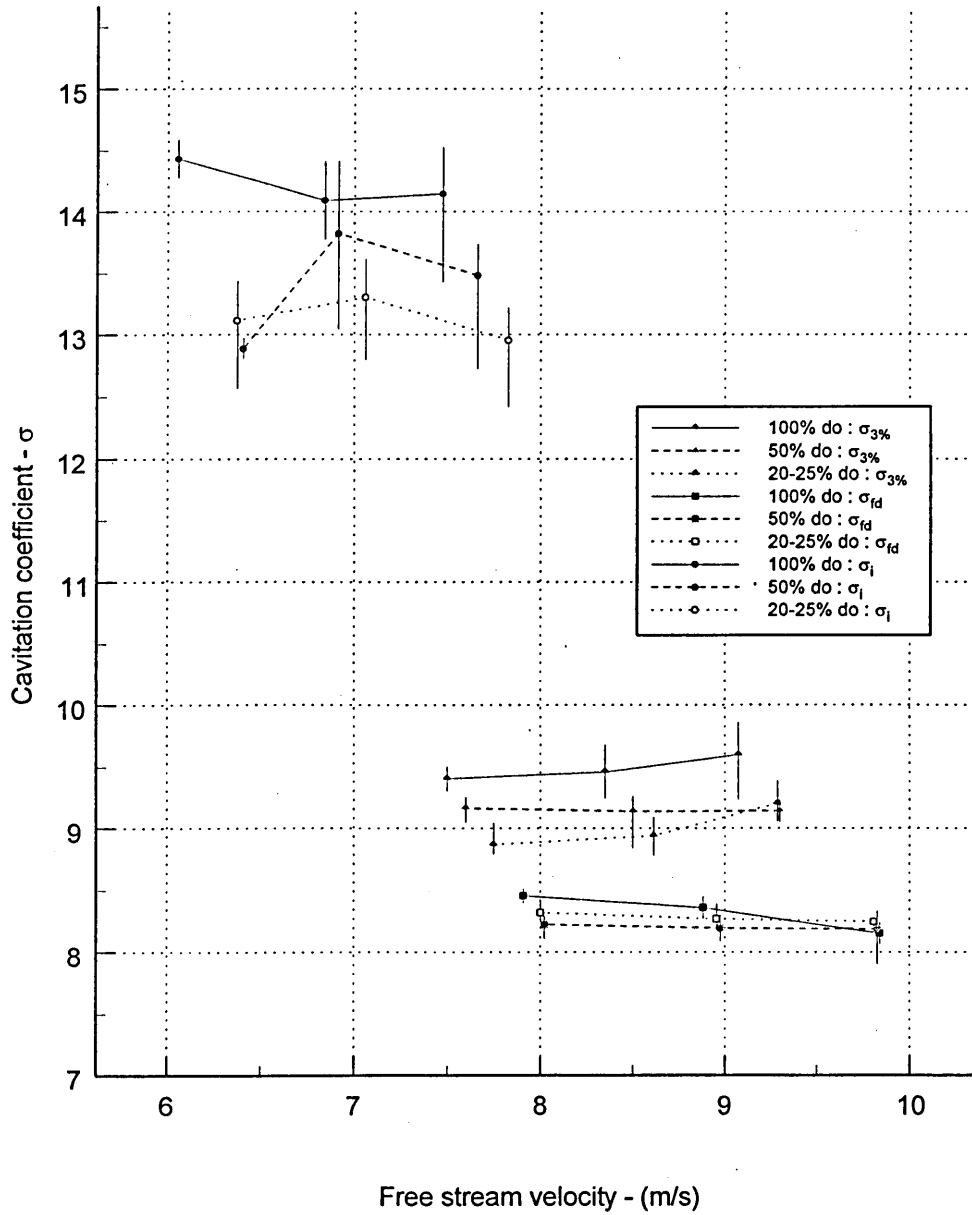


Figure 6.4-10 Effect of free stream velocity on kerosine cavitating in the nozzle.

### 6.4.3 Gas Oil Nozzle Results.

The same tests as performed on kerosine were conducted on gas oil, Therefore the following plots show the effect of temperature at 20°C and 30°C, ( Figures 6.4-11 to 6.4-13 ) on the reference pressures 2.0, 1.5 and 1.0 bar respectively for the three cavitation conditions at three different dissolved oxygen concentrations. As with kerosine, gas oil showed no significant temperature effect over this range so all the results were plotted to see the effect of dissolved oxygen on the cavitation conditions  $\sigma_i$ ,  $\sigma_{3\%}$  and  $\sigma_{fd}$ , Figure 6.4-14 and the effect of free stream velocity, Figure 6.4-15.

Temperature effect on the cavitation coefficient  $\sigma$  for the nozzle (Gas oil).

For inception, 3% efficiency drop and fully developed cavitation at various dissolved oxygen content levels and reference pressure 2.0 bar

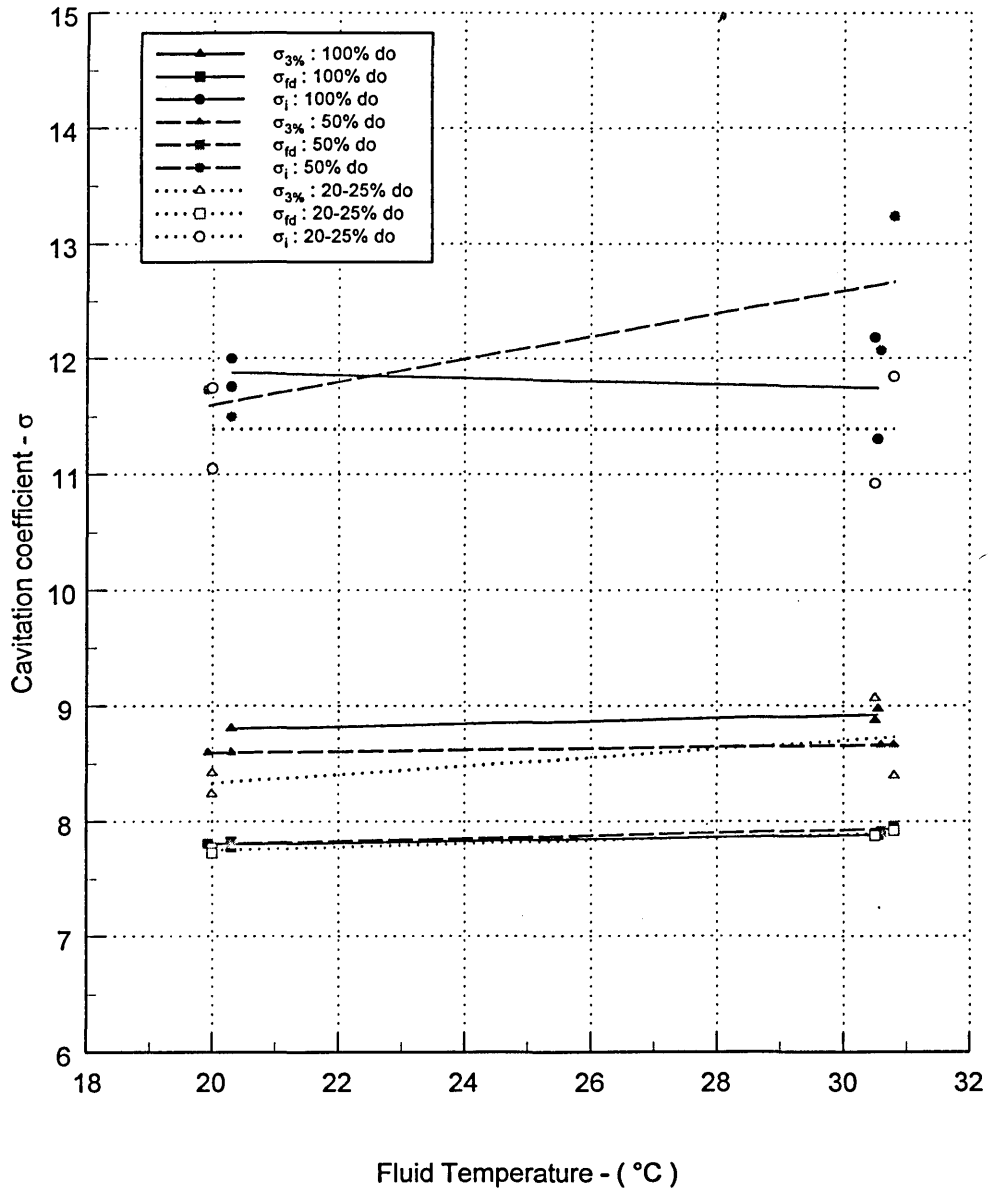


Figure 6.4-11 Effect of temperature on gas oil cavitating in the nozzle. (Ref. pressure 2.0 bar)

Temperature effect on the cavitation coefficient  $\sigma$  for the nozzle (Gas oil).

For inception, 3% efficiency drop and fully developed cavitation at various dissolved oxygen content levels and reference pressure 1.5 bar

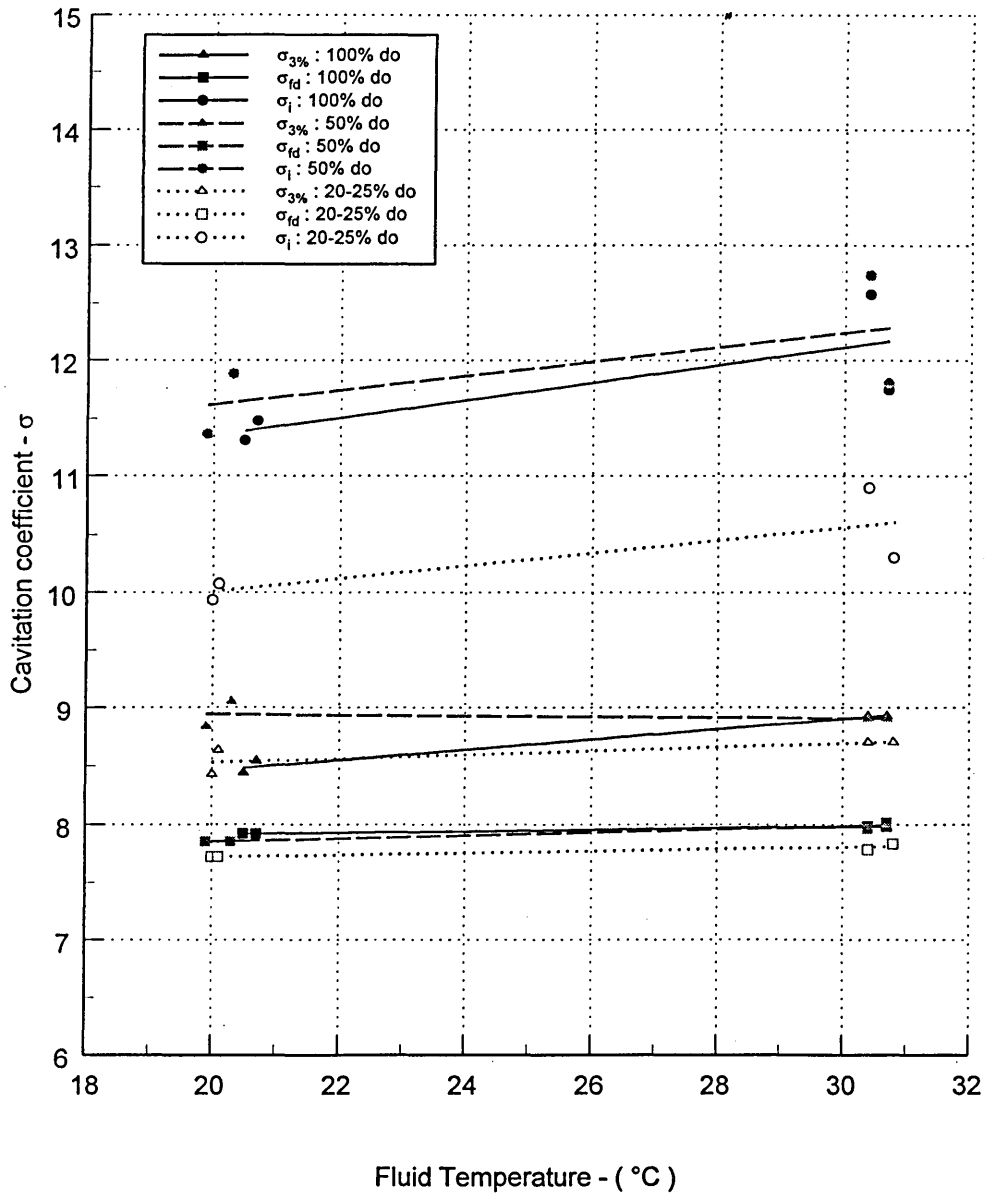


Figure 6.4-12 Effect of temperature on gas oil cavitating in the nozzle. (Ref. pressure 1.5 bar)



Temperature effect on the cavitation coefficient  $\sigma$  for the nozzle (Gas oil).

For inception, 3% efficiency drop and fully developed cavitation at various dissolved oxygen content levels and reference pressure 1.0 bar

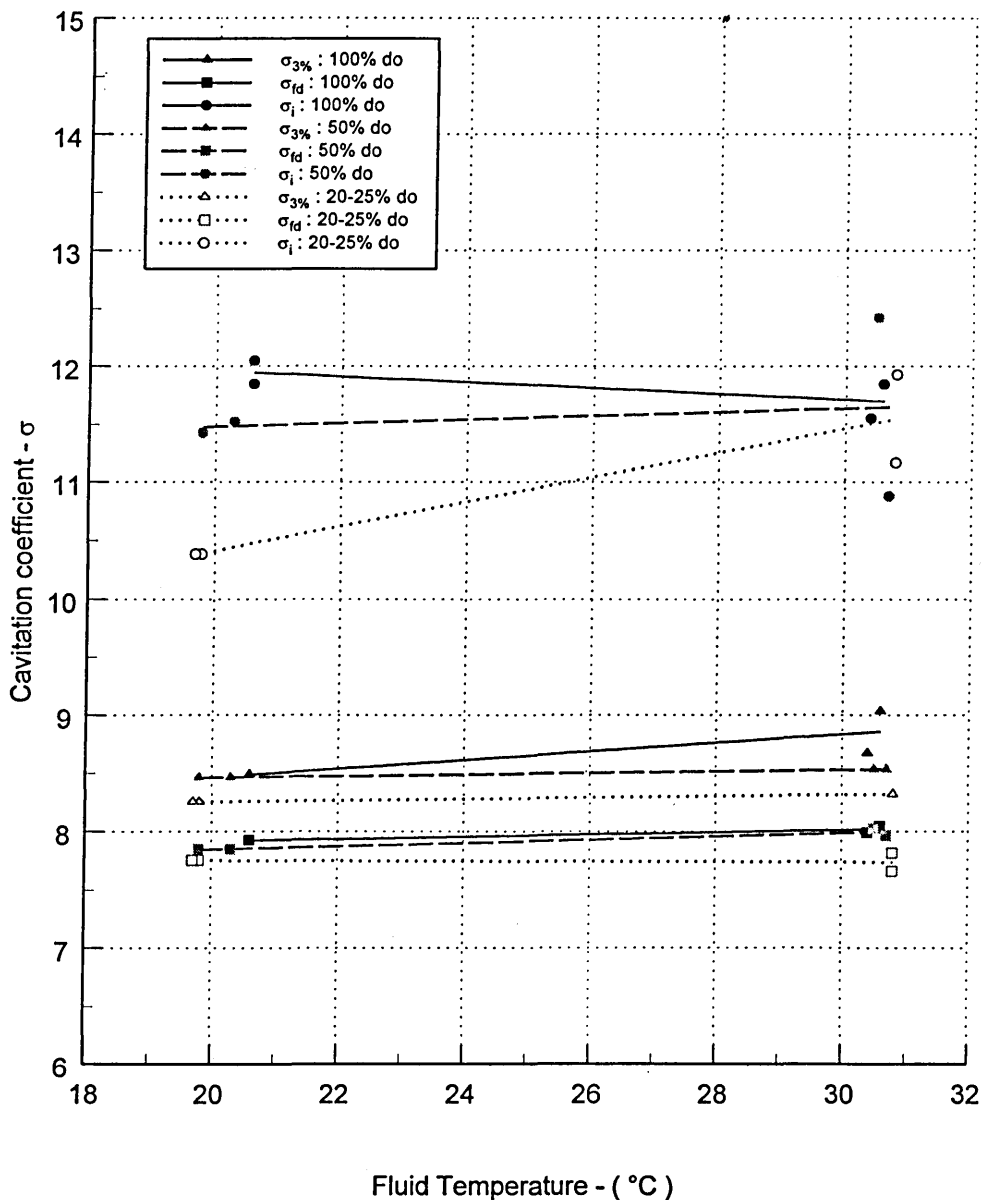


Figure 6.4-13 Effect of temperature on gas oil cavitating in the nozzle. (Ref. pressure 1.0 bar)

Effect of dissolved oxygen on the cavitation coefficient  $\sigma$   
for the nozzle (Gas oil)

For inception  $\sigma_i$ , 3% efficiency drop  $\sigma_{3\%}$  and fully developed  $\sigma_{fd}$  cavitation  
at reference pressures 2.0, 1.5 and 1.0 bar

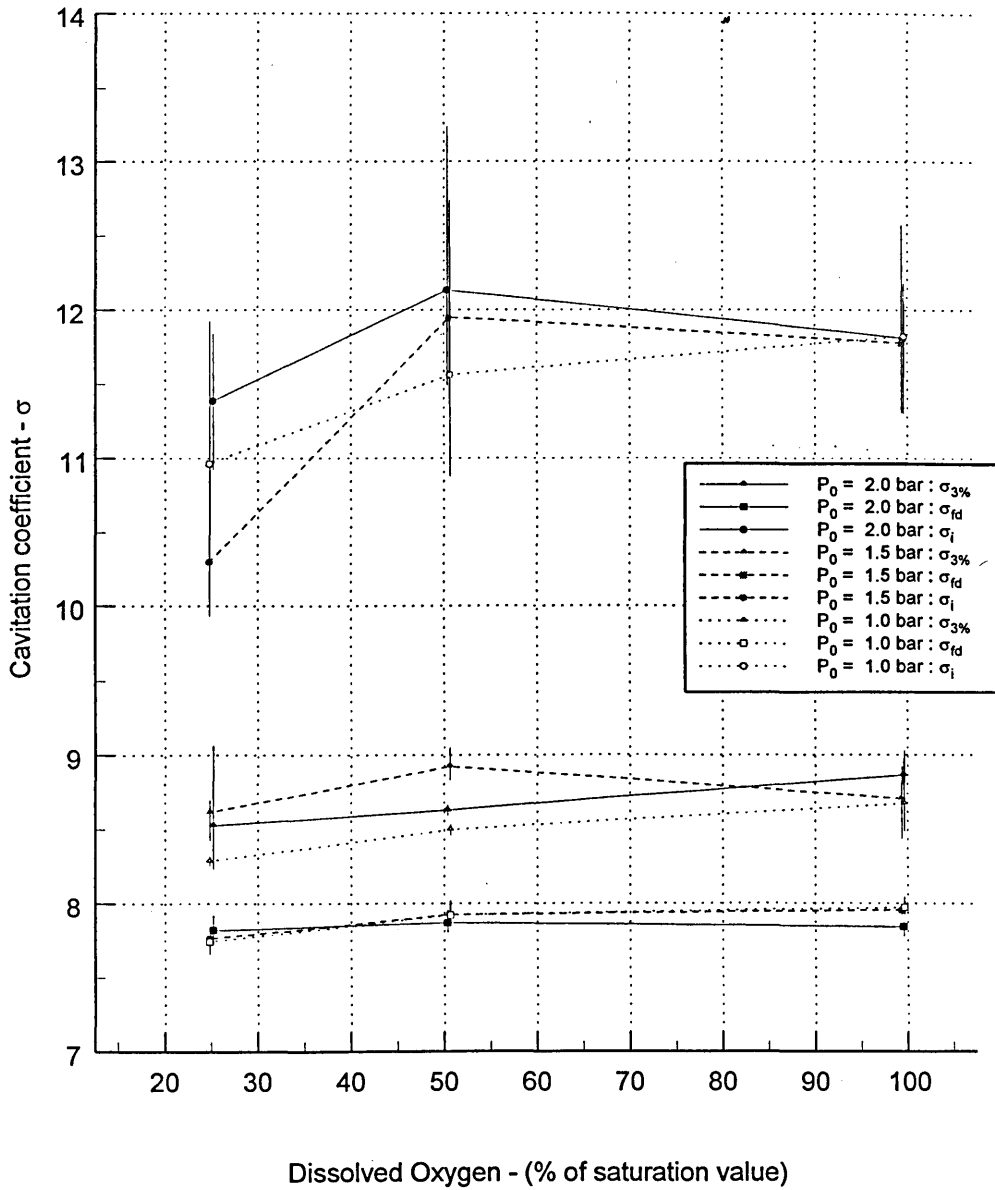


Figure 6.4-14 Effect of dissolved oxygen on gas oil cavitating in the nozzle

Effect of free stream velocity on the cavitation coefficient  $\sigma$   
for the nozzle (Gas oil)

For inception  $\sigma_i$ , 3% efficiency drop  $\sigma_{3\%}$  and fully developed  $\sigma_{fd}$  cavitation.

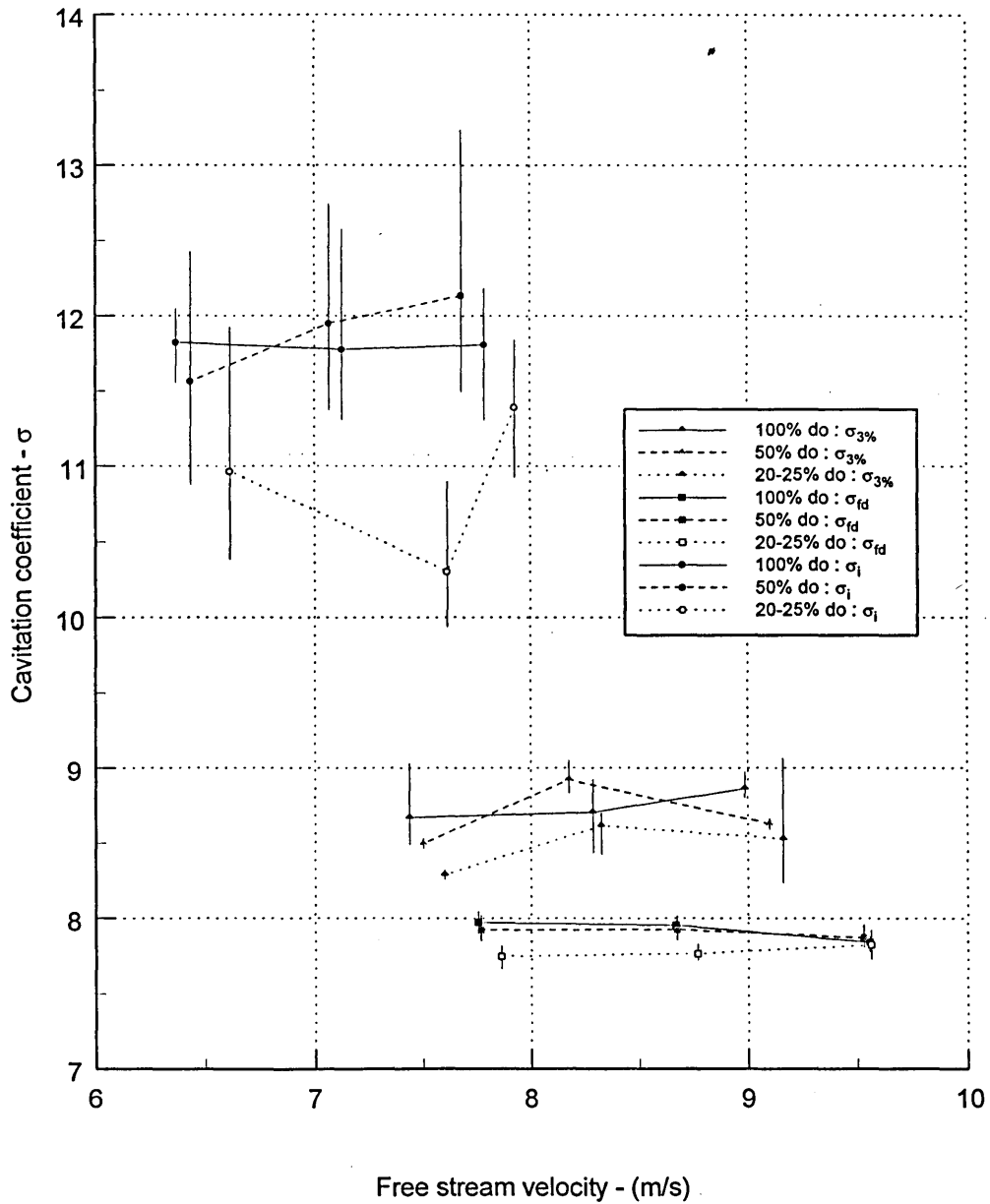


Figure 6.4-15 Effect of free stream velocity on gas oil cavitating in the nozzle.

#### 6.4.4 Comparison of Nozzle Results.

From the results for water, kerosine and gas oil, no temperature effect or significant effect of free stream velocity could be found on the cavitation conditions  $\sigma_i$ ,  $\sigma_{3\%}$  and  $\sigma_{fd}$  over the range tested. Although there is a possibly a small velocity effect for water at  $\sigma_{3\%}$ . However the small increase in the average values of  $\sigma_{3\%}$  as velocity increases is within the band of readings taken and therefore neglected. The major effect on the cavitation for the range of properties tested was the effect of the dissolved oxygen content. The results are presented on a graph of sigma against dissolved oxygen content as a percentage of the saturation value (Figure 6.4-16) and sigma against total air content by volume (%) (Figure 6.4-17). Total air content values are taken from Perry (1984) for water and the hydrocarbon data is taken from Cansdale (1978) and Ross (1970). Approximate values at STP are: Water contains 1.55% dissolved air by volume of which 34% is oxygen : Kerosine contains 16.5% dissolved air by volume of which 32% is oxygen : Gas oil contains 12% dissolved air by volume of which 33% is oxygen. Over the range of temperatures tested the proportion of dissolved oxygen to dissolved air remains relatively constant for all the fluids.

Effect of dissolved oxygen on Inception  $\sigma_i$ , 3% efficiency drop  $\sigma_{3\%}$ , and Fully developed cavitation  $\sigma_{fd}$  for Water, Kerosine and Gas oil

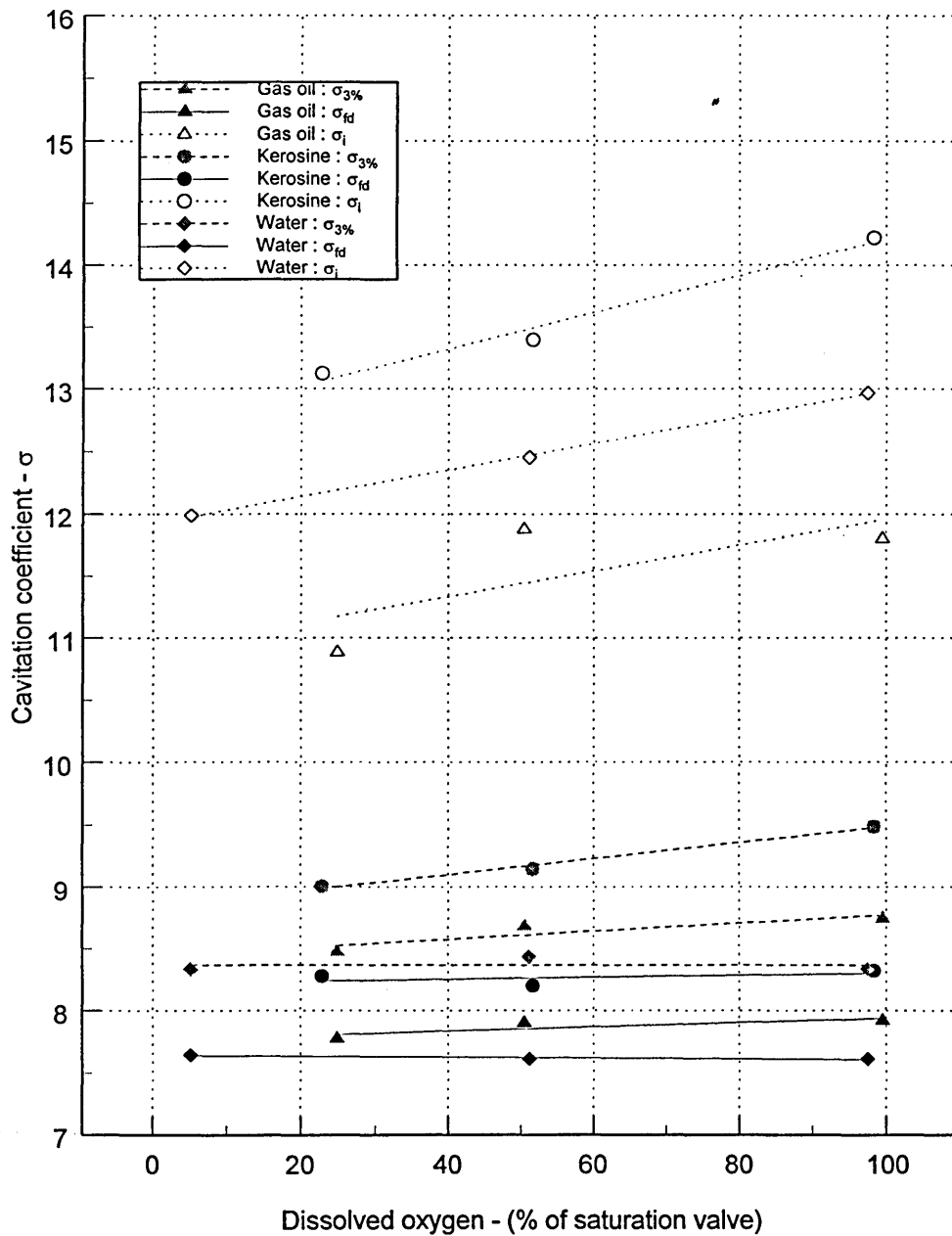


Figure 6.4-16 Effect of dissolved oxygen on water, kerosine and gas oil for various cavitation conditions.

Effect of dissolved air on Inception  $\sigma_i$ , 3% efficiency drop  $\sigma_{3\%}$ , and Fully developed cavitation  $\sigma_{fd}$  for Water, Kerosine and Gas oil

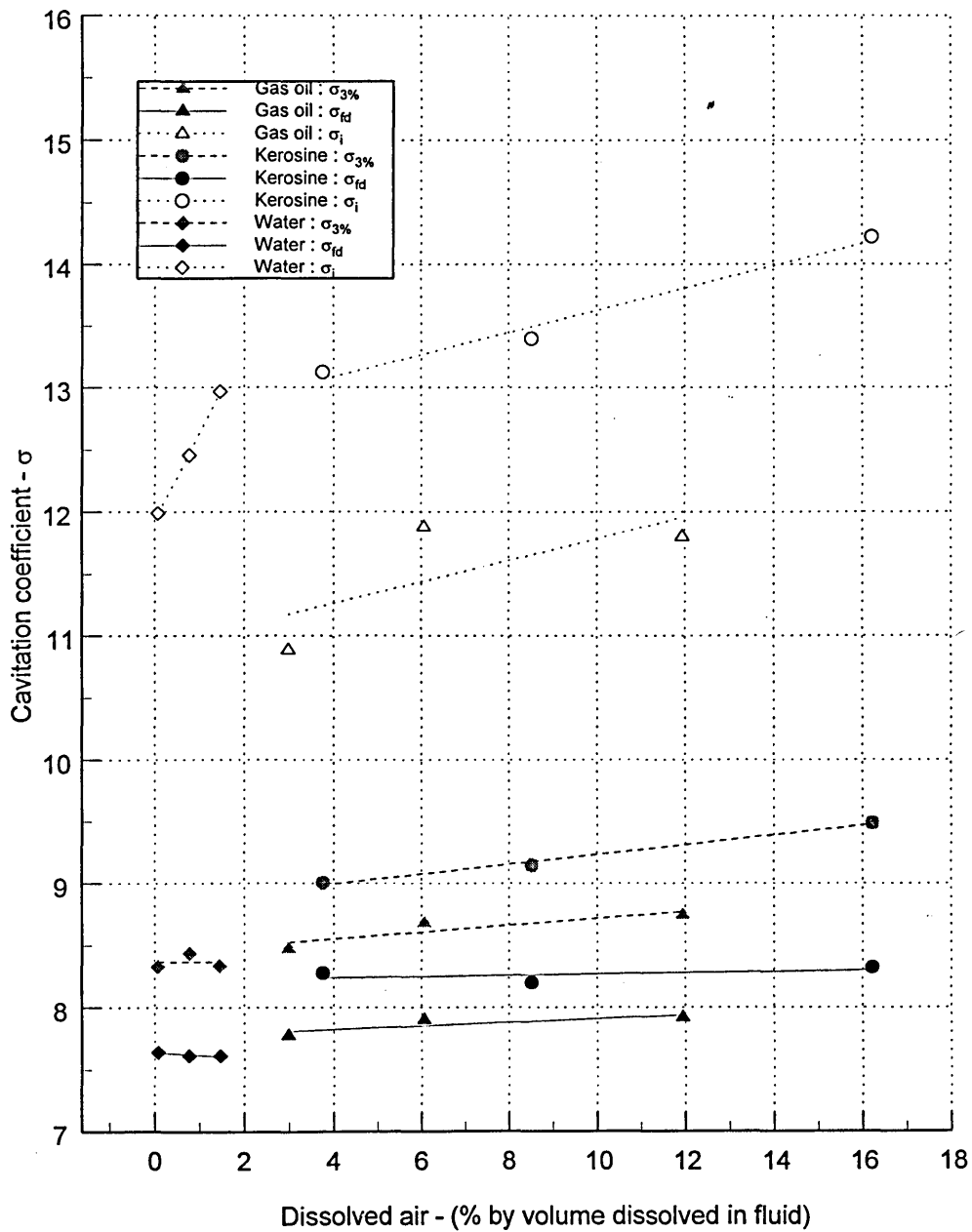


Figure 6.4-17 Effect of dissolved air (% by volume dissolved in the fluid) on water, kerosine and gas oil for various cavitation conditions.

## **6.5 Comparison between pump NPSH tests and nozzle tests.**

The initial comparison that can be made between the pump and the nozzle is between the 3% head drop and 3% efficiency drop data for the fluids. Figure 6.5-1 shows the data for the 20°C vacuum pump NPSH test and the data for the nozzle averaged for temperature and dissolved oxygen.

Comparison of NPSH test results and nozzle efficiency 3% drop results.  
for water kerosine and gas oil

NPSH test results at fluid temperature 20°C : Nozzle results are an average of the data.

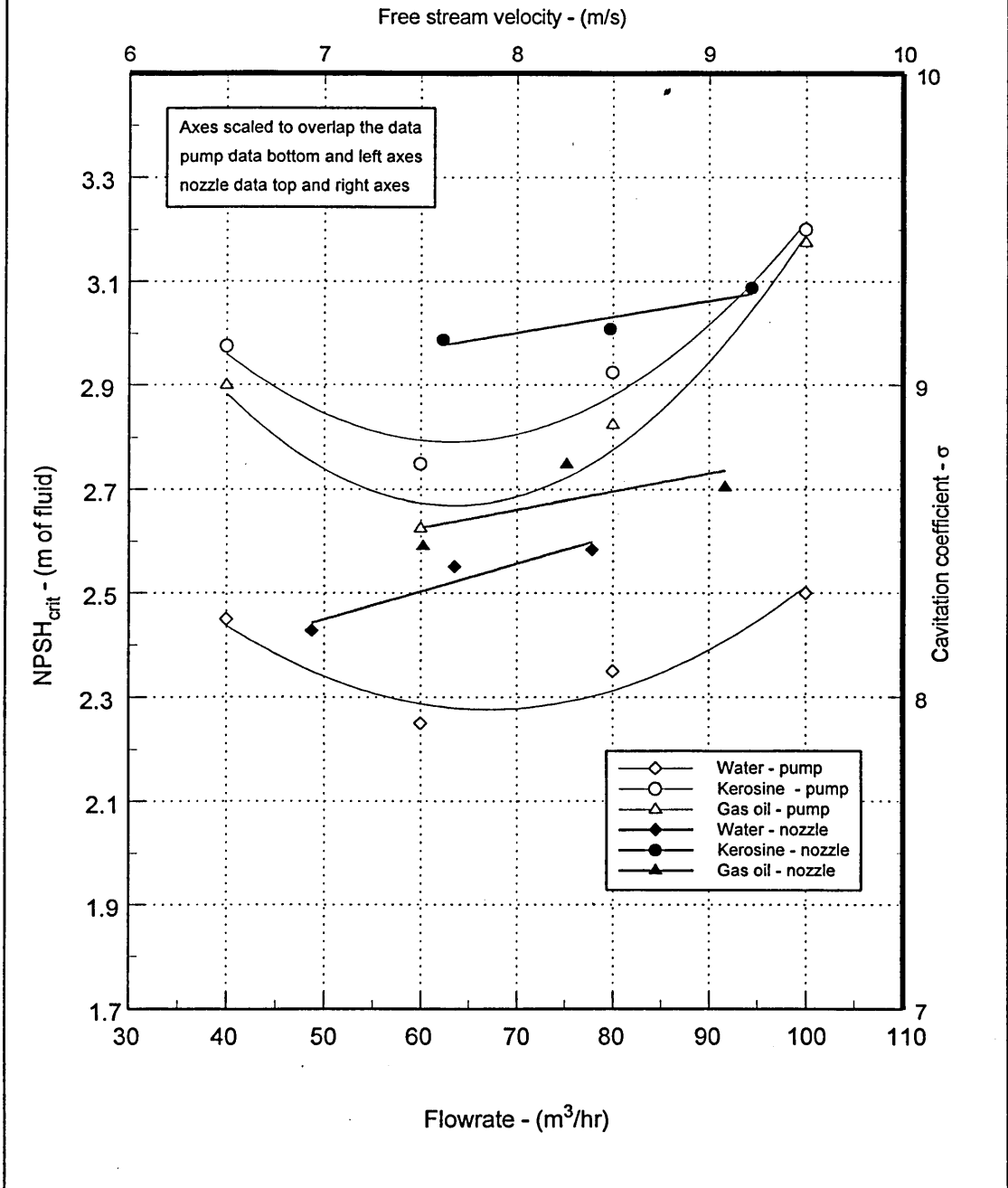


Figure 6.5-1 Comparison of NPSH test and nozzle test data for water, kerosine and gas oil.



## 7. Analysis and discussion of test results.

### 7.1 Introduction.

This chapter aims to discuss the various results of the present work, in detail. Each type of test is discussed in turn, pump performance, pump NPSH tests and nozzle efficiency tests, in an attempt to point out effects of the fluids used on the specific test. The broader discussion of the comparisons between the hydrocarbons and water are left until the end of the chapter, so the pump and nozzle tests can be discussed in conjunction. This is also an attempt to avoid too much repetition, thus some of the effects described in earlier sections are not discussed in full, until near the end of the chapter.

### 7.2 Pump Performance Curves.

This section aims to explain the differences in the tests pumps head efficiency and power characteristics for the three test liquids. Changes in mechanical losses in the bearings (oil lubricated ) and the mechanical seals due to different fluids are ignored as they are assumed to remain relatively constant. Although there is very little data to back this up, as testing is very difficult, losses due to bearings and seals together only account for about 1% in a well designed pump of the size used (Stepanoff (1964)), thus any variations would be negligible. The main factors that therefore affect the characteristic performance curves of the test pump are the fluid densities and viscosities. As a pump is a dynamic machine for a given speed of rotation and volumetric quantity the head in *meters of fluid* will remain constant. So an increase or decrease in the density of the fluid will not effect the head or flow, but it will alter if the flow is expressed as a mass flow rate or the pressure is expressed in the same units e.g. *bar* or *psi*. The change being proportional to the density of the fluid. The power needed to produce, this same head of fluid will therefore decrease with decreasing fluid density, and vice-versa. It can be seen clearly on figure 6.2-1, with reference to table 7.2-1 that the power consumption varies with the test fluid's densities. Disk friction also has an effect on the power

consumption, although this cannot be made clear from these results. Disk friction is the friction loss due to the effects of the fluid in the clearance spaces between the rotating impeller and the stationary volute. The effective result of the disk friction is a retarding torque on the pump impeller and shaft. Disk friction is related to density and viscosity, Anderson (1980) suggests that for a pump that  $\text{Disk friction} \propto \sqrt[5]{\text{viscosity} \times \text{density}}$ .

Fluid	Water				Kerosine		Gas oil	
Temperature (°C & 1 bar)	19	30	40	50	20	30	20	30
Density (kg/m <sup>3</sup> )	998.5	995.7	992.2	988	775	758	849	842
Dynamic Viscosity (cP)	1.03	0.80	0.65	0.54	1.3	1.14	5.4	3.92
Vapour pressure (m of fluid)	0.224	0.43	0.75	1.26	0.138	0.23	31×10 <sup>-6</sup>	82×10 <sup>-6</sup>

**Table 7.2-1 Summary of test fluid properties.**

This would mean that the effect would be greatest on gas oil followed by water then kerosine. However with the type of pump used i.e. with an unshrouded impeller, the disk friction plays a reduced role, as one of the friction surfaces, the top shroud is eliminated.

Leakage losses, which are also affected by fluid properties, are therefore probably the most influential of the losses on the test pumps efficiency. The leakage of the open impeller type is slightly different to that of a shrouded impeller as described earlier in the chapter on pump design. Where the recirculation is from the discharge of the impeller back over the top shroud through the wear ring and back into the eye. The flow in an unshrouded impeller leaks over the impeller blades through the clearance gap between the blades and the volute. The fluid leaks from the pressure side of a blade to the suction side. However this leakage is thought to be no more than the shrouded impeller assuming a minimum clearance is maintained. Anderson (1980) also suggested

these leakage flows rates are proportional to the  $\sqrt[8]{\text{Reynolds number}}$  therefore at the same flow and pump it can be said that:

$$\text{Leakage flow} \propto \sqrt[8]{\frac{\rho}{\mu}} \quad \text{..Equ 7.2-1}$$

The variations in the *head-flow* curves between the fluids, travelling back along the characteristics from best efficiency point BEP (Approximately 100m<sup>3</sup>/hr for all the fluids) to the closed valve head ( 0 m<sup>3</sup>/hr ), are most likely due to a combination of the disk friction and leakage losses. Although most texts suggest viscosity has a reducing effect on the total head at the BEP for shrouded impellers, Stepanoff (1964), little data could be found on effects of viscosity on the open impeller type.

The main implications of viscosity and density on pump design are that a pump design for water will be adequate for pumping fluids with lower densities than water. However fluids with higher densities will need a design with a much more robust mechanical design because of the increased pressure. Higher densities and viscosities also create the need for a more powerful pump driver in line with power consumption increase.

Comparisons to the manufacturers NPSH data for the pump and the experimental data have not been made for two reasons

1. NPSH does not scale well with speed, as shown in the literature review.
2. Manufacturers data tend to be published with a safety margin, so it is unlikely to be a true experimental curve.

### **7.3 Pump cavitation tests on water kerosine and gas oil.**

#### **7.3.1 NPSH test method.**

The difference between the suction valve throttling and the vacuum pump methods of NPSH test (Figures 6.3-4 and 6.3-5 show the comparison for water) is most likely due to air content effects. The low oxygen suction valve test and the vacuum pump tests both

compare well. However the reduced NPSH performance of the suction valve throttling method with the air saturated water is most likely due to the gaseous cavitation created by the throttling valve. This results in the introduction of a two-phase flow of air and water into the impeller eye, thus reducing the pumps NPSH performance. This could not be proved as there were no inspection windows in the pump or suction pipe work. However the suction valve throttling test with water with a reduced air content was much easier to perform than with the saturated water. This was because the movements of the throttling valve were much less sensitive with the low air content. Thus indicating that cavitation caused by the valve was affecting the pump This did not occur with the deaerated suction valve throttling test as there was much less air available to create the two phase flow.

The much larger air content of the hydrocarbons used (gas oil and kerosine approximately 7 to 10 times greater air content by volume respectively) made it impossible to conduct suction valve throttling tests. The reason being similar to the reason why deaerated water gave a better NPSH performance than air saturated water, for the suction valve throttling test method. The throttling valve would cavitate, thus introducing a two-phase flow into the impeller eye. The two-phase flow produced by the hydrocarbons would have a greater proportion of gas to liquid than that produced in water. As a result the flow conditions at the suction inlet of the pump were extremely unstable, meaning the test became impossible to conduct.

### **7.3.2 Cavitation performance of water.**

The comparisons made in this section are made only using the vacuum pump NPSH test method results, as the suction valve results are less reliable, the reasons for this have been stated in the previous section. Figure 6.3-1 shows the effect of temperature on the vacuum pump method of NPSH test for water, it shows approximately a 0.25m (approx. 10%) improvement in  $NPSH_{crit}$  performance due to a temperature increase of 11°C from 19°C. This is much greater than predicted by Stepanoff's (1964) empirical formula for

finding the NPSH correction factor (equation 2.2-11 or equation 7.3-1 shown in its metric form where  $B'$  is in SI units)

$$\Delta h_t = \frac{29}{h_v (B')^{1/3}} \quad \text{..Equ 7.3-1}$$

The adjustment factor  $B'$  being :

$$B' = \frac{C_{P,L}}{J' L^2} T \left( \frac{v_v}{v_L} \right)^2 \quad \text{..Equ 7.3-2}$$

where  $J'$  is the mechanical equivalent of heat  $\approx 102 \text{ kg m/K}$ . Calculating  $\Delta h_t$  for each fluid temperature the  $\Delta NPSH$  can be found from equation 7.3-3.

$$\Delta h_2 - \Delta h_1 = NPSH_1 - NPSH_2 = \Delta NPSH \quad \text{..Equ 7.3-3}$$

Temperature : ( $^{\circ}\text{C}$ )	19	30	40	50
Vapour Pressure : ( <i>bar</i> )	0.022	0.0424	0.0738	0.123
Specific Volume of vapour : ( $\text{m}^3/\text{kg}$ )	61.34	32.93	19.55	12.04
Specific Volume of liquid : ( $\text{m}^3/\text{kg}$ )	0.0010015	0.0010043	0.001008	0.001012
Latent heat : ( $\text{kJ/kg}$ )	2456.7	2430.7	2406.2	2382
Enthalpy of liquid : ( $\text{kJ/kg}$ )	79.7	125.7	167.5	209.3
Specific heat capacity : ( $\text{kJ/kg K}$ )	4.183	4.179	4.179	4.182
$B'$	7443	2259	833	330
$\Delta h_t$ : ( <i>m</i> )	0.00089	0.00226	0.005	0.01
$\Delta NPSH$ ( <i>m</i> ) for 19 to 30 $^{\circ}\text{C}$ change.		0.00137		
$\Delta NPSH$ ( <i>m</i> ) for 19 to 40 $^{\circ}\text{C}$ change.			0.004	
$\Delta NPSH$ ( <i>m</i> ) for 19 to 50 $^{\circ}\text{C}$ change.				0.009

**Table 7.3-1 NPSH adjustment for water between 19 and 30 $^{\circ}\text{C}$ .**

The results of the Stepanoff correction factor seen in table 7.3-1 above are negligible. These become even smaller when as Stepanoff (1964) suggests the resultant change is scaled from the size of the test pump that was used in his experiments. The pump being a 1½-in single stage refinery pump running at 3470 rpm with BEP head and flowrate of 61m and 33m<sup>3</sup>/hr with a 197 mm shrouded impeller.

The larger  $\Delta NPSH$  observed from the test results is probably caused by an increase in leakage as a result of changes in fluid properties due to the temperature rise. The viscosity of water decreases by approximately 23% as the temperature rises from 19 to 30°C. The leakage flow will therefore increase. The leakage flows in a pump with an unshrouded impeller, as used in these tests, flows directly over the impeller blades. The direction of flow being from the pressure side to the suction side of the blade. Whereas in a shrouded impeller it returns to the eye of the impeller over the top shroud and through the wear ring as. This means in the unshrouded impeller type the leakage flow passes directly into the area where cavitation occurs. This would result in a local increase in pressure in the cavitation zone thus temporarily postponing the onset of cavitation and head breakdown. The increased jetting effect of the leakage flow may also contribute by increasing the turbulence in the cavitation zone. As the leakage flow impinges on the main flow between the impeller blades at approximately 90° it would reduce the local fluid velocities, thus reducing the effect of the dynamic pressure head. So although leakage increase could have the effect of decreasing the pumps efficiency, the power meter was not sufficiently accurate to note these changes in efficiency. Its effect of locally increasing the pressure on the suction side of the impeller blades and increasing the turbulence in the zone due to a jetting effect, means the pumps cavitation performance is enhanced. Thus the improvement in NPSH performance would appear to be due to an increase in leakage flow rate, which is in turn inversely related to the fluids viscosity. The changes in these leakage flows would be hard to estimate as very little information is available on unshrouded impeller leakage. It was assumed however that the fluid's viscosity plays a similar role in the amount of leakage as it does with shrouded impellers. It might even play a larger part as the friction forces exerted by the stationary volute also help drive fluid through the clearance gap (See figure 7.3-1), this force being directly related to the viscosity of the fluid. No published work could be found to support this theory. Most work on the thermodynamic effect would appear to have been conducted with shrouded impellers, thus this effect did not appear. There has also been very little work conducted on the leakage effects in unshrouded impellers. Most texts just suggest that the leakage flow for an unshrouded impeller is of the same order as a shrouded impeller, but say no more on the subject.

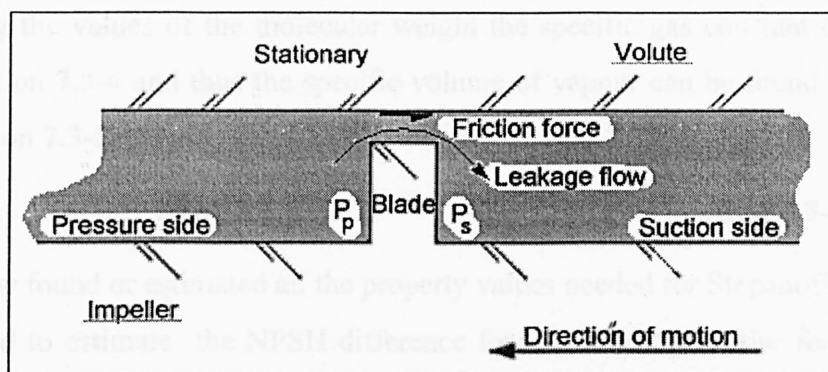


Figure 7.3-4 Schematic of leakage over one blade of an unshrouded impeller.

### 7.3.3 Cavitation performance of Hydrocarbons.

For the analysis of the hydrocarbon data by Stepanoff's theory various thermophysical property values need to be known, most of which can be found in the literature cited in chapter two. However the data for the specific volume of vapour; for kerosine and gas oil could not be found. So a method of estimating  $v_v$  that was proposed by Spraker (1965) was used. The method assumed that the vapour would be a mixture of several pure hydrocarbons which could be identified by the initial boiling range of the fluid under S.T.P. (see table 7.3-2). After an examination of the pure hydrocarbons within this initial boiling range it was found that hydrocarbons with similar boiling points had similar molecular weights. So two hydrocarbons were chosen as representative of the initial boiling point range of kerosine and gas oil.

	Kerosine	Gas oil
Initial Boiling point - ( $^{\circ}K$ )	438	453
10% volume - ( $^{\circ}K$ )	448	488

Table 7.3-2 ASTM distillation for kerosine and gas oil.

Kerosine { 1-METHYL 2-ETHYLBENZENE b.p.  $439^{\circ}K$  Molecular weight 140.3}

Gas oil { N-BUTYLCYCLOHEXANE b.p.  $454^{\circ}K$  Molecular weight 120.2}

Then using the values of the molecular weight the specific gas constant can be found from equation 7.3-4 and thus the specific volume of vapour can be found from the gas law, equation 7.3-5.

$$\tilde{R} = MR \quad \text{..Equ 7.3-5}$$

$$p_v v_v = R T \quad \text{..Equ 7.3-6}$$

Having now found or estimated all the property values needed for Stepanoff's B factor it can be used to estimate the NPSH difference for the temperature rise for each of the fluids. It can be seen from the table 7.3-3 below that Stepanoff predicts a negligible change in NPSH for the

Fluid	Kerosine		Gas oil	
	20	30	20	30
Temperature : ( $^{\circ}\text{C}$ )	20	30	20	30
Vapour Pressure : ( <i>bar</i> )	0.0105	0.017	$2.55 \times 10^{-6}$	$6.81 \times 10^{-6}$
Specific Volume of vapour : ( $\text{m}^3/\text{kg}$ )	19.54	12.5	68977	26710
Specific Volume of liquid : ( $\text{m}^3/\text{kg}$ )	0.00129	0.00132	0.001179	0.00119
Latent heat : ( $\text{kJ}/\text{kg}$ )	226	226	180	180
Enthalpy of liquid : ( $\text{kJ}/\text{kg}$ )	41.8	62.7	41	61.5
Specific heat capacity : ( $\text{kJ}/\text{kg K}$ )	2.09	2.09	2.05	2.05
$B'$	26964	10882	$6.23 \times 10^{11}$	$9.5 \times 10^{10}$
$\Delta h_t$ : ( <i>m</i> )	0.00034	0.0007	$2.1 \times 10^{-10}$	$9.6 \times 10^{-10}$
$\Delta \text{NPSH}$ ( <i>m</i> )		0.00036		$7.5 \times 10^{-10}$

**Table 7.3-3 NPSH adjustment for kerosine and gas oil between 20 and 30°C.**

temperature rise from 20 to 30°C. Referring to figure 6.3-8 we see that this is true for kerosine but this only holds true for gas oil at the low flow condition (40m<sup>3</sup>/hr) but increases significantly towards B.E.P (100m<sup>3</sup>/hr). These differences can also probably be attributed to losses such as leakage for similar reasons to those discussed for water. The dynamic viscosity changes in the fluids over the temperature range 20 to 30°C are much greater for gas oil (and water) than they are for kerosine. Therefore the increase in leakage will be much greater with gas oil (and water) than it will be with kerosine. Although equation 7.2-1 for leakage in a shrouded impeller only predicts small increases in leakage (water 3.2%, gas oil 4% and kerosine 1.4%) it can be seen that the leakage with water and gas oil increase approximately twice as much as with kerosine.



With the unshrouded impeller leakage mechanisms suggested previously these flows may be substantially increased thus the effect on the NPSH performance will be more significant with the gas oil than with kerosine. This is thought to be the only viable explanation for this effect, and without further experimentation and analysis it will remain unproved.

#### **7.4 Nozzle cavitation tests on water, kerosine and gas oil.**

The following section discusses the results for the nozzle tests for all the test fluids used. Water and the hydrocarbons are discussed separately. For the main part the discussion of any comparisons and differences between the hydrocarbons and water are left until near the end of this chapter where they are discuss in conjunction with the pump test results.

##### **7.4.1 Water tests.**

Figures 6.4-1 to 6.4-5 show the effect of temperature on incipient, fully developed and the 3% efficiency drop cavitation conditions. The temperature on the conditions  $\sigma_i$ ,  $\sigma_{3\%}$  and  $\sigma_{fd}$  had a negligible effect over the range 19 to 50°C as was expected from the work by Furness (1973). This is also predicted by Stepanoff's B factor which suggests the '*thermodynamic effect*' has little influence on water for the temperature range 19 - 50°C (Refer to Table 7.3-1). Although this table shows changes in NPSH the  $\sigma$  value used in the nozzle experiments is comparable and a negligible change in one would mean a negligible change in the other. As the nozzle is a passive flow device effects such as leakage and disk friction are not present to interfere with the cavitation process as was the case with the results from the pump.

Having found no temperature effect over the range studied, which was expected as the temperature range was small, and variations in free stream nuclei are most likely to be the cause of any variation. And as can be seen from the data positive negative and null relationships are observed. The results were therefore combined to show the averaged

effect of dissolved oxygen on  $\sigma_i$ ,  $\sigma_{3\%}$  and  $\sigma_{fd}$ , (figure 6.4-4). The dissolved oxygen equates directly to the dissolved air content of the water as the ratio of air to oxygen is constant over the temperature range studied. There are large variations in the incipient cavitation data which are probably due to the variations in the free stream nuclei number density. The cavitation process itself can result in increasing the nuclei density in a closed loop (Holl and Treaster 1966). This however was hoped to have been minimised by the test rig design. There is very little data on cavitation inception and the effect of nuclei number density. It is very hard to measure the number density and so few experimenters have gathered data on it. However the assumption was made, similar to other researchers, that the nuclei population should vary proportionally with the total air content of the fluid. Also the visual method of quantifying cavitation inception is subjective in nature and could have added more variance into the data, acoustic detection would have been less subjective and would be advised for further work. Taking the above points into consideration was found that the averaged inception data provides us with a linear relationship (seen more clearly on figure 6.4-16) between the dissolved air content and incipient cavitation value. The lower the air content the better the incipient cavitation performance. Although the variance is large and straight line could be drawn in some cases to show no variance of  $\sigma_i$  with dissolved oxygen, the general trend appears to be a proportional relationship, it also appeared to be the trend during testing when examining the raw data from test to test. This effect is backed up by the several experimenters such as Keller (1974) and Pearsall et al (1955) and the relationship (Equ 7.4-1) stated in Arndt (1981) and (Holl 1960), which relates the air content of the fluid to the critical cavitation number (i.e. incipient or decinent cavitation). This relationship will be discussed later in conjunction with the hydrocarbon data.

$$\sigma_{crit} = C_{pm} + \frac{E\alpha\beta}{\frac{1}{2}\rho U^2} \quad \text{..Equ 7.4-1}$$

As stated in the gas content section of Chapter 2, the magnitude of the effect appears to differ dependent on the type of experiment and test rig used. Most likely due to the

effect of nuclei populations in the fluid, so no comparisons with other published experimental data have been made as it would be futile until an established method of predicting the number density of nuclei can be found. Unfortunately most of the techniques that have been suggested are very complex, taking three dimensional holographic photographs of sample volumes of test liquid, being one example. Billet (1985) provides a relatively recent review of nuclei measurement and more recently Avellan (1993). However this research project is more concerned with the more advanced stages of cavitation which affect performance, which seem much less dependent on free stream nuclei Brennen (1994<sup>2</sup>), so further discussion of the cavitation inception in water will not be entered into. Finally air content effects in water would seem to be negligible at both the 3% efficiency drop and fully developed stages of cavitation in the nozzle as has been demonstrated by previous experimenters. This is assumed to be the effect of vaporous cavitation becoming more dominant over the gaseous (air) cavitation. Air bubbles grow at a much slower rate to that of vapour bubbles as they pass through the low pressure cavitation zone. This is because the diffusion of dissolved air into the cavity is a slow process, and as they pass through the cavitation zone their size grows very little. Where as the vaporisation of fluid to grow vapour bubbles is a much faster process. So at the point of 3% efficiency drop and beyond where vaporous cavitation is well established. The vapour bubbles having grown much larger than the air bubbles have a more significant choking effect, the total void fraction of all the small air bubbles being much lower than the total void fraction of vapour bubbles. This means that as the gaseous cavitation has little effect the variation in the total air content also has very little effect.

#### **7.4.2 Hydrocarbon tests.**

Figures 6.4-6 to -8 and 6.4-11 to -13 show the temperature effect on kerosine and gas oil for conditions at cavitation inception, breakdown and for a 3% drop in nozzle efficiency. The temperature change for these tests is only ten degrees, it would have been preferable to test over a larger range of temperatures as it would have been for water. The limitations of the test rig being the confining factor. This 10° range in

temperature was more of a check to make sure there were no large effects for changes in temperature. So the small changes during a constant temperature test, typically 0.3°C could be discounted. The thermodynamic change was not expected, and the test showed that there was no significant change for either gas oil or kerosine. The data shows both positive and negative effects for similar conditions throughout the three pressure ranges tested for both the hydrocarbon liquids. However no pattern could be found so it was assumed to be part of the general variance of the cavitation data.

Kerosine exhibited a similar relationship to that of water for the incipient cavitation data, where  $\sigma_i$  reduced linearly with the air content of the fluid. The large variance in the data is probably due to the free stream nuclei although no data has been published for these hydrocarbon fuels and no readings were taken

For gas oil Figure 6.4-14 there was little change, possibly even a slight decrease in the incipient cavitation performance as the air content was reduced from 100% air saturation to 50% of the saturation value for reference pressures 1.5 and 2.0 bar. As the air content was reduced yet further to 25% of the saturation value the incipient cavitation performance gets better. The 1.0 bar condition however has more of a linear relationship similar to that of kerosine. It is still uncertain whether the effect at the 1.5 and 2.0 bar conditions is a genuine effect of the dissolved air content. Or whether it is a phenomenon due to a relatively static nuclei population, and the resultant effect that this would cause, as has been discussed earlier. A relatively static nuclei population could be a result of the gas oils viscosity which is three to five times larger than that of kerosine or water. The nuclei therefore take much longer to rise to the surface of the fluid, and are retained more readily within the fluid body. This is easily observed by simultaneously shaking separate samples of the test fluids for several seconds. Then placing them on a bench to observe the different rates at which the entrained bubbles rise. This could mean during the deaeration process of gas oil a smaller percentage of the gas nuclei were removed in the 1.5 and 2.0 bar tests than in the 1.0 bar test, making the assumption that the nuclei population is proportional to the dissolved air content incorrect. As no deaeration times or standing times were taken, it is not known whether

the 1.5 and 2.0 bar tests were conducted more quickly after deaeration than the 1.0 bar tests. In the absence of this data it is assumed the relationship would be comparable to that of kerosine, this is the reason a linear relationship has been shown for the averaged data in figures 6.4-16 and 6.4-17.

As the air content of the two hydrocarbons was only reduced to 25% it is not known if there is a dramatic improvement in the cavitation inception performance as the air content is reduced to very low levels. At 25% of saturation both hydrocarbons contain 3 to 4% dissolved air by volume, which is more than the total air content of water at 100% saturation (NB. constant temperature). It is thought unlikely that it would be the case, and the incipient cavitation in the hydrocarbons should follow the same relationship as water, Equation 7.4-1. Therefore it can be stated from equ 7.4-1 that for a given temperature, pressure and flow, the incipient cavitation condition for water, kerosine and gas oil is a function of the dissolved gas content;

$$\sigma_i = f(\alpha) \quad \text{..Equ 7.4-2}$$

Further experimentation however will reveal if this relationship holds for low dissolved air levels in the hydrocarbon fuels .

Both kerosine and gas oil both exhibit a linear improvement in the 3% efficiency drop cavitation value  $\sigma_{3\%}$  as the dissolved air level is reduced. Kerosine having a slightly more pronounced effect than gas oil. The improvement is of a similar order to that of the incipient cavitation data. It is interesting to note that the 1.5 bar data set for gas oil has a similar effect, to that of the 1.5 and 2.0 bar data mentioned in the paragraph above. There is a slight rise in  $\sigma_{3\%}$  as the air content is lowered to 50% of saturation , but then the performance gets better as it is lowered further to 25%. The 1.0 and 2.0 bar data for the  $\sigma_{3\%}$  data are both linear in nature. Although nuclei are not thought to have any effect at these later stages of cavitation, most of the work conducted in this area has

been performed on water. Thus little is known about nuclei effect in more viscous liquids such as gas oil. Finally it can be seen that the performance of the fully developed cavitation condition has little or no dependence on the dissolved air content of the fuels over the range studied.

### **7.4.3 Cavity appearance.**

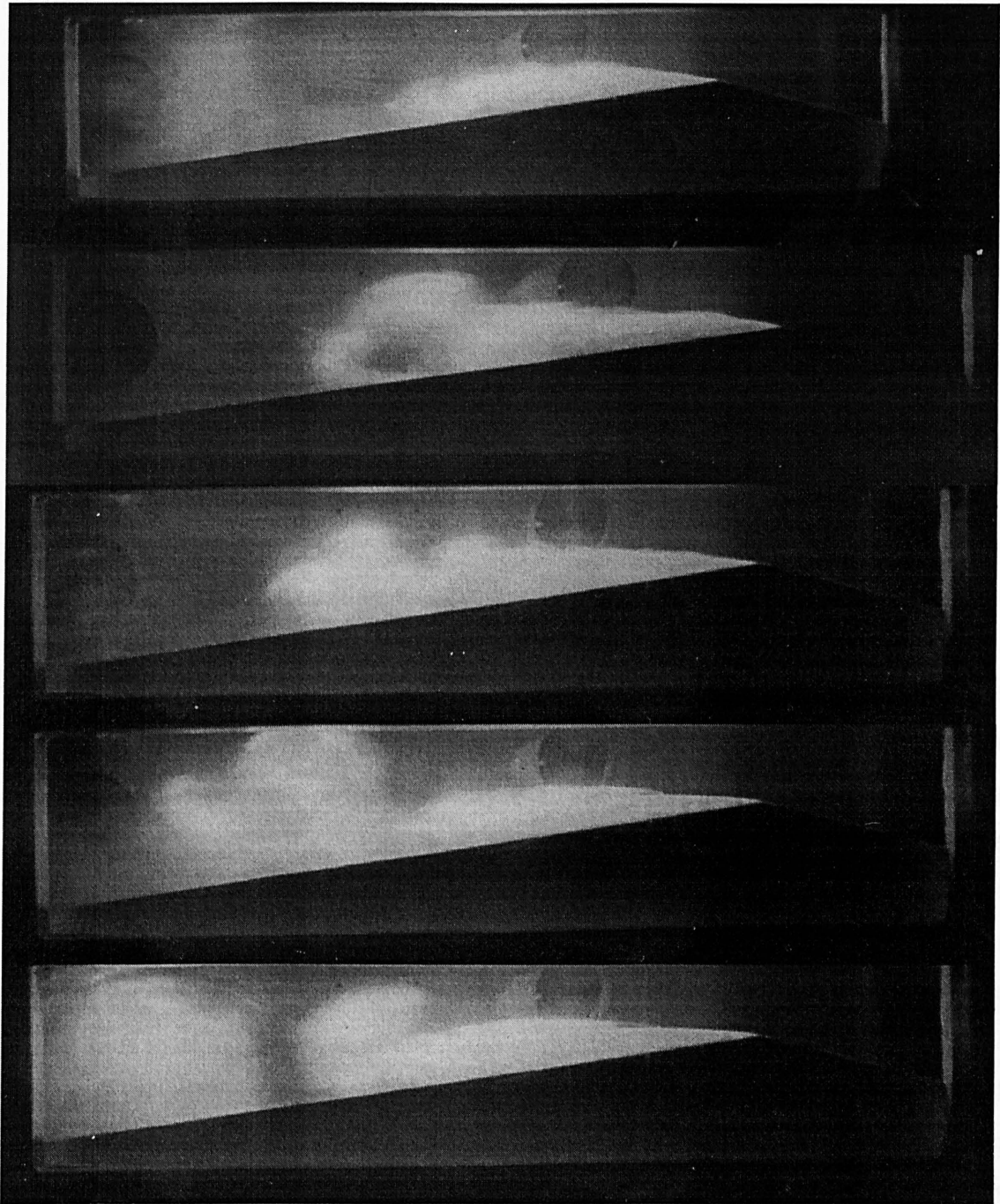
The following section describes the observations made of the cavitation seen in the nozzle test section. This was by no means a major part of this work and this area has constituted whole research projects in itself. The only measurements made were of the average fixed cavity lengths as the velocity was increased through the test section. These were taken using a strobe light and a rule. The basic observations made were only to help in the understanding of the processes at work for the different fluids.

#### **7.4.3.1 Water cavities.**

The cavity appearance of water in the venturi nozzle was found to be similar to those described by many authors including Furness (1973) and Lush et al (1986). From inception which starts with a row of tiny bubbles across the down stream edge of the throat. This then developed into a fixed cavity that gradually lengthened as the velocity through the test section was increased. The fixed cavity was opaque in nature appearing to be filled with both large and small frothy bubbles. The extremity of the cavity was fairly rough covered in a layer of smaller frothy bubbles. The end of this fixed cavity would break off and collapse further down stream. This partial cavity break-off occurs in the range of milli seconds, the frequency being independent of average cavity length (Lush et al 1986). The measured length of the cavity appears to decrease with air content, for a given cavitation condition. Although the precision of the measurements is not thought sufficiently accurate to quantify this any further. At much larger velocities when the tail of the cavity extended beyond the viewing window, the observable wall of the cavity interface became smooth and transparent. Also the cavity itself in this 'supercavitation' condition became void of any bubbles. The noise produced was a

distinctively loud sharp crackling sound, which was observed to increase as the air content was lowered, presumably due to reduced cushioning effect of the air, as more vaporous cavities collapse with more violence than air cavities, and thus more noise.

The following set of five stills taken with a normal 35mm stills camera (Figure 7.4-1) shows the fixed cavity, with a partial break off. The pictures were not taken consecutively, they were chosen from a large number of stills and rearranged to illustrate this unstable nature of the cavity, although they were all taken under the same fluid conditions and the same value of cavitation coefficient  $\sigma$ .



**Figure 7.4-1 Stills of water cavitation in the nozzle**  
**( $\sigma=8.0$  : Dissolved air 100% of saturation value : Reference pressure 2.0 bar)**

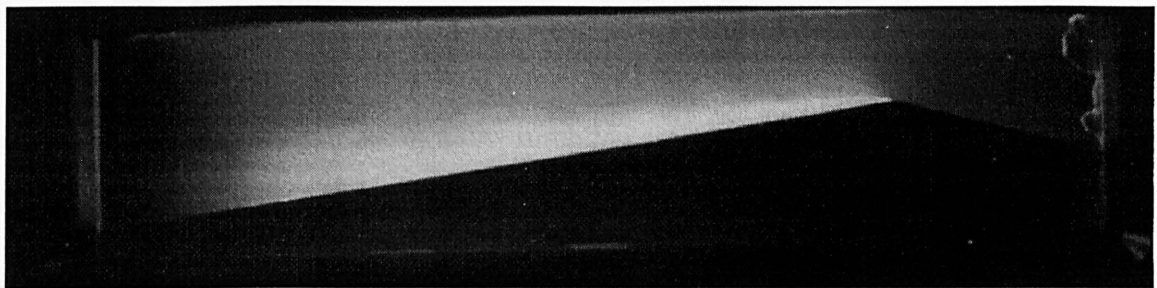
(Note: The picture quality of these stills has not been lost by using electronically scanned and printed photographs. The stills were not of brilliant quality, and this method of display seems to have actually improved definition.)



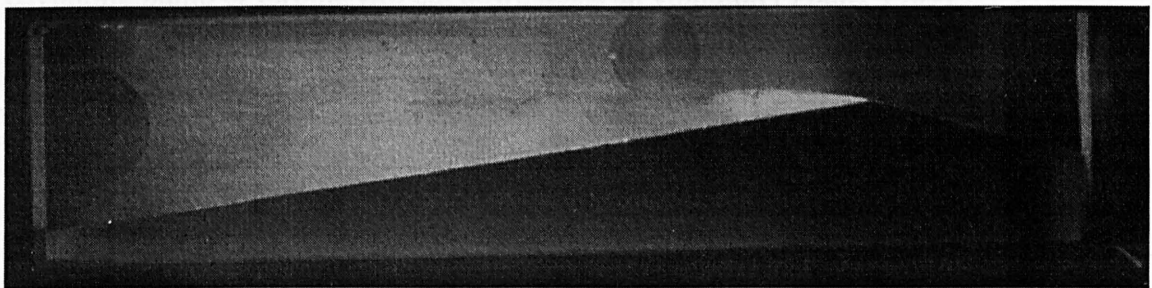
#### 7.4.1.1 Hydrocarbons cavities and how they compare to water.

The appearance of both kerosine and gas oil were very similar, except for the obvious colour difference gas oil having had its distinctive clear red dye, kerosine being clear, so they will both be described together. The inception of the hydrocarbons appeared similar to water on the sharp edge of the nozzle throat just on the down stream side. However the incipient bubbles that formed with the hydrocarbons were much larger than those of water. No measurements were taken but at an estimate they had about 10-20 times larger diameters. This is most likely due to surface tension effects (Knapp et al 1970), gas oil and kerosine have similar surface tension coefficients 27 and 26mN/m at 25°C. Where as water's is almost three times as large; 73mN/m at 25°C . Surface tension has the effect of decreasing the rate of cavity growth. The higher the surface tension the slower the growth, note it only works in one direction. On very small cavities surface tension is not uniform, therefore this explanation might be questionable, it is however the most reasonable explanation (further discussion of this will continued in section 7.5). As the velocity through the section was increased it became very apparent that the mode of cavitation was significantly different from that of water. At 100 % dissolved air saturation a 6% increase in fluid velocity from the incipient velocity would cause a dense trail of very small entrained bubbles to flow down the diverging edge of the nozzle section from their inception at the nozzle throat. These bubbles were not absorbed back into the fluid within the confines of the viewing window of the test section. As the velocity increased further this cloud of bubbles became much more dense, thus masking the view of any fixed cavity that might of formed (Figures 7.4-2 and 7.4-3 are stills for kerosine and water for similar cavitation conditions. The trail of bubbles on the kerosine can be clearly seen, Further colour photographs can be found in Appendix G). However at the reduced air content of 50% of the saturation value, this trail of bubbles was less dense, meaning it was possible to see a fixed cavity up to the length of 10mm ( Velocity increase of 15% from inception ), similar to that of water, before the increasing bubble density of the trail obscured it from further observations. A similar increase in observable cavity length was seen due to the decrease in air content to the 20 to 25% of saturation condition. The cavity was observable up to about 50mm

(Velocity increase of 25% from inception) before the bubble density in the trail again increased to a point where the fixed cavity was obscured. So this trail of obscuring bubbles would therefore seem to be the dissolved air in the hydrocarbons being drawn out of solution in the low pressure zone of the nozzle throat. Once out of solution these bubbles seem to take much longer to reabsorb back into the fluid than purely vaporous cavitation would have (Plesset et al 1977) and they also seemed to vary very little in size (Although eye sight is not very accurate at this small scale). However it could be said that the volume of air released from solution was much larger than the possibly more 'vaporous' cavitation occurring in the fixed cavities.



**Figure 7.4-2 Kerosine cavitation just preceding the 3% efficiency drop value**  
 ( $\sigma=10.5$  : Dissolved air 100% of saturation value : Reference pressure 2.0 bar)



**Figure 7.4-3 Water cavitation just preceding the 3% efficiency drop value**  
 ( $\sigma=9.5$  : Dissolved air 100% of saturation value : Reference pressure 2.0 bar)

As the stage of cavitation progressed the cavity became a mass of turbulent frothy bubbles, the top layer of which becomes roughly parallel to the top wall of the test section (Figure 7.4-4). There seemed to be little change in this cavity until the condition which would have been the 'supercavitation' condition with water was reached. The cavity void, as it was with water, was



**Figure 7.4-4 Kerosine cavitation, comparable condition, to that of water in fig 7.4-1  
( $\sigma=8.2$  : Dissolved air 100% of saturation value : Reference pressure 2.0 bar)**

now filled with an opaque mass of frothy bubbles turbulently flowing in the direction of the main stream. The cavity interface was not smooth as it was for water, it was a very rough turbulent interface. The noise produced was also distinctively different to that of water. Instead of the distinctive loud sharp crackling sound, the noise signature of the hydrocarbons was much more of a low rumbling sound and definitely not as loud as the water cavitation. These descriptions of the cavitation noise apply equally to both the nozzle and the centrifugal test pump. The much quieter and less violent sound of the cavitating hydrocarbons is due to the cushioning effect of the air, as the bubbles collapse much less violently. It has been shown that the injection of air into the inlet of a cavitating pump or turbine will cut down noise and vibration (Young 1989).

#### **7.4.1.2 Conclusion.**

There is one main conclusion that arises from the observations of the test fluids cavitating in the convergent divergent nozzle. The air content of the hydrocarbons would appear to play a large part in the mode of cavitation occurring. The volume of air appears to make up a larger proportion of the void fraction in the cavitation zone for the hydrocarbons than for water. This more significant air void fraction must therefore have a greater effect on the performance characteristic of the nozzle. The dissolved air in the hydrocarbons should therefore play an equally large role in the effect of cavitation on the performance of a centrifugal pump.

## 7.5 Thermodynamic and gas content affects on water and hydrocarbons.

In this last section the thermodynamic effects of pumped hydrocarbons will be discussed. That is, why do hydrocarbons have a different cavitation performance to that of cold clean water? This part of the discussion draws together the results from the pump NPSH tests and the results and observations of cavitation in the nozzle test section, in an attempt to understand the different effects of the fluids on cavitation. This discussion of the cavitation effects of the fluids is divided into two parts.

1. The effect on the 3% head and efficiency drops for the pump and nozzle respectively. This is the main criteria the cavitation performance hydraulic machines are judged on so the effect of the fluid type on this point is the most interest. The effect on the fully developed cavitation will be mentioned in this section, although this has little significance to hydraulic machines, as a pump with fully developed cavitation will be completely vapour locked and will not operate.
2. The effect on cavitation inception, this is significant if trying to avoid cavitation all together. This would be important if the avoidance of erosion damage is a critical factor, as mentioned previously, erosion starts well before performance is effected.

Although a large amount of test data was gathered during the duration of this project it is felt that there is still not enough information to quantify the effects fully. Therefore for the main part trends in the data are described rather than fully quantified.

### 7.5.1 Performance.

Both sets of performance data, for the pump and the nozzle, show that cold clean water has a lower  $NPSH_R$  than the hydrocarbons (Refer to figure 6.5-1)<sup>b</sup> and gas oil has lower  $NPSH_R$  than kerosine (For the pump  $\Delta NPSH_{kero} \approx 0.5m$  and  $\Delta NPSH_{gas\ oil} \approx 0.4m$ ),

---

<sup>b</sup> Although it can be seen from figure 6.3-7 that the water gave a better cavitation performance than the hydrocarbons, at 30°C, the pump data used for comparison purposes is the data taken at approximately 20°C. The reason for this is to discount the possible leakage effects discussed earlier in this chapter and so other effects (hydraulic effects) are not mistaken as thermodynamic effects.

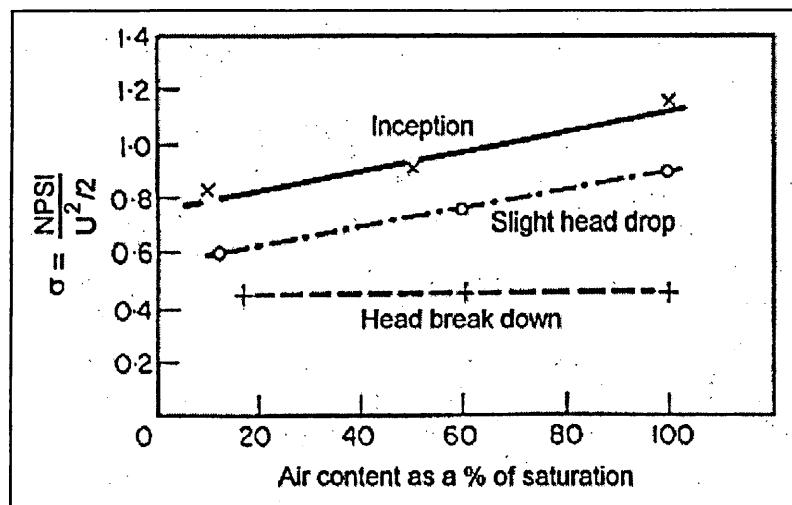
although the magnitude of performance difference is dependent on the test device. This is most likely due to the fact that the pump is a dynamic machine thus has losses etc., as discussed previously, the nozzle on the other hand is only a passive flow device thus has no dynamic effect on the fluid. This result was not entirely expected, most texts including Stepanoff (1957 and 1965), Knapp et al (1970), Anderson (1980) and Brennen (1994<sup>Ⓞ</sup>) all state that other liquids particularly hydrocarbons can operate with a lower  $NPSH_R$  than that of cold clean water. However after having discounted all sources of error in calculation and the tests, it was concluded that the result was a legitimate effect. Thus an explanation of the result needed to be found.

As most thermodynamic NPSH adjustment methods have their foundation in Stepanoffs *B* theory, it was used as a indicator of whether these methods would predict this effect. It can be seen from the  $\Delta h_t$  data in tables 7.3-1 and 7.3-3 and equation 7.3-3 that Stepanoffs NPSH adjustment factor predicts a negligible change in NPSH for these hydrocarbons from the 19°C water data. Thus the predicted change of  $\sigma_{3\%}$  for the fluids will be similarly negligible. However on closer inspection of the *B* factor theory it is not possible to obtain a negative adjustment.

As the *B* -factor method and similar prediction method are based on the on the assumption of vaporous cavitation, and that these methods do not model the effect found, we are led away from a totally vaporous cavitation problem. Assuming now there is another effect that might contribute to this earlier performance break down. It is found the only other possible influence could be gaseous cavitation i.e. dissolved air being drawn out of solution in the low pressure zones to form air bubbles. This assumption would seem to be backed up by the observations of large amounts of dissolved air released in the cavitating nozzle. The fact that at the test temperatures the hydrocarbons used have a 12 to 16 % volume of air dissolved in the fluid. This percentage is reduced during the pump NPSH tests due to the vacuum pump method of reducing the suction pressure. However the dissolved air content at around the 3% head drop criterion was still relatively large, typically 30-40% of the saturation value. The rates of bubble growth are not as fast as vapour cavity growth, so they would not grow

as large in the time taken to traverse the divergent part of the nozzle or from inlet to discharge of the impeller. Therefore the smaller air bubbles would at first not seem to have the nozzle or pump choking effects as compared to the vapour bubbles. However the sum of the volumes of the large number of small air bubbles observed is assumed to create a significant choking effect in the impeller and nozzle passages.

The assumption of gaseous cavitation seems to be backed up by the nozzle results for the 3% efficiency drop (Figure 6.4-17). The results show clearly the effect of dissolved air on the cavitation efficiency. There seems to be no air content effect on water, but both gas oil and kerosine show a marked improvement in cavitation performance as the air content was reduced. It is not known exactly how this scales to a pump, but as there is a great deal more turbulence in a pump it is thought that air will be more readily drawn out of solution. Thus have a greater effect. This would seem to be the case referring to Figure 7.5-1 (Pearsall 1972),



**Figure 7.5-1 Air content effect of water on cavitation in a centrifugal pump.  
(Original source Schoeneberger 1956 - not found by author)**

Although it is not clear what percentage drop the '*slight head*' drop refers to (1,3 or 5% are all used), it is quite clear even in water air content can have an effect on this performance drop indicator in a pump. Although no effect is present at complete head breakdown. Not too many conclusions can be drawn from this as the details of the original work could not be found. However the larger air content of kerosine and gas oil

should show an even more pronounced effect, as it did for the nozzle. For a comparable pressure drop the approximately 10 times more air is available in the hydrocarbons for release as there is for water.

Vaporous cavitation would still play a significant part in the performance breakdown as vapour bubble growth, at the low temperatures tested, is faster compared to the growth if the tests had been carried out at higher temperatures. This is because at low temperatures there is a high specific volume of vapour. This means the mass rate of evaporation of the liquid required for bubble growth is small, thus the latent heat needed to effect the evaporation of liquid is also small thus the change in temperature across the bubble gas liquid interface is small thus there is little thermal effect on the internal vapour pressure of the fluid, whose differential pressure from the bulk fluid pressure is the driving force behind the bubble growth. For higher temperatures the inverse is true, the specific volume of vapour is much lower so the heat needed for the same volume of evaporation is much greater thus the temperature differential across the interface is much larger, artificially lowering the internal vapour pressure, this decreases the pressure differential driving force of bubble growth.

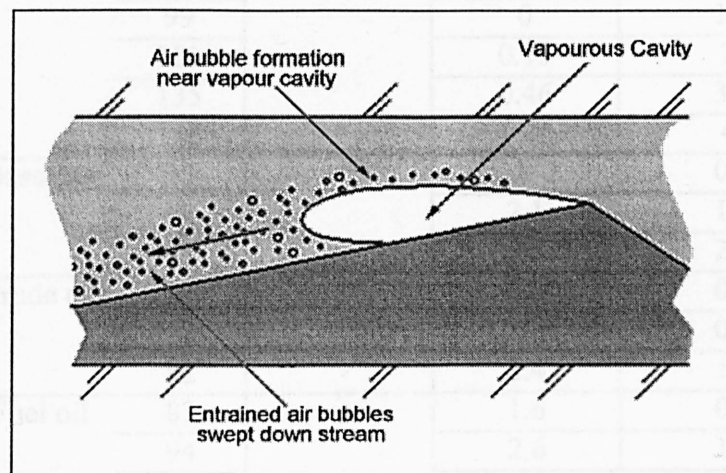
So this reduced cavitation performance would seem to be a consequence of gaseous cavitation combining with vaporous cavitation. The ambient temperatures at which the test were conducted would seem to have increased this dual action effect. At ambient temperatures the percentage of dissolved air in the fuels are high because of the low vapour pressure of the fluid : Henry's Law states *'the volume of gas dissolved is proportional to the partial pressure of the gas above the liquid'*. So as the temperature rises the vapour pressure increases thus assuming a constant pressure above the liquid the amount of dissolved air is decreased proportionately to the rise in vapour pressure. So as temperature rises the cavitation performance will improve for two reasons;

1. The air content will be reduced thus decreasing the effect of gaseous cavitation on performance.



2. The increase in vapour pressure means the vapour bubble growth is slower, for the reasons stated above, so it also has less of an effect on performance.

A suggestion of the mechanism by which this dual action cavitation works, is as follows (refer to figure 7.5-2). After inception the initial cavity formation is mainly vaporous. The bulk fluid pressure is above atmospheric pressure, so dissolved air remains in solution, however near and at the cavity boundary the local pressure falls below that of atmospheric pressure. So the vaporous cavity acts similarly to a free surface under vacuum, drawing the dissolved air out of solution to form air bubbles which are subsequently swept down stream. The larger the 'free surface' of the cavity more air that will be drawn out of solution. This would explain the observation that the lower the air content of the hydrocarbons the larger the cavity would have to grow before drawing enough air out of solution to obscure it from vision.



**Figure 7.5-2 Formation of air bubbles around vapour cavity.**

It would appear therefore that the main reason Stepanoff's theory did not predict this negative adjustment is because it does not include the effects of dissolved gas content. Also no other prediction method could be found that compensates for these gas content effects. This is possibly due to the fact that there is very little published experimental data on thermodynamic effects, to base a comprehensive theory on. The fluids on which Stepanoff (1961) used to formulate his theory apart from the ubiquitous water were



methane, propane, butane, freon 11, ammonia, liquid nitrogen and liquid oxygen the dissolved air content of which are all very low (Information from various sources ICI, Air Products Ltd. and fluid property data reference books) and the vapour pressures are all relatively high, for the range of temperatures tested (at STP). Thus the effects gaseous cavitation effects were negligible. The most similar experimental data to that of the present study is that of Spraker (1965) who conducted experiments on water, gasoline, crude oil and fuel oil and several other fluids. Some of the results are tabulated below in table 7.5-1 These results are fairly representative of the results he compiled on hydrocarbons.

Fluid	Temp (°C)	NPSH (m of fluid)	$\Delta$ NPSH (m of fluid)	Vapour Pressure (bar)
Water	23	9.8	0	0.03
	60		0	0.20
	99		0	1.01
	121		0.15	2.1
	135		0.46	3.25
	146		1.28	4.4
Gasoline	38		0	0.83
	62		2.1	1.70
	83		3.5	2.65
Crude oil	33		0.2	0.50
	42		1.2	0.90
	82		2.4	1.50
Fuel oil	83		1.6	0.67
	94		2.6	1.17
	115		3.2	2.16

**Table 7.5-1 Sprakers data for a top suction pump  
( 3550 rpm : 71m head : 136 m<sup>3</sup>/hr )**

The temperatures at which Sprakers study was carried out for these hydrocarbons started at around 40°C and up to about 115°C. At STP the hydrocarbons he studied would have contained similar quantities of dissolved air to the hydrocarbons in the present study, typically 12-16% air by volume. However at these elevated temperatures the vapour pressures are much higher thus the partial pressure of the air above the fluid is much less meaning the total air content would be much smaller. The amount of air dissolved

reduces with the increasing vapour pressure (temperature). Thus by conducting the tests at higher temperatures the effect found in this study were not found. Although it can be seen at the lower temperature ranges the  $\Delta$ NPSH is small to non existent. Thus with further reduction in temperature and a decrease in vapour pressure and an increase in air content, it is not unfeasible to assume the cavitation performance would have reduced yet further.

On a graph of air content of a fluid against the fluids vapour pressure, there will be a zone within which gaseous cavitation and vaporise cavitation both contribute to a more advanced performance break down. Within this zone the  $\Delta$ NPSH will be negative and outside the zone it will be positive, the border being a negligible change in NPSH.

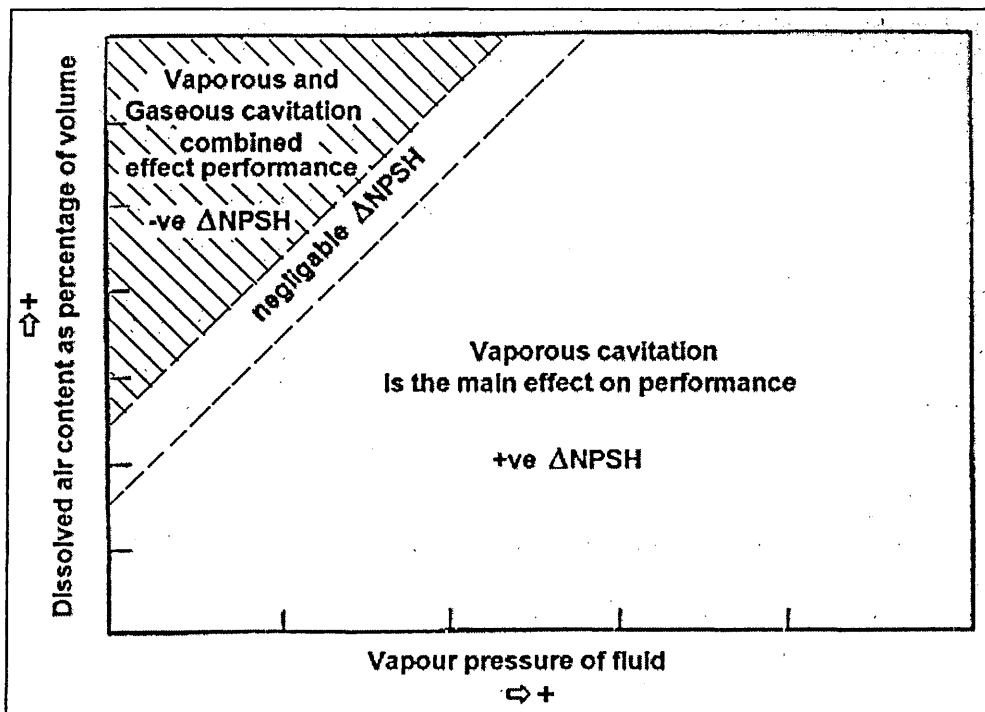
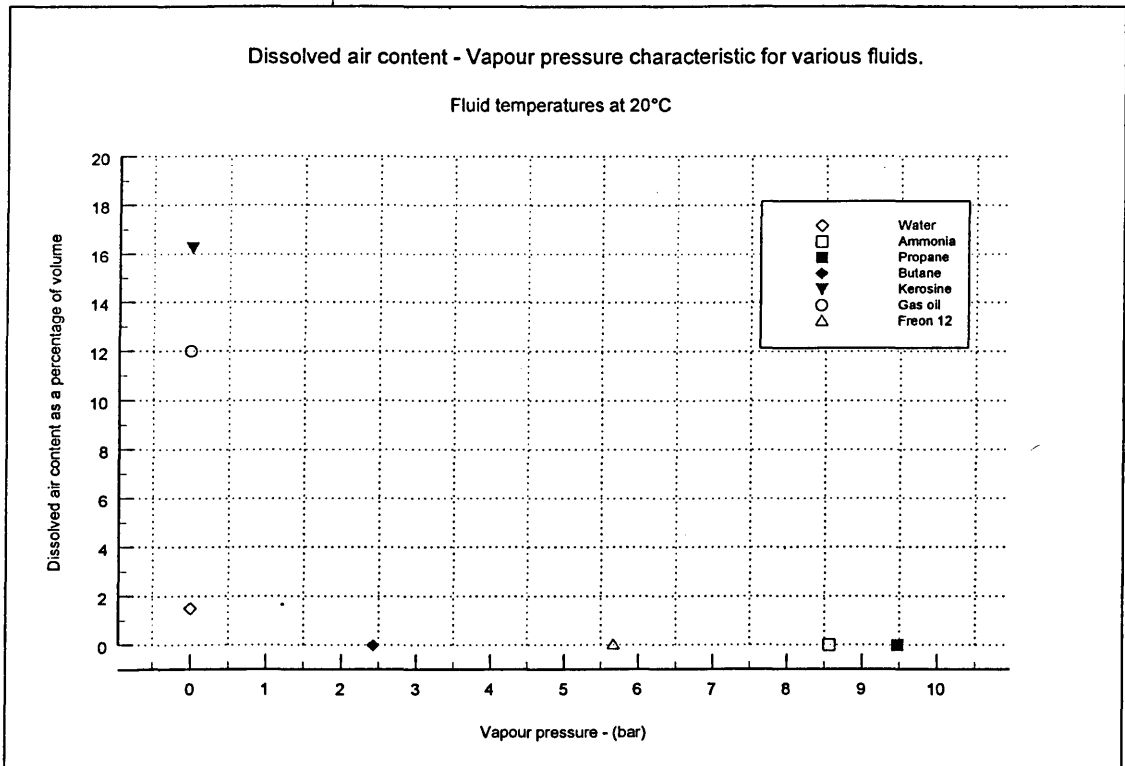


Figure 7.5-3 Zone of gas content effect on cavitation performance.

There is not enough data on enough fluids to characterise a chart such as this. The temperature restrictions of the rig meant that the cross over point from negative to positive adjustment of the fuels could not be found. However as the knowledge of cavitation on fluids other than water is increased it may prove to be a useful tool in

deciding whether the air content will effect the cavitation performance. For a particular fluid this graph could be plotted for a range of temperatures, the air content decreasing as temperature, thus vapour pressure increase. Or in the case of figure 7.5-4 a range of fluids at constant temperature. This shows kerosine and gas oil are in the area of negative  $\Delta NPSH$  and the other fluids, which have been used in cavitation research, are in the vaporous thus positive  $\Delta NPSH$  adjustment zone.



**Figure 7.5-4 Gaseous - vaporous cavitation characteristic graph for several fluids.**

### 7.5.2 Inception.

As noted in previous sections cavitation inception;  $\sigma_1$  appears to be closely related to the population of the free stream nuclei, although many experiments only show the relationship of air content to inception, as it is much easier to measure and control. As no attempt was made to control or measure these nuclei in the present study it is not

known how reliable the data is. The large variation in the data is evident, most likely due to the variations in free stream nuclei, as the variance is several orders of magnitude greater than the estimated instrumentation errors. However very little data is available on cavitation inception in hydrocarbons, or many other fluids except water for that matter, so any information will help push the frontier of knowledge forward.

The results from the incipient data in the nozzle would seem to indicate that the processes at work are different to those of the more fully developed cavitation at the 3% efficiency drop and fully developed cavitation (Refer to figures 6.4-16 and 6.4-17). The main observations from the results are as follows:

1. Gas oil gave the best  $\sigma_i$  performance followed by water then kerosine, which is a different order to that of the 3% efficiency drop data.
2. The inception number appears to be dependent on the dissolved air as a percentage of the saturation value even for fluids with high saturation volumes of dissolved gas.

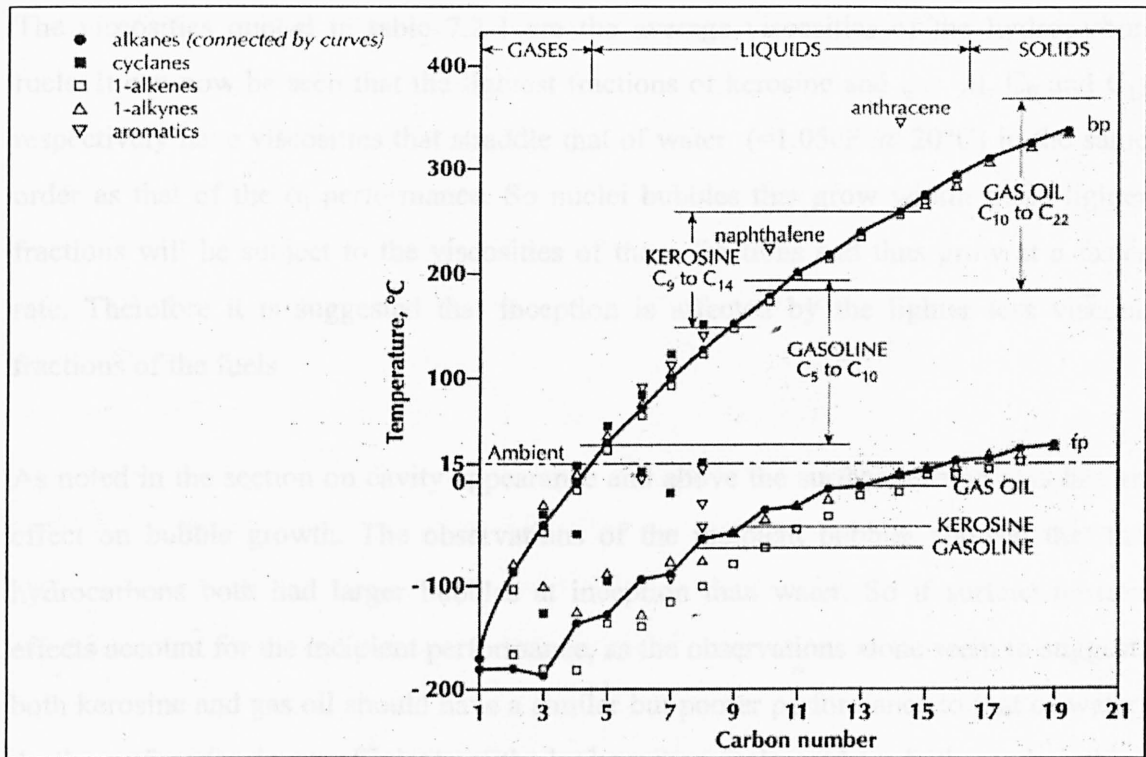
$$\sigma_i = f(\alpha)$$

The scaling of cavitation inception to that of other fluids is an area where there is very little data. However from the work on water the main influence on cavitation inception would appear to be the Reynolds number (Arndt 1974), ignoring the effect of air and nuclei content for the time being. There are two reasons for this, first is that the turbulence of the flow can have an effect on inception because the pressures at the centre of turbulent vortices can be significantly lower than that of the main body of flow. The second factor is involved with the residence time of the nuclei in the low pressure zone. There is a critical time for a bubble to grow to an observable size in the low pressure zone, this time is dependent on the viscosity (effectively the Re number) but the surface tension also affects bubble growth, this factor will be discussed after the effect of viscosity.

The viscosity of a fluid has a damping effect on the growth of a bubble within the bulk of that fluid. The higher it is the slower the bubble growth and collapse, so the larger the critical residence time. As the velocities at inception for all of the fluids are of the same order ( $V_o \approx 5-8m/s$ ) the residence times in the low pressure area in the throat of the test section are similar. Also a cavitation nuclei needs to reach a certain critical size before they will grow explosively Arndt (1981) and Brennen (1994<sup>2</sup>) to a visible cavitation bubble. Therefore assuming the residence times in the low pressure zone are similar a bubble nuclei growing in fluids with a high viscosity will need much greater tensions to achieve the critical size, than a bubble growing in a low viscosity fluid. As the greater pressure differential is needed to overcome the larger damping effects of the higher viscosity fluid. This means that high viscosity fluids will sustain higher tensions i.e. lower cavitation numbers before inception occurs for comparable flow rates.

One of the main effects on  $\sigma_i$  would therefore appear to be the viscosity. The greater the viscosity the better the incipient cavitation performance, as the nuclei do not have the chance to grow to the critical size in the low pressure area. This is backed up by Rood (1989) in his conclusion to several Reynolds number experiments on various axisymmetric bodies in water, where he states that “ *in the absence of information about nuclei spectra, that viscous effects are factors in the determination of both the form of cavitation and the inception conditions*”

Now referring to table 7.2-1 it can be seen that gas oil has the largest viscosity then kerosine and lastly water. So Reynolds number scaling would not appear to be applicable to these hydrocarbon fuels. However as bubble nuclei growth is at the micro scale, the chemistry of the hydrocarbons should be looked at more closely.



**Figure 7.5-5 Boiling range of typical petroleum fuels.**  
(Source Goodger (1993))

Hydrocarbon fuels are made up of a range of pure hydrocarbon fluids which fall into certain boiling ranges, and denoted by their carbon number;  $C_n$ . Kerosine is made up of a range of fluids that fall into the bracket of  $C_9$  to  $C_{14}$  and the gas oil specification covers the range  $C_{10}$  to  $C_{22}$  (see figure 7.5-5). From an examination of these pure hydrocarbon fluids it was found that : fluids with similar carbon numbers had similar viscosities but as the carbon number increased so did the viscosity. A study was then made of the fluids within the boiling ranges of kerosine and gas oil a few examples of which can be seen below from in table 7.5-2

Molecular Formula	Name	Viscosity (cP) @ 20°C
$C_9H_{18}$	1-Nonene	0.80
$C_{10}H_8$	Napthalene	1.65
$C_{11}H_{10}$	1-Methlnepthalene	1.75
$C_{14}H_{10}$	Anthracene	2.79
$C_{15}H_{32}$	n-Pentadecane	2.61

**Table 7.5-2 Viscosities of some constituent fluids of kerosine and gas oil.**

The viscosities quoted in table 7.2-1 are the average viscosities of the hydrocarbon fuels. It can now be seen that the lightest fractions of kerosine and gas oil, C<sub>9</sub> and C<sub>14</sub> respectively have viscosities that straddle that of water (=1.05cP @ 20°C) in the same order as that of the  $\sigma_i$  performance. So nuclei bubbles that grow within these lighter fractions will be subject to the viscosities of those fractions and thus grow at a faster rate. Therefore it is suggested that inception is affected by the lighter less viscous fractions of the fuels.

As noted in the section on cavity appearance and above the surface tension also has an effect on bubble growth. The observations of the incipient bubbles showed that the hydrocarbons both had larger bubbles at inception than water. So if surface tension effects account for the incipient performance, as the observations alone seem to suggest, both kerosine and gas oil should have a similar but poorer performance to that of water. As the surface tension coefficients of the hydrocarbon fuels used are both nearly a third of that of water, the bubbles should grow faster, thus larger in a similar residence time. One questionable point about the surface tension effect on bubble growth is its applicability to the very small bubble nuclei that are the starting point for inception (Knapp et al 1970). This is because the surface of the bubble can only contain a limited number of molecules thus the surface tension, which is based on molecular attraction can no longer be considered constant<sup>Fr</sup>.

Therefore it is suggested that the viscosity is the is the most influential fluid property in determining when inception occurs. But once the nuclei has passed the critical size and has grown explosively, i.e. inception, the bubbles have grown large enough for the surface tension of the fluid to have more of an effect. The surface tension then almost instantaneously starts effecting the incipient bubble size. Thus as gas oil is the more viscous of the fluids (lightest fraction viscosity; C<sub>14</sub>) it has the best incipient cavitation

---

<sup>Fr</sup> No data could be found on the surface tensions of the pure fractions of hydrocarbons making up kerosine and gas oil. But as the surface tensions are nearly the same for the two different ranges of carbon number. The variation in carbon number over the total range, C<sub>9</sub> to C<sub>22</sub> is not thought to have a significant effect on the magnitude of the surface tension coefficient.

performance, but as the surface tension is low compared to that of water, the bubbles grow to a much larger size.

The effect of air content is a much harder phenomenon to explain as most work carried out on inception has been conducted on water and a few other fluids such as liquid hydrogen oxygen and nitrogen. Brennen (1997) states there is no published data on air content in hydrocarbon fuels but possibly there is some related work of air content in hydraulic oil valves, although none could be found. Having made no nuclei measurements, the only general conclusion that can be drawn is that the incipient cavitation appears to be dependent on the air content as a percentage of the saturation value of fluids and not the total air content. This means that the relationship stated in equation 7.4-2 ( $\sigma_i = f(\alpha)$ ) holds true for fluids, even those with large volumes of dissolved air.

It is not known how significant comparisons between the inception data and the performance data of the nozzle would be, due to the uncertainty of the inception data, as nuclei density information was not collected. It can be seen however from figures 6.4-16 and 6.4-17 that the fluid orders between cavitation criteria  $\sigma_i$  and  $\sigma_{3\%}$  change. Gas oil performing better than water at inception but worse at the 3% efficiency drop. This shows that there must be fundamental differences between the mechanisms at work at inception and the more fully developed stages of cavitation which will need to be further investigated.



## 8. Conclusions and Further work.

### 8.1 Conclusions.

The discussion of the results show how complex a phenomenon cavitation is and how near impossible producing an all encompassing analytical solution would be. Visual observations of inception through to fully developed cavitation by themselves show the large variance in type of cavitation from fluid to fluid. There is a long way to go before all the effects of the thermophysical and thermochemical properties of fluids on cavitation are understood. Theoretical analysis of cavitation helps a great deal in the understanding of the processes at work, but without good experimental results and observations in a wide range of fluids to back up these theories their application is limited.

The time spent designing, constructing and developing the dual test facility with multi fluid capabilities meant a more comprehensive test schedule could not be undertaken, such a using mixtures of kerosine and gas oil. However the large volume of tests that were conducted have discovered several areas of key importance to cavitation in hydrocarbon fuels and which have possible applications to wider cavitation issues. The main elements of the findings are listed below, along with some of the main problem areas encountered so as to help further researchers avoid them.

- Suction valve throttling tests are impossible to conduct on hydrocarbons because of the large dissolved air content. Two phase flow conditions are created by cavitation of the suction throttle valve and creates pump inlet conditions that are too unstable.
- Small changes in fluid viscosity (small increase in temperature) would appear to affect the cavitation performance of an unshrouded impeller. A small temperature increase was shown to have significant improvement in the cavitation performance of the pump possibly by increasing leakage effect, which directly affects the zone of

cavitation. This was found for both water and gas oil, whose viscosity changes are large in comparison to that of kerosine were the effect did not manifest itself. The effect was not found in the nozzle as it is a passive flow device consequently there are no leakage effects.

- For water cavitation in the nozzle, the fluid temperature range of 20 to 50°C had no significant effect on cavitation performance.
- The reduction of the air content of water gave a linear improvement in the incipient cavitation performance of water, but had no effect on the 3% efficiency drop or fully developed cavitation.
- For hydrocarbon cavitation in the nozzle, the fluid temperature range of 20 to 30°C had no significant effect on any of the cavitation conditions.
- The reduction of the air content of the hydrocarbons linearly improved the incipient cavitation performance and the 3% efficiency drop values but had little to no significance on the fully developed stage of cavitation.
- Incipient cavitation is dependent on the air content as a percentage of the saturation value but the 3% drop in efficiency cavitation criteria is dependent on the total air content as a percentage of volume.
- It is unwise to assume all hydrocarbons have a better cavitation performance than cold clean water, as most texts suggest. Particular care should be taken at ambient temperature air saturated fuels. The larger dissolved air content of hydrocarbons fuels at ambient temperatures causes an additional effect on the vaporous cavitation, causing the cavitation performance to be worse than that of cold clean water. This was found in both the pump and the convergent divergent nozzle.

- The viscosity of the fluids would appear to be one of the main influencing factors in incipient cavitation performance. High viscosity fluids slow down the bubble growth rate which can stop it reaching the critical size at which explosive growth occurs. This means for a system with the same residence time (flowrate), the higher the viscosity fluid that is used the higher the pressure differential is needed to increase the growth rate so the bubble passes the critical size for the bubble to grow explosively and inception to occur. Therefore the greater the viscosity the better the incipient cavitation performance. However after the point of inception the surface tension also begins to effect on bubble growth. Thus fluids with low surface tensions have larger incipient bubbles. NB for the hydrocarbon fuels the viscosity of importance is that of the lightest petroleum fraction within the fuel (i.e. lowest carbon number) and not the average fuel viscosity.
  
- The other influence on the incipient performance is the air content as a percentage of the saturation value. As the percentage of saturation is reduced the incipient performance gets better. NB it is not effected by the total air content of the liquid. Therefore it would appear the number of cavitation nuclei present in a fluid is independent of total air content. But varies with the percentage of saturation of that air content.

One final point is that although experimentation with gas oil and kerosine provided very interesting results, further work with hydrocarbons should make use of the pure hydrocarbon fractions. Although they are very expensive (Note : this is the reason they were not used in this project) they should produce much clearer data to be theoretically analysed than the mixture of pure fluids in kerosine and gas oil. It would seem that the lighter fractions are responsible for both inception (lower viscosity) and the more developed stages of cavitation (lighter fractions have the higher vapour pressure), therefore use of a C<sub>9</sub> hydrocarbon and a C<sub>14</sub> hydrocarbon instead of kerosine and gas oil respectively, would probably have produced similar results. However the property values for the pure hydrocarbons are much easier to find.

## 8.2 Further work.

The opportunity for further work in this field would seem to be inexhaustible as there is very little published data on cavitation in other fluids compared to that of the data on water. The obvious target for the study of other fluids is hydrocarbons, as next to water they are probably the most pumped fluid. Theoretical work needs sound experimental data and observations to be based on, so initially any further work should be based firmly in the experimental camp. The scope for suggesting further experimental work is enormous. The following points are therefore areas where the author feels that this research could not answer due to time considerations or temperature limitations the test rig.

- The effect of viscosity on the leakage in an unshrouded impeller and its subsequent effect on cavitation performance, so that these effects can be compensated for or discounted when investigating the thermodynamic effects of fluids .
- The characterisation of the change between negative and positive NPSH adjustment factors to find a gaseous cavitation tendency quotient that would indicate the possibility of a worse cavitation performance than the cold water condition. Possibly based on a air content - vapour pressure ratio.
- As very low air content tests were not possible on the test rig the effect of very low dissolved air concentrations in hydrocarbons were not discovered. Although it is not thought that it will vary from the linear relationship found, experimental work will confirm this.
- No cavitation nuclei measurements and their effect on inception could be found on fluids other than water. This linked with the fact that the inception appeared to varied with the air content as a percentage of saturation, would seem to make an excellent area for further experimental work.

Finally the test rig constructed for this project is thought a very reliable and useful tool in the study of cavitation. There is scope for further development of the test rig such as increasing its temperature range, and improving the air content control. However as it stands it should continue to provide a source of invaluable experimental data, to aid the search for a solution to the problem of cavitation.

---

## REFERENCES

---

- ANDERSON H.H. *Centrifugal pumps*, 3<sup>rd</sup> edition, Trade & Technical Press Ltd. Surrey, ISBN 85461-076-6, 1980.
- ARNDT R.E.A. 'Cavitation inception and how it scales; A review of the problem with a summary of recent research' Symposium of High Powered Propulsion of Large Ships, Wageningen, paper 21, p1-65 1974.
- ARNDT R.E.A. 'Cavitation in fluid machinery and hydraulic structures' Annual Review of Fluid Mechanics, 13 p273-328, 1981.
- AVELLAN F. *Cavitation tests of hydraulic machines : procedure and instrumentation*, ASME Cavitation inception FED v177 p91-102, 1993
- BARNABY S.W. and THORNYCROFT J. *Torpedo boat destroyers*, Proc. Inst. Civil Eng. 122,57,1895
- BARENBOIM A.B. *Cavitation for modelling cavitation phenomena in pumps for refrigeration liquids*, BHRA, T-865, October 1966 (Translated from the Russian *KHOLODIL'NAIA TEKHNIKA I TEKHNLOGIA*, 1 pp95-103, 1965 )
- BESANT W.H. *Hydrostatics and hydrodynamics*, Deighton Bell, Cambridge p170, 1859.
- BILLET M.L. *Cavitation nuclei measurements - a review*, Proceedings of the ASME Cavitation and multiphase flow forum, FED 23, p31-38, 1985
- BILLET M.L., HOLL J.W. and WIER D.S. *Correlation of thermodynamic effects for developed cavitation*, Journal of Fluids Engineering 97,4, December 1975, pp507-514.
- BIRKETT P. *Private communication to the author containing property data on gas oil calculated by a fluid properties prediction program PPDS-2*, From LUCAS AEC, Solihull, 14<sup>th</sup> December 1995.
- BLAKE J.R. *Cavitation bubbles near boundaries*, Annual Review of Fluid Mechanics, v19 p99-123, 1987
- BLAKE J.R. and ROBINSON P.B. *Pressures on a rigid boundary due to motion of a collapsing cavitation bubble*, Cavitation and Multiphase Flow, ASME FED v210 p181-185, 1985
- BRENNEN C.E. *Cavitation and bubble dynamics*, Oxford University Press, 1994<sup>Ⓟ</sup>

- BRENNEN C.E. *Hydrodynamics of pumps*, Oxford University Press, 1994<sup>©</sup>
- BRENNEN C.E. *Subject Re : Cavitation-air content-hydrocarbons*, Private comunicaton to the author by e-mail : brennen@piccolo.cco.caltech.edu , 1997.
- CANSDALE J.T. *The effect of using jet transfer pumps on the dissolved air content of fuel in aircraft*. Royal Aircraft Establishment, Technical report 78024, February 1978.
- CHALABY A.A. and THEW M.T. *Cavitation in small centrifugal pumps : Effects of some variation in impeller geometry and comparison of water antifreeze mixtures*, IAHR Symposium: Operating problems of pump stations and power plants, Amsterdam, 1982.
- CHALABY A.A. and THEW M.T. *Cavitation in a binary mixture of polar liquids (Water-Antifreeze) in a small centrifugal pump*, IMechE Conference on Cavitation C199/83 , 1983
- CHIVERS T.C. *The effect of fluid properties on cavitation in a centrifugal pump: Theory and Experiment* , PhD Thesis University Collage Cardiff Sept 1967.
- CHIVERS T.C. *Temperature effects on cavitation in a centrifugal pump: Theory and Experiment* , Proceedings of the IMechE Fluid Plant and Machinery group, Vol. 184 Part 1 Number 2, First Paper 1970.
- CHIVERS T.C. *Correlation of cavitating performance for a centrifugal pumps handling various liquids*, Proceedings of the IMechE Fluid Plant and Machinery group, Vol. 184 Part 1 Number 2, Second Paper 1970.
- COOPER M.G. and CHANDRATILLEKE T.T. *Growth of diffusion-controlled vapour bubbles at a wall in a known temperature gradient*, Journal of Heat and Mass Transfer, 24, 9, pp1475-1492, 1981.
- COOPER M.G. and STONE C.R. *Boiling of binary mixtures - study of individual bubble*, Journal of Heat and Mass Transfer, 24, 12, pp1937-1950, 1981.
- COOPER M.G., JUDD A.M. and PIKE R.A. Proceedings of the 6th International Conference on Heat and Mass Transfer, Toronto Paper PB-1, 1978.
- COOPER M.G., MORI K. and STONE C.R. *Behaviour of vapour bubbles growing at a wall with forced flow*, Journal of Heat and Mass Transfer, 26, 10, pp1937-1950, 1983.
- CRUMP S.F. *Determination of critical pressures for inception of cavitation in fresh water and sea water as influenced by air content of the water*, DTMB (David Taylor Model Basin, US Navy), Report 575, 1949

- CRUMP S.F. *Critical pressure for inception of cavitation in a large scale Numachi Nozzle as influenced by air content of the water*, DTMB (David Taylor Model Basin, US Navy), Report 770, 1951
- ESSO *Correction of observed density to density at 15°C*, ESSO Measurement tables advisory panel, Table E53B-Products, 1981
- FURNESS R.A. *A Basic cavitation studies in a convergent divergent nozzle*, PhD Thesis, Dept of Mech. Eng., University of Southampton, March 1973.
- FURNESS R.A. *Studies of the mechanics of "Fixed" cavities in a two-dimensional convergent-divergent nozzle*, IMechE Conference on Cavitation, C160/74, pp119-128, June 1974.
- GELDER T.F., MOORE R.D. and RUGGERI R.S. *Incipient cavitation of Freon-114 in a tunnel venturi*, NASA Technical Note D-2662, February 1965.
- GELDER T.F., RUGGERI R.S. and MOORE R.D. *Cavitation similarity considerations based on measured pressure and temperature depressions in cavitated regions of Freon-114*. NASA Technical Note D-3509, July 1966.
- GILMORE F.R. *Cavitation*, Engineering Monographs, Knapp Daily and Hammitt, McGraw Hill Book Company pp117-123, 1970.
- GONGWER C.A. *A theory of cavitation flow in centrifugal pump impellers*, Transactions of ASME 1941, 63, pp29-40
- GOODGER E.M. *Alternative Fuel Technology Series Vol. 2 Comparative properties of conventional and alternative fuels*, Cranfield Press. ISBN 0-902937-669, 1982
- GOODGER E.M. *An appreciation of hydrocarbon fuel chemistry*, Landfall press, Norwich 1993
- GOODGER E.M. *Jet fuel supply and quality*, Landfall press, Norwich, ISBN 0-9520186-16, December 1994
- HAMMITT F.G. *Effect of gas content upon cavitation inception, performance and damage*, Journal of Hydraulic Research Vol. 10, no 2 1972, p259-287
- HAMMITT F.G., IAFFERTY J.F. et al *Gas content, size, temperature and velocity effects on cavitation inception in a venturi* ASME Winter Annual Meeting November 12-17 1967, 67-WA/FE-22
- HARRISON M. *Experimental study of single bubble cavitation noise* Journal of the Acoustic Society of America, 24 pp776, 1952



- HOLL J.W. *An effect of air content on the occurrence of cavitation*, Journal of Basic Engineering, (82) December 1960, p 941-946
- HOLL J.W. , BILLET M.L. and WIER D.S. *Thermodynamic effects on developed cavitation* , Journal of Fluids Engineering 103, December 1981, pp534-541.
- HOLL J.W. and TREASTER A.L. *Cavitation hysteresis*, ASME Journal of Basic Engineering, v88 p 199-212, 1966.
- HUTTON S P and FURNESS R.A. *Thermodynamic scale effects in cavitating flows and pumps*, IMechE Conference on cavitation , C184/74 pp329-340, June 1974 .
- HYDRAULIC INSTITUTE *Hydraulic institute standards for centrifugal, rotary and reciprocating pumps*, 14<sup>th</sup> edition , Hydraulic institute, Ohio, USA, January 1983.
- IVANY R.D. and HAMMITT F.G. *Cavitation bubble collapse in viscous compressible liquids - Numerical analysis*, Journal of Basic Engineering, pp977-985 1965.
- IYENGAR K.S. and RICHARDSON E.G. *The role of cavitation nuclei*, IBID 46, Fluids report No. 57, August 1957
- JACOBS R.B, MARTIN K.B. and HARDY R.J. *Direct measurement of net positive suction head*, Journal of basic engineering ,June 1959 pp147- 152.
- JACOBS R.B, *Prediction of symptoms of cavitation*, Journal of Research, V 65C, No 3, July - September 1961
- KAMIYAMA S. and YAMASAKI T. *Prediction of gaseous cavitation occurrence in various liquids based on two-phase flow analogy*, Journal of Fluids Engineering 103, December 1981, pp551-556 .
- KAMIYAMA S. and YAMASAKI T. *Critical condition of cavitation occurrence in various liquids* , International Symposium on Cavitation Inception, Winter Annual meeting of ASME New Orleans, FED-Vol.16, December 9-14 1984 , pp103-107.
- KELLER A.P. *Investigations concerning scale effects of the inception of cavitation*, Proc IMechE, Conference on cavitation p109-117, 1974.
- KIRKWOOD J.G. and BLETHE H.A. *A pressure wave produced by an underwater explosion*, OSRD Report 588, 1942.
- KNAPP, DAILY and HAMMITT *Cavitation, Engineering Societies Monographs* Mcgraw Hill Book Company 1970.

- LAMB H. *Hydrodynamics*, 6th ed., Cambridge university press, London 1932, (reprint by Dover ,1942).
- LEHMAN A.F. and YOUNG J.O. *Experimental investigations of incipient and desinent cavitation* , Journal of Basic Engineering, June 1964 , p 275-284
- LIDE D.R. and KEHIAIAN *CRC handbook of thermophysical and thermochemical data*, CRC Press, ISBN 0-8493-0197-1 , 1994
- LOBANOFF V.S. and ROSS R.R. *Centrifugal pumps design and application*, Gulf Publishing Company USA, 1985.
- LORD RAYLEIGH *On the pressure developed in a liquid during the collapse of a spherical cavity*, Philosophy Magazine Vol.34, pp94-98, 1917.
- LUI Z., KUHN DE CHIZELLE Y. and BRENNEN C.E. *Cavitation event rates and nuclei distributions*, ASME, FED Cavitation inception Vol. 177, p13-23
- LUSH P.A. and SKIPP R.S. *High speed cine observations of cavitating flow in a duct*, Int. Journal of heat and fluid flow, V7 No.4 December 1986.
- LUSH P.A. *Materials for minimum cavitation: Part 2*, Chartered Mechanical Engineer, October, pp31-33, 1987
- MATSUMOTO Y. and NISHIKAWA H. *Performance of cascade of blade in two phase flow (Modelling and Numerical calculations)*, JSME International Journal, Series II v31, n4, p652-659 1988.
- MATSUMOTO Y. and YAMADA M. *Behaviour of a gas bubble in an oscillatory pressure field*, The Second International Symposium on cavitation, Tokyo p288-296, April 1994
- MATSUMOTO Y. and TAKEMURA F. *Influence of internal phenomena on gas bubble motion (Effects of thermal diffusion, phase change on the gas-liquid interface and mass diffusion between vapour and non-condensable gas in the collapsing phase)*, JSME International Journal, Series B 37,2, 1994.
- McNULTY P.J. and PEARSALL I.S. *Cavitation inception in pumps*, ASME International symposium on cavitation inception p163-170, 1979.
- MEYER R.S., BILLET M.L. and HOLL J.W. *Free-stream nuclei and cavitation*, Proc. International symp on cavitation inception, ASME FED , p55-62, 1989.

- MOORE R.D. and RUGGERI R.S. *Venturi scaling studies on thermodynamic effects of developed cavitation of Freon-114*, NASA Technical Note D-4387, February 1968.
- MOORE R.D., and RUGGERI R.S. *Prediction of thermodynamic effects of developed cavitation based on Liquid -Hydrogen and Freon-114 data in scaled venturis*, NASA Technical Note D-4899, November 1968,
- MOORE R.D., RUGGERI R.S. and GELDER T.F. *Effects of wall pressure distribution and liquid temperature on incipient cavitation of Freon-114 and water in venturi flow*, NASA Technical Note D-4340, January 1968.
- NEUMANN B. *The interaction between geometry and performance of a centrifugal pump*, Mechanical Engineering Publications Ltd. London, ISBN 0-85296-755-2, 1991
- NEWTON I. *Optiks*, Dover Publications, New York, p207 1704.
- PEARSALL I.S. and McNULTY P.J. *Cavitation inception and efficiency of a two dimensional diffuser*, N.E.L. fluids note 36, 1955
- PEARSALL I.S. *Cavitation*, Mills & Boon Ltd. London , ISBN 0.263.05000.9 , 1972
- PEARSALL I.S. *Cavitation* , The Chartered Mechanical Engineer, July 1974 pp79-85
- PERRY R.H., GREEN D.W. and MALONEY J.O. *Perry's chemical engineers handbook*, 6<sup>th</sup> Edition, ISBN 0-07-049479-7, 1984
- PLESSET M.S. and PROSPERETTI A. *Bubble dynamics and cavitation*, Annual Review of Fluid Mechanics v9, pp145-185, 1977.
- PLESSET M.S. *The dynamics of cavitation bubbles*, Journal of Applied Mechanics 16, 1949.
- PLESSET M.S. and CHAPMAN R.B. *Journal of Fluid Mechanics* n47 283, 1971.
- PORITSKI H. *The collapse or growth of a spherical bubble or cavity in a viscous fluid*, Proceedings of the First US National Congress on Applied Mechanics (ASME) pp813-821, 1957.
- REYNOLDS O. *Transactions of the Institute of Naval Architecture*, V14 Sci. Papers 1,56, 1873
- ROLLS-ROYCE LTD. *Aviation fuel and oil properties*, ACS 20361, Issue A, November 1981.

- ROSS K. *The solubility of air in aviation turbine fuels*, Shell Research LTD, Report K186, September 1970.
- RUGGERI R.S. and GELDER T.F. *Effects of air content and water purity on liquid tension at incipient cavitation in venturi flow*, NASA Technical Note D1459, 1963.
- RUGGERI R.S. and GELDER T.F. *Cavitation and effective liquid tension of nitrogen in a tunnel venturi*, NASA Technical Note D2088, February 1964.
- RUGGERI R.S. and MOORE R.D. *Method for prediction of pump cavitation performance for various liquids, liquid temperatures and rotative speeds*. NASA Technical Note D-5292, June 1969.
- RUGGERI R.S., MOORE R.D. and GELDER T.F. *Incipient cavitation of Ethylene Glycol a tunnel venturi*. NASA Technical Note D-2722, March 1965.
- SALEMANN V. *Cavitation and NPSH requirements of various liquids*, Journal of basic engineering, June 1959 pp167-180.
- SALISBURY A.G. *Current concepts in centrifugal pump hydraulic design*, IMechE, C177/82 p1-15, 1982.
- SARÓSDY L.R. and ACOSTA A.J. *Note on observations of cavitation in different fluids*, Journal of Basic engineering, September 1961 pp399-400.
- SCHOENEBERGER W. *'Cavitation tests in radial pump impellers'* PhD Thesis, TU Damstadt 1965.
- SPIERS H.M. *Technical data on fuel*, 5th ed., The British national committee world power conference, 1950
- SPRAKER W.A. *The effects of fluid properties on cavitation in centrifugal pumps*, Journal of engineering for power, 87 series A pp309-318 1965.
- STAHL H.A. and STEPPANOFF A.J. *Thermodynamic aspects of cavitation in centrifugal pumps*, Transactions of the ASME, November 1956 pp1691-1693.
- STEPANOFF A.J. *Centrifugal and Axial flow pumps*; 2nd ed., J Wiley & Sons Inc., 1957.
- STEPANOFF A.J. *Pumps and Blowers Two-phase flow*, J Wiley & Sons Inc. 1965.
- STEPANOFF A.J. *Cavitation in centrifugal pumps with liquids other than water*, Journal of engineering for power, January 1969 pp79-89.

STEPANOFF A.J. *Cavitating properties of liquids*, *Journal of engineering for power*, April 1964 pp195-200

TAKEMURA F. and MATSUMOTO Y. *Influence of internal phenomena on gas bubble motion (Effect of transport phenomena and mist formation inside bubble in the expanding phase)*, *JSME International Journal, Series B* 37,4, 1994.

TAKEMURA F. and MATSUMOTO Y. *Internal phenomena on bubble motion*. Kluwer Academic Publishers, J R Blake et al. (Eds.), *Bubble dynamics and Interface phenomena*, pp467-477, 1994.

THEW M.T. and HADJI-SHEIKE M. *Cavitation behaviour of water glycol mixtures in small centrifugal pumps*, NEL Fluid Mech, Silver Jubilee Conference, UK, November 1979.

WHEELER W. H. *Indentation of metals by cavitation* ASME Transaction, Series D, 82, 1, 184-94, 1960

WILLIAMS P.E. and MCNULTY P.J. *Some factors affecting the inception of cavitation*, NPL Symposium, *Cavitation in Hydrodynamics*, 1955, HMSO London, 1956

WARD T. and SUTTON M. *A review of the literature on cavitation in centrifugal pumps with various liquids*, BHRA, TN 892, April 1967

WEAST R.C. and LIDE D.R. *CRC handbook of chemistry and physics*, CRC Press 70<sup>th</sup> Edition, 1990

YOUNG F.R. *Cavitation*, McGraw Hill Book Company, London ISBN 0-07-707094-1 ;1989

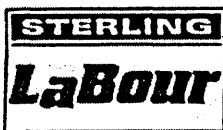
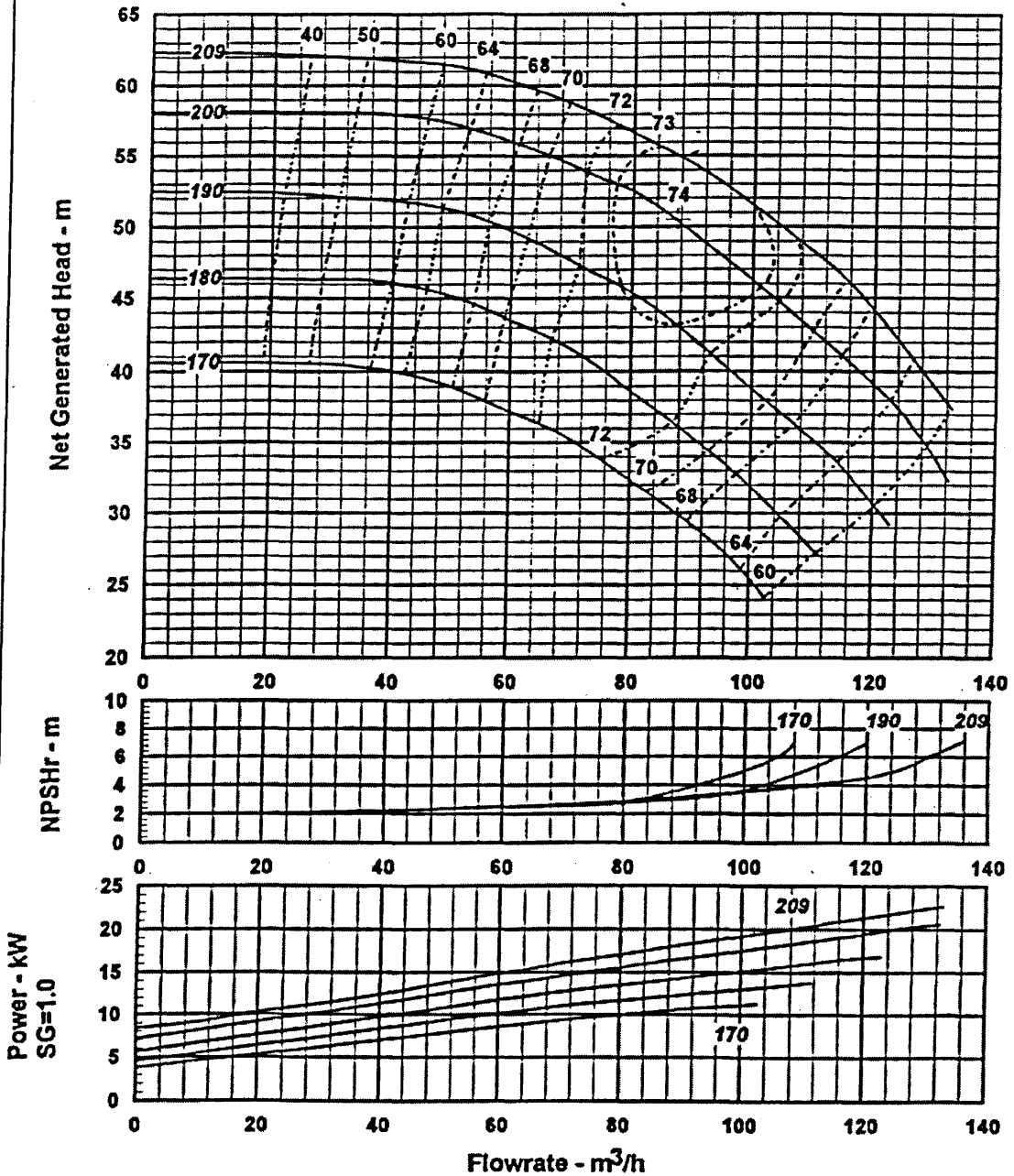
ZIEGLER G. *Tensile stresses in flowing water*, NPL Symposium, *Cavitation in Hydrodynamics*, 1955, HMSO London, 1956



**Appendix A - Test rig pump details.**

This appendix contains the details of the main pump used for the hydrocarbon cavitation test rig. The pump was the research and development model of a Sterling LaBour, *ProChem* (PC80-50-200) pump with an impeller diameter of 209mm, for further details contact the manufacturer.

<b>PUMP</b> PC80-50-200	<b>SPEED</b> 2900 RPM	<b>CURVE REF</b> 52-8520a	<b>DATE</b> 27/11/95
----------------------------	--------------------------	------------------------------	-------------------------



LaBour NORTHAMPTON  
 ENGLAND NN4 7YJ  
 Tel. 01604 700338  
 Fax 01604 700064

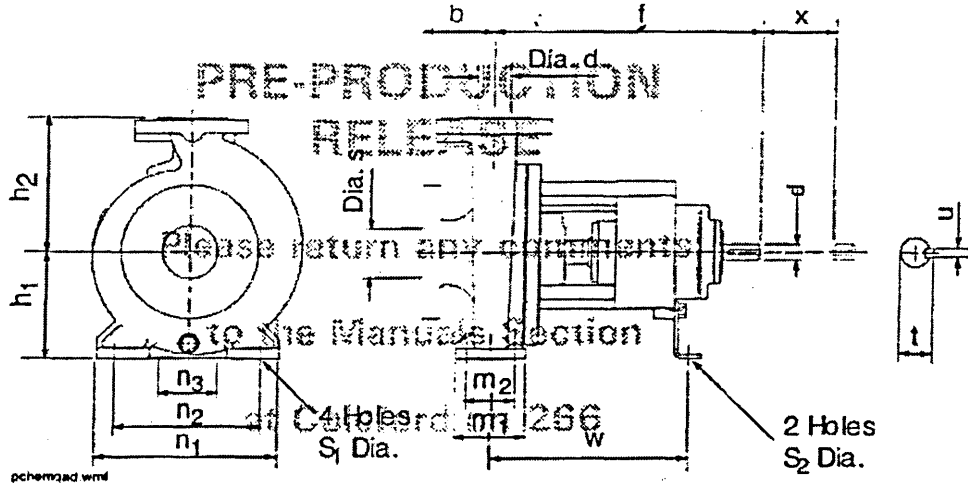
<b>PUMP TYPE</b>	<i>ProChem</i>
<b>Size</b>	<i>PC80-50-200</i>
<b>Max/Min Impeller Dia</b>	<i>209/170 mm</i>
<b>Suction Branch</b>	<i>80 mm</i>
<b>Discharge Branch</b>	<i>50 mm</i>
<b>Shaft Dia at Seal</b>	<i>35 mm</i>

Figure A-1 Manufacturers pump curves for the main circulating pump.



Section 8 Pump Information

8.1 Pump Dimensions & Weights



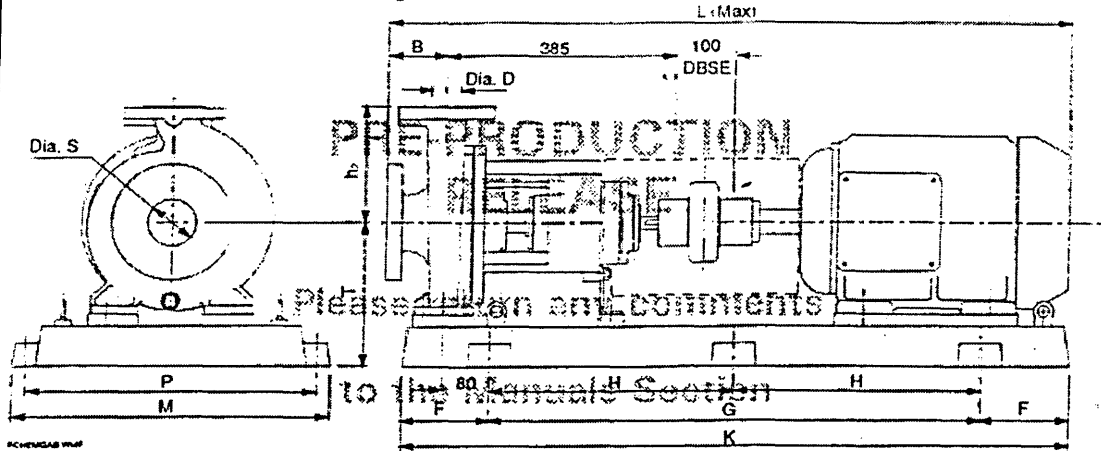
Pump Size	Dim.	50	32	160	65	40	160	80	50	160	50	32	200	65	40	200	80	50	200		
Pump Dimensions	Dia. s	50	65	80	50	65	80														
	Dia. d	32	40	50	32	40	50														
	a	80	80	100	80	100	100														
	f	385	385	385	385	385	385														
	h <sub>1</sub>	132	132	160	160	160	160														
Foot Dimensions	h <sub>2</sub>	160	160	180	180	180	200														
	m <sub>1</sub>	100	100	100	100	100	100														
	m <sub>2</sub>	70	70	70	70	70	70														
	n <sub>1</sub>	240	240	265	240	265	265														
	n <sub>2</sub>	190	190	212	190	212	212														
	n <sub>3</sub>	110	110	110	110	110	110														
	s <sub>1</sub>	14	14	14	14	14	14														
	s <sub>2</sub>	14.5	14.5	14.5	14.5	14.5	14.5														
Shaft Dimensions	w	285	285	285	285	285	285														
	x	100	100	100	100	100	100														
	d	24	24	24	24	24	24														
	l	50	50	50	50	50	50														
Weight (Maximum)	t	27	27	27	27	27	27														
	u	8	8	8	8	8	8														
	Kg.	47	50	55	53	57	58														
Nominal Maximum Power at 2900 rpm.	Kw.	7.5	11	15	15	22	30														
Estimated Noise Level	Db(A)																				

**Baseplate Dimensions and Weights**

Standard Baseplate Details	K	F	G	H	P	M	Bolts	No.	Weight Kg
Baseplate Code C	890	150	590	-	410	450	M12	4	45
Baseplate Code D	1000	150	700	350	430	470	M12	4	57
Baseplate Code E	1120	150	820	410	480	530	M16	6	83
Baseplate Code F	1220	150	920	450	530	580	M16	6	98

Figure A-2 Dimensions of the main circulating pump

8.2 Pumpset Dimensions & Weights

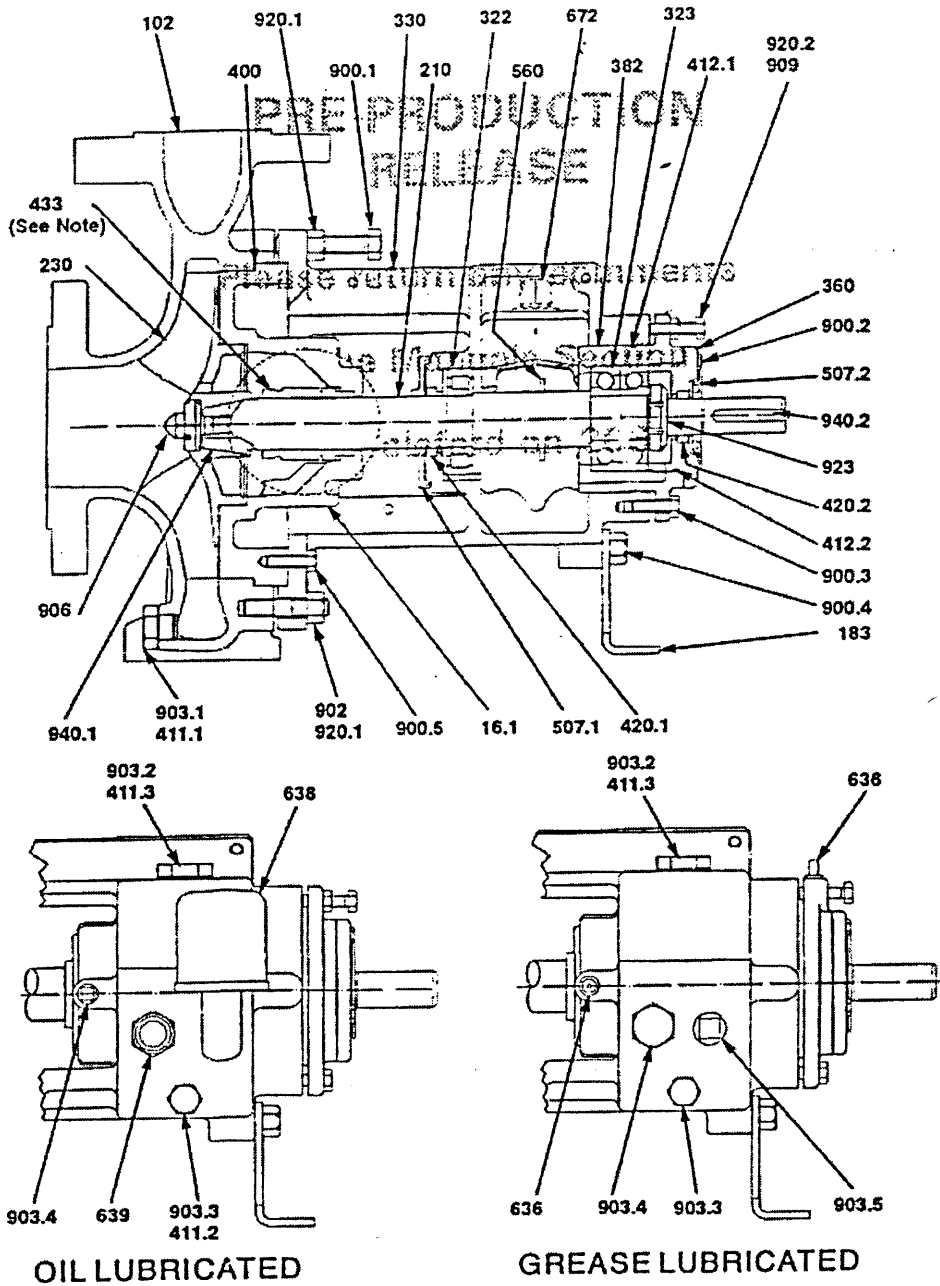


Pump Size   Dim		Motor Frame Size												
		70	80	90S	90L	100L	112M	132S	132M	160M	160M	180M	180L	200L
Baseplate:		C					D			E		F		
50 32 160	h <sub>2</sub>	160					160			160				
	B	80					80			80				
	T	182					210			230				
	L	816	860	879	904	936	842	1026	1063	1170	1170			
Weight	Kg	113	123	127	130	131	143	181	193	274	294			
65 40 160	h <sub>2</sub>	160					160			160				
	B	80					80			80				
	T	182					210			230				
	L	880	879	904	936	942	1025	1063	1170	1170				
Weight	Kg	126	129	133	134	145	184	196	277	297				
80 50 160	h <sub>2</sub>	180					180			180		180		
	B	100					100			100		100		
	T	210					210			230		250		
	L	880	899	924	956	962	1045	1083	1190	1190	1251			
Weight	Kg	134	137	140	141	155	194	206	279	299	342			
50 32 200	h <sub>2</sub>	180					180			180				
	B	80					80			80				
	T	210					210			230				
	L	860	879	904	936	942	1025	1063	1107					
Weight	Kg	132	135	138	139	153	192	230	277					
65 40 200	h <sub>2</sub>	180					180			180		180		
	B	100					100			100		100		
	T	210					210			230		250		
	L	880	899	924	956	962	1045	1083	1190	1190	1251			
Weight	Kg	136	139	142	143	157	196	208	281	301	347			
80 50 200	h <sub>2</sub>	200					200			200		200		
	B	100					100			100		100		
	T	210					210			230		250		
	L	899	924	956	962	1045	1083	1190	1190	1256	1256	1335		
Weight	Kg	140	143	144	158	197	209	282	302	348	368	429		

(Weight based on stainless steel pump with an IP55 TEFV motor)

Figure A-3 Pump set details of the main circulating pump.

8.3 Pump Cross Section



NOTE - REFER TO THE SEAL ASSEMBLY DRAWING  
FOR DETAILS OF THE MECHANICAL SEAL

Figure A-4 Cross section of the main circulating pump.

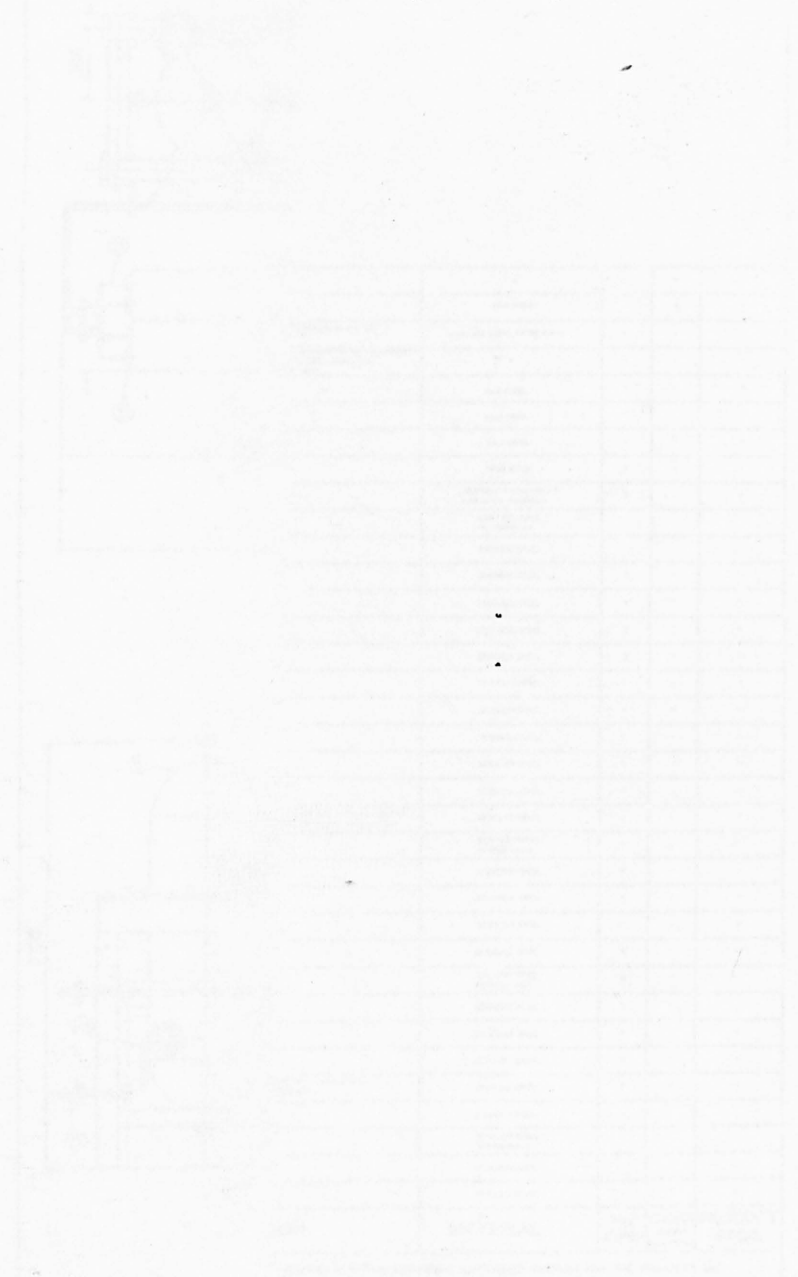
Parts Identification List - (Numbers as shown on cross section drawing)

Part	Description:	Part	Description:	Part	Description:
102	Volute Casing	420.1	Lip Seal (Pump End)	900.4	Screw (Support Foot)
161	Casing Cover	420.2	Lip Seal (Drive End)	900.5	Screw (Bearing Housing)
183	Support Foot	433	Mechanical Seal	900.6	Screw (Guard - Not
210	Pump Shaft	507.1	Flinger (Pump End)	902	Stud (Casing)
230	Impeller	507.2	Flinger (Drive End)	903.1	Plug (Volute Drain)
322	Bearing Pump End Roller	554	Washer (Not Shown)	903.2	Plug (Oil Filler)
323	Bearing Drive End Thrust	560	Pin (Oil Splash)	903.3	Plug (Oil Drain)
330	Bearing Bracket	636	Grease Nipple	903.4	Plug (Sight Glass/Nipple)
360	Bearing Cover	638	Constant Level Oiler	903.5	Plug (Oiler Tapping)
382	Bearing Carrier	672	Oil Breather Plug	906	Impeller Screw
400	Gasket (Volute / Casing)	685.1	Seal Guard (No Shown)	909	Adjustment Screw
411.1	Gasket (Volute Drain)	685.2	Top Guard (Not Shown)	920	Nut
411.2	Gasket Ring (Oil Drain)	685.3	Bottom Guard (Not Shown)	920.1	Nut
411.3	Gasket (Oil Filler Plug)	900.1	Screw (Casing Push-off)	923	Locking Nut (Bearing)
412.1	'O' Ring (Bearing Carrier)	900.2	Screw (Bearing Cover)	940.1	Impeller Key
412.2	'O' Ring (Bearing Cover)	900.3	Screw (Bearing Carrier)	940.2	Drive Coupling Key

Figure A-5 Cross section parts list.

**Appendix B - HCTR layout drawing.**

This appendix contains the layout drawings for the hydrocarbon cavitation test rig.



(Over leaf)

**Figure B-1 Main layout engineering drawing of the HCTR. (p160)**

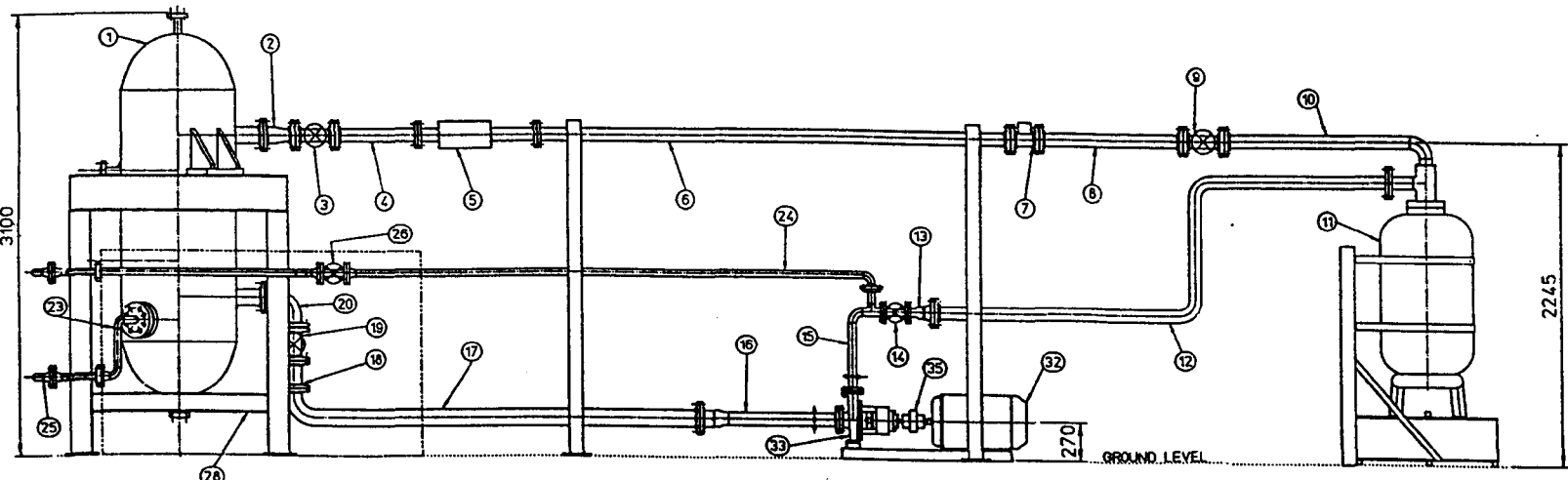
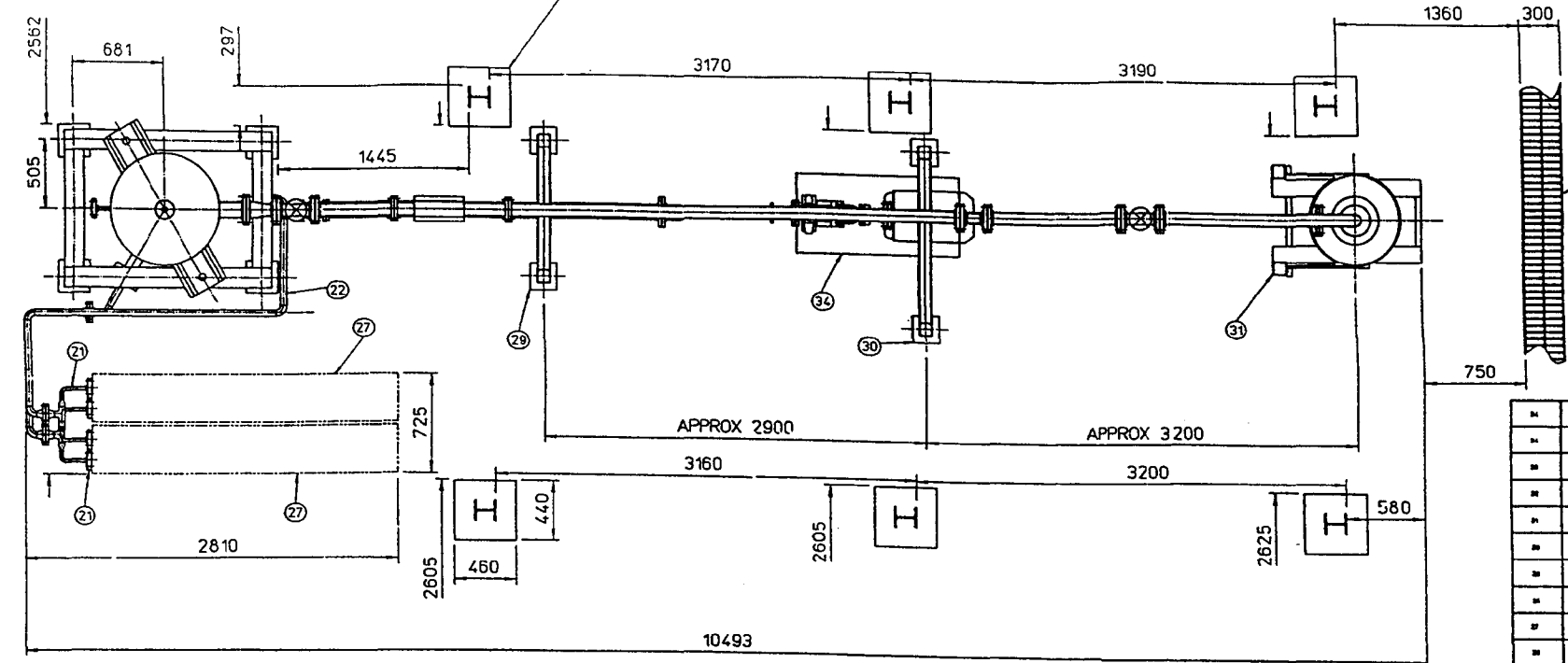
**Figure B-2 Main flow loop engineering drawing. (p161)**

THIRD ANGLE PROJECTION

A1

EXISTING 152x152mm (37kg/m) VERTICAL COLUMNS x 6 WITH 460x440mm BASES, SUPPORTS THE MEZZANINE FLOOR NOT SHOWN IN PROJECTION BELOW

EXISTING DRAINAGE CHANNEL NOT SHOWN IN PROJECTION BELOW



ITEM No.	DRAWING No.	DESCRIPTION	MATERIAL	No. OFF	O/N/O CODE	PRODUCT SPEC.
21	-	WELDED	-	1	-	-
22	-	BASE PLATE - SEE REF 1, 2	MILD STEEL	1	-	-
23	-	2" WELDED PIPE, 10-10.5mm WALL THICKNESS, 10-10.5mm FLANGED SECTION, WELDED TO 2" WELDED PIPE	STAINLESS STEEL WETTED PARTS	1	-	-
24	-	2" WELDED PIPE, 10-10.5mm WALL THICKNESS, 10-10.5mm FLANGED SECTION, WELDED TO 2" WELDED PIPE	-	1	-	-
25	SLT_SF003	WELDED 1" WELDED SUPPORT PLATE	MILD STEEL	1	-	-
26	SLT_SF003	1" WELDED SUPPORT PLATE	MILD STEEL	1	-	-
27	SLT_SF003	2" WELDED SUPPORT PLATE	MILD STEEL	1	-	-
28	SLT_SF003	WELDED 1" WELDED SUPPORT PLATE	MILD STEEL	1	-	-
29	SLT_SF003	2" WELDED SUPPORT PLATE	MILD STEEL	1	-	-
30	SLT_SF003	2" WELDED SUPPORT PLATE	MILD STEEL	1	-	-
31	SLT_SF003	2" WELDED SUPPORT PLATE	MILD STEEL	1	-	-
32	SLT_SF003	2" WELDED SUPPORT PLATE	MILD STEEL	1	-	-
33	SLT_SF003	2" WELDED SUPPORT PLATE	MILD STEEL	1	-	-
34	SLT_SF003	2" WELDED SUPPORT PLATE	MILD STEEL	1	-	-
35	SLT_SF003	2" WELDED SUPPORT PLATE	MILD STEEL	1	-	-

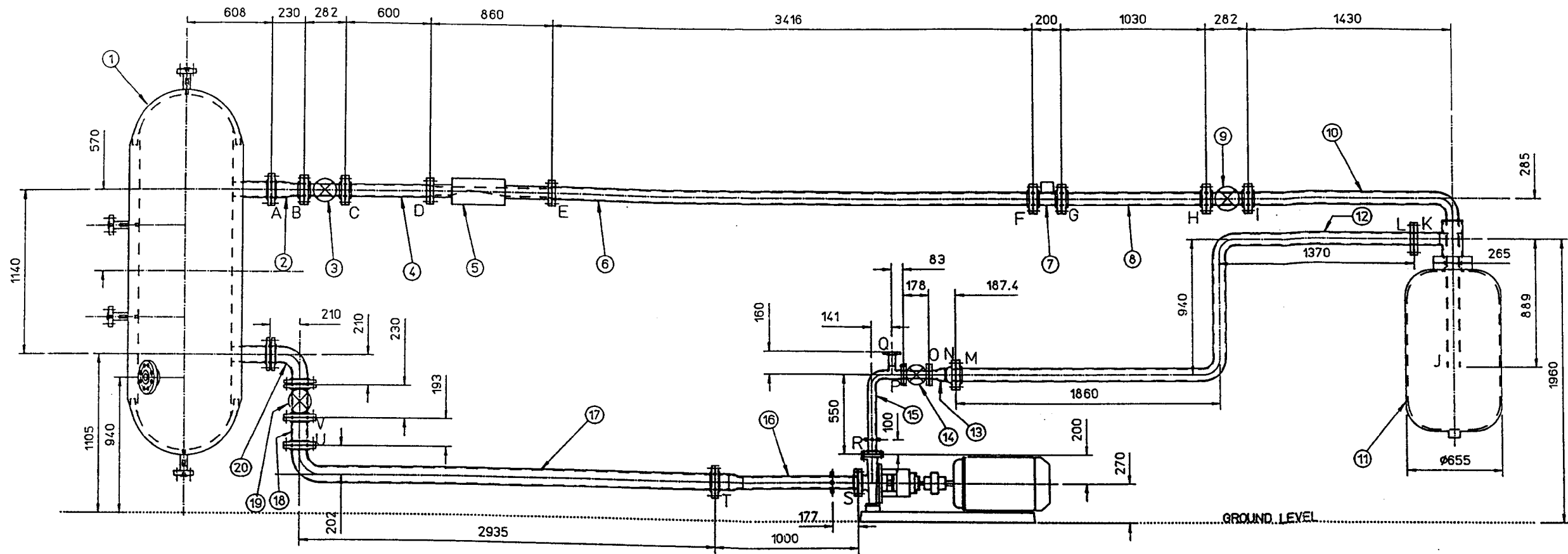
DRAWN DATE  
S.L-T  
APPROVED DATE  
ENG.  
Q.A.

<p>HAYWARD TYLER FLUID DYNAMICS</p> <p>TBL (1582) 31144 FAX (1582) 452198</p>	THIS DRAWING AND THE COPYRIGHT CONTAINED THEREIN ARE THE PROPERTY OF HAYWARD TYLER FLUID DYNAMICS, LUTON, BEDFORDSHIRE, ENGLAND. © 1996	
	TITLE OVERALL TEST RIG LAYOUT WITH PIPE AND VESSEL SUPPORTS	
	DRAWING No. SLT_SF003	ISSUE 1

ISSUE	CHANGE	DRAWN DATE	CHECKED DATE	ENG. APPROVED/DATE	Q.A.

THIRD ANGLE PROJECTION


A2



ITEM No.	DRAWING No.	DESCRIPTION	MATERIAL	No.	C/N/C CODE/ NON CODE	PRODUCT SPEC.
20	-	4" 304 LAP JOINT FLANGE END CONNECTIONS & 4" SCH 40 ELBOW	-	-	-	-
19	-	4" BALL VALVE WITH 4" 304 FLANGE END CONNECTIONS	STAINLESS STEEL	1	-	-
18	S.L.T.04	4" 304 FLANGE END CONNECTIONS (U & V) 4" SCH 40 PIPE	STAINLESS STEEL	1	-	-
17	-	4" 304 FLANGE END CONNECTIONS 4" SCH 40 PIPE & ELBOW	STAINLESS STEEL	1	-	-
16	S.L.T.05	4" 304 ANGE FLANGE (U) TO 4" 304 ANGE FLANGE (V) PIPE & REDUCER BOMBS VAMP FOR PRESSURE TAP	STAINLESS STEEL	1	-	-
15	S.L.T.06	2" 304 ANGE FLANGE END CONNECTIONS (P&R) WITH A 1/2" TEE CONNECTION TO A 1/2" 304 ANGE LAP-JOINT FLANGE (S) & SCH 40 STUD END VAMP FOR PRESSURE TAP	STAINLESS STEEL	1	-	-
14	-	2" GATE VALVE 304 ANGE	STAINLESS STEEL	1	-	-
13	S.L.T.08	3" 304 ANGE FLANGE (N) REDUCING TO 2" 304 ANGE FLANGE (O)	STAINLESS STEEL	1	-	-
12	S.L.T.02	3" 304 PIPE / 3" 304 ANGE FLANGE (N) TO 4" 304 ANGE FLANGE (L)	STAINLESS STEEL	1	-	-
11	-	SECONDARY NON PRESSURE STORAGE VESSEL	STAINLESS STEEL	1	-	-
1						

ISSUE	DRAWN	DATE	CHECKED	DATE	ENG. APPROVED	DATE	Q.A.	DATE	CHANGE	
1										

ITEM No.	DRAWING No.	DESCRIPTION	MATERIAL	No. OFF	C/N/C CODE/ NON CODE	PRODUCT SPEC.
10	S.L.T.03	TANK CONNECTION INLET 4" 304 ANGE FLANGE (Q) OUTLET 4" 304 ANGE FLANGE (R)	STAINLESS STEEL	1	-	-
9	-	3" GATE VALVE	STAINLESS STEEL	1	-	-
8	S.L.T.04	3" 304 PIPE / 3" 304 ANGE FLANGE (N) TO 3" 304 ANGE FLANGE (O)	STAINLESS STEEL	1	-	-
7	-	3" TURBINE FLOW METER	STAINLESS STEEL	1	-	-
6	S.L.T.05	3" 304 PIPE / 3" 304 ANGE FLANGE (N) TO 2.5" 304 PIPE (REDUCING) (O)	STAINLESS STEEL	1	-	-
5	-	CHANGES / PURCHASE CONNECTIONS (MATERIAL SPECIFICATION CHANGE, 2507000 TUBING & 2.5" 304 PIPE (REDUCING) CONNECTIONS)	STAINLESS STEEL	1	-	-
4	S.L.T.04	3" 304 PIPE / 3" 304 ANGE FLANGE (N) TO 2.5" 304 PIPE (REDUCING) (O)	STAINLESS STEEL	1	-	-
3	-	3" GATE VALVE	STAINLESS STEEL	1	-	-
2	S.L.T.02	4" TO 3" REDUCER BOMBS 4" 304 ANGE FLANGE (U) TO 3" 304 ANGE FLANGE (V)	STAINLESS STEEL	1	-	-
1	-	NON STORAGE VESSEL	STAINLESS STEEL	1	-	-

DRAWN DATE S.L.-T		 <b>HAYWARD TYLER FLUID DYNAMICS</b> TEL. (1582) 31144 FAX. (1582) 452198	THIS DRAWING AND THE COPYRIGHT CONTAINED THEREIN ARE THE PROPERTY OF HAYWARD TYLER FLUID DYNAMICS, LUTON, BEDFORDSHIRE, ENGLAND. © 1996			
APPROVED DATE ENG.			TITLE Hydrocarbon Cavitation Test Rig			
Q.A.			Main Flow Loop			
		DRG. No. SLT_CVR2		ISSUE 1		

**Appendix C - Hydraulic design information.**

This appendix contains the data used in the hydraulic design of the test rig.

Loss coefficient		
Through pipe		
Sudden enlargement (A <sub>1</sub> < A <sub>2</sub> ) (To Pipe to tank)		
Sudden contraction (A <sub>1</sub> > A <sub>2</sub> ) (Tank supply)		
	0.1	
	0.2	
	0.5	
	0.7	
	0.9	
Gradual contraction		
Gradual enlargement included angle = 90°		
	40°	
	30°	
	20°	
	10°	
Gate valve		
Open		
Three quarters open		
Half open		
One quarter open		
Globe valve		
Open		
Three quarters open		
Half open		
One quarter open		
Foot valve with siphon		
Hinged		
Ball		
Check valve		
Hinged		
Ball		
LC		

Table C.1.1. Loss coefficients for typical fittings



FITTING	K FACTOR
Return bend (close)	2.2
Standard 45° elbow	0.4
Standard 90° elbow	0.9
Long radius 90° elbow	0.6
Union screwed	0.05
Tee Along line of flow	0.4
Through side	1.8
Sudden enlargement ( $A_1 < A_2$ ) (1= Pipe to tank)	$\left(1 - \frac{A_1}{A_2}\right)^2$
Sudden contraction $A_2 / A_1 = 0$ (Tank supply)	0.5
0.1	0.45
0.3	0.4
0.5	0.3
0.7	0.2
0.9	0.08
Gradual contraction	Negligible
Gradual enlargement Included angle $> 50^\circ$	1.0
40°	0.9
30°	0.7
20°	0.4
10°	0.15
Gate valve Open	0.2
Three quarters open	0.9
Half open	5.0
One quarter open	24.0
Globe valve Open	0.2
Three quarters open	0.9
Half open	5.0
One quarter open	24.0
Foot valve with strainer Hinged	2.0
Lift	10.0
Check valve Hinged	2.5
Ball	4.0
Lift	15.0

**Table C-1 K factors for typical fittings .**

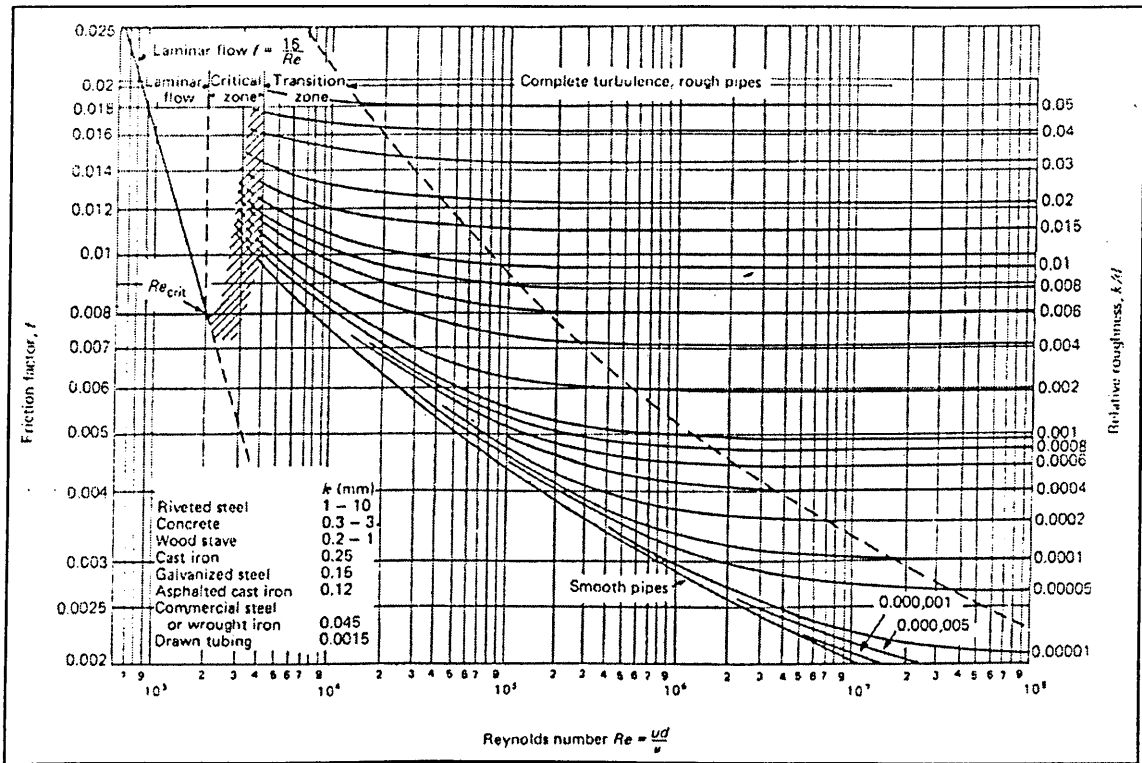
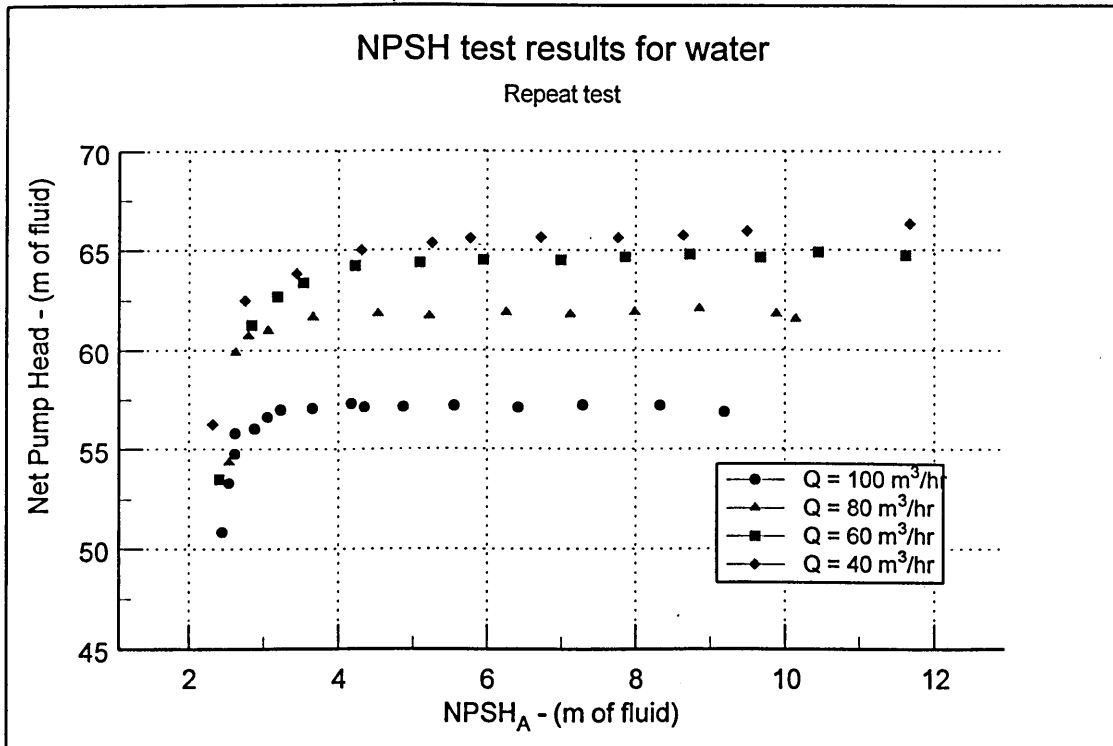
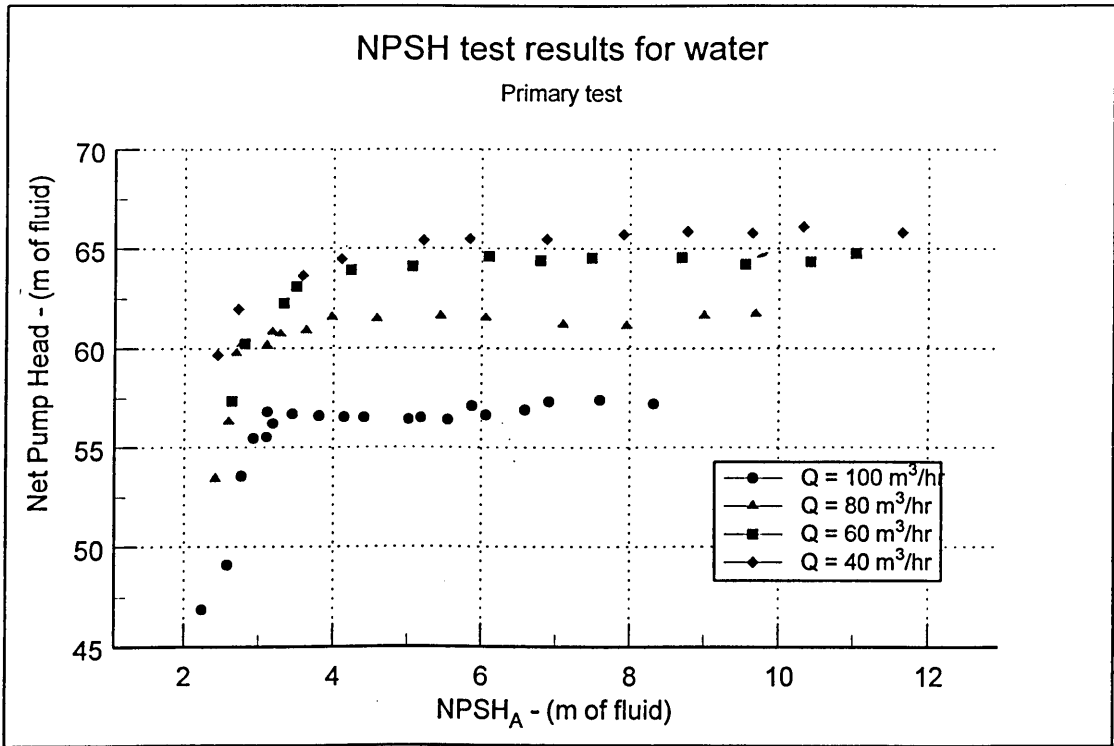


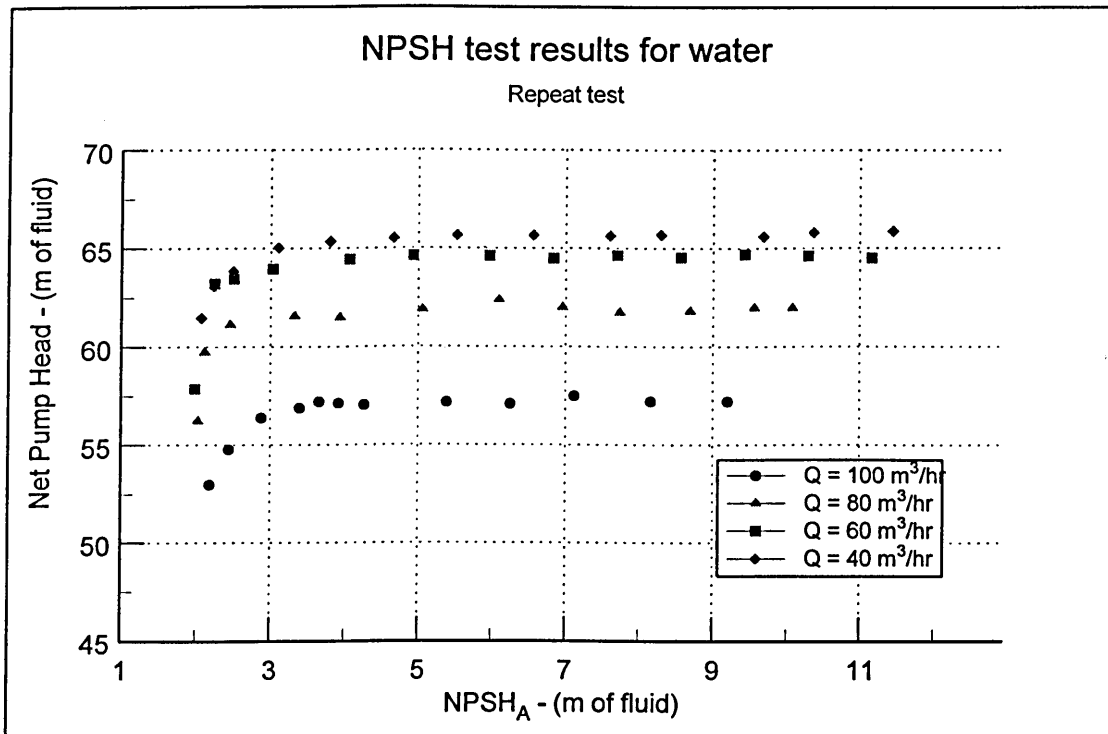
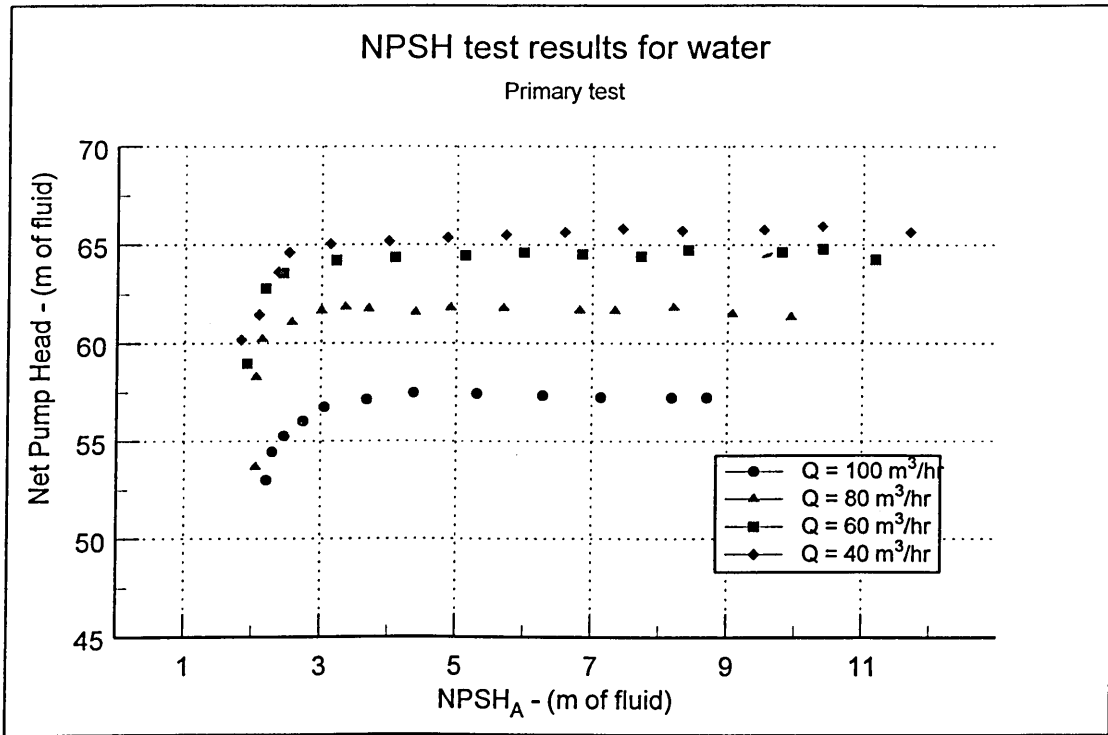
Figure C-1 Moody Friction factor chart.

**Appendix D - Pump and nozzle curves for water.**

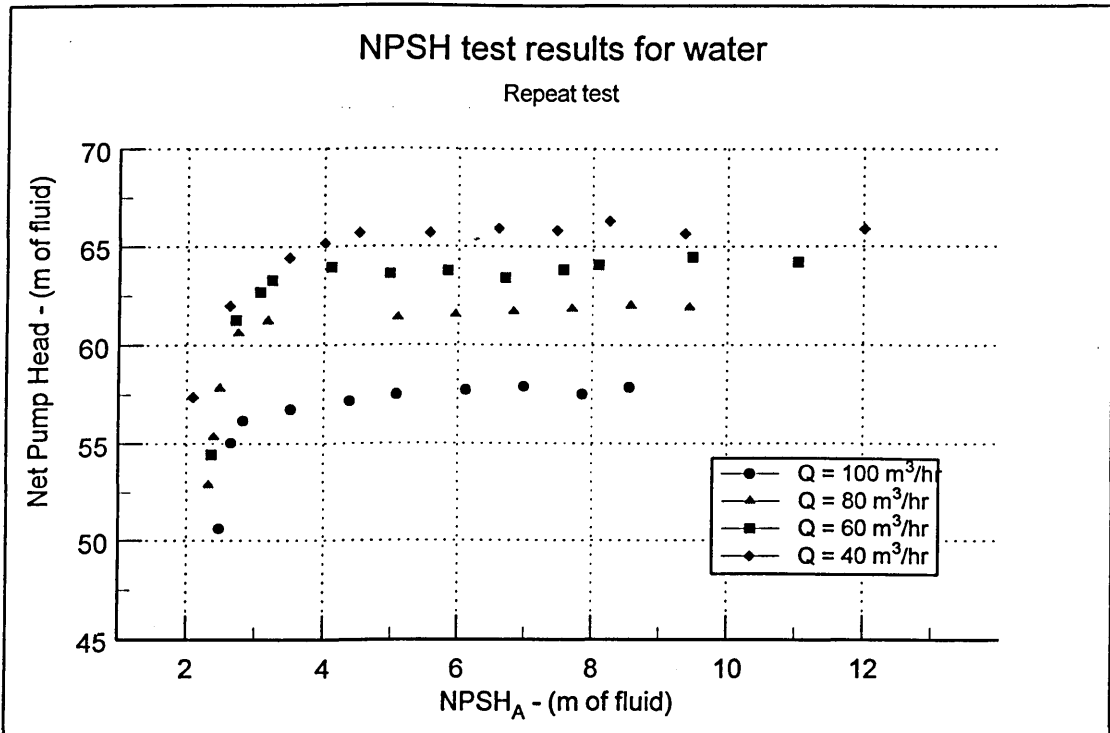
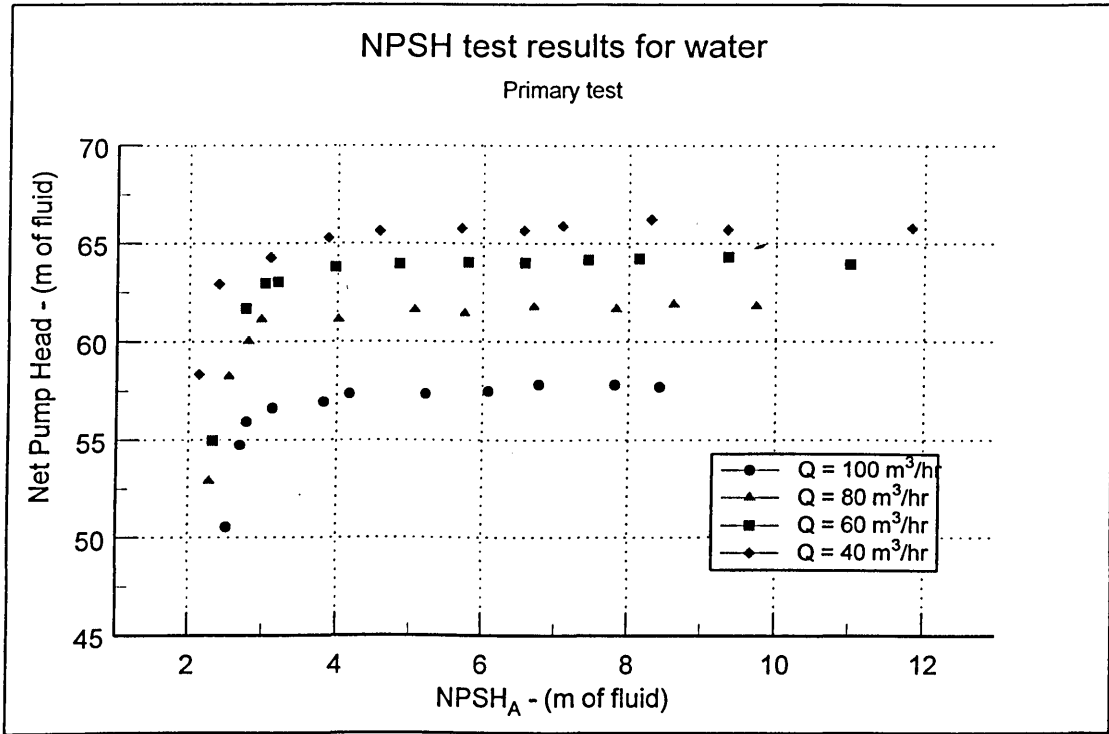
This appendix contains the NPSH curves (Figures D-1 to D-6) and tests section efficiency curves (Figures D-7 to D-18) for the tests on water. Each figure contains two graphs, the primary test and the repeat at the same conditions. The conditions given are approximate (to within a °C or a few percent).



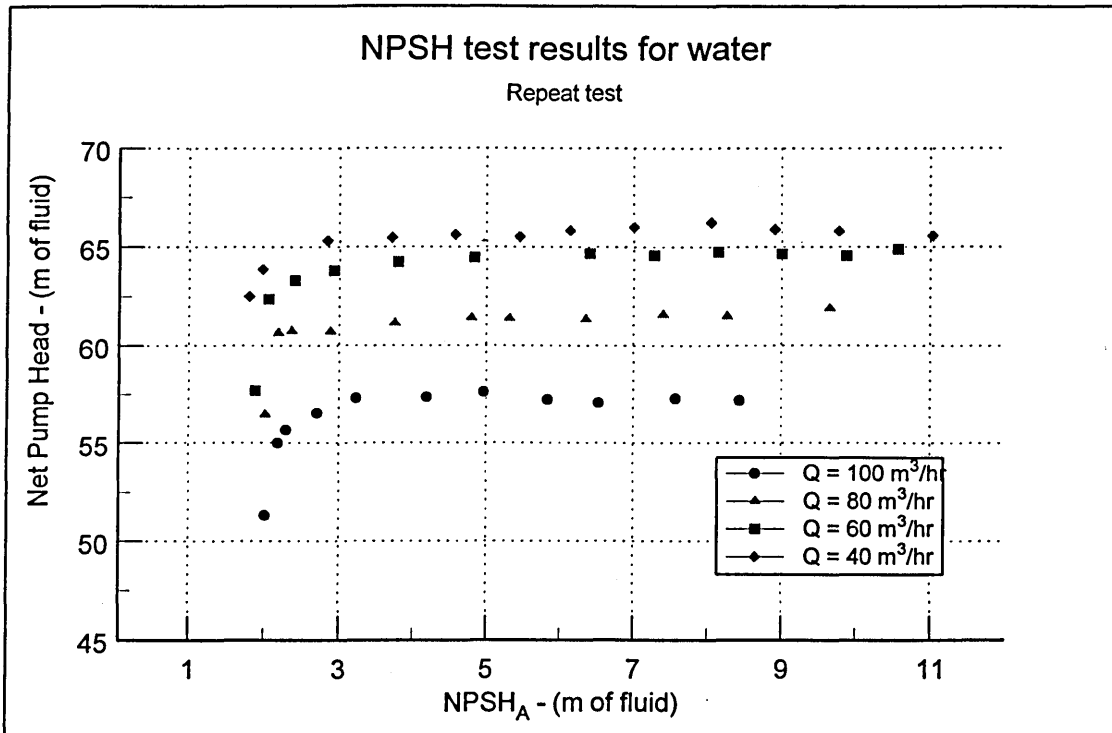
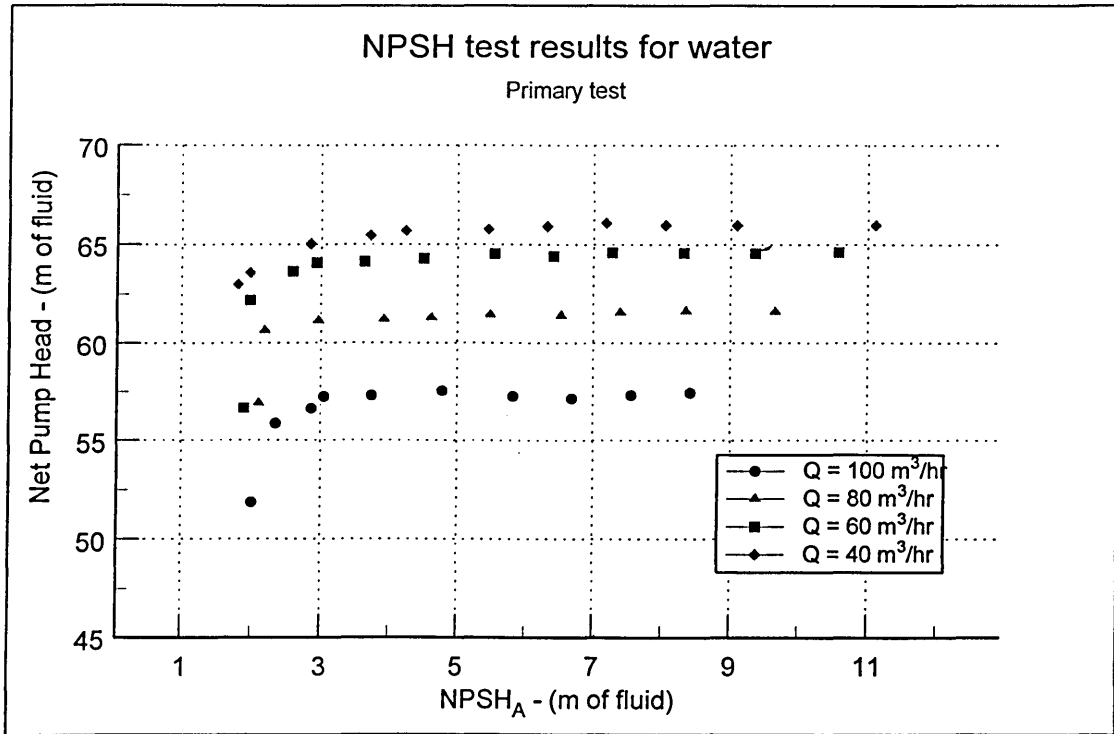
**Figure D-1 NPSH curves for water - Suction valve throttling**  
**Dissolved oxygen 100% of saturation value : Fluid temperature 20°C**



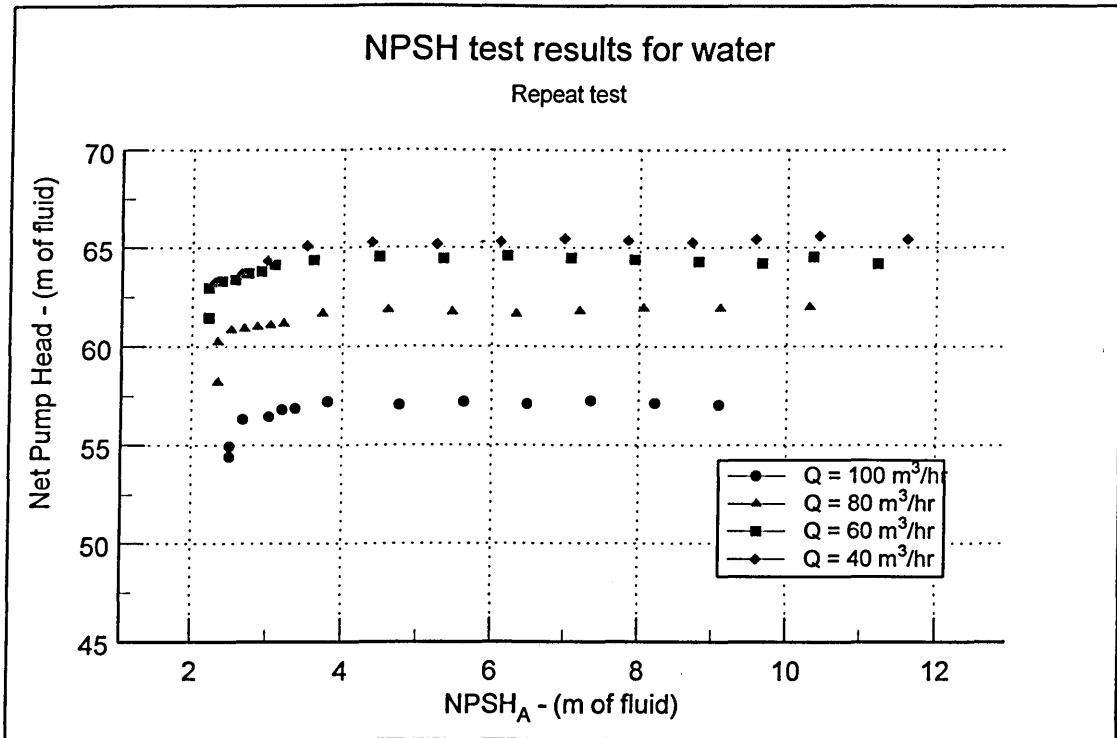
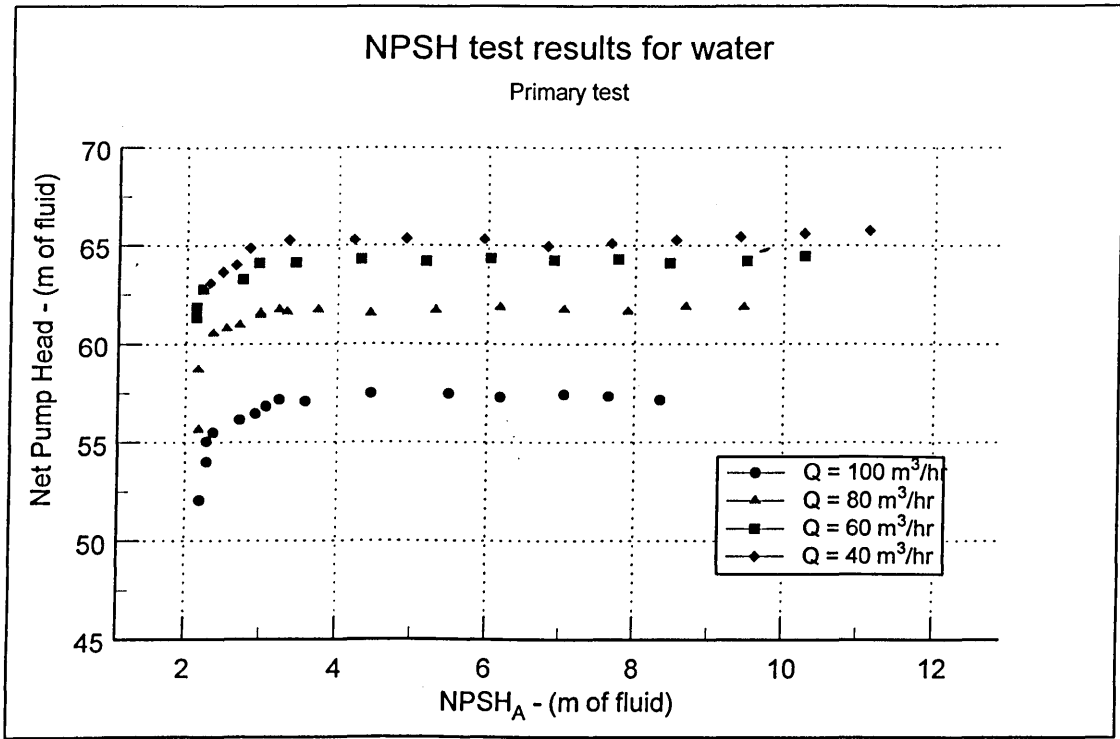
**Figure D-2 NPSH curves for water - Suction valve throttling**  
**Dissolved oxygen <10% of saturation value : Fluid temperature 20°C**



**Figure D-3 NPSH curves for water - Suction valve throttling  
Dissolved oxygen <10% of saturation value : Fluid temperature 30°C**

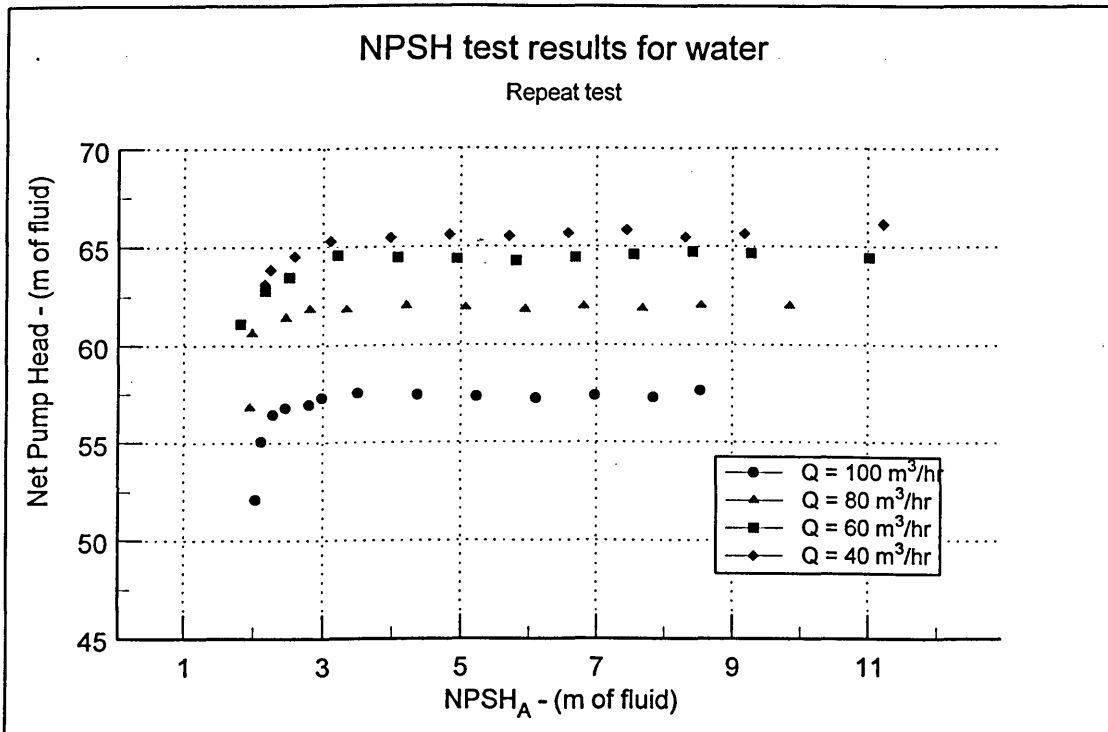
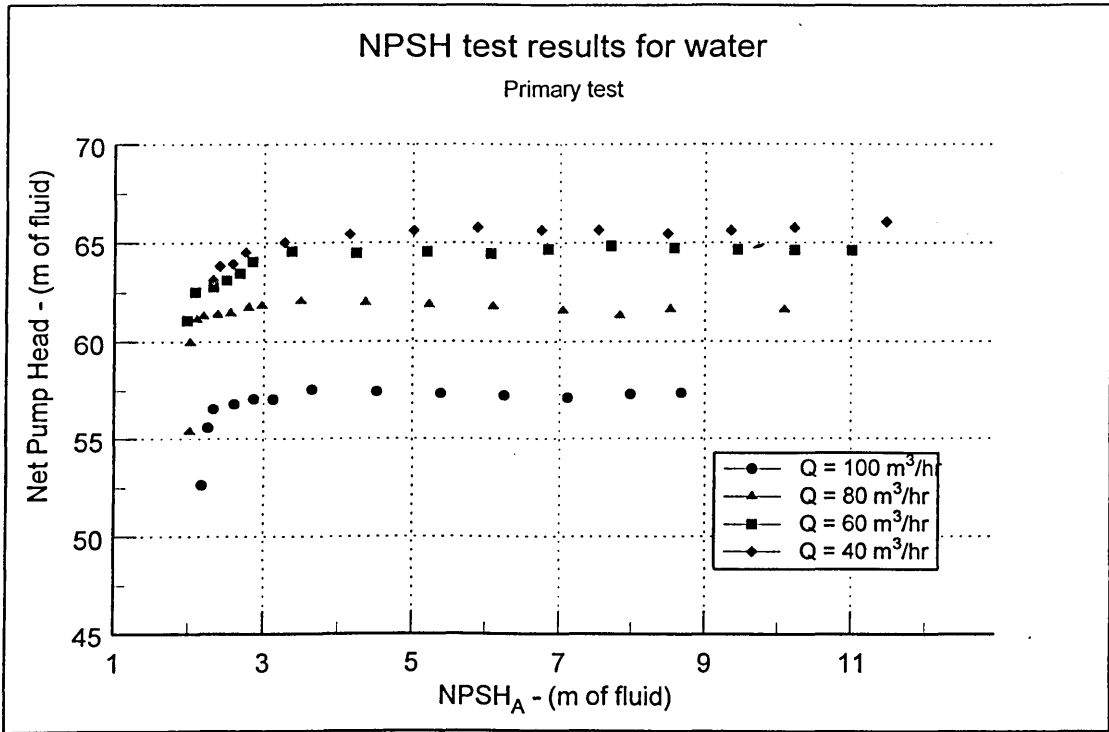


**Figure D-4 NPSH curves for water - Suction valve throttling**  
**Dissolved oxygen 100% of saturation value : Fluid temperature 30°C**

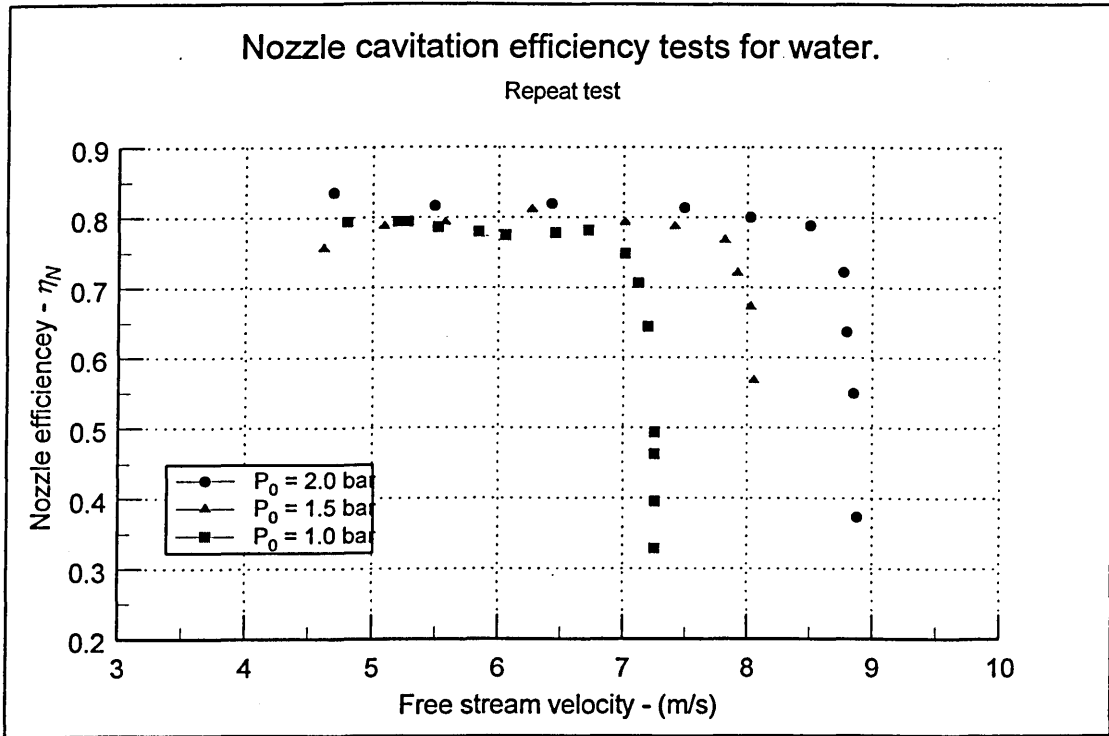
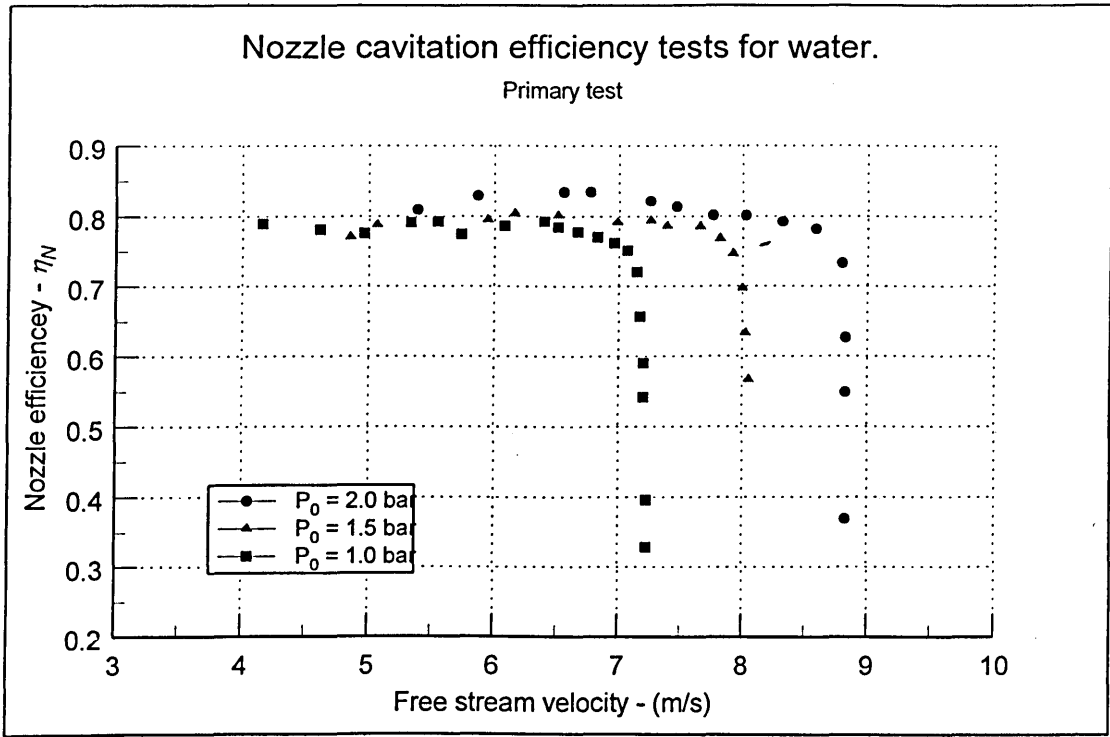


**Figure D-5 NPSH curves for water - Vacuum pump method**  
 Dissolved oxygen  $\approx$  30-40% of saturation value at 3% head drop : Fluid temperature 20°C

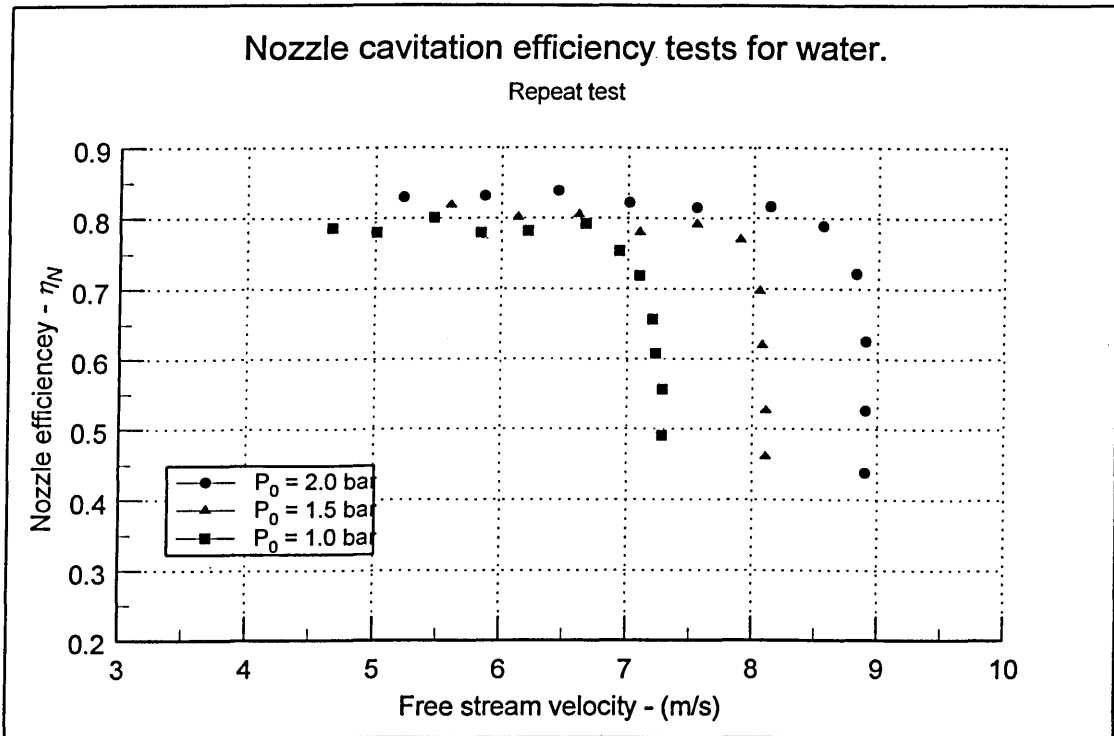
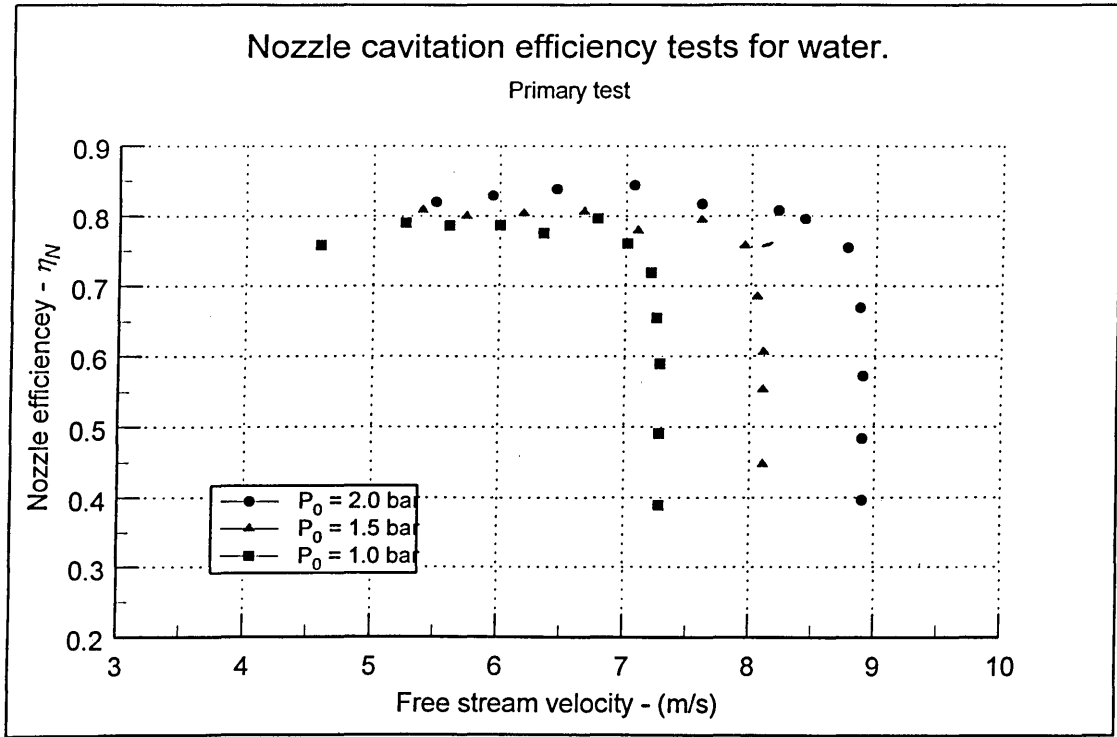




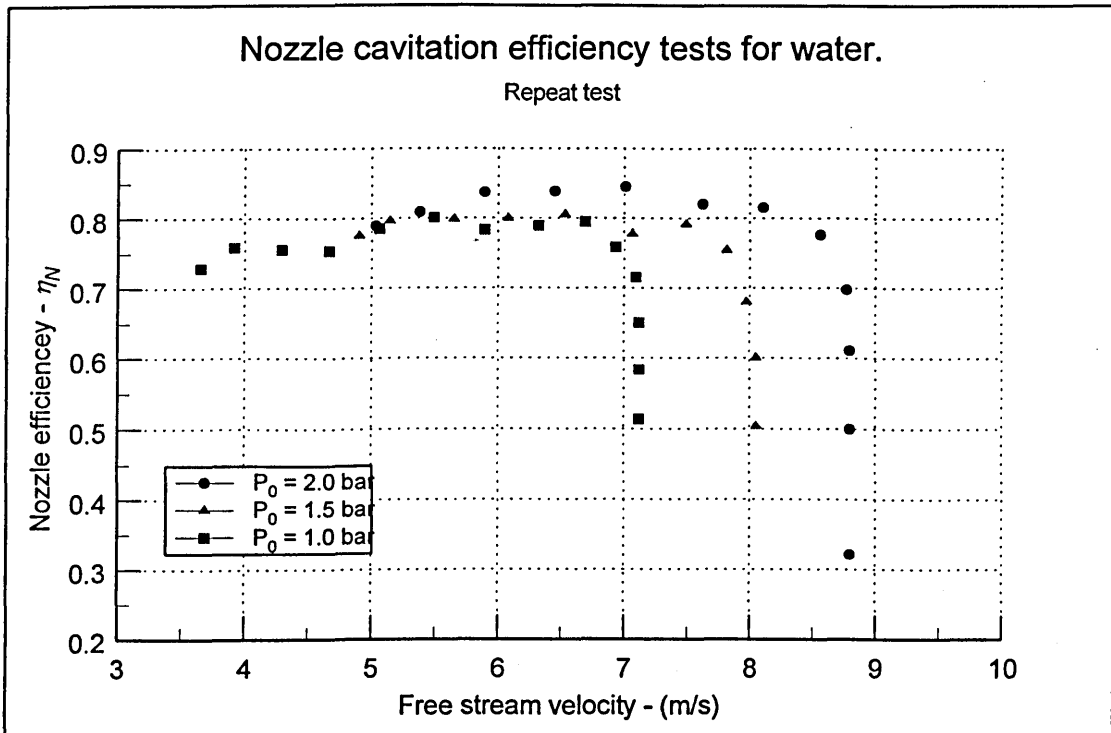
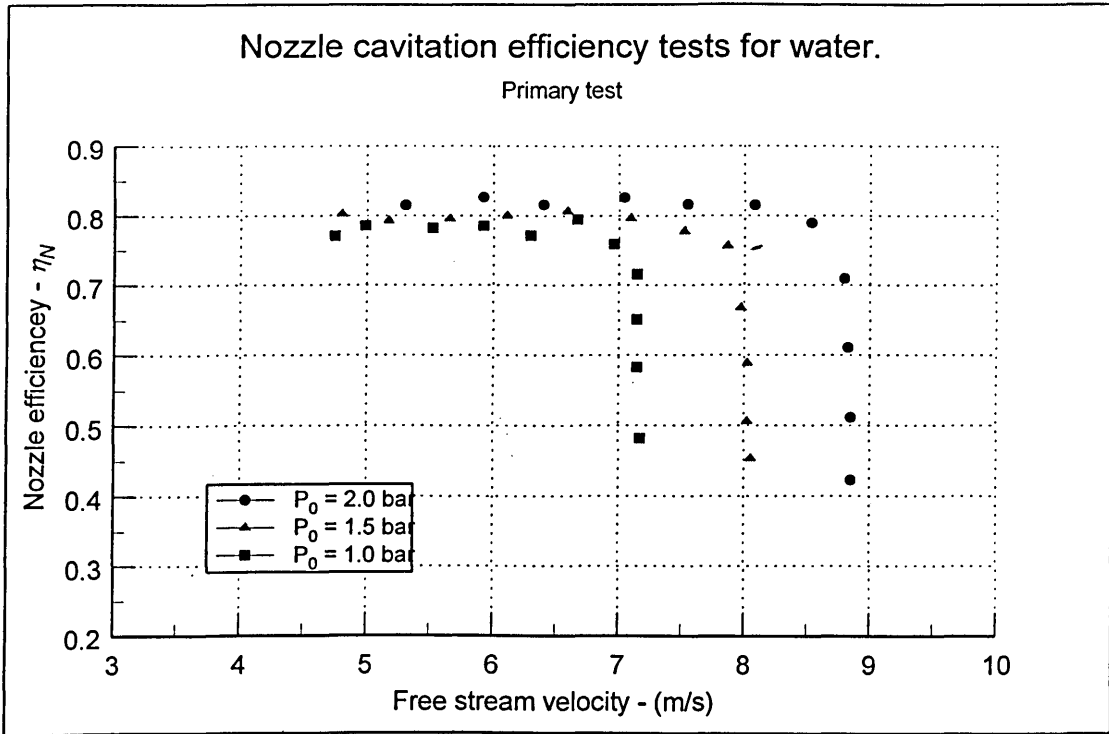
**Figure D-6 NPSH curves for water - Vacuum pump method**  
Dissolved oxygen  $\approx$  30-40% of saturation value at 3% head drop : Fluid temperature 30°C



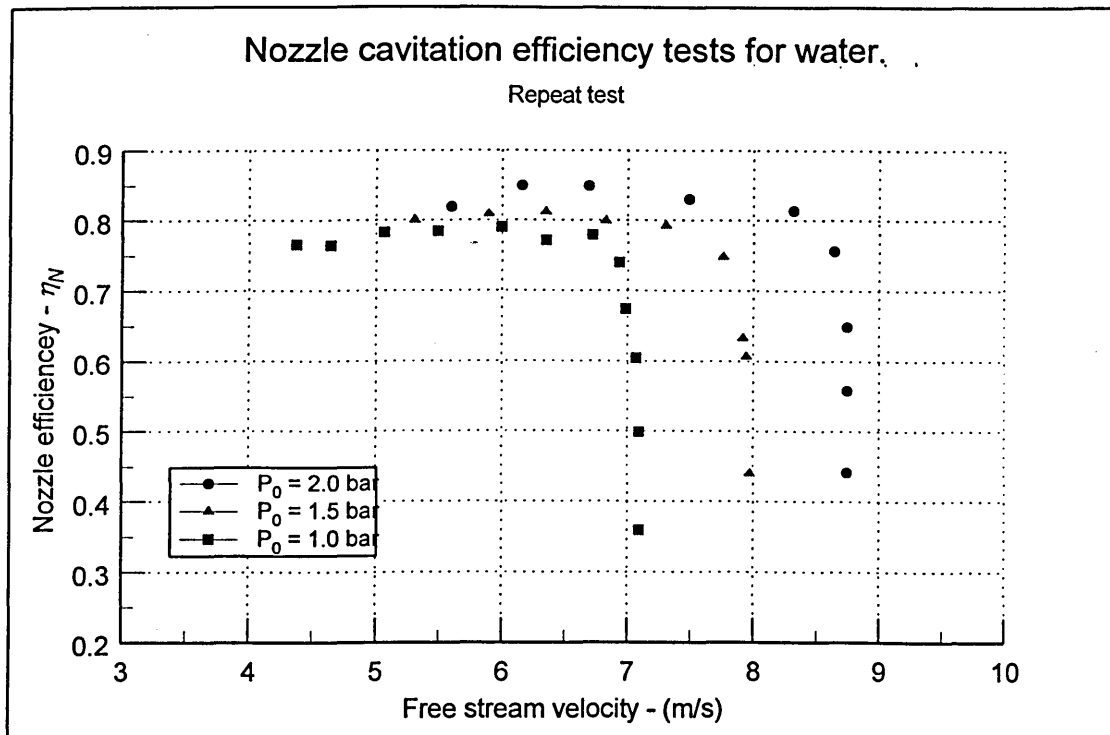
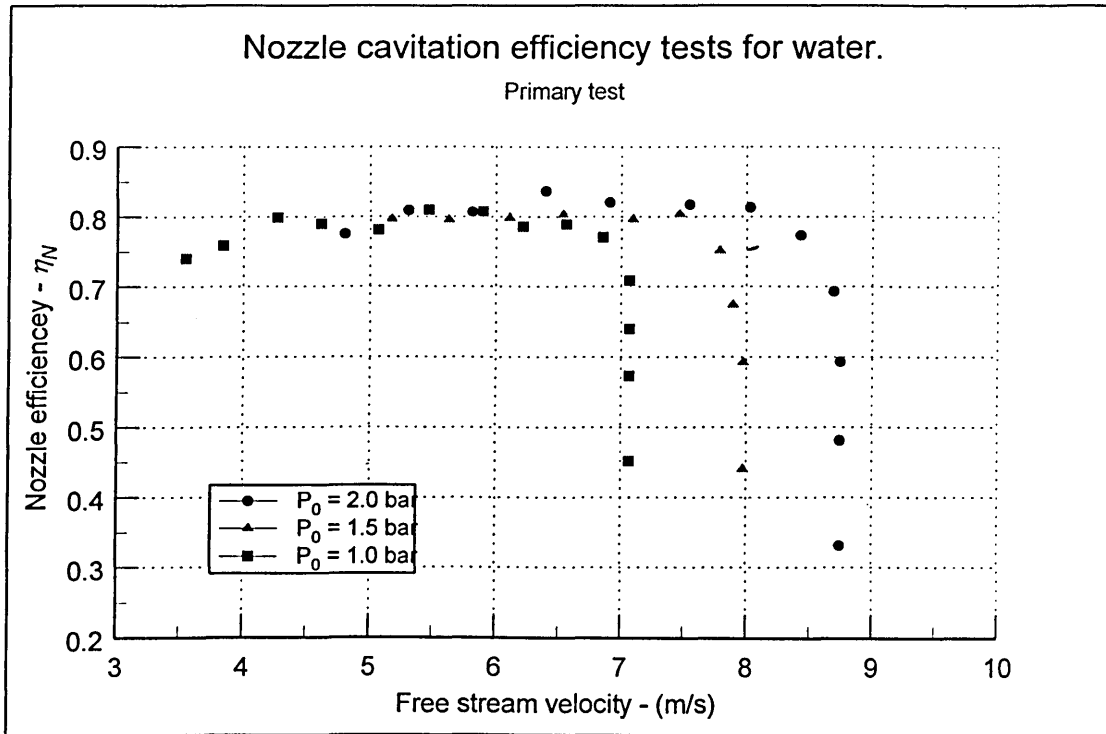
**Figure D-7 Nozzle efficiency tests for water : Dissolved oxygen  $\approx$  100% of saturation value : Fluid temperature 20°C**



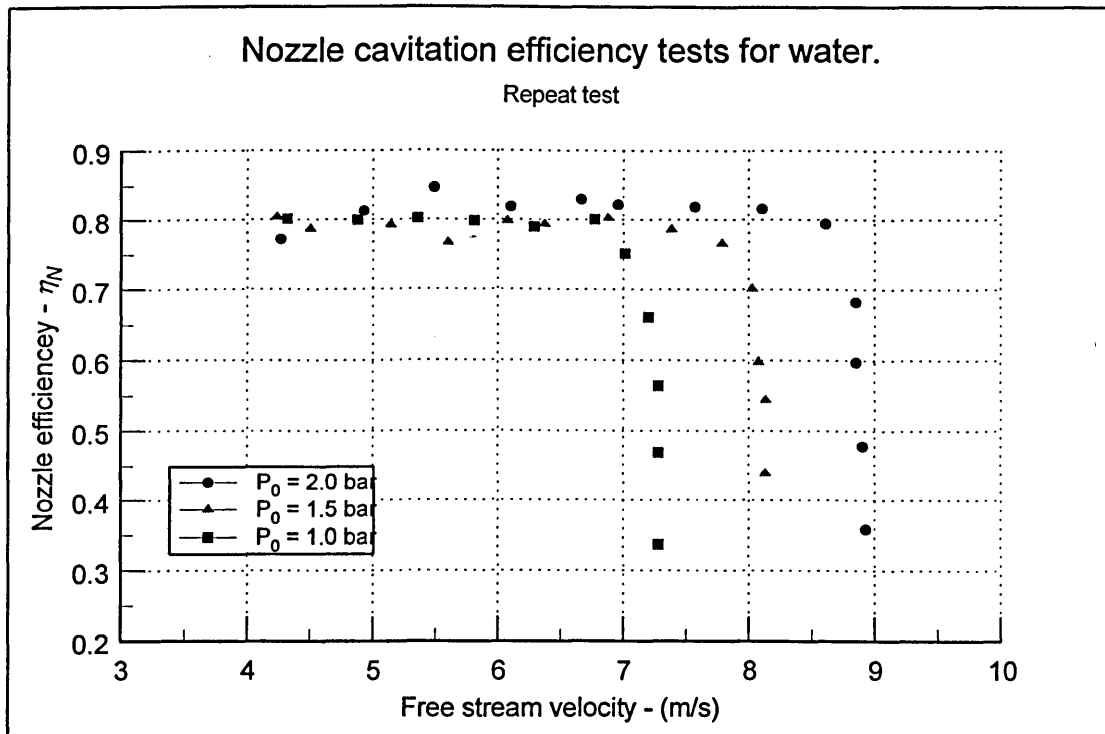
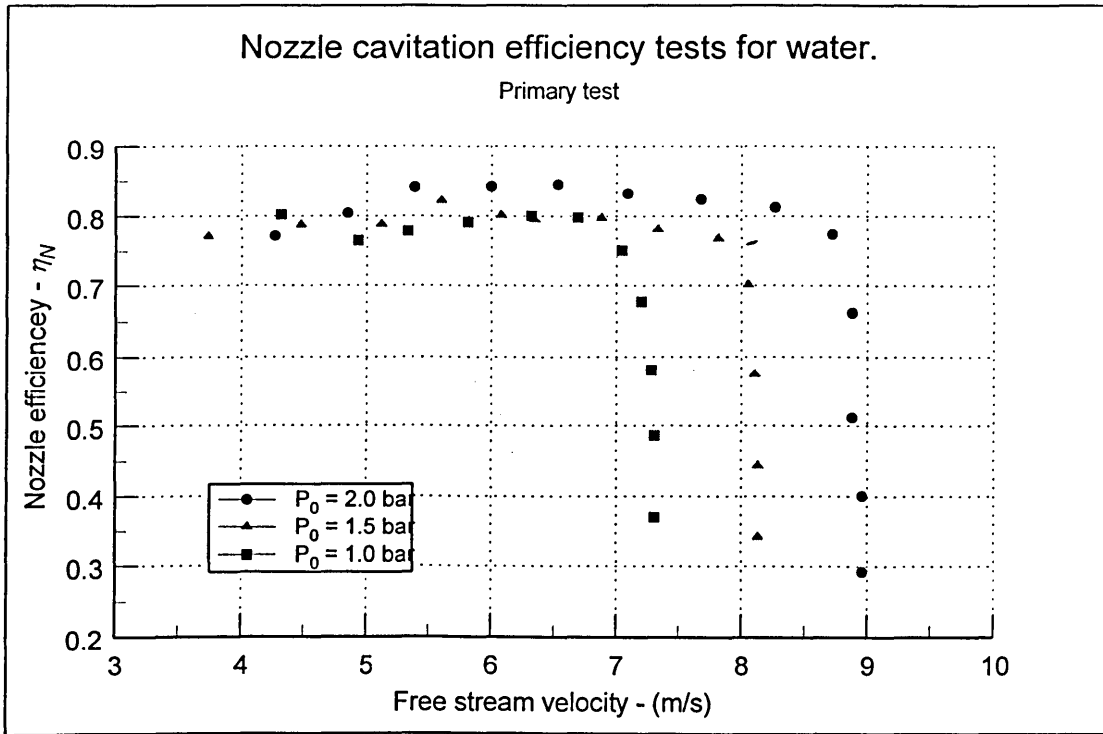
**Figure D-8 Nozzle efficiency tests for water: Dissolved oxygen  $\approx$  100% of saturation value : Fluid temperature 30°C**



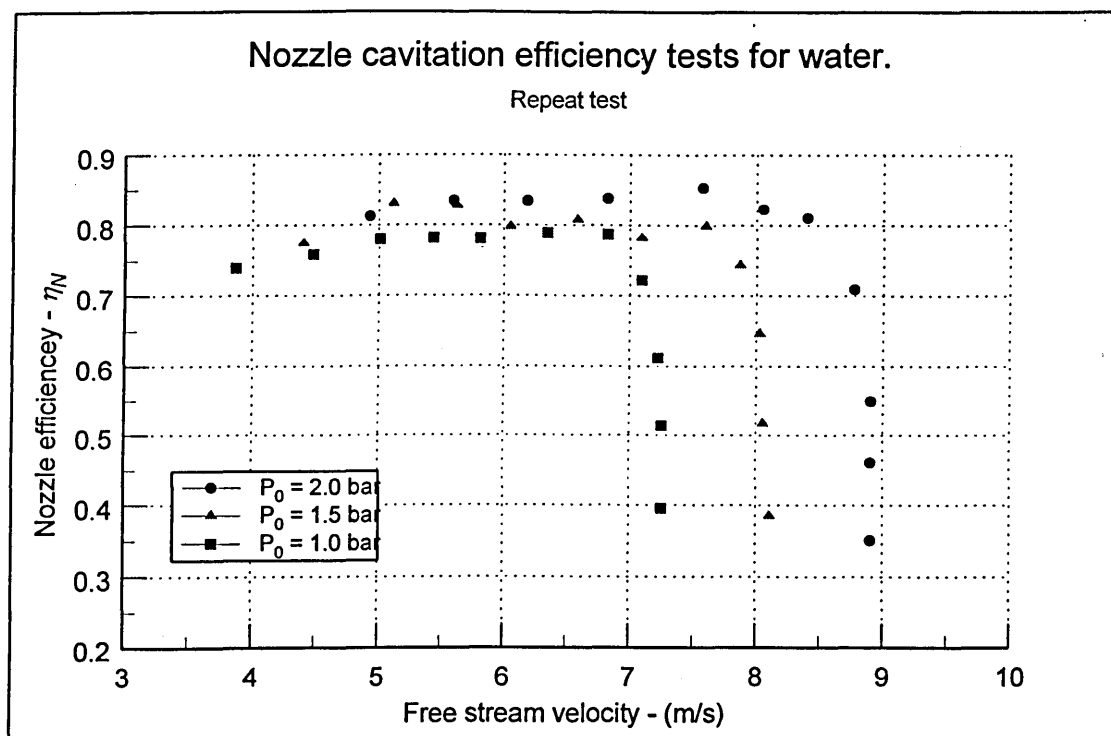
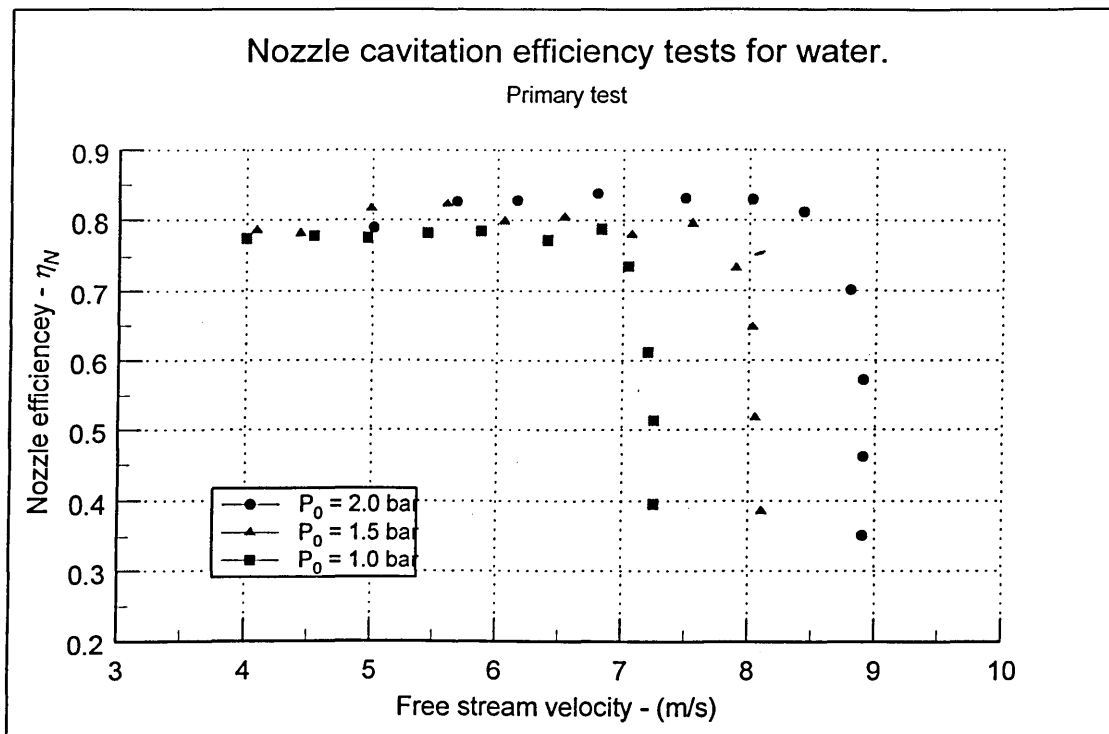
**Figure D-9 Nozzle efficiency tests for water : Dissolved oxygen  $\approx$  100% of saturation value : Fluid temperature 40°C**



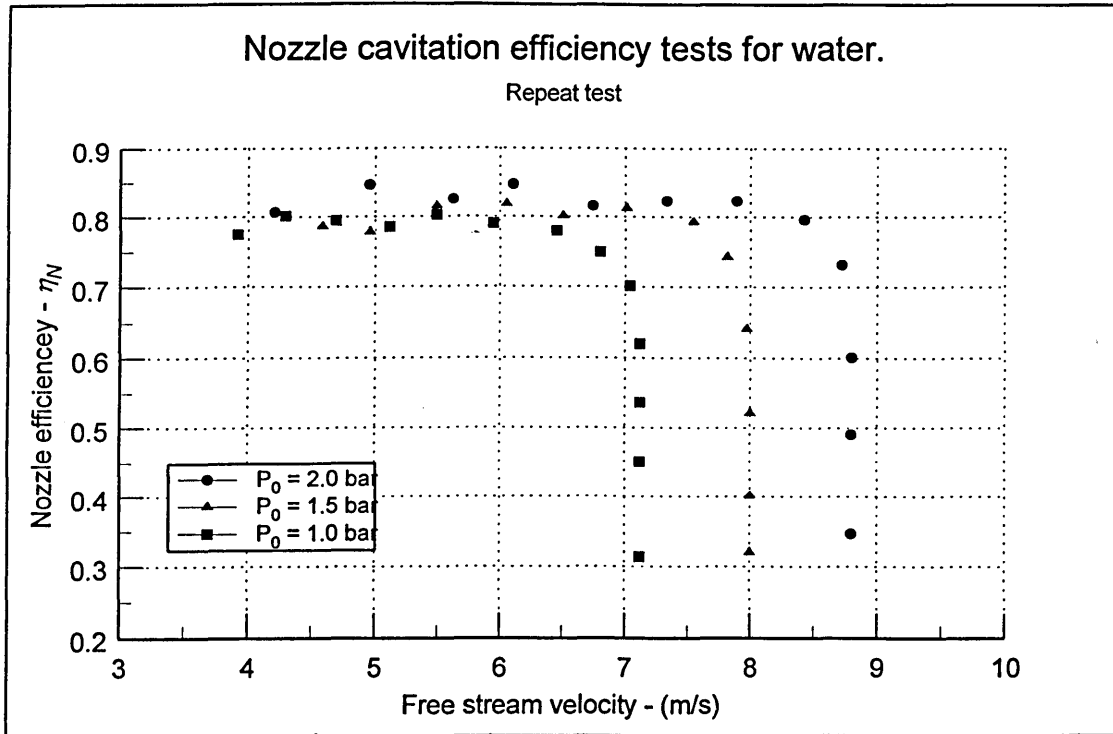
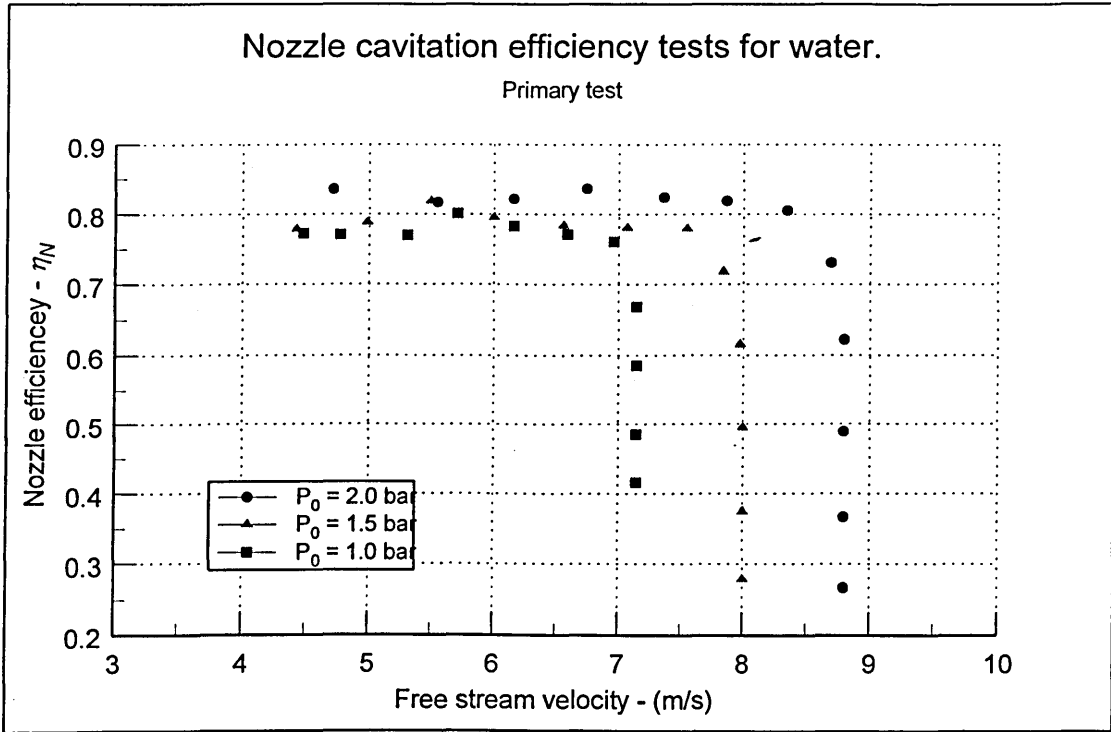
**Figure D-10 Nozzle efficiency tests for water : Dissolved oxygen  $\approx$  100% of saturation value : Fluid temperature 50°C**



**Figure D-11 Nozzle efficiency tests for water : Dissolved oxygen  $\approx$  50% of saturation value : Fluid temperature 20°C**

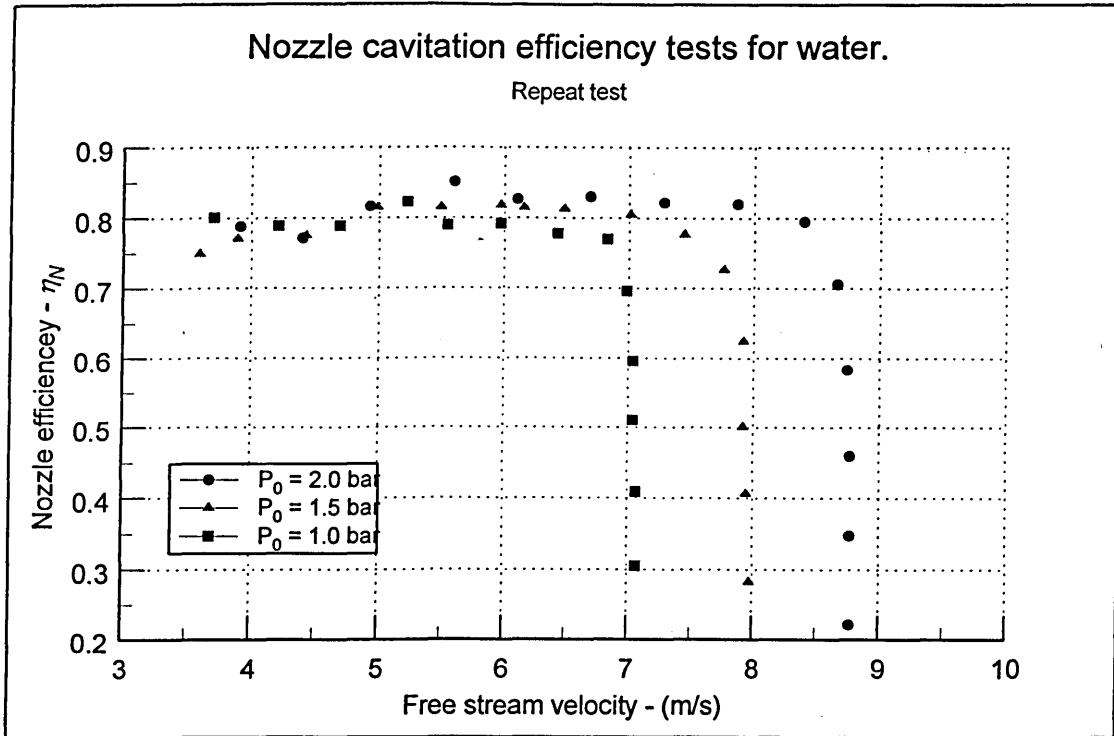
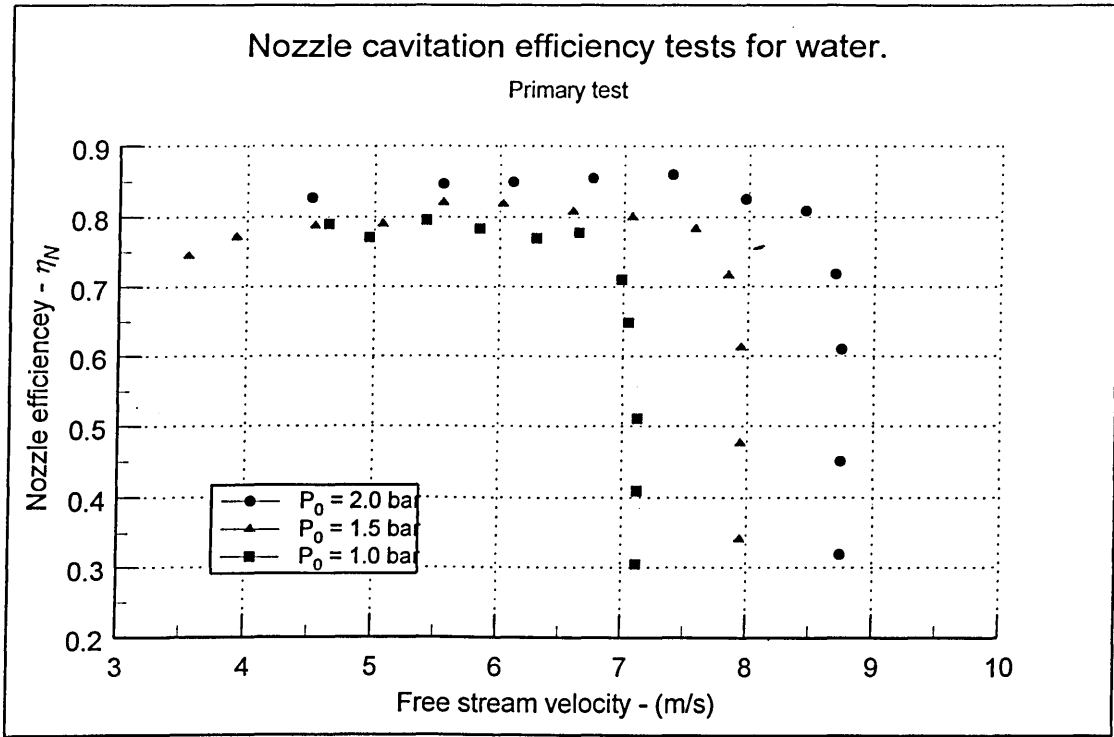


**Figure D-12 Nozzle efficiency tests for water : Dissolved oxygen  $\approx$  50% of saturation value : Fluid temperature 30°C**

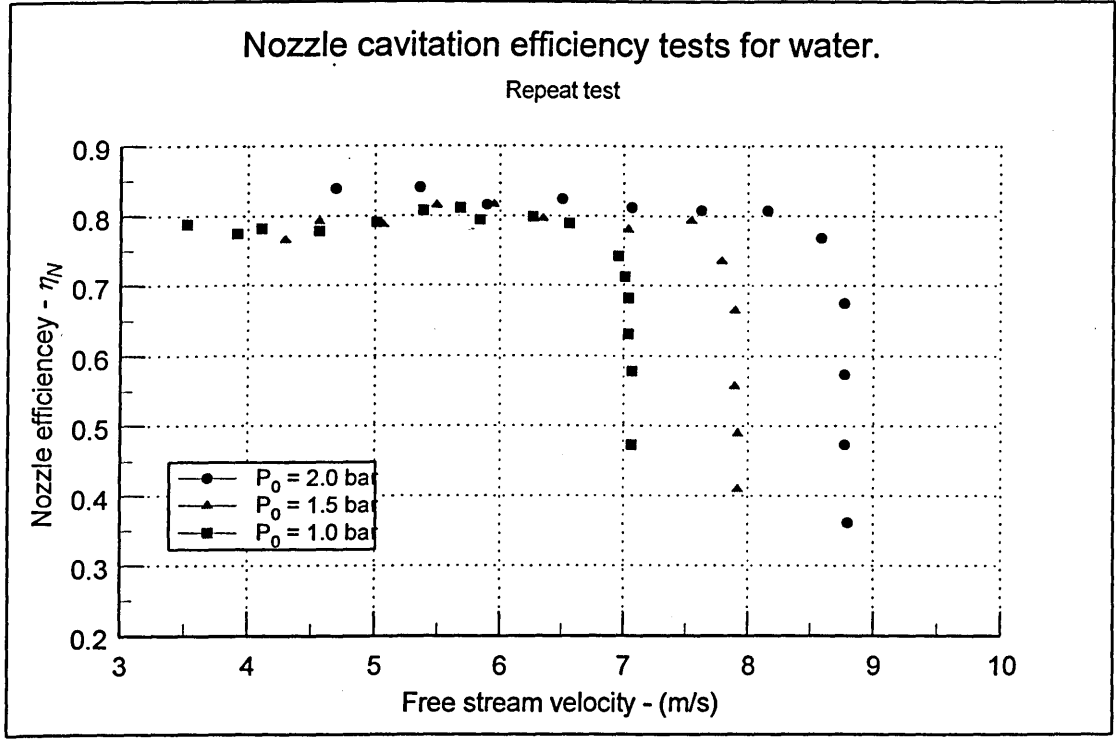
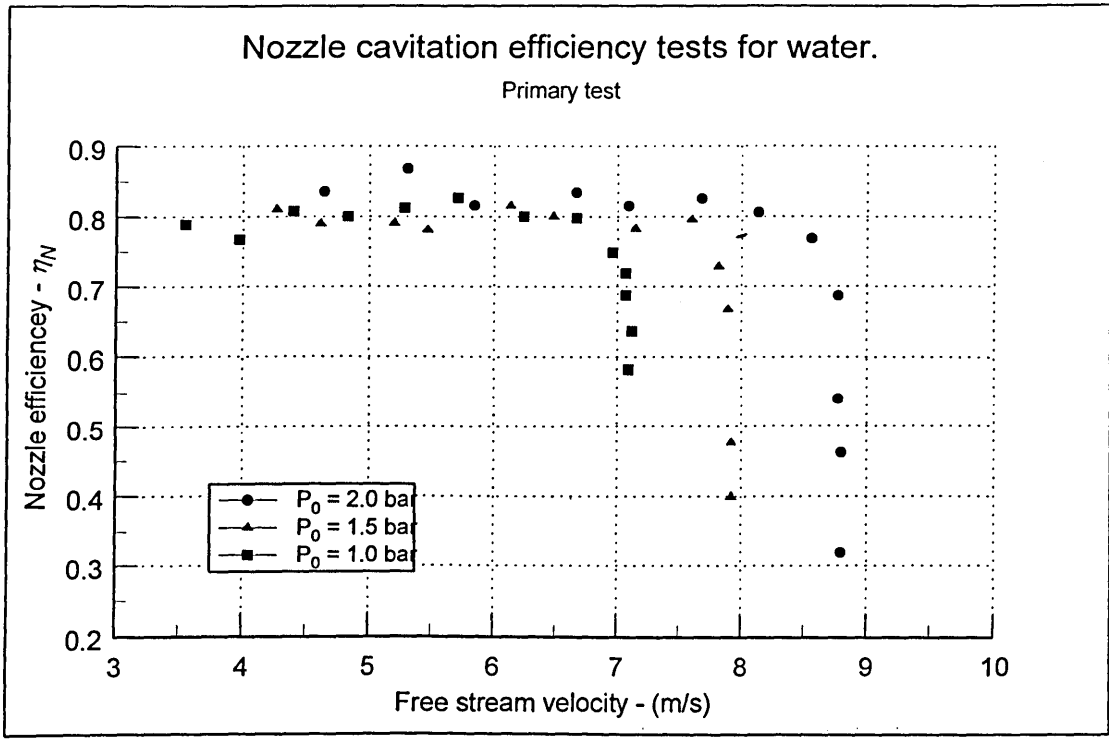


**Figure D-13 Nozzle efficiency tests for water : Dissolved oxygen  $\approx$  50% of saturation value : Fluid temperature 40°C**

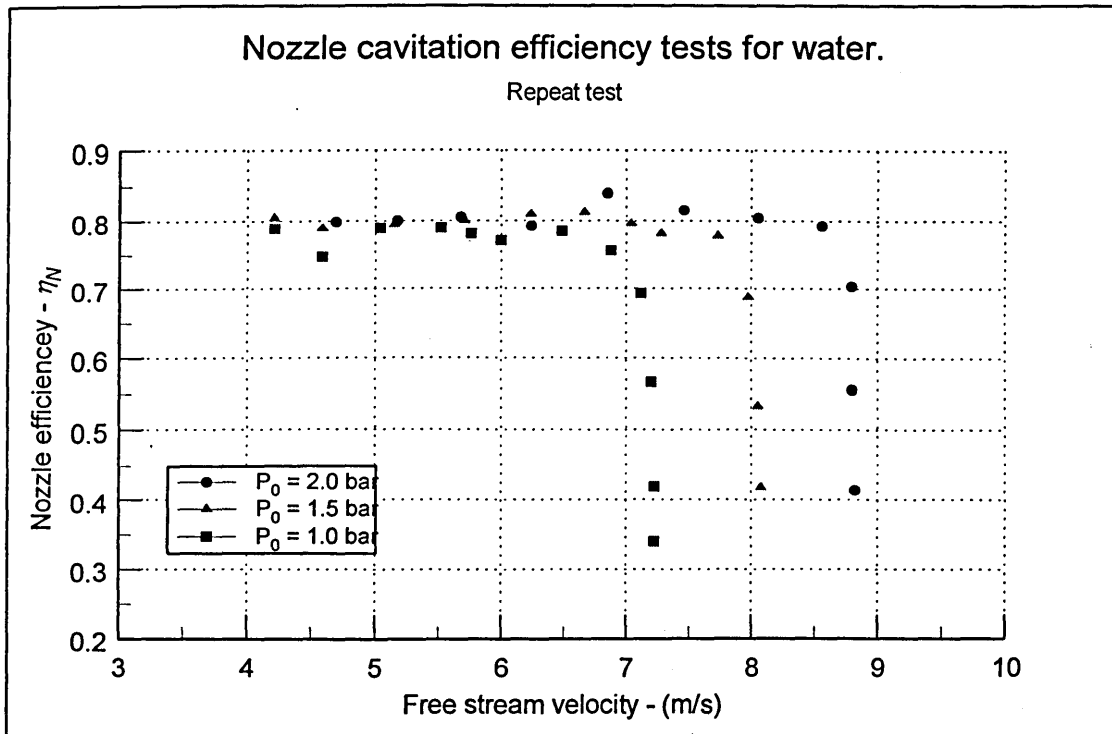
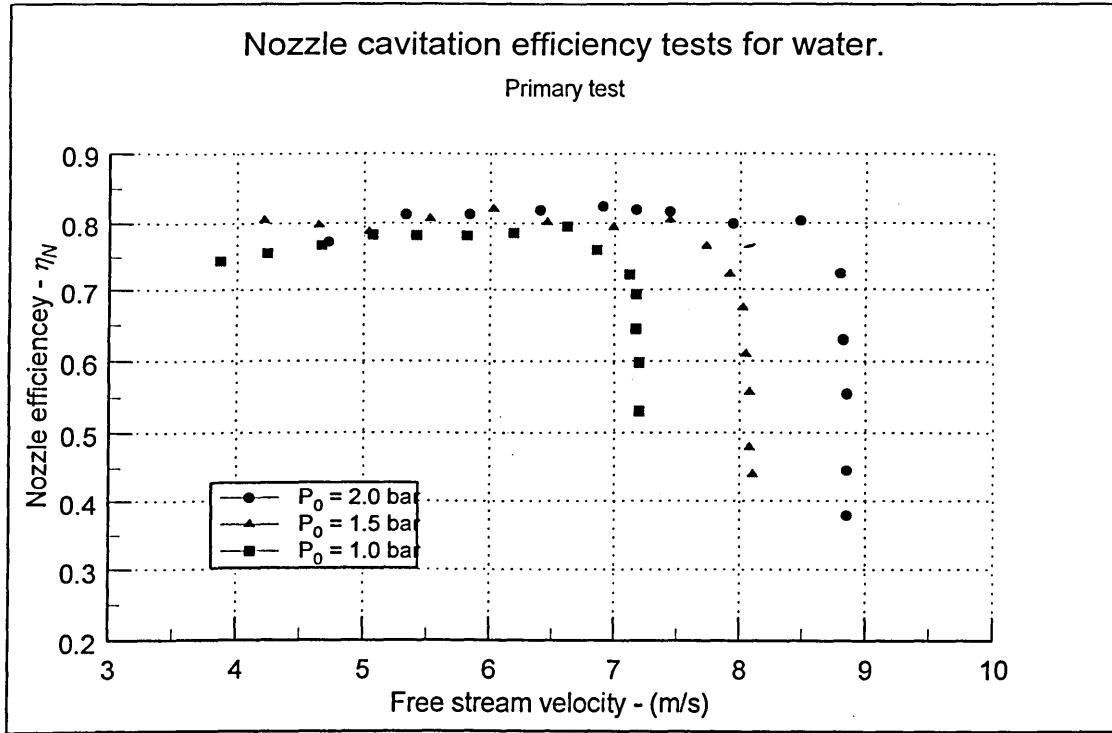




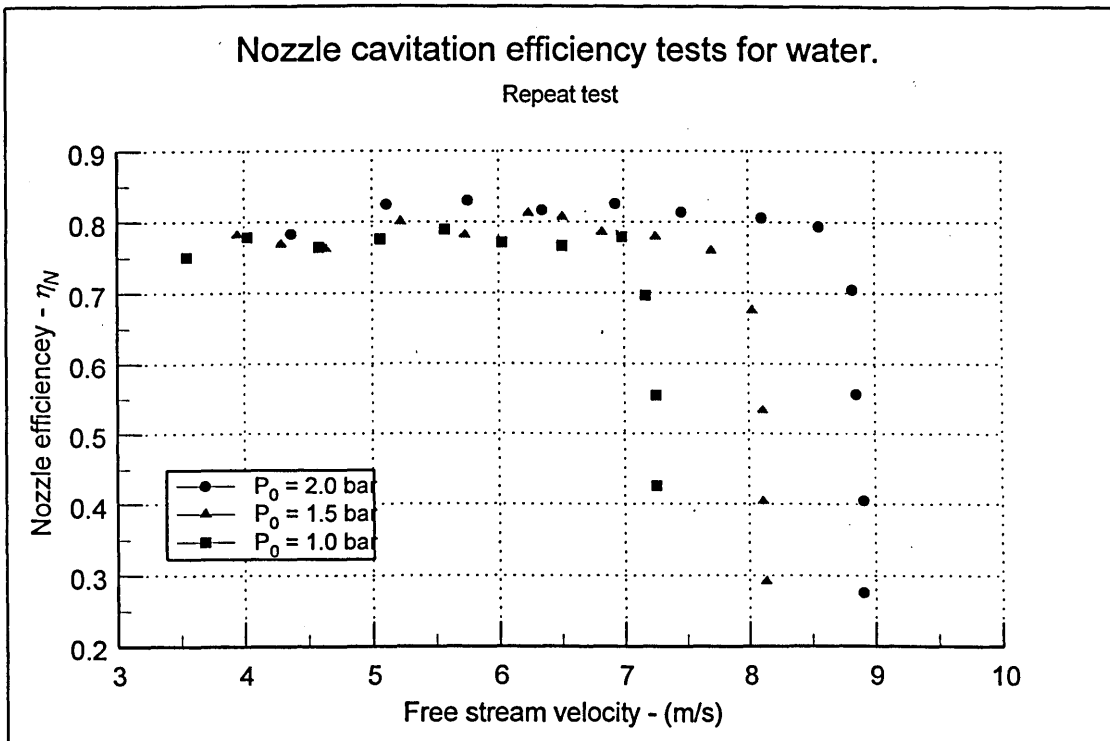
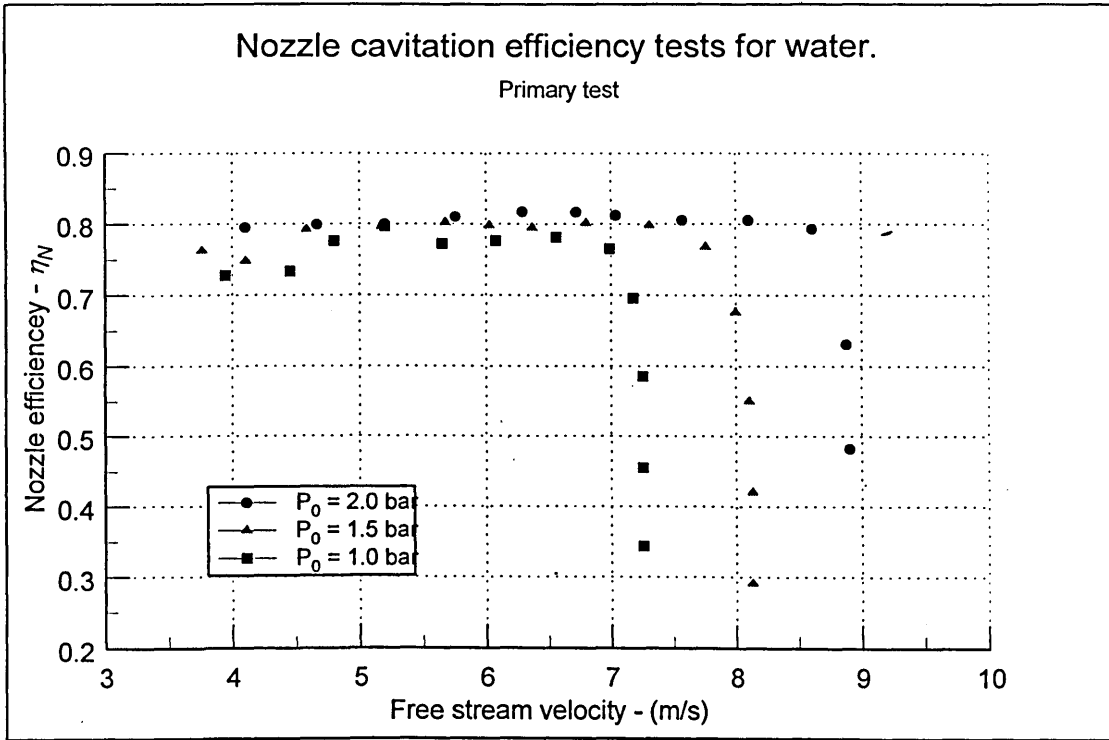
**Figure D-14 Nozzle efficiency tests for water : Dissolved oxygen  $\approx$  50% of saturation value : Fluid temperature 50°C**



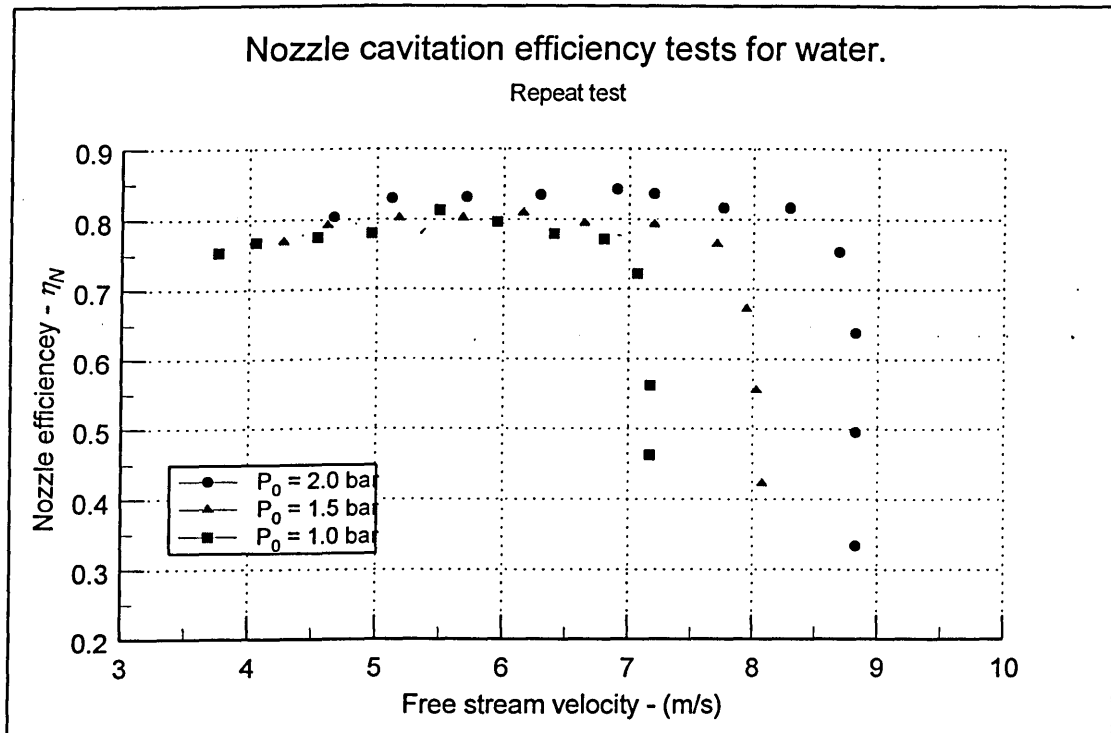
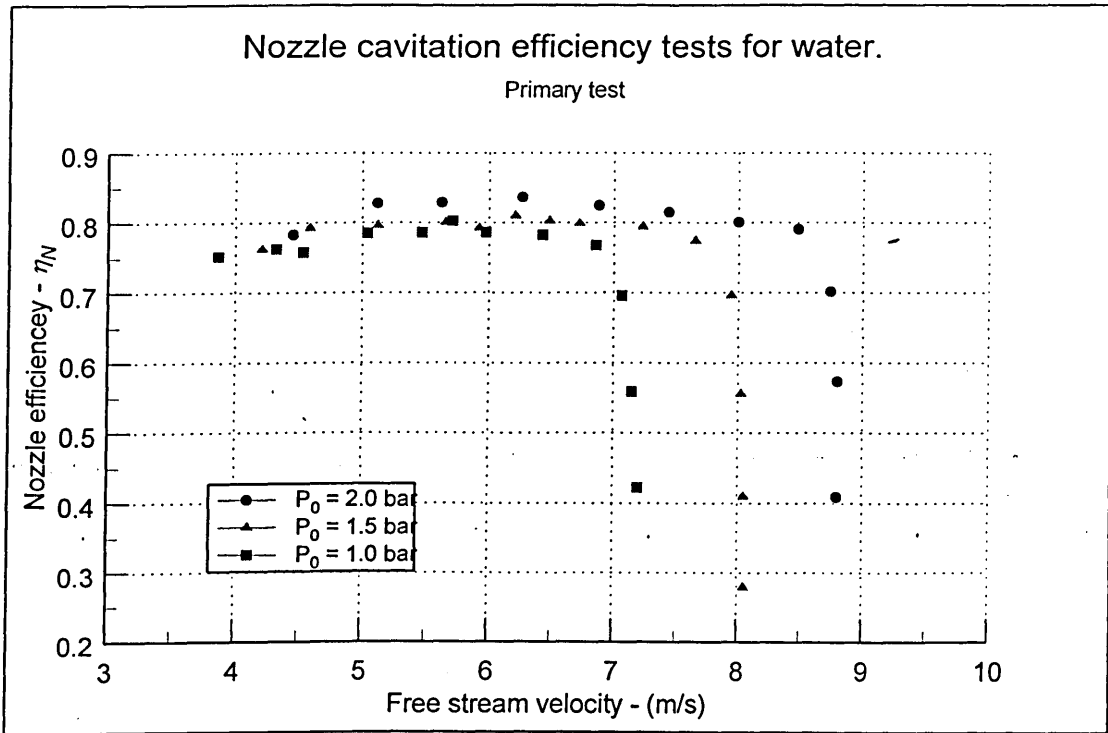
**Figure D-15 Nozzle efficiency tests for water : Dissolved oxygen <10% of saturation value : Fluid temperature 50°C**



**Figure D-16 Nozzle efficiency tests for water : Dissolved oxygen <10% of saturation value : Fluid temperature 30°C**



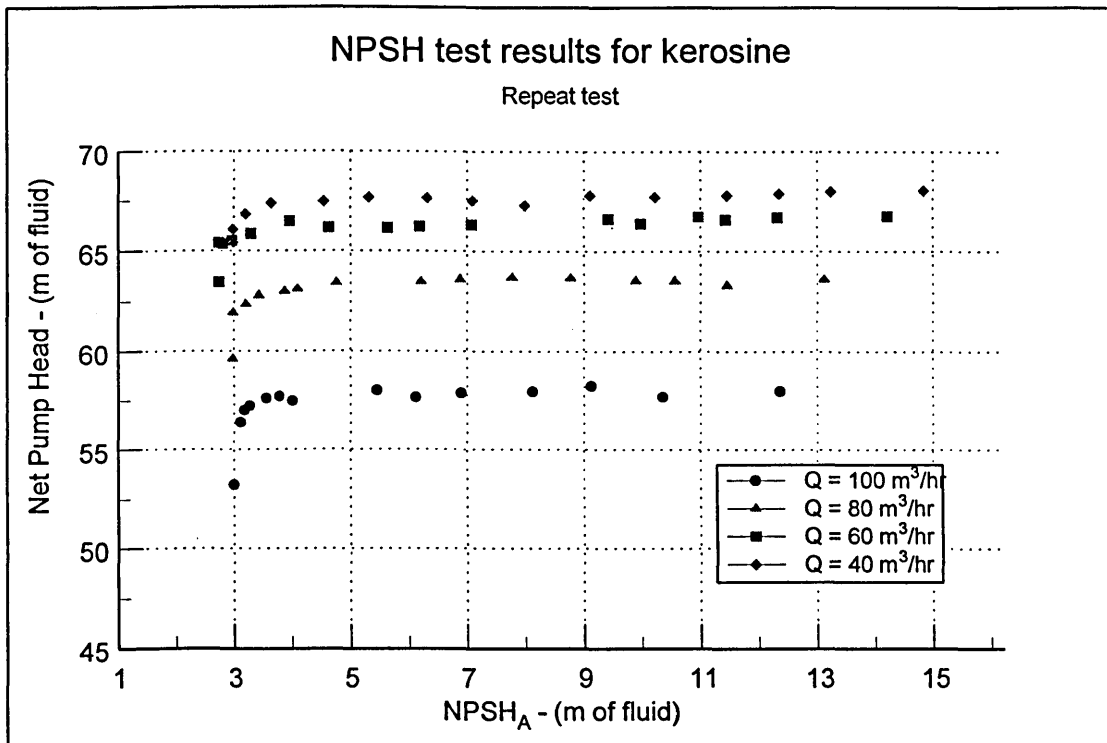
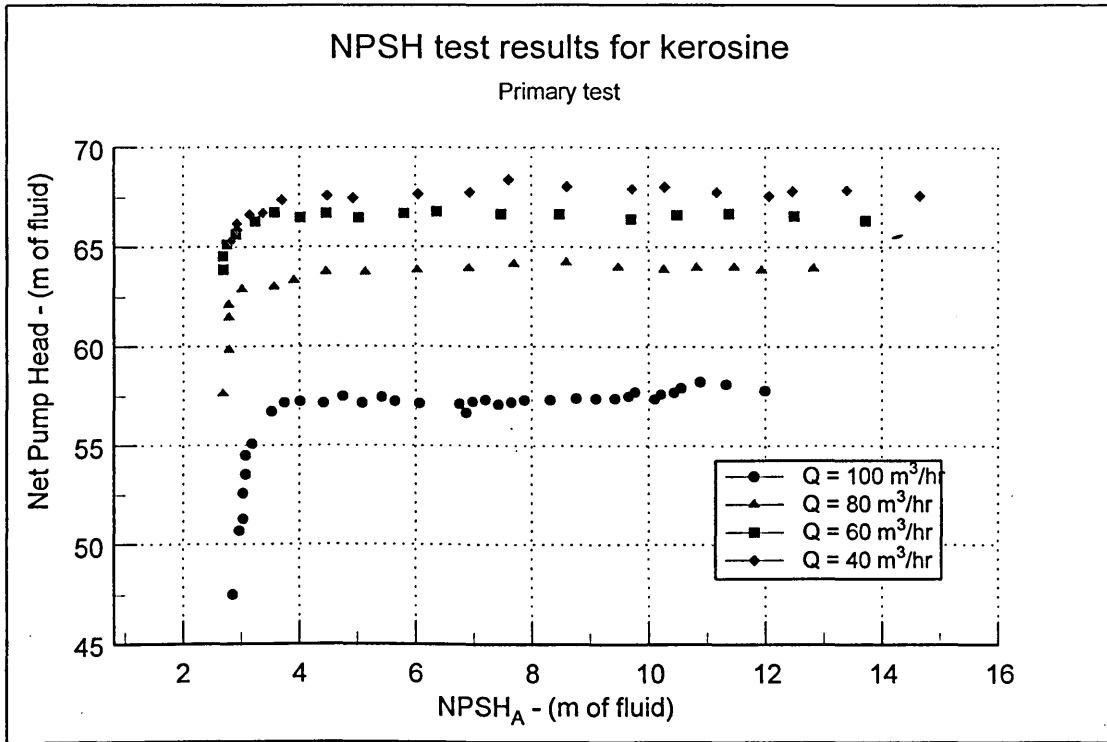
**Figure D-17 Nozzle efficiency tests for water : Dissolved oxygen <10% of saturation value : Fluid temperature 20°C**



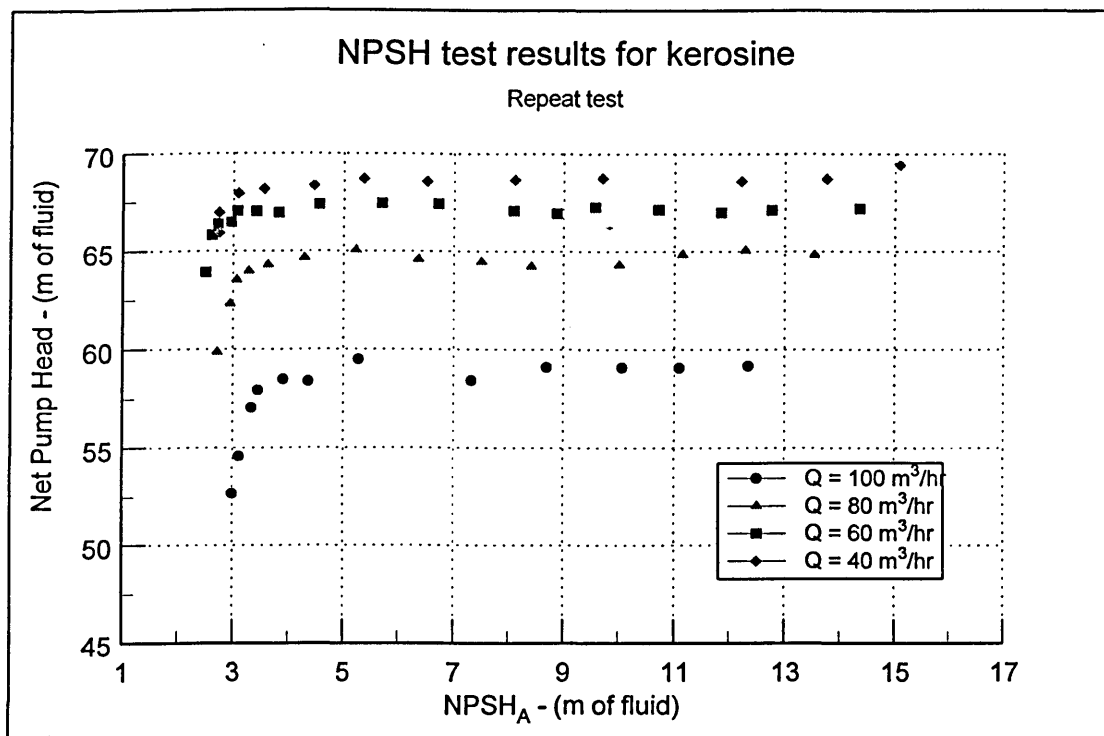
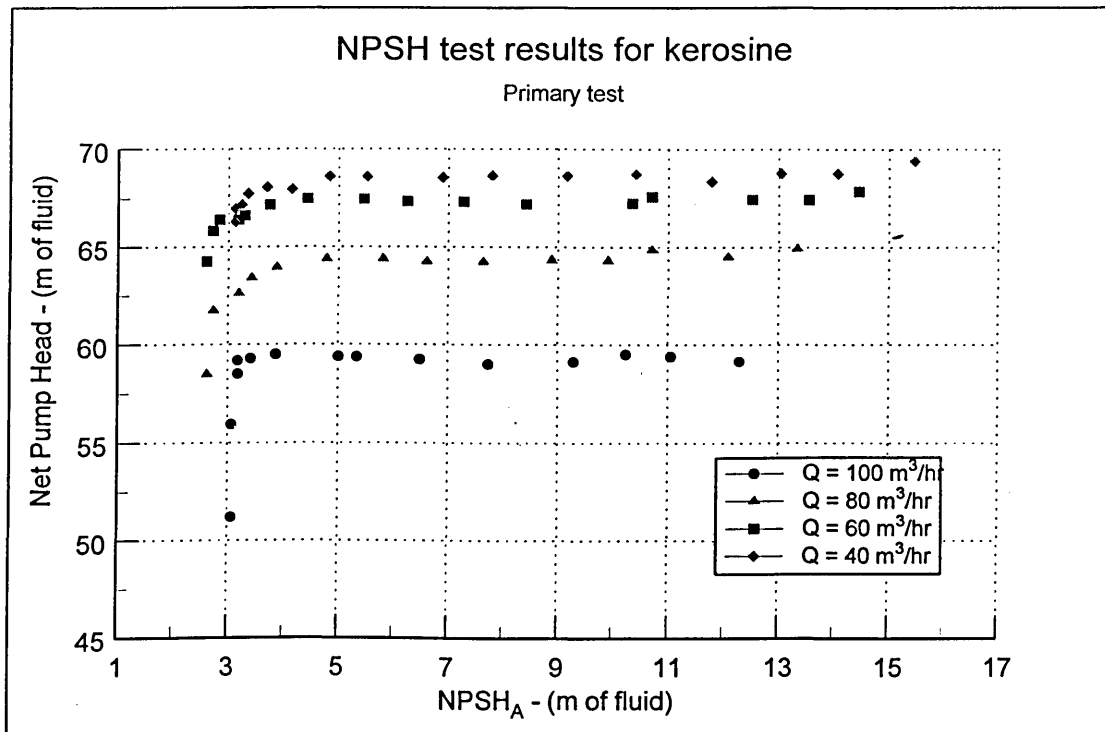
**Figure D-18 Nozzle efficiency tests for water : Dissolved oxygen <10% of saturation value : Fluid temperature 40°C**

**Appendix E - Pump and nozzle curves for kerosine.**

This appendix contains the NPSH curves (Figures E-1 to E-2) and tests section efficiency curves (Figures E-3 to E-8) for the tests on kerosine. Each figure contains two graphs, the primary test and the repeat at the same conditions. The conditions given are approximate (to within a °C or a few percent).

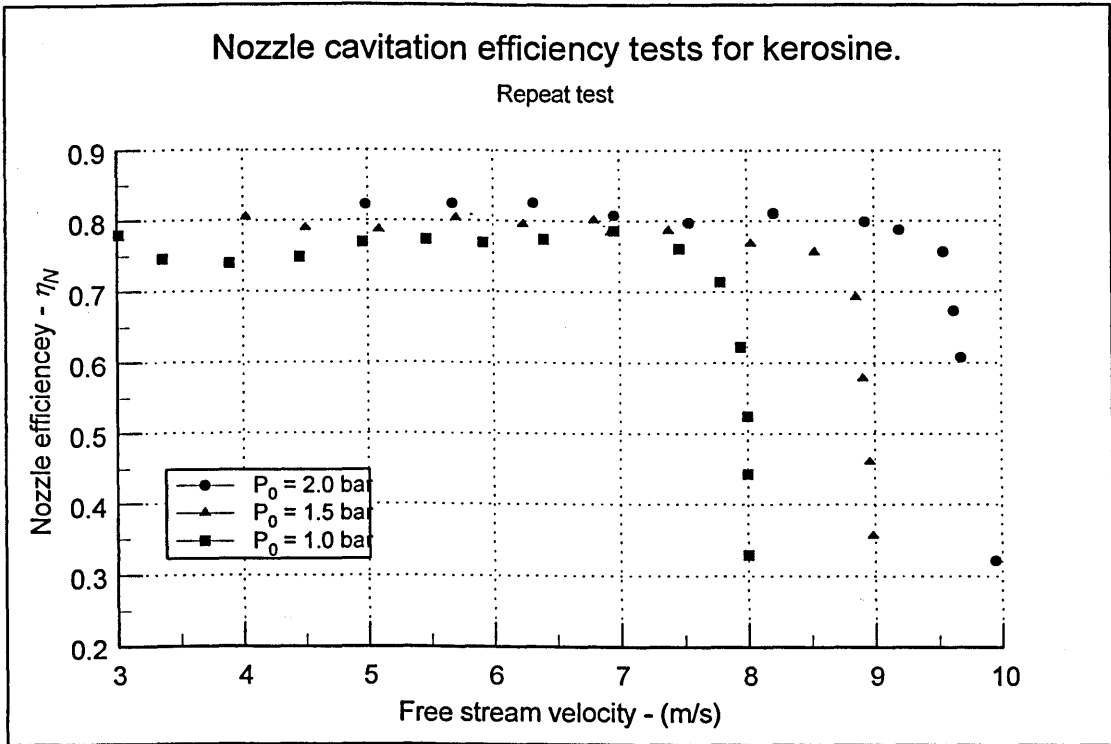
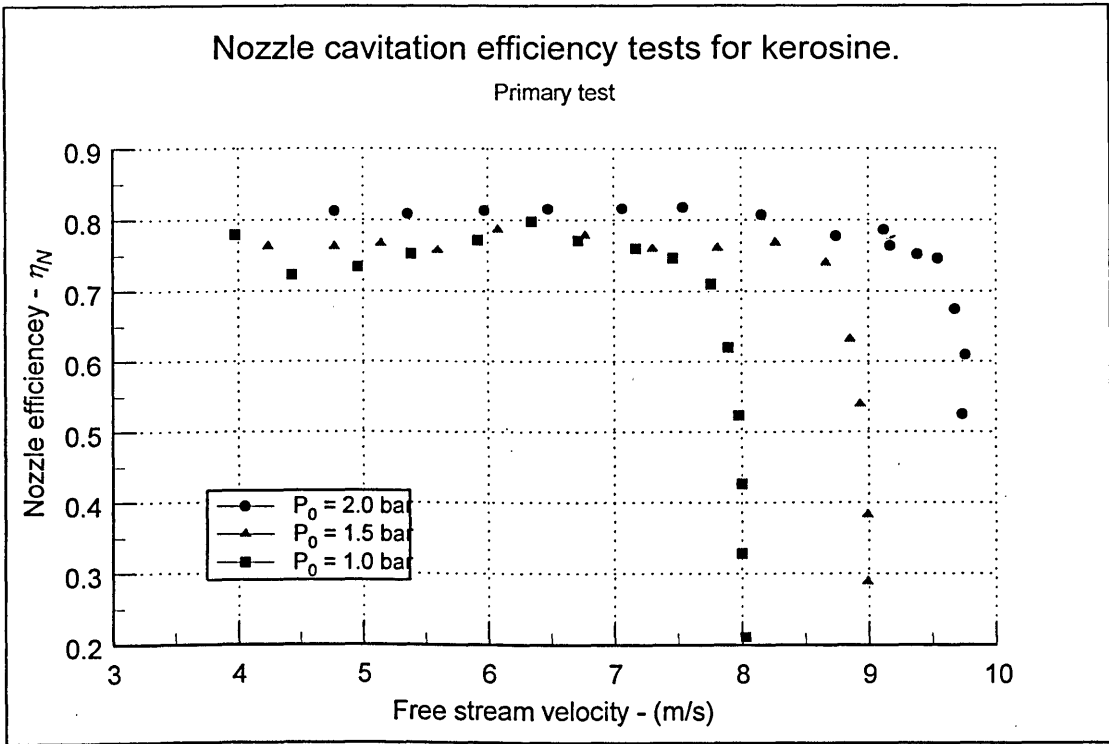


**Figure E-1 NPSH curves for kerosine - Vacuum pump method**  
 Dissolved oxygen  $\approx$  20% of saturation value at 3% head drop : Fluid temperature 20°C

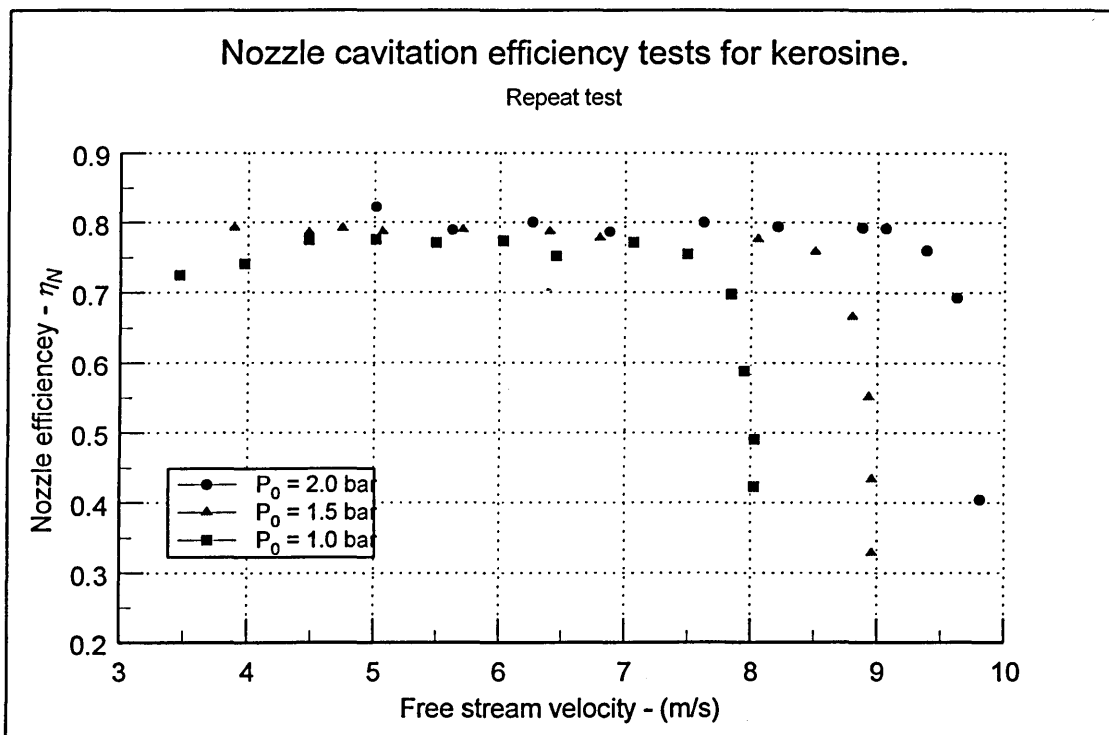
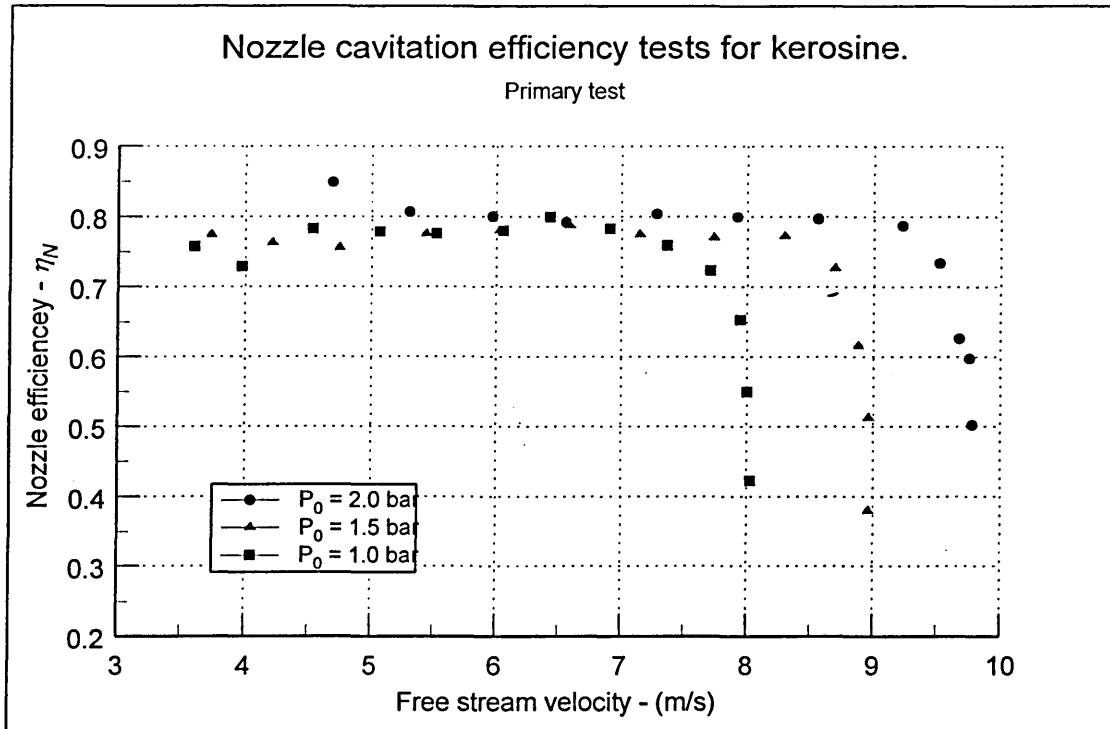


**Figure E-2 NPSH curves for kerosine - Vacuum pump method**  
 Dissolved oxygen  $\approx$  20% of saturation value at 3% head drop : Fluid temperature 30°C

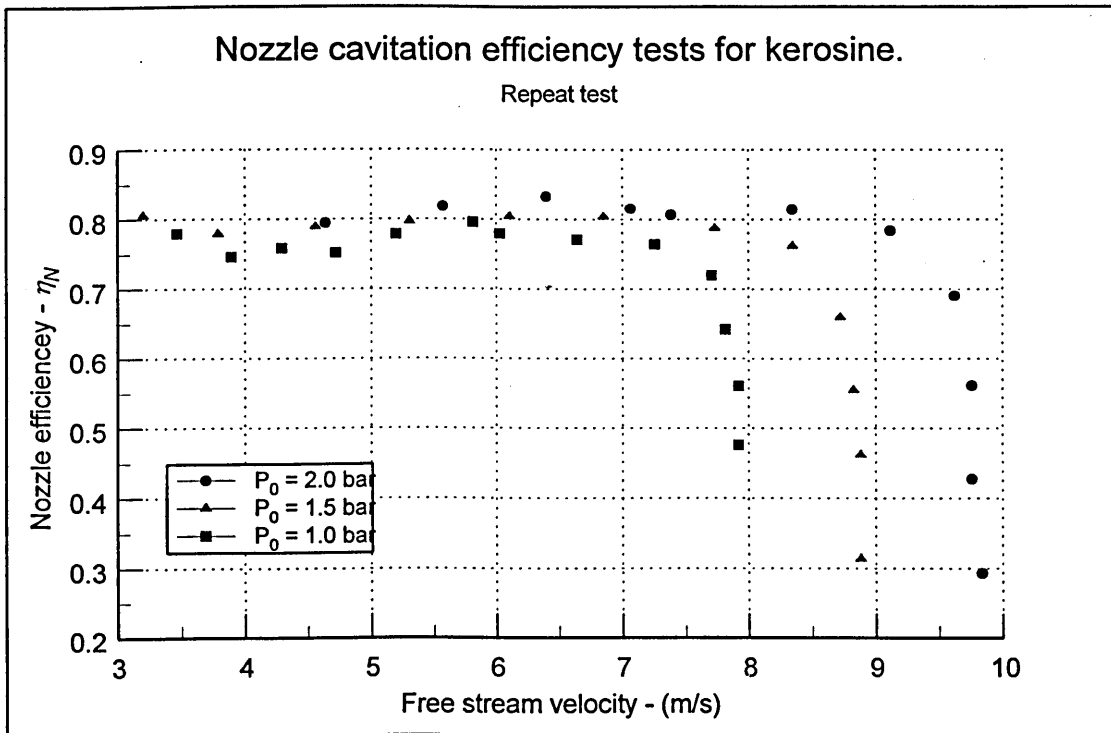
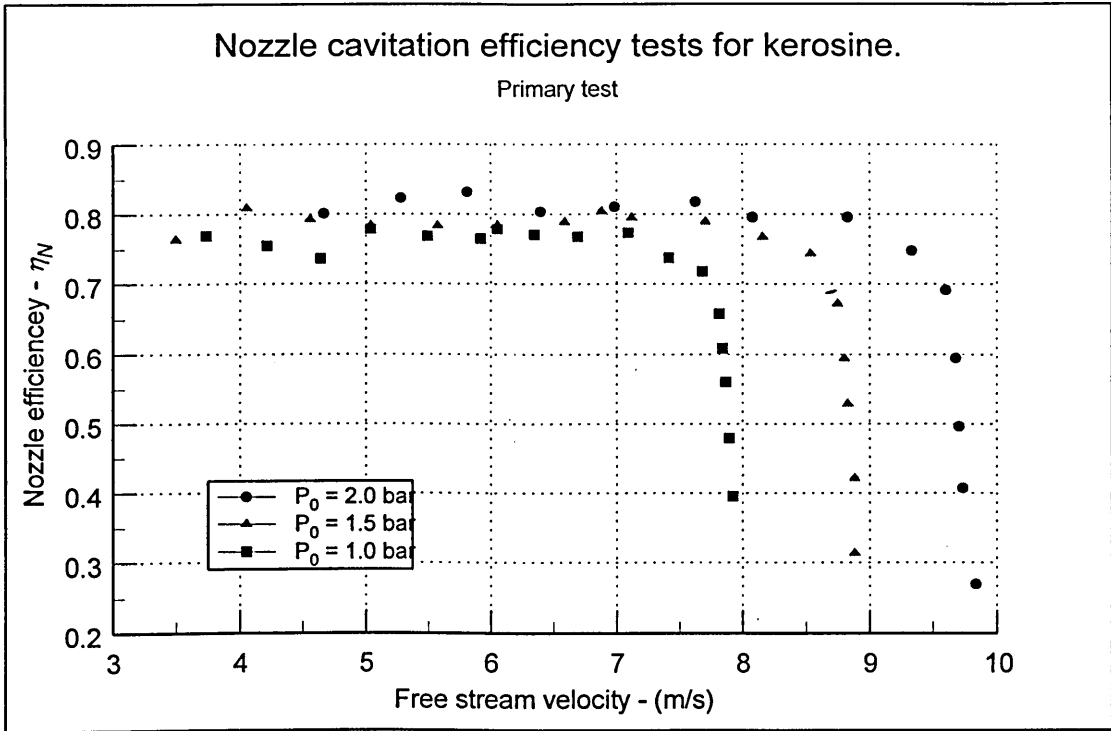




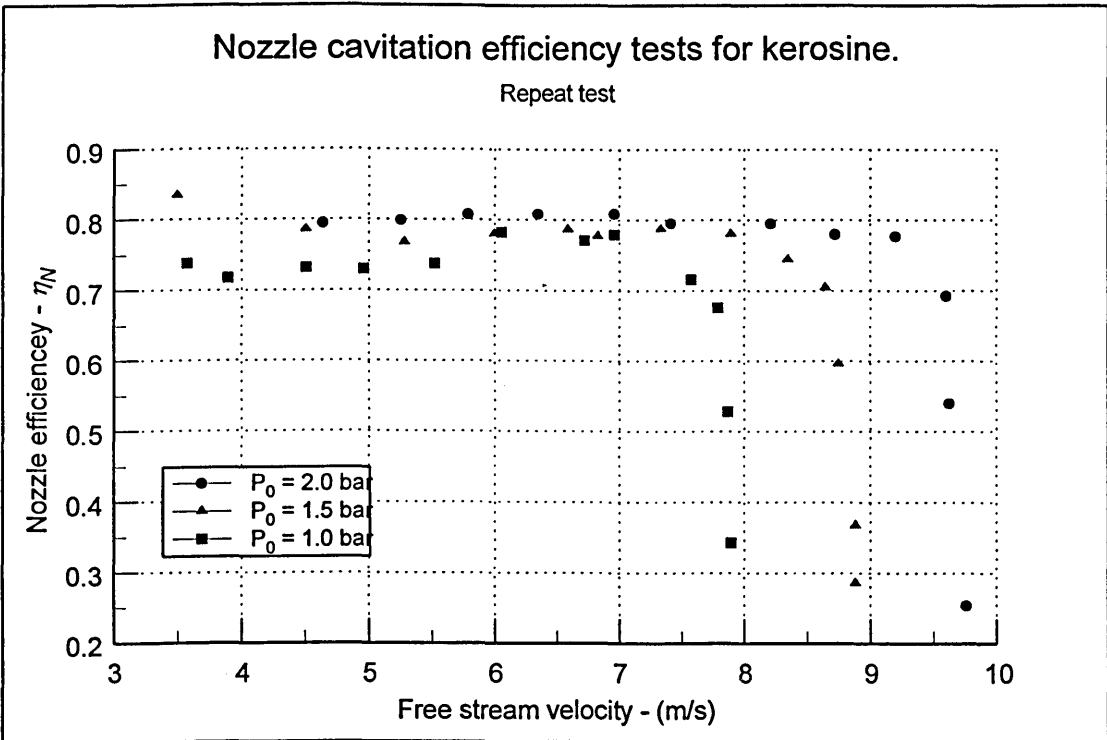
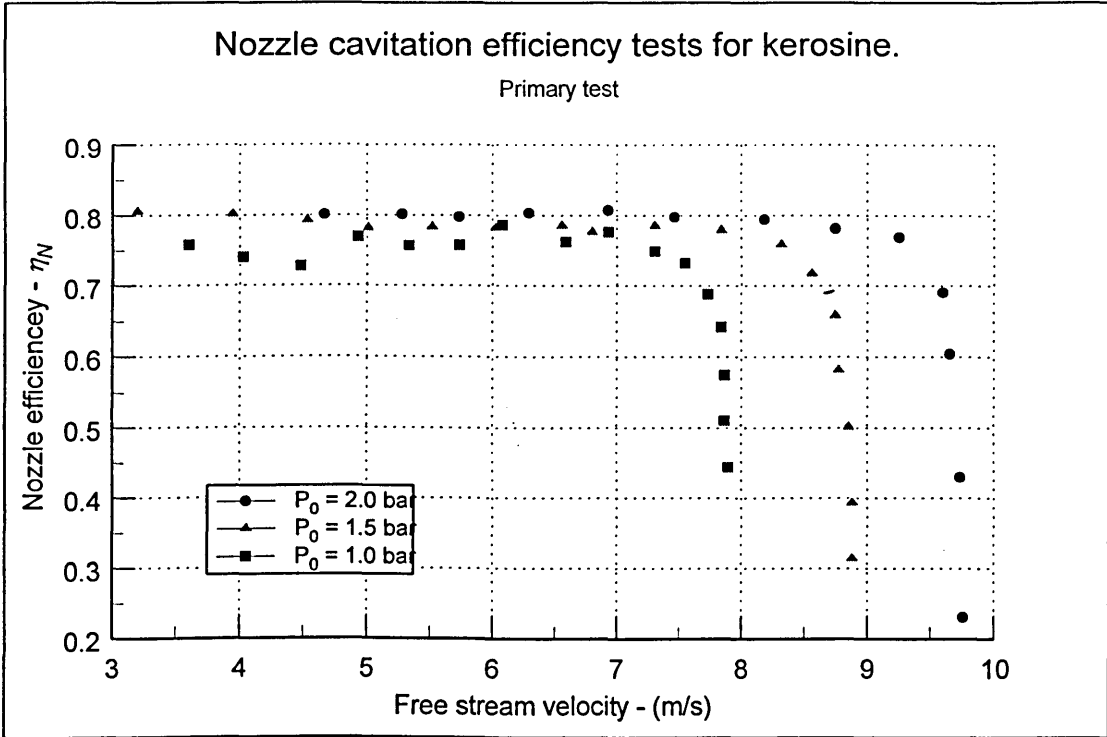
**Figure E-3 Nozzle efficiency tests for kerosine : Dissolved oxygen  $\approx$  50% of saturation value : Fluid temperature 20°C**



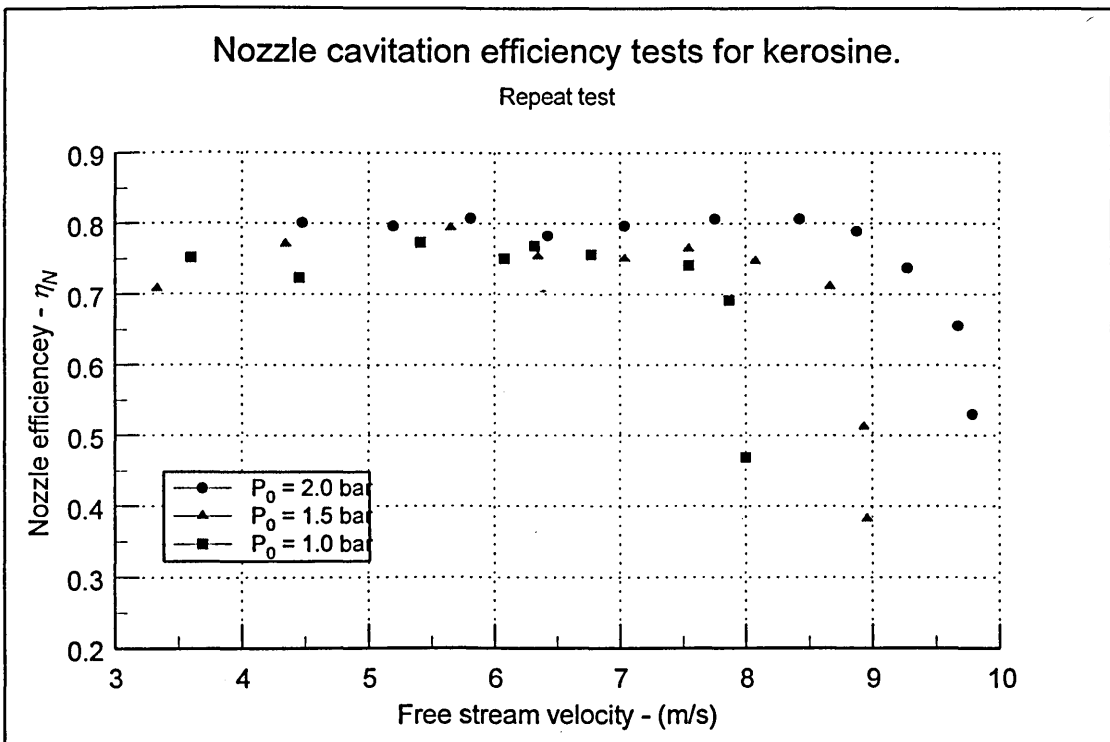
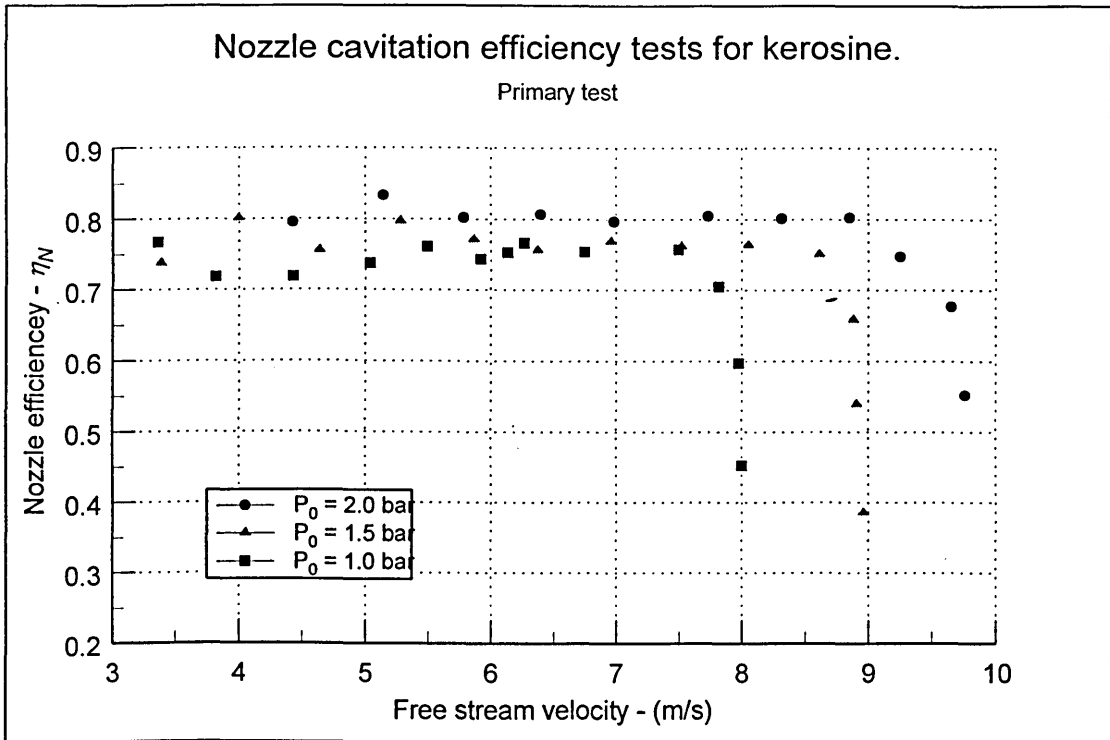
**Figure E-4 Nozzle efficiency tests for kerosine: Dissolved oxygen  $\approx$  50% of saturation value : Fluid temperature 30°C**



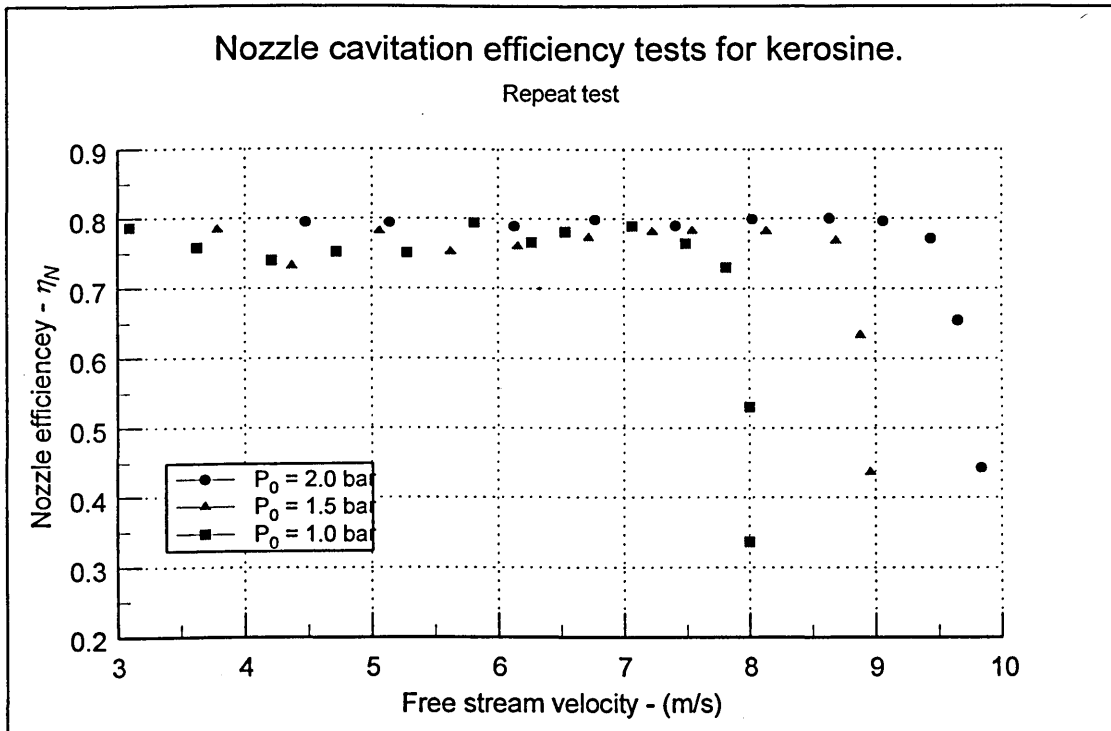
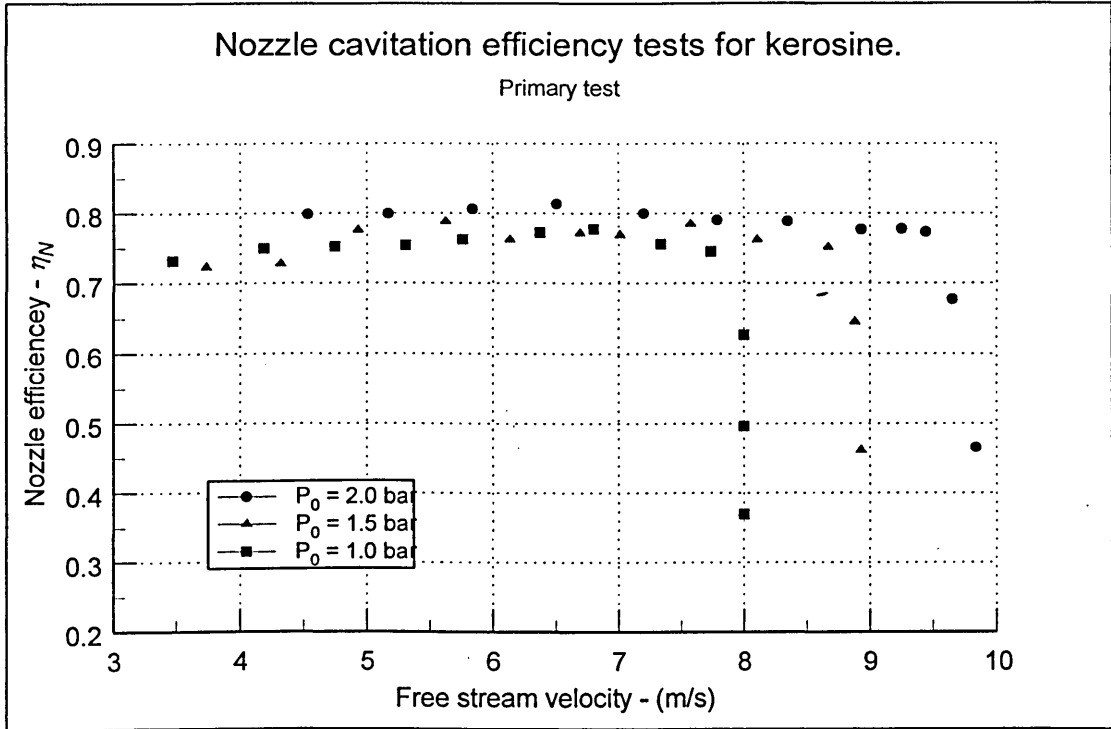
**Figure E-5 Nozzle efficiency tests for kerosine : Dissolved oxygen  $\approx$  100% of saturation value : Fluid temperature 30°C**



**Figure E-6 Nozzle efficiency tests for kerosine: Dissolved oxygen  $\approx$  100% of saturation value : Fluid temperature 20°C**



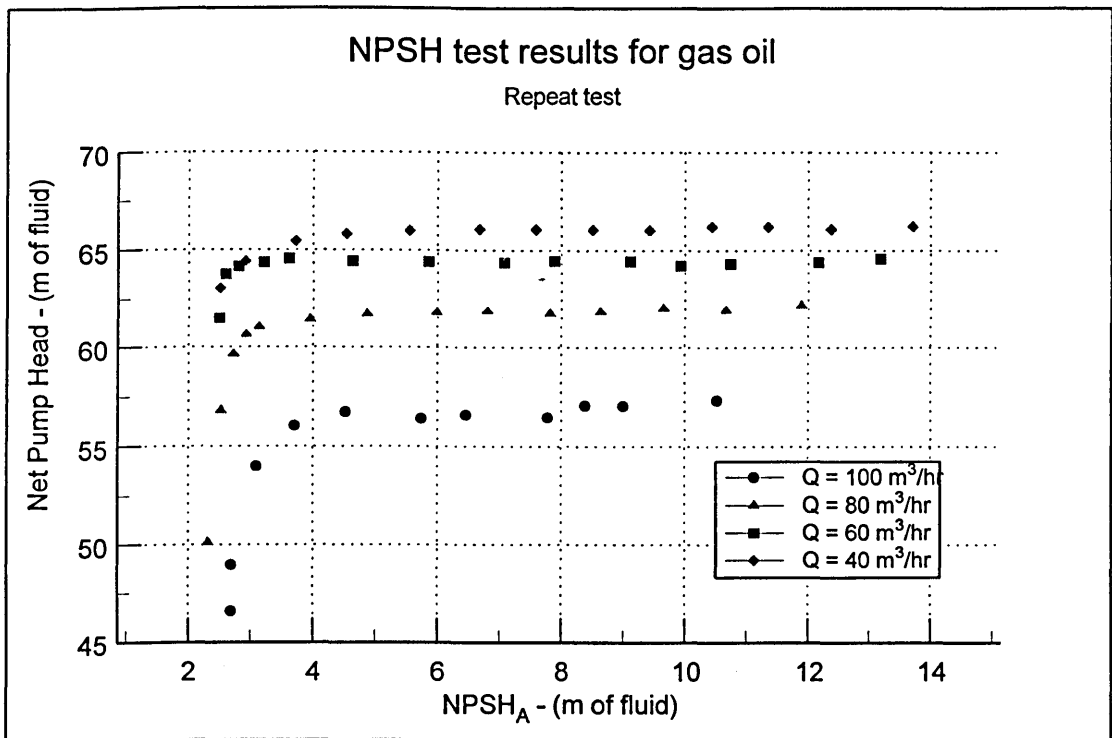
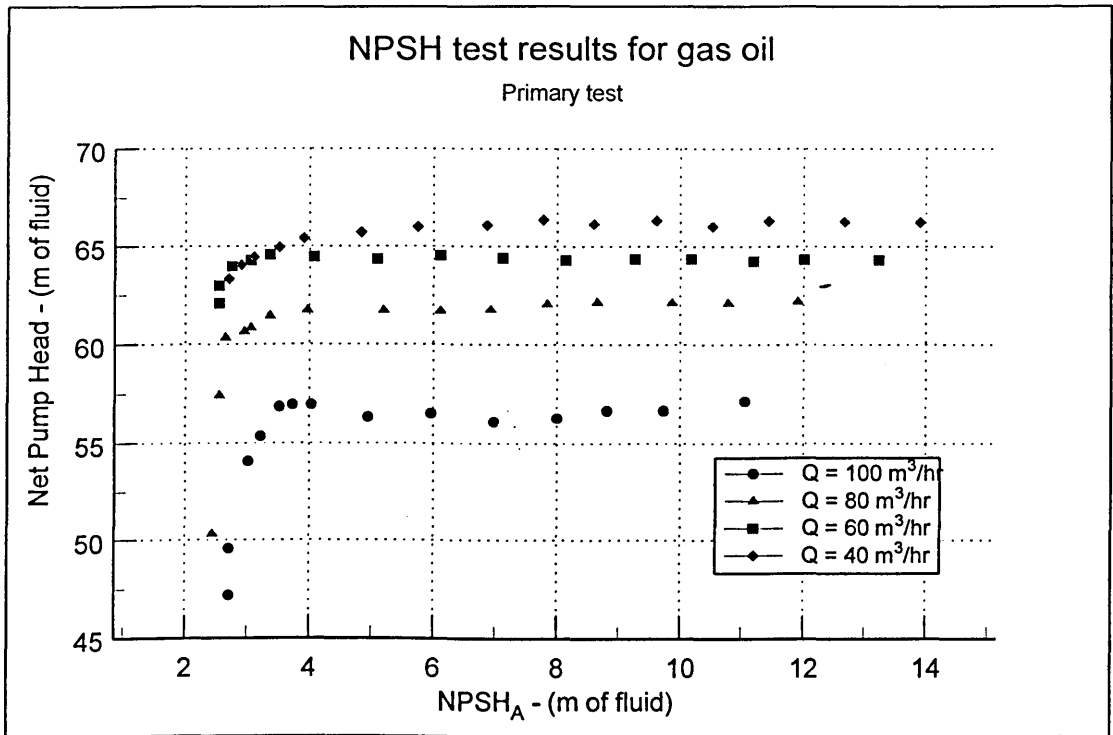
**Figure E-7 Nozzle efficiency tests for kerosine : Dissolved oxygen  $\approx$  20-25% of saturation value : Fluid temperature 20°C**



**Figure E-8 Nozzle efficiency tests for kerosine : Dissolved oxygen  $\approx$  20-25% of saturation value : Fluid temperature 30°C**

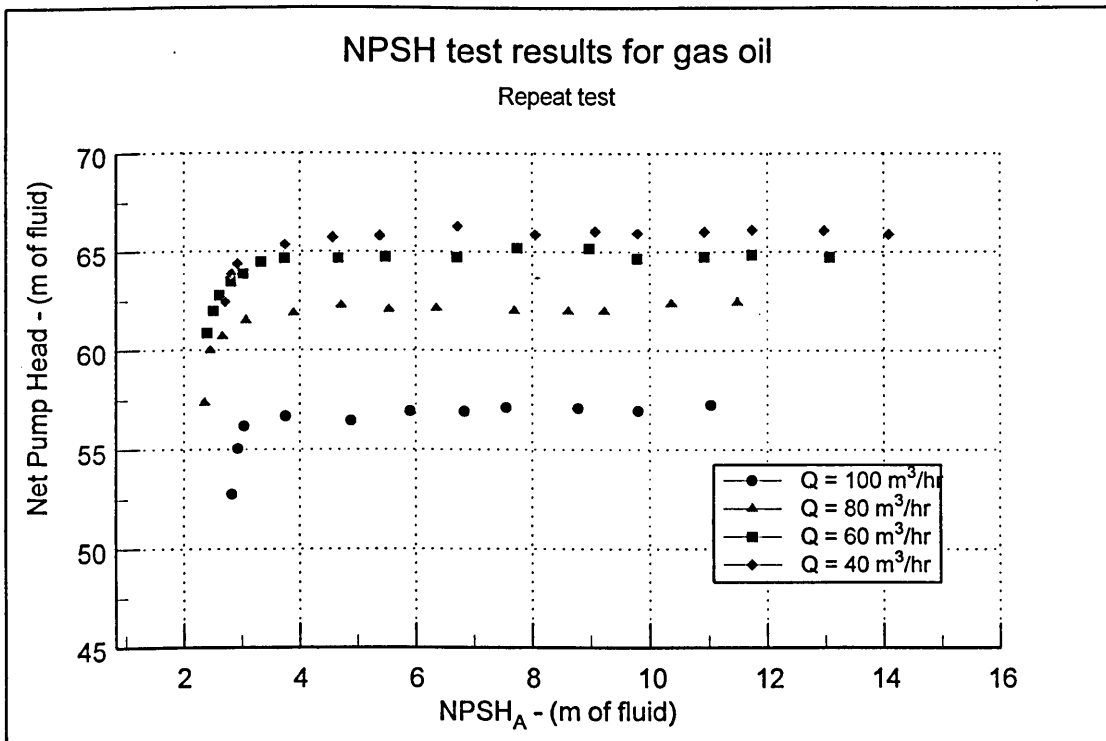
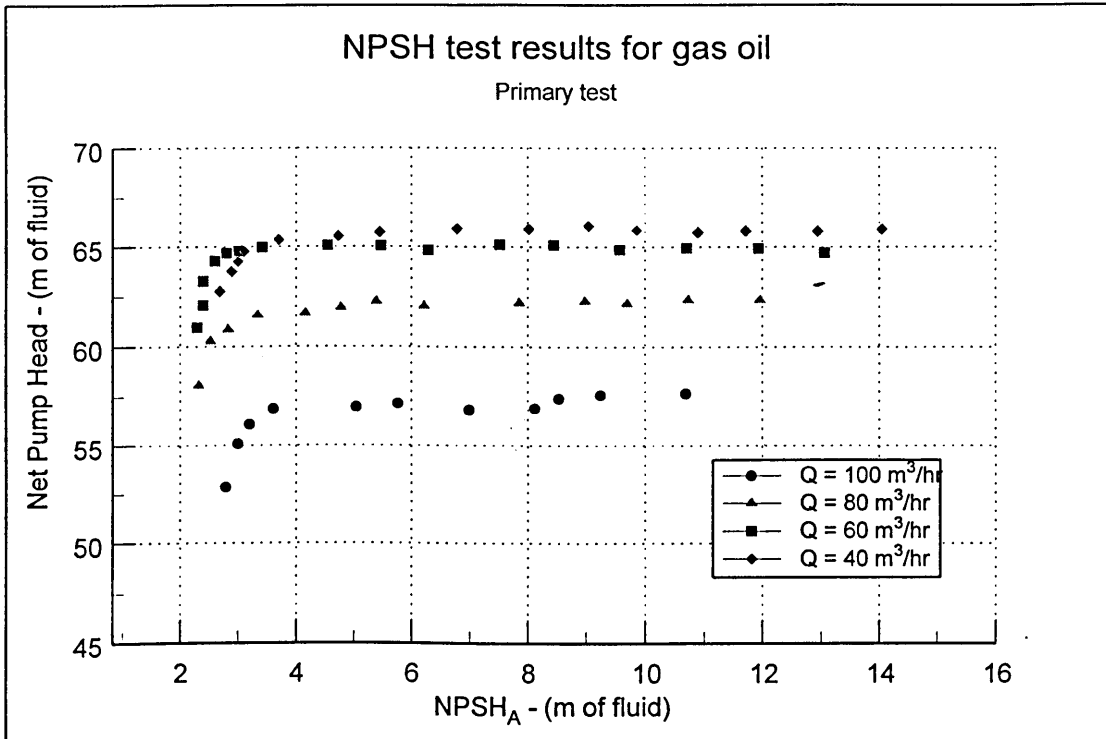
**Appendix F - Pump and nozzle curves for gas oil.**

This appendix contains the NPSH curves (Figures F-1 to F-2) and tests section efficiency curves (Figures F-3 to F-8) for the tests on gas oil. Each figure contains two graphs, the primary test and the repeat at the same conditions. The conditions given are approximate (to within a °C or a few percent).

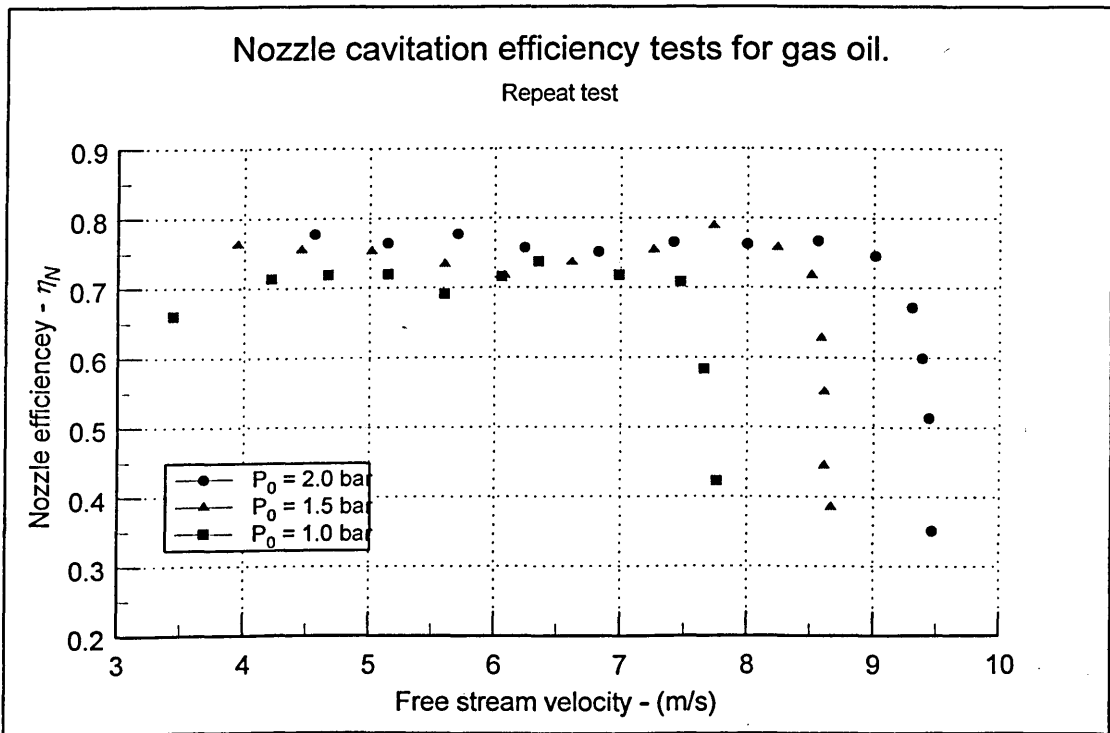
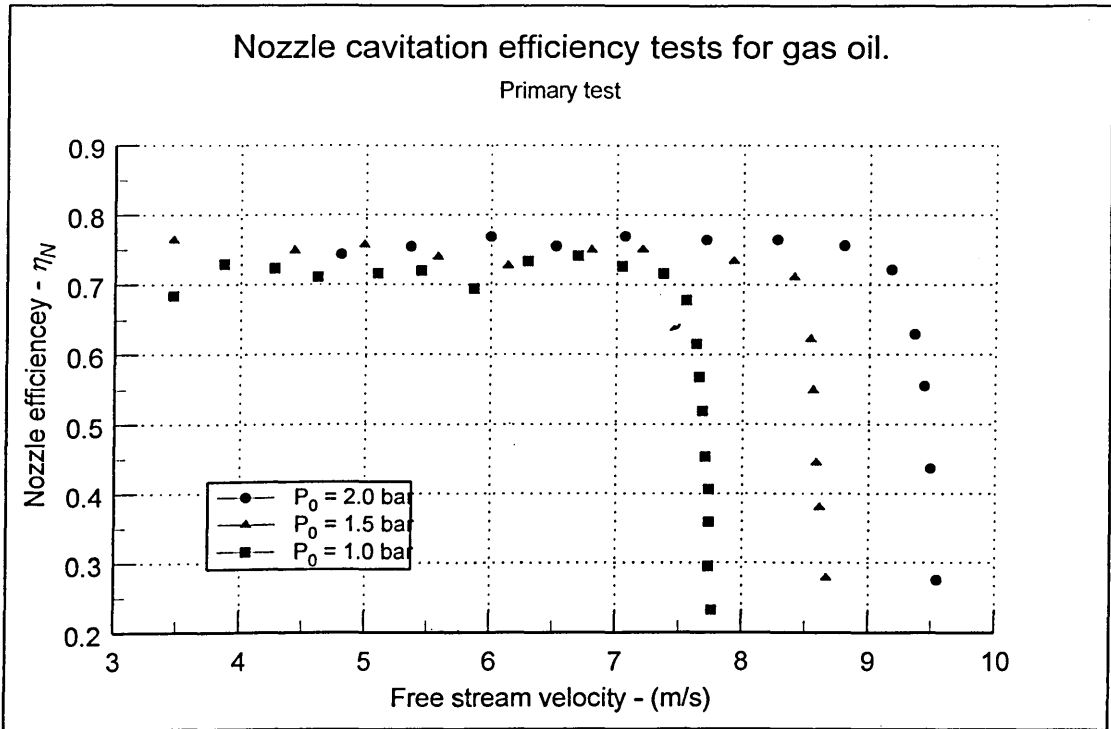


**Figure F-1 NPSH curves for gas oil - Vacuum pump method**  
 Dissolved oxygen  $\approx$  20% of saturation value at 3% head drop : Fluid temperature 20°C

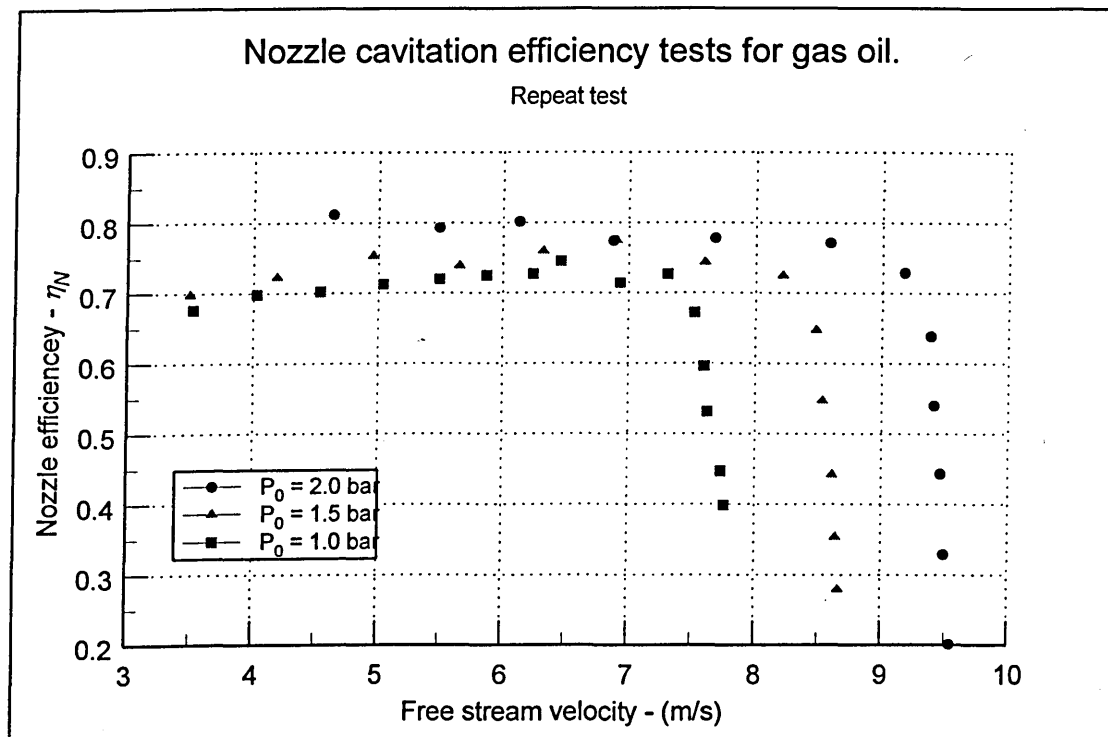
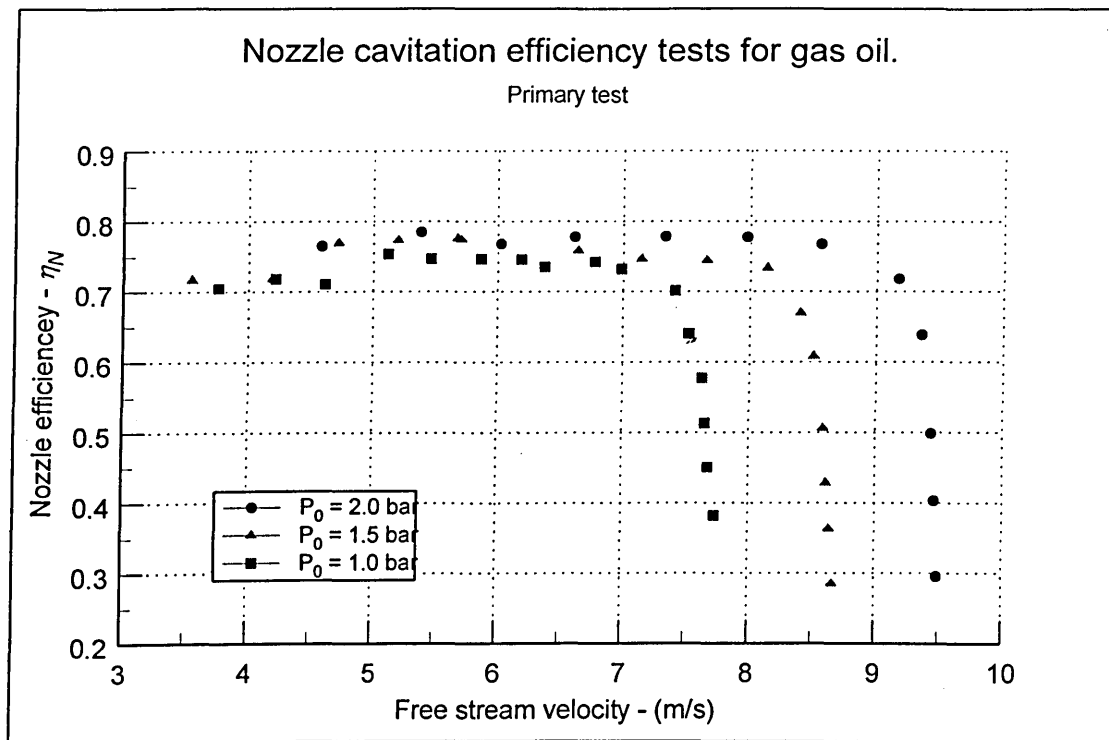




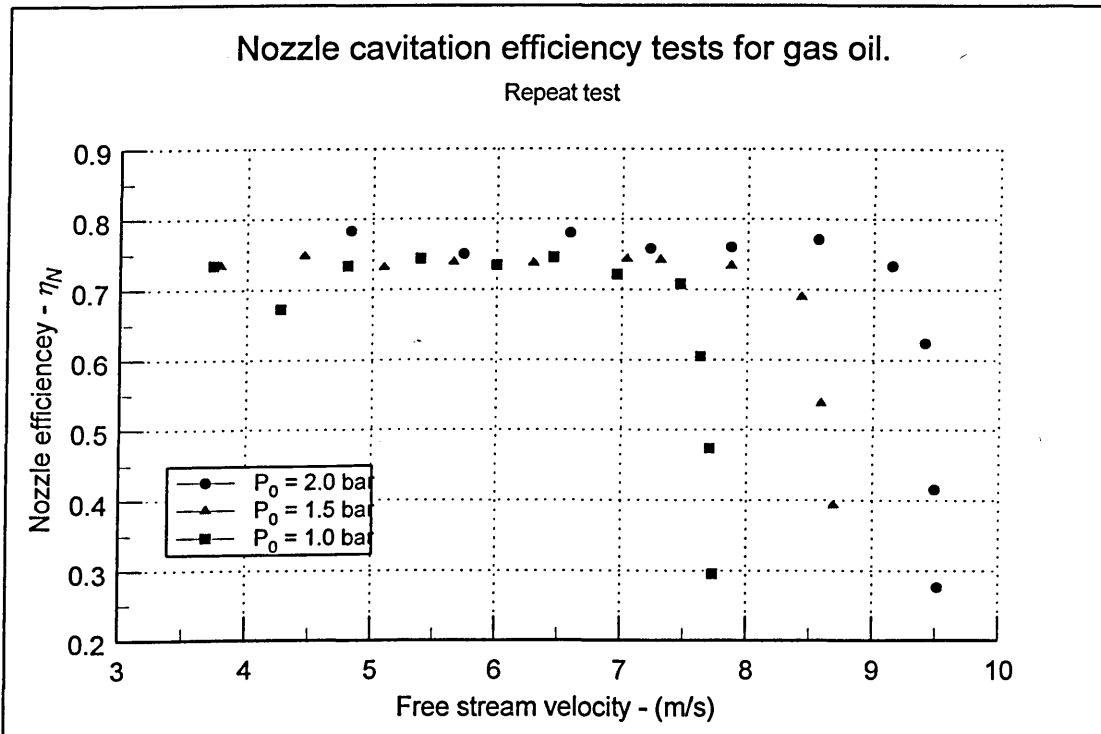
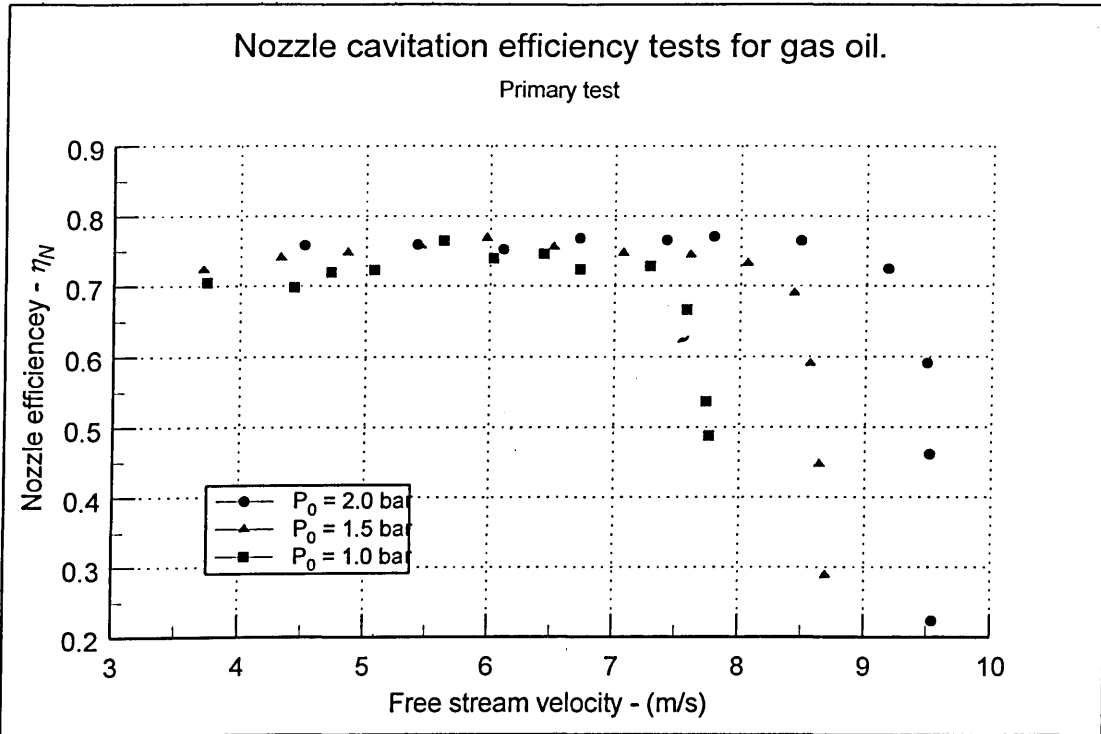
**Figure F-2 NPSH curves for gas oil - Vacuum pump method**  
 Dissolved oxygen  $\approx$  20% of saturation value at 3% head drop : Fluid temperature 30°C



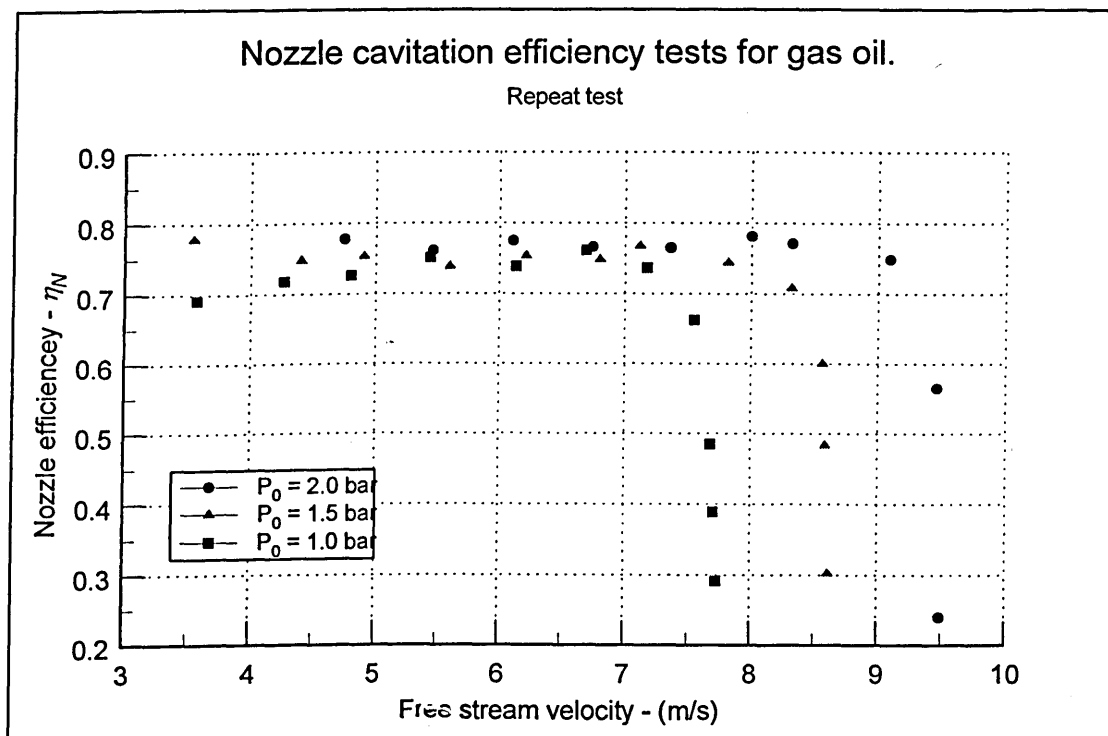
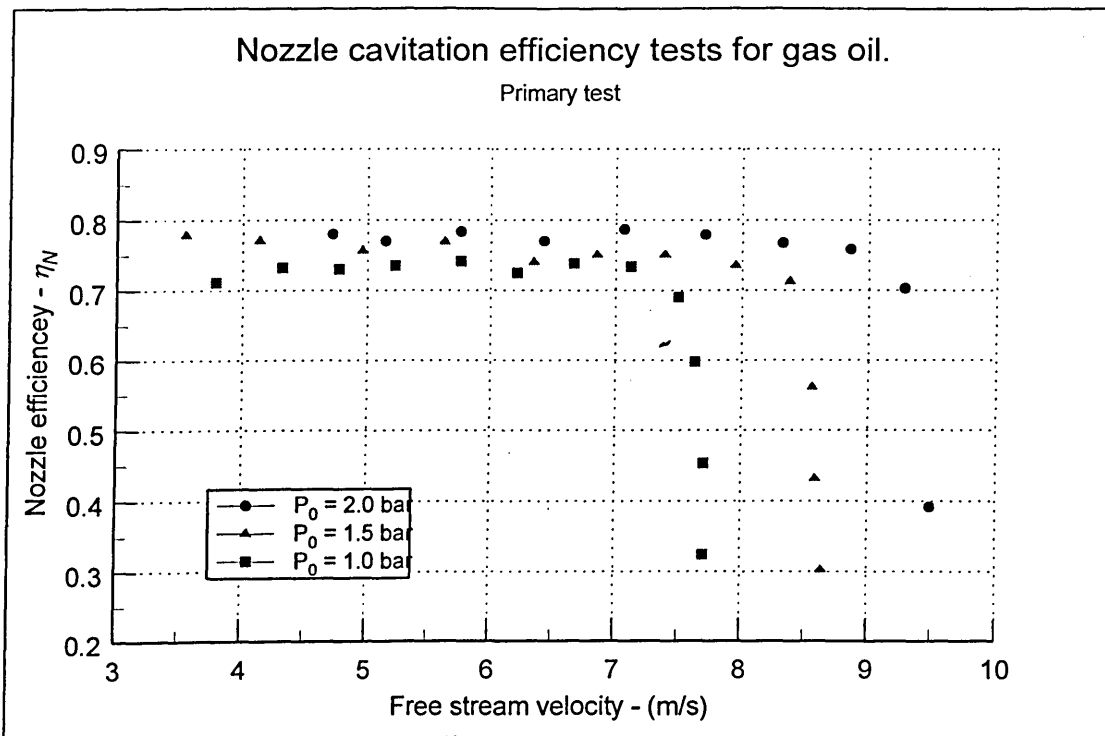
**Figure F-3 Nozzle efficiency tests for gas oil : Dissolved oxygen  $\approx$  100% of saturation value : Fluid temperature 20°C**



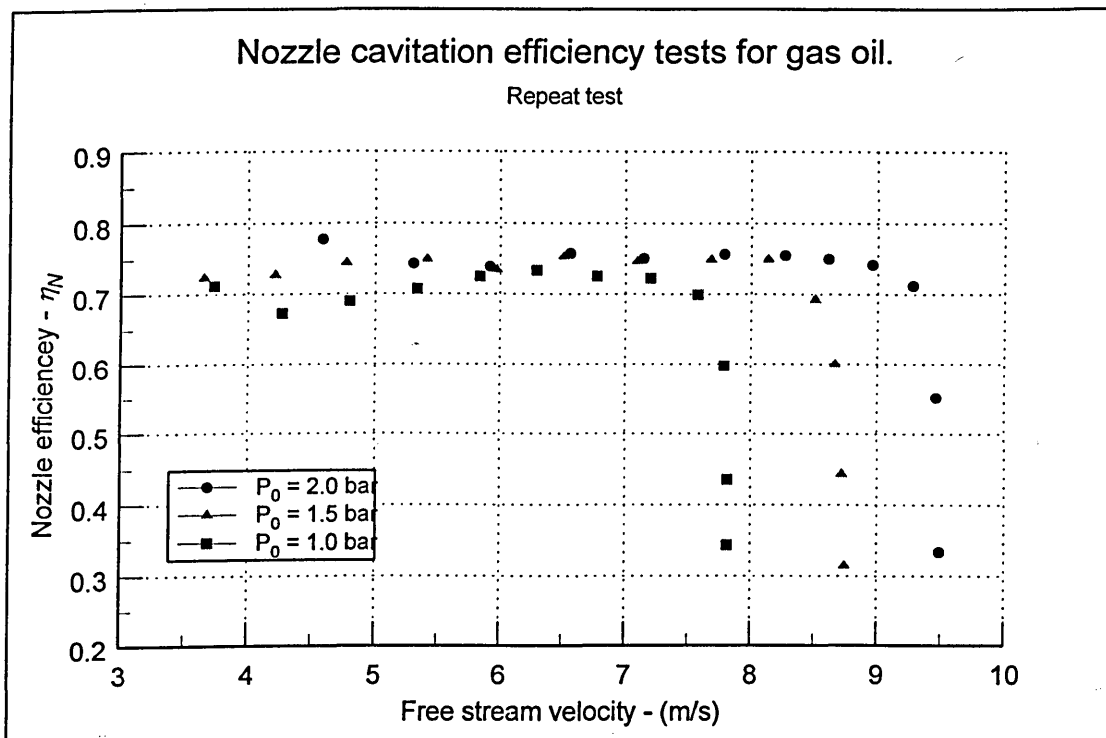
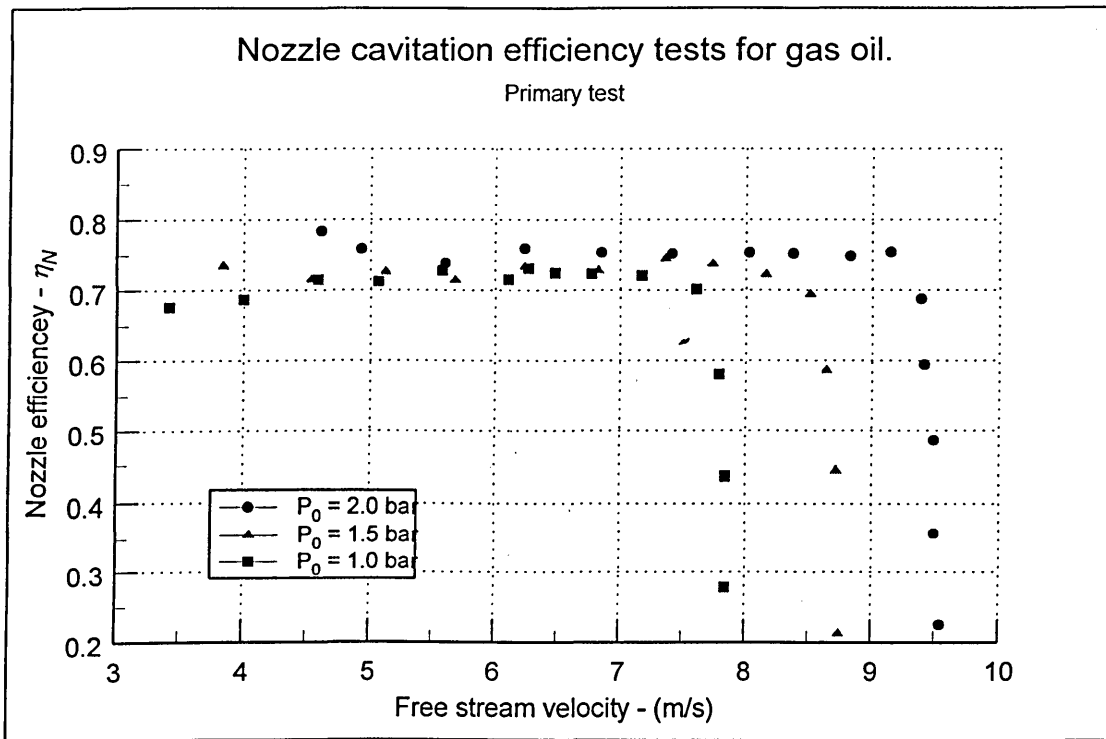
**Figure F-4 Nozzle efficiency tests for gas oil: Dissolved oxygen  $\approx$  100% of saturation value : Fluid temperature 30°C**



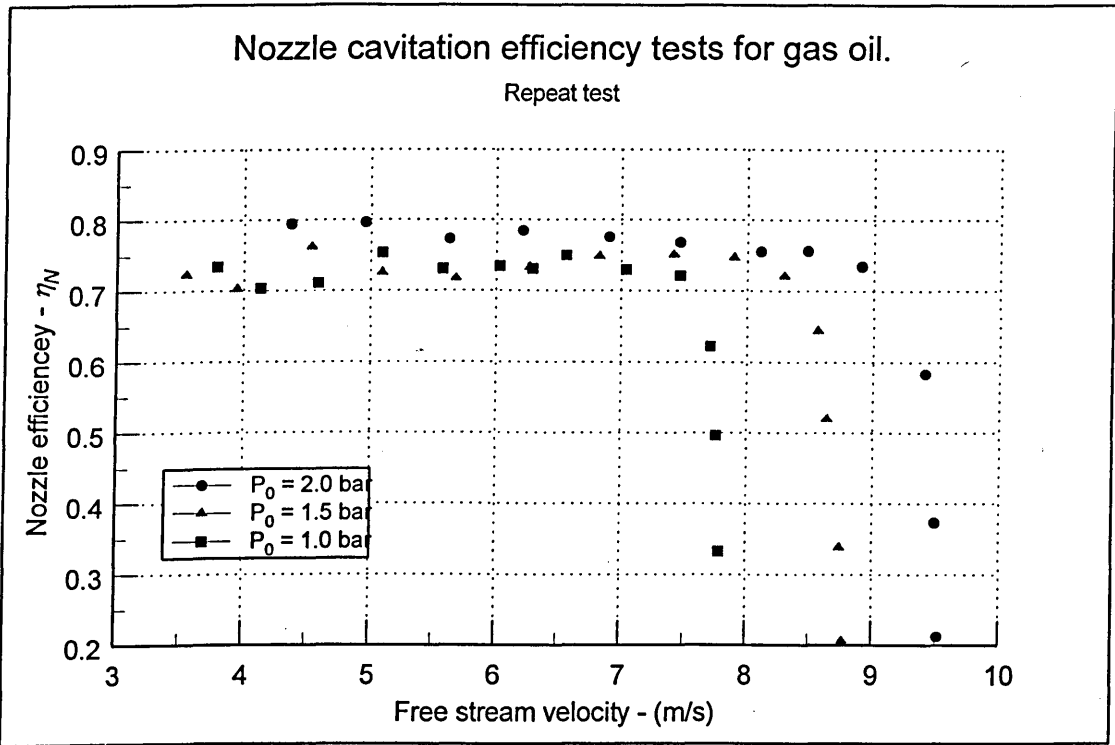
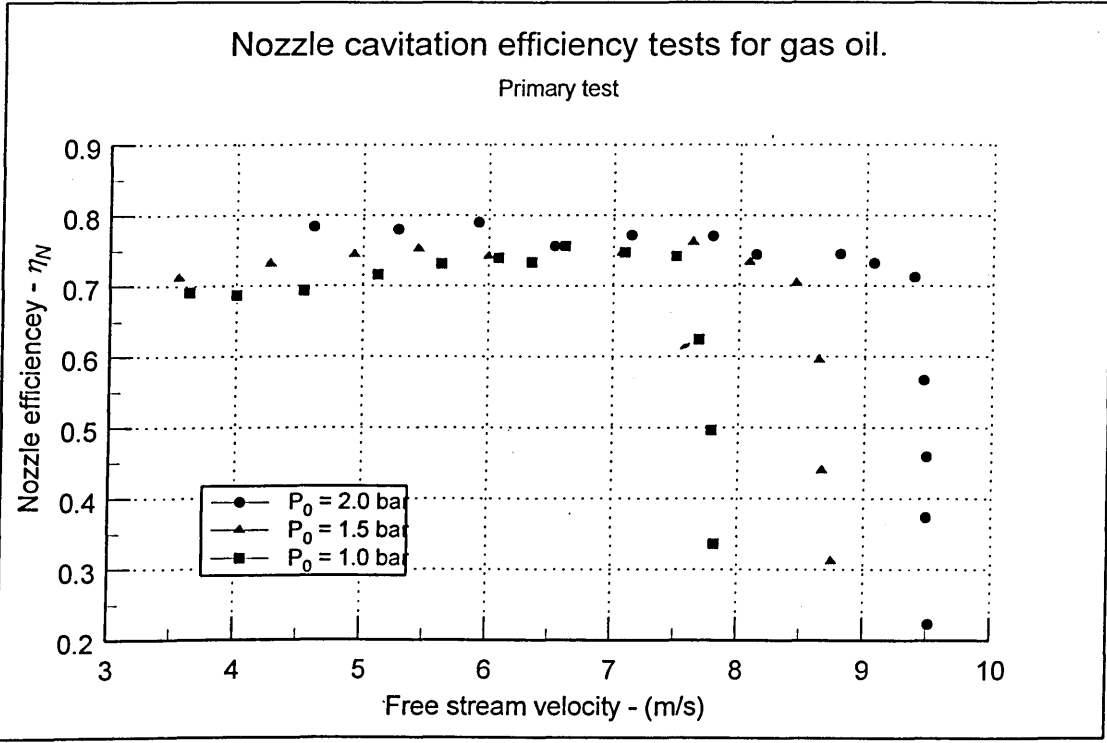
**Figure F-5 Nozzle efficiency tests for gas oil : Dissolved oxygen  $\approx$  50% of saturation value : Fluid temperature 30°C**



**Figure F-6 Nozzle efficiency tests for gas oil: Dissolved oxygen  $\approx$  50% of saturation value : Fluid temperature 20°C**



**Figure F-7 Nozzle efficiency tests for gas oil : Dissolved oxygen  $\approx$  20-25% of saturation value : Fluid temperature 20°C**



**Figure F-8 Nozzle efficiency tests for gas oil : Dissolved oxygen  $\approx$  20-25% of saturation value : Fluid temperature 30°C**

## **Appendix G - Photographs.**

This appendix contains a photograph of the test rig and some colour photos of cavitation in the test section with gas oil.

(Over leaf)

**Figure G-1 Hydrocarbon cavitation test rig ; Main circuit (p 203)**

**Figure G-2 Early cavitation growth in gas oil (p 204)**

**Figure G-3 Approximately 3% efficiency drop cavitation condition in gas oil (p205)**

**Figure G-4 Fully developed cavitation in gas oil (p 206)**

**Figure G-5 'Supercavitation' condition in gas oil (p 207)**



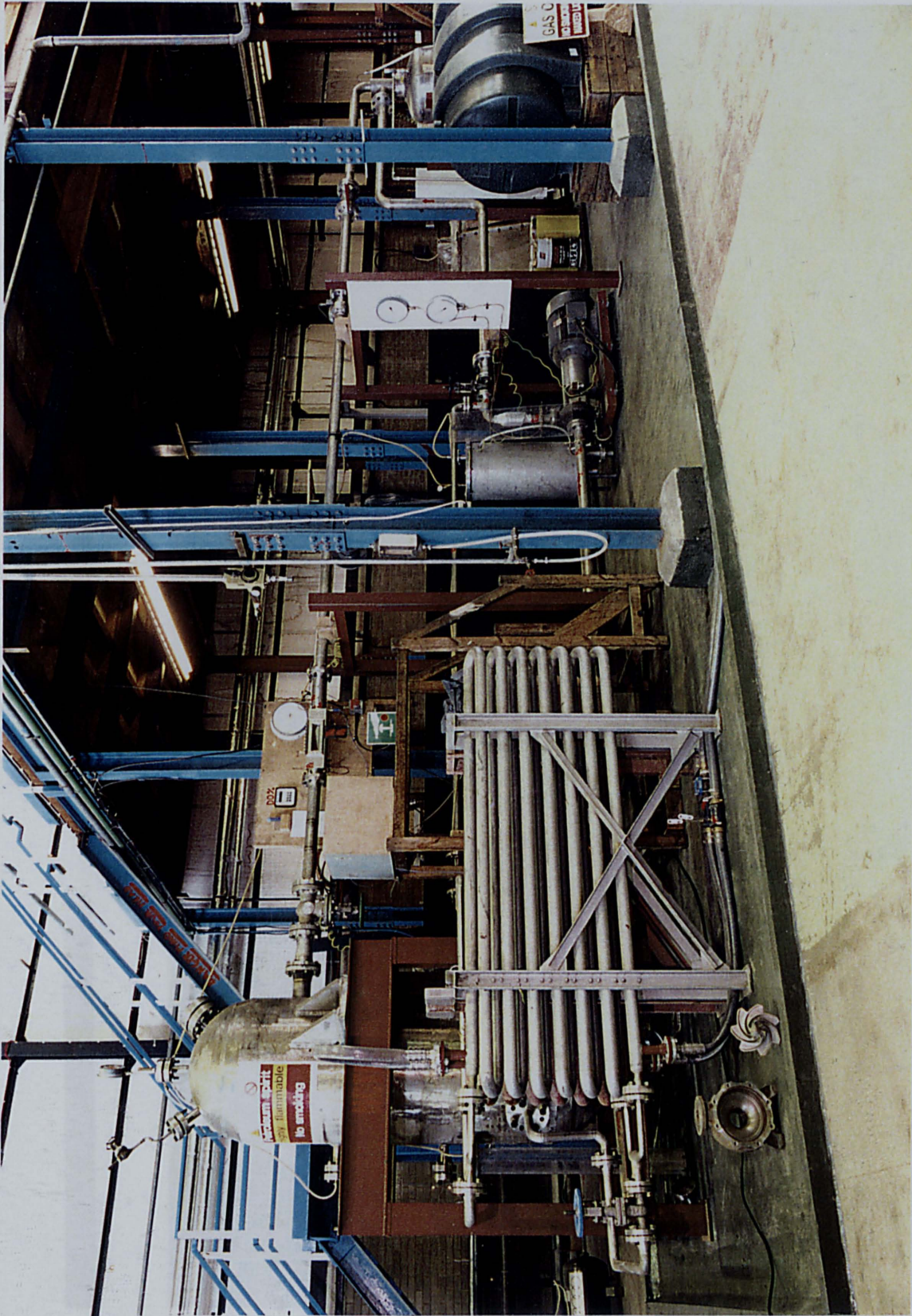


Figure G-1





Figure G-2

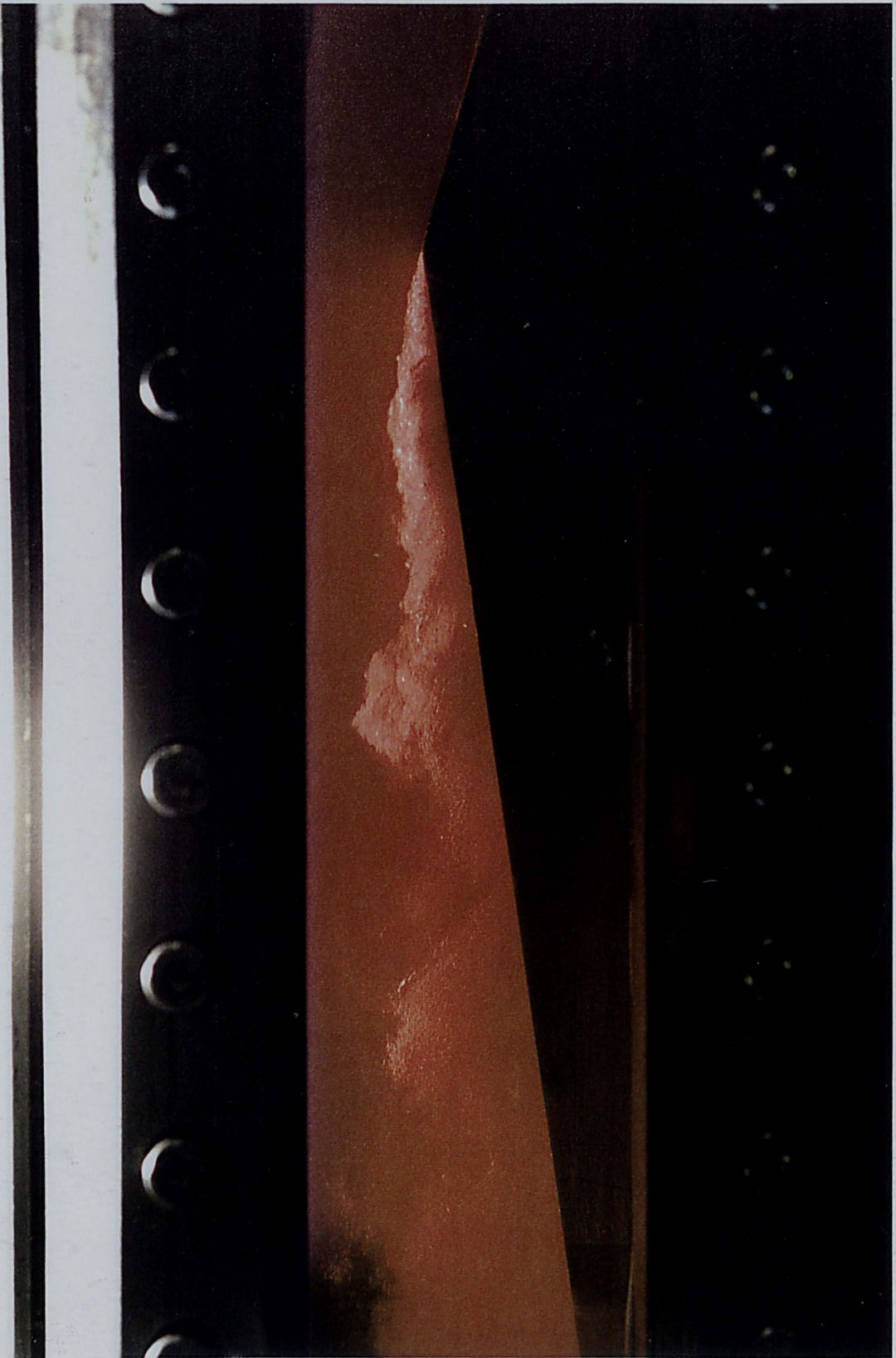


Figure G-3



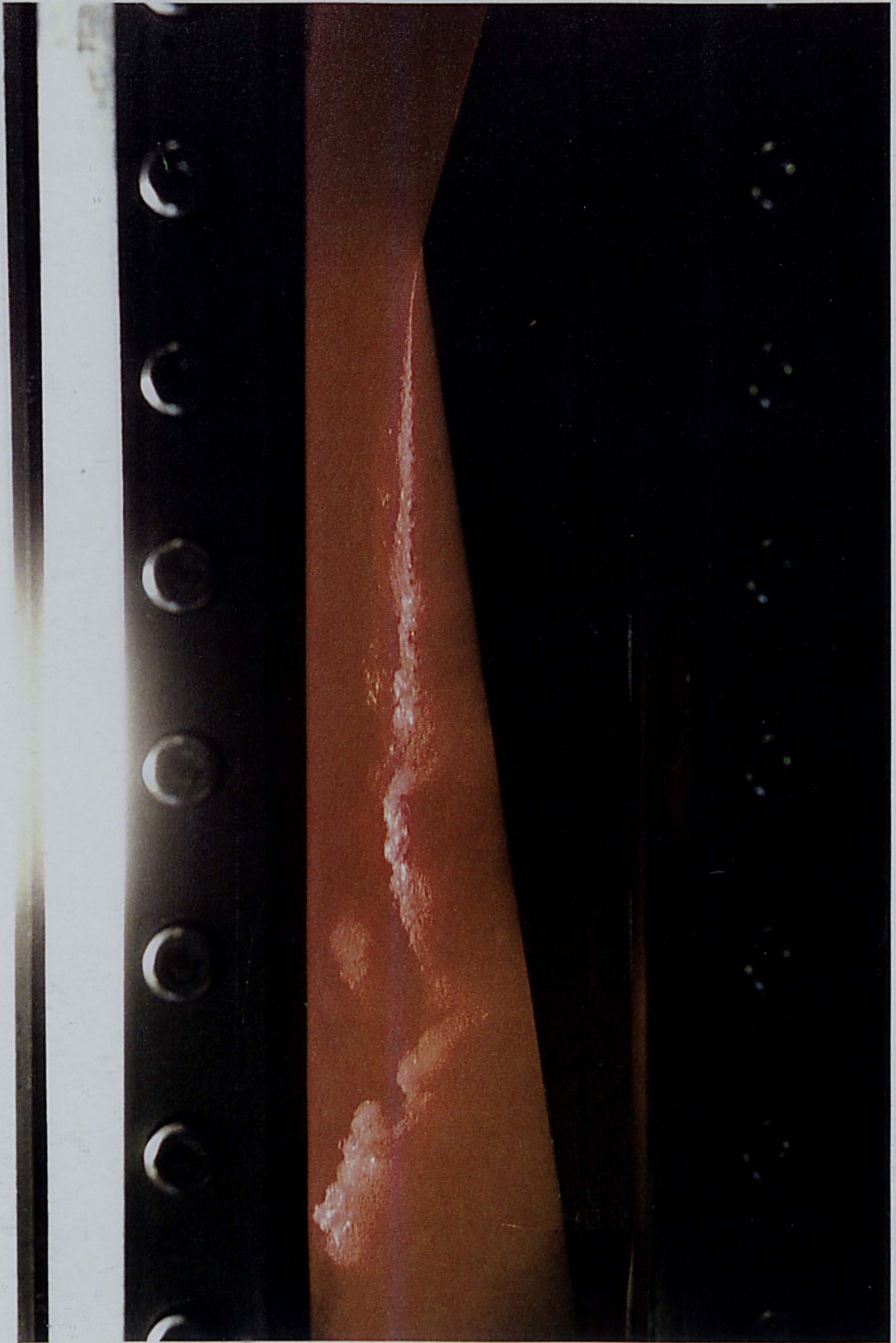


Figure G-4

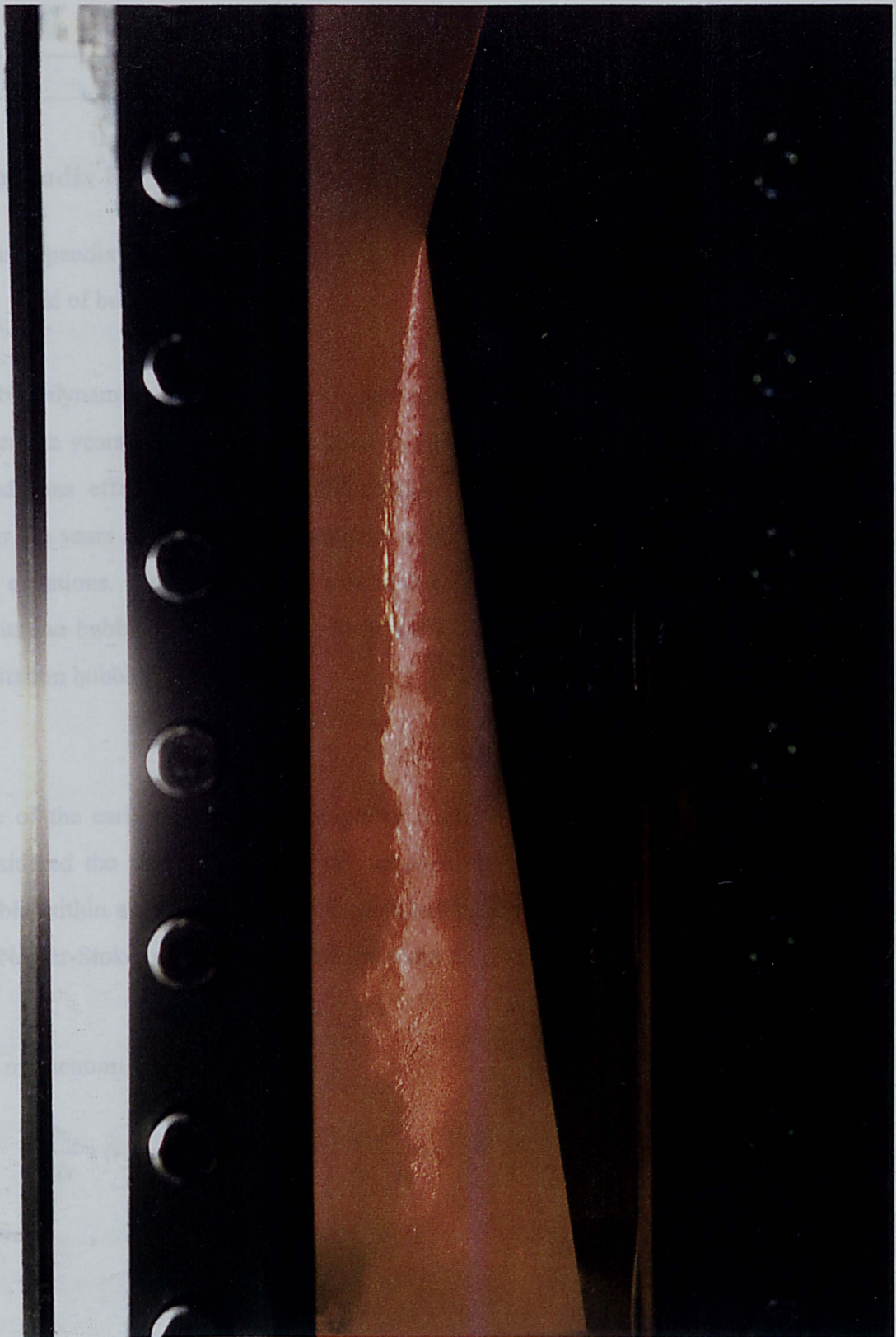


Figure G-5

## Appendix H - Bubble dynamics.

This appendix contains a descriptive overview of some of the major work completed in the field of bubble dynamics.

Bubble dynamics is a mathematical approach to the study of cavitation on a micro scale. Over the years, researchers have tried to find out how fluid properties, and boundary conditions effect bubble growth and collapse. The analysis has increased in complexity over the years and increasing amounts of computer power have been needed to solve the equations. This subject area was studied to give an overview of the physics of cavitation bubbles and to give an insight into what effect fluid properties have on the cavitation bubbles.

One of the earliest recorded attempts to model a bubble was by Besant (1859). He considered the very simple case of an expanding and contracting empty spherical bubble within an invicid fluid. The equations of motion for the bubble were based on the Navier-Stokes equations in spherical polar co-ordinates.

The momentum equations are;

$$\frac{\partial u_r}{\partial t} + (v. grad)u_r - \frac{u_\theta^2 + u_\phi^2}{r} = \frac{1}{\rho} \frac{\partial p}{\partial r} + v \left[ \Delta u_\theta - \frac{2 \cos \theta}{r^2 \sin^2 \theta} \frac{\partial u_\phi}{\partial \phi} + \frac{2}{r^2} \frac{\partial u_r}{\partial \theta} - \frac{u_\theta}{r^2 \sin^2 \theta} \right]$$

Where

$$(v. grad)f = u_r \frac{\partial f}{\partial r} + \frac{u_\theta}{r} \frac{\partial f}{\partial \theta} + \frac{u_\phi}{r \sin \theta} \frac{\partial f}{\partial \phi}$$

$$\Delta f = \frac{1}{r^2} \frac{\partial}{\partial r} \left( r^2 \frac{\partial f}{\partial r} \right) + \frac{1}{r^2 \sin \theta} \frac{\partial}{\partial \theta} \left( \sin \theta \frac{\partial f}{\partial \theta} \right) + \frac{1}{r^2 \sin^2 \theta} \frac{\partial^2 f}{\partial \phi^2}$$

for a spherical bubble  $\frac{\partial u_r}{\partial \phi} = 0$  ; and  $\frac{\partial u_r}{\partial \theta} = 0$

and for invicid flow;  $v = 0$

$$\frac{\partial u_r}{\partial t} + u_r \frac{\partial u_r}{\partial r} - \frac{u_\theta^2 - u_\phi^2}{r} = -\frac{1}{\rho} \frac{\partial p}{\partial r}$$

considering only radial expansion and contraction;  $u_\phi = u_\theta = 0$

Therefore;

$$\frac{\partial u_r}{\partial t} + u_r \frac{\partial u_r}{\partial r} = -\frac{1}{\rho} \frac{\partial p}{\partial r} \quad \text{..Equ H-1}$$

Consider continuity

$$\frac{1}{r^2} \frac{\partial (r^2 u_r)}{\partial r} + \frac{1}{r \sin \theta} \frac{\partial (u_\theta \sin \theta)}{\partial \theta} + \frac{1}{r \sin \theta} \frac{\partial u_\phi}{\partial \phi} = 0$$

$$\frac{1}{r^2} \frac{\partial (r^2 u_r)}{\partial r} = 0$$

This implies;

$$\frac{\partial (r^2 u_r)}{\partial r} = 0 \quad \text{..Equ H-2}$$

So equations 2.3-1 and 2.3-2 can be solved for the motion of a cavity wall, for this simple case. Besant did not however continue with any analysis or apply his solution to the cavitation case.

A most significant early contribution to cavity dynamics was provided by Lord Rayleigh (1917). He considers an expanding and contracting empty spherical bubble in an inviscid fluid, similar to Besant. After initially applying momentum and continuity considerations, as Besant's analysis, Rayleigh used an energy balance. He came up with expressions for the time taken for a cavity to collapse, pressures at the cavity wall and for cavity wall velocities. He then went on to include internal gas effects in his analysis but to no great success. The main draw back with the Rayleigh analysis is that the only



liquid property to be considered was density. Properties such as viscosity, surface tension, compressibility and other properties were neglected from his analysis.

The equations H-1 and H-2 derived by Besant were the starting point for Rayleigh's analysis of a spherical bubble in an incompressible fluid.

By integrating Equ. 2.3-2

$$r^2 u_r = \text{Constant}$$

Therefore

$$\begin{aligned} r^2 u_r &= R^2 U_R = R^2 \dot{R} \\ \Rightarrow u_r &= \frac{\dot{R} R^2}{r^2} \quad \text{..Equ H-3} \end{aligned}$$

The capital letters denote quantities measured at the bubble wall.

Now substituting Equ H-3  $\rightarrow$  H-1

$$\frac{\partial}{\partial t} \frac{\dot{R} R^2}{r^2} + \frac{\dot{R} R^2}{r^2} \frac{\partial}{\partial r} \frac{\dot{R} R^2}{r^2} = -\frac{1}{\rho} \frac{\partial p}{\partial r} \quad \text{..Equ H-4}$$

Differentiating using the product rule gives

$$\frac{\ddot{R} R^2}{r^2} + \frac{2\dot{R}^2 R}{r^2} + \frac{2\dot{R}^2 R^4}{r^5} = -\frac{1}{\rho} \frac{\partial p}{\partial r}$$

And integrating between  $r = r$  and  $r = \infty$

$$\begin{aligned} \ddot{R} R^2 \int_r^\infty \frac{dr}{r^2} + 2\dot{R}^2 R \int_r^\infty \frac{dr}{r^2} + 2\dot{R}^2 R^4 \int_r^\infty \frac{dr}{r^5} &= -\frac{1}{\rho} \int_p^{p_\infty} dp \\ \frac{\ddot{R} R^2}{r} + \frac{2\dot{R}^2 R}{r} + \frac{2\dot{R}^2 R^4}{4r^4} &= -\frac{1}{\rho} (p_\infty - p) \quad \text{..Equ H-5} \end{aligned}$$

And at the bubble wall  $r = R$  and  $p = P_{(R)}$



$$\ddot{R} R + \frac{3\dot{R}^2}{2} = \frac{1}{\rho} (P_{(R)} - p_{\infty}) \quad \text{..Equ H-6}$$

This is the Rayleigh equation for bubble wall motion.

Rayleigh decided that a better method for analysing the problem would be by using an energy balance. Rayleigh's main assumptions for this theory were;

1. The velocity is  $u$  at a radius  $r$ .
2. The cavity wall has a radius  $R$  and a velocity  $U$  at a time  $t$
3.  $r > R$
4. Radial flow is irrotational for spherical symmetry.

The velocity potential and velocities are given by

$$\phi = \frac{UR^2}{r} \quad \text{and} \quad \frac{u}{U} = \frac{R^2}{r^2} \quad \text{..Equ H-7}$$

$$\text{Kinetic energy} \quad KE = \frac{1}{2} (\rho V) u^2$$

Therefore the kinetic energy for a liquid at a time  $t$  can be found by integrating a concentric fluid shell of thickness  $dr$  from  $R$  to  $\infty$ , see Figure H-1.

$$KE_{LIQ} = \int_R^{\infty} \frac{1}{2} \rho V u^2 = \frac{\rho}{2} \int_R^{\infty} u^2 4\pi r^2 dr \quad \text{..Equ H-8}$$

substituting (Equation H-7)<sup>2</sup> into H-8 gives;

$$KE_{LIQ} = 2\pi\rho U^2 R^3 \quad \text{..Equ H-9}$$

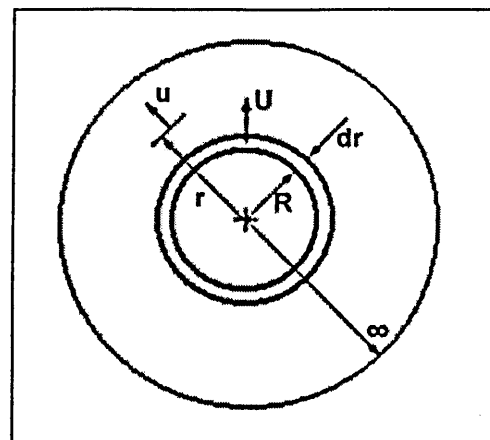


Figure H-1 Rayleigh energy analysis.

The work done on the fluid as the cavity collapses from an initial radius  $R_0$  to  $R$  is the product of the pressure at infinity  $p_\infty$  and the change in volume of the cavity. There is no work done at the cavity wall as  $P_{(R)} = 0$

$$\therefore \text{Work Done} = p_\infty \frac{4\pi}{3} (R_0^3 - R^3) \quad \text{..Equ H-10}$$

Assuming the liquid to be inviscid and incompressible, the work done on the fluid will be equal to the kinetic energy of the liquid, so equations H-9 and H-10 can be equated.

$$\text{Work done} = KE_{LIQ}$$

$$p_\infty \frac{4\pi}{3} (R_0^3 - R^3) = 2\pi\rho U^2 R^3$$

$$\Rightarrow U^2 = \frac{2p_\infty}{3\rho} \left( \frac{R_0^3}{R^3} - 1 \right)$$

$$U = \sqrt{\frac{2p_\infty}{3\rho} \left( \frac{R_0^3}{R^3} - 1 \right)} \quad \text{..Equ H-11}$$

Where equation H-11 is an expression for the bubble wall velocity.

An expression for the time for the cavity to collapse can be found as  $U = dR/dt$ .

$$dt = \sqrt{\frac{3\rho}{2p_\infty} \left( \frac{R^3}{R_0^3 - R^3} \right)} dR$$

$$t = \sqrt{\frac{3\rho}{2p_\infty}} \int_R^{R_0} \left( \frac{R^3}{R_0^3 - R^3} \right) dR$$

$$\text{let } \beta = R/R_0$$

$$t = \sqrt{\frac{3\rho}{2p_\infty}} \int_R^{R_0} \left( \frac{\beta^{3/2}}{(1-\beta^3)^{1/2}} \right) d\beta$$

..Equ H-12

Equation H-12 can be evaluated for the time of total collapse  $\tau$  ie  $\beta=0$  by means of  $\Gamma$  functions.

$$\tau = R_0 \sqrt{\frac{3\rho}{2p_\infty} \frac{\Gamma(3/2) \Gamma(1/2)}{\Gamma(2)}}$$

$$\tau = 0.91489 R_0 \sqrt{\frac{\rho}{p_\infty}} \quad \text{..Equ H-13}$$

It can be seen from equation H-11 that as  $R \Rightarrow 0$   $U \Rightarrow \infty$

$$U = \sqrt{\frac{2p_\infty}{3\rho} \left( \frac{R_0^3}{R^3} - 1 \right)}$$

To avoid this, Rayleigh assumed that the gas in the cavity compressed isothermally instead of having zero or constant pressure at the cavity wall. This means that the energy balance now involves equating equations H-9 and H-10 and the work done compressing the gas (Equ H-14).

ork done compressing the gas;  $W = - \int_R^{R_0} p dV$

$$W = \left[ p_1 V_1 \ln \left( \frac{V_2}{V_1} \right) \right]_R^{R_0}$$

$$W = -4\pi Q R_0^2 \ln \left( \frac{R}{R_0} \right)$$

..Equ H-14

$$U^2 = \frac{2p_\infty}{3\rho} \left( \frac{R_0^3}{R^3} - 1 \right) - \frac{2Q}{\rho} \left( \frac{R_0^3}{R^3} \right) \ln \left( \frac{R_0}{R} \right) \quad \text{..Equ H-15}$$

For any positive initial pressure  $Q$  the cavity will not collapse completely and  $U \Rightarrow 0$  for a finite  $R$ . The limiting size of the cavity can be found by setting  $U=0$ . Let  $z = R_0^2/R^3$

$$p_{\infty} \left( \frac{z-1}{z} \right) - Q \ln(z) = 0 \quad \text{..Equ H-16}$$

Although this has been derived for an isothermal process, any thermodynamic process can be used. The next step was to assess the pressure field around the bubble. The liquids acceleration  $a_r$  is can be written as the total differential of the liquids velocity  $u$  at radius  $r$ .

$$\begin{aligned} a_r &= -\frac{du}{dt} \\ &= -\frac{\partial u}{\partial t} - u \frac{\partial u}{\partial r} \\ &= \frac{1}{\rho} \frac{\partial p}{\partial r} \end{aligned}$$

Taking the partial derivatives of Equations H-7 and H-11 it can be shown that

$$\frac{1}{p_{\infty}} \frac{\partial p}{\partial r} = \frac{R}{3r^2} \left[ \frac{(4z-4)}{r^3} R^3 - (z-4) \right] \quad \text{..Equ H-17}$$

here  $z = (R_0/R)^3$  and  $r > R$

integrating H-17

$$\frac{p}{p_{\infty}} - 1 = \frac{R}{3r} (z-4) - \frac{R^4}{3r^4} (z-1) \quad \text{..Equ H-18}$$

The pressure distribution at the instant of release is obtained when  $R = R_0 \Rightarrow z = 1$

$$p = p_{\infty} \left( 1 - \frac{R_0}{r} \right) \quad \text{..Equ H-19}$$

Now applying some boundary conditions we can find out more about the cavity.

At the initiation of collapse  $z = 1$

for  $1 < z < 4$  it can be seen that  $p_{\max} = p_{\infty}$  and occurs at  $R/r = 0$  i.e. where  $r \rightarrow \infty$

for  $4 < z < \infty$  it can be seen that  $p_{\max} > p_{\infty}$  and occurs at a finite  $r/R$

as  $z \rightarrow \infty$  the value of  $r/R=1.59$

A graph was obtained from solving equation H-18 for various values of  $z$ , and can be seen in Figure H-2. The location of the maximum pressure in the liquid  $r_{\max, p}$  may be found by setting  $dp/dr=0$  in equation H-17. therefore the maximum value of  $p$  occurs where;

$$\frac{r_m^3}{R^3} = \frac{4z-4}{z-4} \quad \text{..Equ H-20}$$

substituting H-20 into H-18 the maximum value of  $p$  can be found.

$$\frac{p_{\max}}{p_{\infty}} = 1 + \frac{(z-4)^{4/3}}{4^{4/3}(z-1)^{1/3}} \quad \text{..Equ H-21}$$

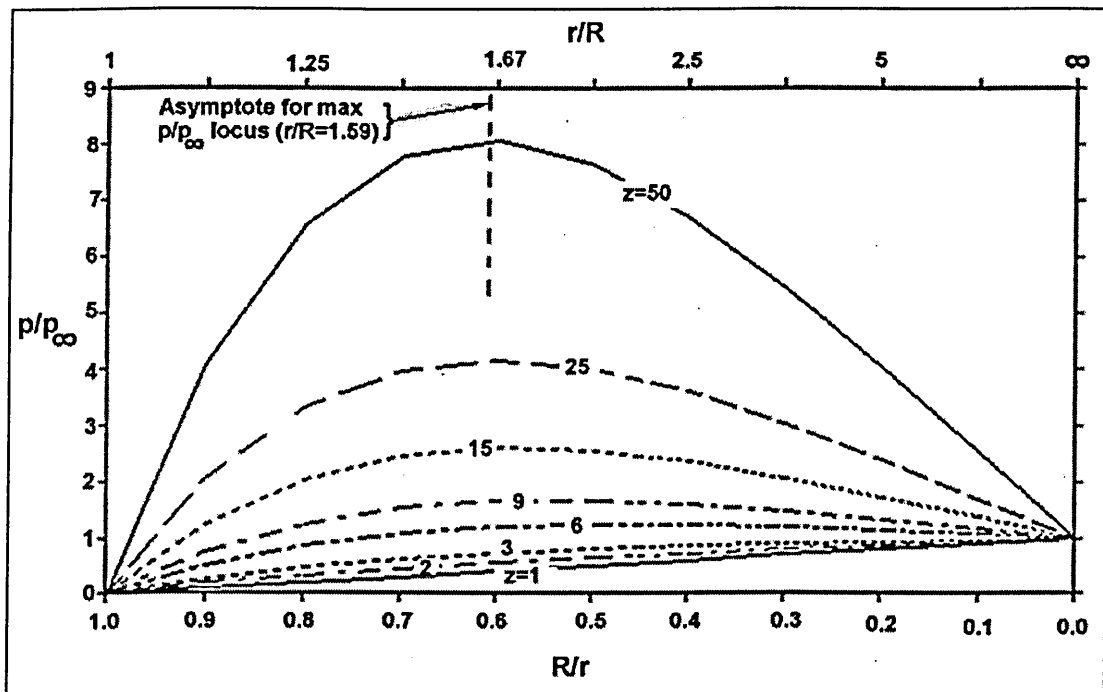


Figure H-2 Rayleigh analysis: Pressure profile near a collapsing bubble.

Equations H-20 and H-21 show that as the cavity gets very small ( $z \rightarrow \infty$ ) the pressure in the liquid becomes very large, however the pressure at the bubble wall is always zero.

This would suggest the possibility that, in compressing the liquid, energy is stored which would add an extra term to equation H-11 and therefore invalidating the assumption of incompressibility.

Plesset (1949) went on to include internal vapour, surface tension effects and improve the pressure field analysis by Rayleigh by including a time variance. A summary of the analysis can be found below. He compared the predicted results from the analysis with observed cavitation bubbles. The agreement was close but the analysis gave more rapid growth and collapse times than was seen in practice. This was thought to be due to 'wall effects', because the theory assumes a bubble in an infinite fluid, where as experimentally, it had physical boundaries.

From Rayleigh's basic equation Equ. H-6.

$$\ddot{R}R + \frac{3\dot{R}^2}{2} = \frac{1}{\rho} (P_{(R)} - p_{\infty})$$

We can say in this equation that;

$$P_{(R)} = \Sigma (\text{Vapour pressure, Gas pressure, \& Surface tension})$$

$$P_{(R)} = p_v + p_{gas} + p_{st}$$

For a fixed mass of gas

$$p_{gas} = \frac{m\tilde{R}T}{V} = \frac{m\tilde{R}T}{\frac{4}{3}\pi R^3} = \frac{3m\tilde{R}T}{4\pi R^3}$$

$$\frac{3m\tilde{R}}{4\pi} = \text{Const} = N$$

$$p_{gas} = \frac{NT}{R^3}$$

For a sphere

$$p_{st} = \sigma \left( \frac{1}{R_1} + \frac{1}{R_2} \right)$$

$$R_1 = R_2$$

$$p_{st} = \frac{2\sigma}{R}$$

$$\frac{R\ddot{R}}{\rho} + \frac{3\dot{R}^2}{2\rho} = p_v - p_{\infty} - \frac{2\sigma}{R} + \frac{NT}{R^3} = f(R, T) \quad \text{..Equ H-22}$$

For equilibrium	$f(R, T) = 0$	For stability	$\partial f / \partial R < 0$
For growth	$f(R, T) = +ve$	For instability	$\partial f / \partial R > 0$
For collapse	$f(R, T) = -ve$	The critical radius is at	$\partial f / \partial R = 0$

Soon after, Poritski (1957) developed the model of an expanding and contracting spherical bubble in an incompressible fluid with internal vapour and gas, surface tension effects and the inclusion of viscosity. The effect of viscosity is to reduce the effective pressure differential at the bubble wall, therefore reducing the rates of growth or collapse. This explains why Plesset's analysis predicted more rapid growth than experimental results, his analysis did not include the effect of viscosity. However there is a 'viscosity paradox', the Navier-Stokes equations for spherical symmetry in an incompressible fluid can be arranged, so there is no viscosity term present. This paradox was solved by Poritski using the following analysis, see Figure H-3.

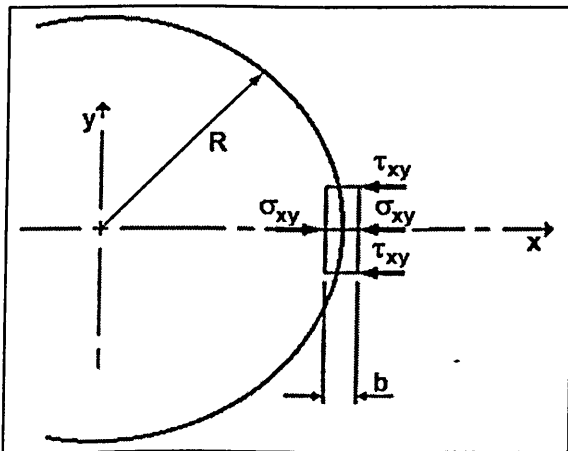


Figure H-3 Poritski analysis

For the one dimensional incompressible case, the stresses on a control volume thickness  $b$ , must balance. The relationship between these stresses and pressure are as follows

$$\sigma_x = -p + 2\mu \frac{\partial u}{\partial x} \quad \text{..Equ H-23}$$

$$\text{here } p = \bar{\sigma} = \frac{1}{3}(\sigma_x + \sigma_y + \sigma_z)$$

Assuming the gas/vapour viscosity is small in comparison with the liquid viscosity it may be neglected, then;

$$P_g = -\sigma_x = P_{(R)} - \mu_L 2 \frac{\partial u}{\partial x} \quad \text{..Equ H-24}$$

and from continuity we have;

$$\frac{\partial u}{\partial r} = -\frac{2u}{r} \quad \text{..Equ H-25}$$

at the bubble wall  $u = \dot{R}$  and  $r = R$  and also combining a surface tension term the following equation is arrived at.

$$P_{(R)} = P_g - \frac{2\sigma}{R} + 4\mu_L \frac{\dot{R}}{R} \quad \text{..Equ H-26}$$

To include the effects of the gas and vapour viscosity an extra term has to be added

$$P_{(R)} = P_g - \frac{2\sigma}{R} + 4(\mu_L + \mu_g) \frac{\dot{R}}{R} \quad \text{..Equ H-27}$$

These terms can then be used within Rayleigh's basic Equation H-6.

Gilmore (1970) went on to include compressibility effects in the analysis developed by Poritski. Compressibility in liquids only starts to take effect at high Mach numbers. The sonic velocity for water is approximately 1500 m/s and this sort of velocity is unlikely in normal flow conditions. However with a collapsing bubble as  $r \Rightarrow 0$  large Mach numbers are achieved and therefore compressibility will make an effect. Gilmore was one of the first researchers to include the effects of compressibility in his analysis which follows.

From the Navier-Stokes equations, assuming;

1. No body forces.
2. Spherical symmetry i.e.  $curl \vec{v} = 0$ .

$\therefore$

Momentum in vector form.

$$\frac{D\vec{v}}{Dt} = -\frac{1}{\rho} grad p + \frac{4\mu}{3\rho} grad(div\vec{v}) \quad \text{..Equ H-28}$$

Continuity in vector form.

$$\frac{D\rho}{Dt} + \rho(div\vec{v}) = 0 \quad \text{..Equ H-29}$$



$$\frac{D\vec{V}}{Dt} = -\frac{1}{\rho} \text{grad } p + \frac{4\mu}{3\rho} \text{grad} \left( -\frac{1}{\rho} \frac{Dp}{Dt} \right) \quad \text{..Equ H-30}$$

The viscous and compressibility effects are small, and as they appear in equation H-30 as a product of each other they can be neglected. This does not mean that compressibility is neglected, as it appears in the continuity equation and the viscosity will appear in the boundary conditions.

$$\frac{D\vec{V}}{Dt} = -\frac{1}{\rho} \text{grad } p \quad \text{..Equ H-31}$$

If it is also assumed that the liquid's density is only a function of the fluid's pressure, and that the enthalpy for isentropic compression is defined as.

$$h(p) = \int_{p_\infty}^p \frac{dp}{\rho} \quad \text{..Equ H-32}$$

$$\text{grad } h = \text{grad} \left( \frac{p - p_\infty}{\rho} \right)$$

∴

$$\rho \frac{\partial h}{\partial r} = \text{grad } p \quad \text{..Equ H-33}$$

∴

Substituting H-33 into H-31 gives;

$$\frac{D\vec{V}}{Dt} = -\frac{\partial h}{\partial r} \quad \text{..Equ H-34}$$

defining the sonic velocity,  $c$  as;

$$c^2 = \frac{dp}{d\rho} \quad \text{..Equ H-35}$$

The continuity equation H-29 can be written as;

$$-\frac{1}{c^2} \frac{Dh}{Dt} = \text{div } \vec{V} \quad \text{..Equ H-36}$$

Now we have two differential equations H-36 and H-34 with three dependant variables  $\bar{V}$ ,  $h$ ,  $c$  and two independent variables  $r$  and  $t$ . These can be reduced to two independent and two dependant variables by equating  $c$  and  $h$  in equations H-35 and H-32. The two differential equations must then be solved simultaneously. From the Lamb (1942) acoustic equation for divergent spherical waves:

$$\left(\frac{\partial}{\partial t} + c \frac{\partial}{\partial r}\right) r \phi = 0$$

And the Kirkwood-Blethe (1942) hypothesis that characteristic quantity  $r((u^2/2)+h)$  is propagated outwards in the liquid with a characteristic of  $(c+u)$  the following relation between  $r$  and  $t$  is obtained;

$$\frac{\partial}{\partial t} \left[ r \left( h + \frac{u^2}{2} \right) \right] + (c+u) \frac{\partial}{\partial r} \left[ r \left( h + \frac{u^2}{2} \right) \right] = 0 \quad \text{..Equ H-37}$$

Substituting equations H-34 and H-36 into the above equation for the motion of a point on the bubble wall, a single ordinary differential equation with one independent variable, either  $r$  or  $t$ .

$$RU \frac{dU}{dR} \left( 1 - \frac{U}{C} \right) + \frac{3}{2} U^2 \left( 1 - \frac{U}{3C} \right) = H \left( 1 + \frac{U}{C} \right) + \frac{RU}{C} \frac{dH}{dR} \left( 1 - \frac{U}{C} \right) \quad \text{..Equ H-38}$$

He came up with these governing equations which can be solved by numerical means, however at the time the computing power to solve them was not available.

They were eventually solved by Ivany and Hammitt (1965), using numerical analysis. Ivany and Hammitt's results showed that surface tension and viscosity do not generally effect the collapse behaviour of the bubble. However bubbles collapsing in incompressible liquids collapse at greater speeds to those collapsing in a compressible liquid, because less of the available energy appears as kinetic energy.

From these basic studies by Rayleigh, Poritski and Gilmore, a large number of studies have been undertaken, continually increasing the complexities of the models. A good review of the work done up until the late seventies is given by Plesset and Prosperetti (1977). As computer availability and power have increased it has been possible to vastly increase the complexity of these studies. The remainder of this section will describe

some of the studies that have been conducted since the late seventies. The complexity and the number of studies that have been conducted in recent years is too great to contemplate giving a full review, the passage however gives some good references as starting points for further reading.

Cooper et al (1978,1981<sup>P1</sup> & 1983) undertook a large program of work, both analytical and experimental. Vapour bubbles were studied growing with various boundary conditions. Starting with the simple case of a slow growing bubble at a wall with a stagnant fluid, isothermal conditions and zero gravity. These studies gradually increased in complexity to include conditions such as , fast growing bubbles, gravity, temperature gradients between boundary walls and fluid, moving fluids, horizontal and vertical walls, and even different wall materials. Among the conclusions were that, slow growing bubbles grew spherically where as fast growing bubbles grew hemispherically. With a thermal gradient bubbles will depart from the wall where they are growing, even in zero gravity, whereas the bubble will not depart with isothermal conditions. They also found that liquid flow increased the growth rate, due to increased heat transfer by convective effects.

Blake (1987 & 1995) has conducted a large amount of work concerned with the growth and collapse of cavitation bubbles near to boundaries, both numerically and experimentally. He has particularly concentrated on using different materials for the boundary walls. For example he showed that using a surface that will deform (rubber) can greatly modify the bubbles motion.

Some of the most recent studies were by Matsumoto et al (1988 & 1994<sup>P2</sup>) and Takemura et al (1994 & 1995). These studies were based on the effect of the cavities internal phenomena such as thermal diffusion, phase change and mass diffusion on its

---

<sup>P1</sup> Two papers in this year

<sup>P2</sup> Two papers in this year

motion. These studies have included both numerical analysis and experimental investigations of laser induced bubbles, the correlation's of which are extremely good.

### **Concluding comments.**

This subject gives an insight into the mechanisms at work during the cavitation process: How the bubbles grow and collapse and the factors affecting this process. Bubble dynamics cannot yet predict the start of a cavitation bubble and at present its practical use is limited. It however can only help to aide in the understanding of the cavitation process. For further reading see Brennen (1994<sup>①</sup>).